

MDL

# Neuroscience Bulletin

The Official Journal of The Chinese Neuroscience Society

神经科学通报

Volume 36  
Number 3  
March 2020



ACC

ACC-to-MDL Projection Modulates  
Vicarious Freezing Behavior

SIBS Springer

www.neurosci.cn

## About the Cover

Emotional contagion, a primary form of empathy, is present in rodents. Among its associated behaviors, the social transmission of fear is the most studied. In this issue, Zheng *et al.* applied fMRI and virus-dependent strategies to identify the brain regions and neural circuits involved in vicarious freezing behavior. In the cover image, a demonstrator rat (left) elicits freezing behavior when a cat comes into sight. Meanwhile, the threat-experienced observer rat (right) also shows freezing behavior—vicarious freezing—when seeing the freezing response of the demonstrator. See pages 217–229. (Cover image provided by Prof. Zuoren Wang)

Volume 36 Number 3  
March 2020



## Editorial

### 199 Neuronal Network Dissection with Neurotropic Virus Tracing

Xiaoping Rao · Jie Wang

## Original Articles

### 202 Rabies Virus Pseudotyped with CVS-N2C Glycoprotein as a Powerful Tool for Retrograde Neuronal Network Tracing

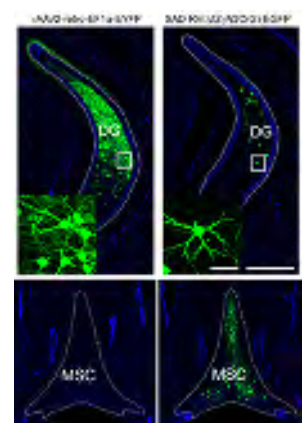
Xutao Zhu · Kunzhang Lin · Qing Liu · Xinpei Yue · Huijie Mi · Xiaoping Huang · Xiaobin He · Ruiqi Wu · Danhao Zheng · Dong Wei · Liangliang Jia · Weilin Wang · Anne Manyande · Jie Wang · Zhijian Zhang · Fuqiang Xu

### 217 Projection from the Anterior Cingulate Cortex to the Lateral Part of Mediodorsal Thalamus Modulates Vicarious Freezing Behavior

Chaowen Zheng · Yanwang Huang · Binshi Bo · Lei Wei · Zhifeng Liang · Zuoren Wang

### 230 Dopamine D2 Receptor-Mediated Modulation of Rat Retinal Ganglion Cell Excitability

Ning Yin · Yu-Long Yang · Shuo Cheng · Hong-Ning Wang · Xin Hu · Yanying Miao · Fang Li · Zhongfeng Wang



p 209

**243 Scorpion Venom Heat-resistant Peptide is Neuroprotective against Cerebral Ischemia-Reperfusion Injury in Association with the NMDA-MAPK Pathway**

Xu-Gang Wang · Dan-Dan Zhu · Na Li · Yue-Lin Huang · Ying-Zi Wang · Ting Zhang · Chen-Mei Wang · Bin Wang · Yan Peng · Bi-Ying Ge · Shao Li · Jie Zhao

**254 AVP(4-8) Improves Cognitive Behaviors and Hippocampal Synaptic Plasticity in the APP/PS1 Mouse Model of Alzheimer's Disease**

Xiumin Zhang · Fang Zhao · Chenfang Wang · Jun Zhang · Yu Bai · Fang Zhou · Zhaojun Wang · Meina Wu · Wei Yang · Junhong Guo · Jinshun Qi

**263 Role of Elevated Thrombospondin-1 in Kainic Acid-Induced Status Epilepticus**

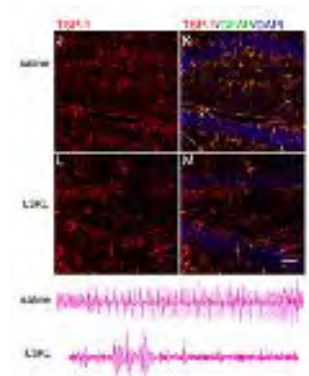
Yurong Zhang · Mengdi Zhang · Wei Zhu · Xiaohong Pan · Qiaoyun Wang · Xue Gao · Chaoyun Wang · Xiuli Zhang · Yuxia Liu · Shucui Li · Hongliu Sun

**277 NLRP3 Deficiency Attenuates Secondary Degeneration of Visual Cortical Neurons Following Optic Nerve Injury**

Zhou Zhang · Wenyi Liu · Yubin Huang · Linlin Luo · Xiaofeng Cai · Yunjia Liu · Liqianyu Ai · Jun Yan · Sen Lin · Jian Ye

**289 Propofol Attenuates  $\alpha$ -Synuclein Aggregation and Neuronal Damage in a Mouse Model of Ischemic Stroke**

Yuzhu Wang · Dan Tian · Changwei Wei · Victoria Cui · Huan Wang · Yanbing Zhu · Anshi Wu · Yun Yue



p 269

## Letter to the Editor

**299 The Risk and Prevention of Novel Coronavirus Pneumonia Infections Among Inpatients in Psychiatric Hospitals**

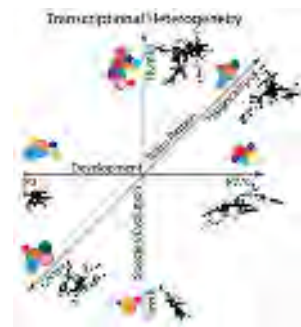
Yuncheng Zhu · Liangliang Chen · Haifeng Ji · Maomao Xi · Yiru Fang · Yi Li

## Insight

- 303 Microglia Research in the 100th Year Since Its Discovery**  
Anthony D. Umpierre · Long-Jun Wu

## Reviews

- 307 Expert Consensus on the Care and Management of Patients with Cognitive Impairment in China**  
Academy of Cognitive Disorders of China (ACDC) · Yuliang Han · Jianjun Jia · Xia Li · Yang Lv · Xuan Sun · Shanshan Wang · Yongjun Wang · Zhiwen Wang · Jintao Zhang · Jiong Zhou · Yuying Zhou
- 321 A Review of Functional Near-Infrared Spectroscopy Studies of Motor and Cognitive Function in Preterm Infants**  
Quan Wang · Guang-Pu Zhu · Li Yi · Xin-Xin Cui · Hui Wang · Ru-Yi Wei · Bing-Liang Hu



p 304



# Neuronal Network Dissection with Neurotropic Virus Tracing

Xiaoping Rao<sup>1</sup> · Jie Wang<sup>1,2</sup>

Received: 12 January 2020 / Accepted: 17 January 2020 / Published online: 17 February 2020  
© Shanghai Institutes for Biological Sciences, CAS 2020

The brain is a marvel of biological evolution, a highly complex organ including hundreds of different types of about 100 billion neurons. Understanding the structure and function of the brain is one of the most challenging scientific questions in the 21st century. Crucially, the structure of neural circuits and the mechanisms of neuronal information processing related to brain function are still poorly understood [1]. A neural circuit is composed of a large number of synaptically connected neurons of different types and characteristics. It is the structural basis for the execution of various functions, such as perception, emotion, memory, and imagination, as well as other activities. Revealing the structure of neural circuits is the basic premise for understanding the mechanism of information processing in the brain [2].

Traditional neural circuit-tracing methods, such as electron microscopy and Golgi staining, along with dyes and protein/peptide tracers, can depict the morphology of neurons in one brain region and their projections to other regions, as well as trans-synaptic labeling [3]. However, there are some limitations to these tracers and methods, such as extensive deposition, indirect signaling, uncertain direction of spreading, and severe post-synaptic signal

attenuation [4]. Neurotropic viruses are a class of viral vectors that can infect neurons and propagate along the neural connections (Fig. 1), such as pseudorabies virus (PRV), herpes simplex virus type 1 (HSV), rabies virus (RV), and vesicular stomatitis virus (VSV) [5]. In addition, some recombinant non-trans-synaptic viral vectors can efficiently label the fine morphology of neurons *in vivo*, such as Semliki forest virus (SFV) [6], or act as a helper virus to express exogenous genes, such as recombinant adeno-associated virus (AAV) and lentivirus (LV). They can also be used to dissect upstream projections, such as canine adenovirus 2 (CAV2) (Table 1) [5].

Compared with the traditional tracers, the neurotropic viruses have the following characteristics: (I) transmission across synapses, (II) control of the anterograde or retrograde direction of trans-synaptic transmission, (III) replication after crossing synapses without any signal attenuation, and (IV) compatibility with various genetic markers [7]. These characteristics provide unique advantages in the study of structural and functional neural circuits. Nevertheless, there are some limitations or problems for the existing viral tracer systems: (I) tracer tools do not work consistently for different animal models, especially there is a lack of efficient viral tracing tools for primates, (II) the toxicity of existing tools limits their application, such as the long-term functional analysis of neural circuits, (III) low efficiency of expression for some viruses complicates the experimental process, (IV) preparation processes need to be upgraded urgently for the efficient production of high-quality viral vectors, (V) sparse labeling virus systems suitable for local neural circuits need improvement, (VI) the mechanisms by which some viral particles infect neurons are not clear, so the direction of spread across synapses is uncertain, leading to unclear interpretation, and (VII) due to the lack of

✉ Jie Wang  
jie.wang@wipm.ac.cn

<sup>1</sup> Center of Brain Science, State Key Laboratory of Magnetic Resonance and Atomic and Molecular Physics, National Center for Magnetic Resonance in Wuhan, Key Laboratory of Magnetic Resonance in Biological Systems, Wuhan Institute of Physics and Mathematics, Innovation Academy for Precision Measurement Science and Technology, Chinese Academy of Sciences, Wuhan 430071, China

<sup>2</sup> The Second Hospital of Shijiazhuang, Shijiazhuang 050051, China

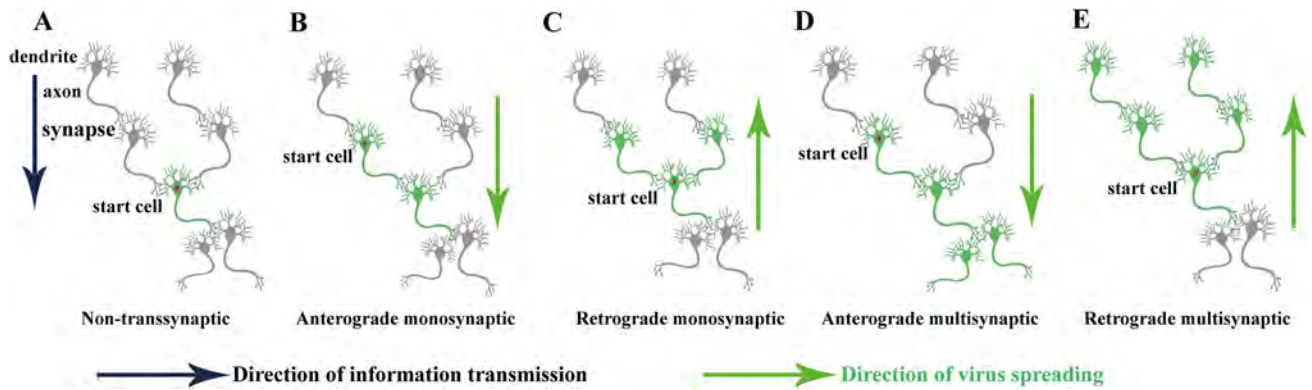


**Fig. 1** Direction and numbers of steps of virus spread in neural circuit tracing.

**Table 1** Advantages and disadvantages of recombinant viral vectors commonly used in neural circuit tracing [4, 7].

Type	Virus tracer	Advantages	Disadvantages
<b>Non-trans-synaptic</b>	Adeno-associated virus	Various serotypes, low immunogenicity, low cytotoxicity, cell-type specific labeling available, structural and functional dissection	Vector capacity $\leq 5$ kb, higher titer and high purity required in primates
	rAAV-retro	Retrograde tracer, efficient axon terminal absorption	Lower subcortical infection
	Canine adenovirus	Wide range of hosts, retrograde tracer, efficient axon terminal absorption	Cytotoxicity
	Semliki forest virus	Non-specific rapid labeling	High cytotoxicity
	Rabies virus (glycoprotein G-deleted)	Retrograde tracer, efficient infection of axon endings	High cytotoxicity
	Herpes simplex virus amplicon	Retrograde tracer, efficient axon ending absorption, capacity of $\leq 150$ kb, wide cellular tropism, low probability of insertional mutagenesis	Low efficiency, low cytotoxicity
<b>Trans-synaptic</b>			
	<b>Anterograde, monosynaptic</b>		
	Herpes simplex virus (TK-deleted)	Broad host range, anterograde trans-synaptic spread, large capacity, more genetic elements available	Low efficiency, high cytotoxicity, axonal terminal uptake
	Adeno-associated virus, serotype 1	Clear direction of spread, low immunogenicity, low cytotoxicity, downstream cell-type specific labeling and structural and functional dissection available	Unclear trans-synaptic mechanism, high titer required, low trans-synaptic efficiency, small capacity
<b>Retrograde, monosynaptic</b>	Rabies virus, RV $\Delta$ G-EnvA	Clear direction of spread, high efficiency	High cytotoxicity, potential leakage
	Pseudorabies virus (TK-deleted)	Clear direction of spread, more genetic elements available	Low trans-synaptic efficiency, cytotoxicity
<b>Anterograde, multisynaptic</b>	Herpes simplex virus 1, HSV1, H129	Fast and bright labeling, large capacity, broad host range	High cytotoxicity, axon terminal absorption
	Vesicular stomatitis virus	Fast and bright labeling	High cytotoxicity
<b>Retrograde, multisynaptic</b>	Pseudorabies virus, PRV Bartha	Clear direction of spread, large capacity, more genetic elements available	High cytotoxicity, low expression efficiency, does not infect primates
	Rabies virus, RV WT	Clear direction of spread	High cytotoxicity, high pathogenicity

comprehensive understanding of the pathogenicity of various viral tracers in different types of neurons in the same animal, the scope of their applicability is vague, leading to inconsistent results (Table 1). Therefore, further development and improvement of viral tracing tools, as well as the establishment of appropriate instructions for use, have become urgent.

In the present issue of *Neuroscience Bulletin*, Zhu and collaborators [8] compared the efficiency of retrograde gene transduction and neurotropism in three widely-used retrograde virus tracers. They found that the SAD strain of rabies virus [SAD-RV( $\Delta$ G)-N2C(G)], packaged with the N2C glycoprotein from the CVS strain [9], has a retrograde efficiency comparable to rAAV2-retro, but has a broader tropism in different neural types and regions, especially in subcortical regions. However, rAAV2-retro is more suitable for cortical neural circuit tracing [8]. On the other hand, HSV1 strain H129, widely used as an anterograde tracer, also efficiently infects upstream innervating neurons through axon terminal uptake and displays a clear retrograde labeling phenotype, indicating that there are two types of starter cell: locally infected neurons in the injection site and retrogradely infected neurons [10].

The comparison of the infection mechanism, efficiency, and neurotropism of different viral vectors provides valuable information for the selection of appropriate viral tools for individual research designs [3]. In neural circuit tracing, the qualitative and quantitative analyses of labeled images are also necessary for further analysis. Based on the results [8, 10], different neurotropic viruses have different labeling characteristics in the infected cerebral regions. Results from a single tool might be incomplete and inadequate, thus needing verification with multiple techniques. Thus, there is often no ideal viral tool available for tracing various neural circuits. The researcher must be aware of the advantages and disadvantages of the selected tools or methods to avoid inaccuracy or overgeneralization

of the results. At the same time, the results obtained using different tools and methods must be comprehensively compared and analyzed to avoid reaching overgeneralized conclusions.

**Acknowledgements** This work was supported by the Youth Innovation Promotion Association of the Chinese Academy of Sciences (Y6Y0021004). We thank Zengpeng Han and Huadong Wang at Wuhan Institute of Physics and Mathematics for suggestions and comments on the manuscript and creating the picture and table.

## References

1. Poo M, Xu B, Tan T. Brain science and brain-inspired intelligence technology—an overview. *Bull Chin Acad Sci* 2016, 31: 725–736.
2. Luo L, Callaway EM, Svoboda K. Genetic dissection of neural circuits. *Neuron* 2008, 57: 634–660.
3. Lanciego JL, Wouterlood FG. A half century of experimental neuroanatomical tracing. *J Chem Neuroanat* 2011, 42: 157–183.
4. Saleeba C, Dempsey B, Le S, Goodchild A, McMullan S. A student's guide to neural circuit tracing. *Front Neurosci* 2019, 13: 897.
5. Zheng N, Su P, Liu Y, Wang H, Nie B, Fang X, *et al.* Detection of neural connections with *ex vivo* MRI using a ferritin-encoding trans-synaptic virus. *Neuroimage* 2019, 197: 133–142.
6. Jia F, Zhu X, Lv P, Hu L, Liu Q, Jin S, *et al.* Rapid and sparse labeling of neurons based on the mutant virus-like particle of semliki forest virus. *Neurosci Bull* 2019, 35: 378–388.
7. Li J, Liu T, Dong Y, Kondoh K, Lu Z. Trans-synaptic neural circuit-tracing with neurotropic viruses. *Neurosci Bull* 2019, 35: 909–920.
8. Zhu X, Lin K, Liu Q, Yue X, Mi H, Huang X, *et al.* Rabies Virus pseudotyped with CVS-N2C glycoprotein as a powerful tool for retrograde neuronal network tracing. *Neurosci Bull* 2019, 10.1007/s12264-019-00423-3.
9. Reardon TR, Murray AJ, Turi GF, Wirblich C, Croce KR, Schnell MJ, *et al.* Rabies virus CVS-N2c( $\Delta$ G) strain enhances retrograde synaptic transfer and neuronal viability. *Neuron* 2016, 89: 711–724.
10. Su P, Wang H, Xia J, Zhong X, Hu L, Li Y, *et al.* Evaluation of retrograde labeling profiles of HSV1 H129 anterograde tracer. *J Chem Neuroanat* 2019, 100: 101662.



# Rabies Virus Pseudotyped with CVS-N2C Glycoprotein as a Powerful Tool for Retrograde Neuronal Network Tracing

Xutao Zhu<sup>1,2,6</sup> · Kunzhang Lin<sup>3</sup> · Qing Liu<sup>2</sup> · Xinpei Yue<sup>2</sup> · Huijie Mi<sup>4</sup> · Xiaoping Huang<sup>2</sup> · Xiaobin He<sup>2</sup> · Ruiqi Wu<sup>2</sup> · Danhao Zheng<sup>4</sup> · Dong Wei<sup>4</sup> · Liangliang Jia<sup>2</sup> · Weilin Wang<sup>4</sup> · Anne Manyande<sup>5</sup> · Jie Wang<sup>2</sup> · Zhijian Zhang<sup>2</sup> · Fuqiang Xu<sup>1,2,3</sup>

Received: 2 February 2019 / Accepted: 17 June 2019 / Published online: 23 August 2019  
© Shanghai Institutes for Biological Sciences, CAS 2019

**Abstract** Efficient viral vectors for mapping and manipulating long-projection neuronal circuits are crucial in structural and functional studies of the brain. The SAD strain rabies virus with the glycoprotein gene deleted pseudotyped with the N2C glycoprotein (SAD-RV( $\Delta$ G)-N2C(G)) shows strong neuro-tropism in cell culture, but its *in vivo* efficiency for retrograde gene transduction and neuro-tropism have not been systematically characterized. We compared these features in different mouse brain regions for SAD-RV-N2C(G) and two other widely-used retrograde tracers, SAD-RV( $\Delta$ G)-B19(G) and rAAV2-retro. We found that SAD-RV( $\Delta$ G)-N2C(G) enhanced the infection efficiency of long-projecting neurons by  $\sim 10$  times but with very similar neuro-tropism, compared with

SAD-RV( $\Delta$ G)-B19(G). On the other hand, SAD-RV( $\Delta$ G)-N2C(G) had an infection efficiency comparable with rAAV2-retro, but a more restricted diffusion range, and broader tropism to different types and regions of long-projecting neuronal populations. These results demonstrate that SAD-RV( $\Delta$ G)-N2C(G) can serve as an effective retrograde vector for studying neuronal circuits.

**Keywords** Viral vector · N2C glycoprotein · Neuronal circuits · Retrograde tracing

## Introduction

In the central nervous system, distinct brain regions work together through particular circuit connections to process different and complex information [1–7]. Neuronal circuits are the keystone to brain functions and their anatomical and

**Electronic supplementary material** The online version of this article (<https://doi.org/10.1007/s12264-019-00423-3>) contains supplementary material, which is available to authorized users.

✉ Zhijian Zhang  
zhzhj\_hust@126.com

✉ Fuqiang Xu  
fuqiang.xu@wipm.ac.cn

<sup>1</sup> Shenzhen Key Lab of Neuropsychiatric Modulation and Collaborative Innovation Center for Brain Science, Guangdong Provincial Key Laboratory of Brain Connectome and Behavior, CAS Center for Excellence in Brain Science and Intelligence Technology, Brain Cognition and Brain Disease Institute (BCBDI), Shenzhen Institutes of Advanced Technology, Chinese Academy of Sciences, Shenzhen-Hong Kong Institute of Brain Science-Shenzhen Fundamental Research Institutions, Shenzhen 518055, China

<sup>2</sup> State Key Laboratory of Magnetic Resonance and Atomic and Molecular Physics, Key Laboratory of Magnetic Resonance in Biological Systems, Wuhan Center for Magnetic Resonance, Wuhan Institute of Physics and Mathematics, Chinese Academy of Sciences, Wuhan 430071, China

<sup>3</sup> Wuhan National Laboratory for Optoelectronics, Huazhong University of Science and Technology, Wuhan 430071, China

<sup>4</sup> College of Life Sciences, Wuhan University, Wuhan 430071, China

<sup>5</sup> School of Human and Social Sciences, University of West London, London, UK

<sup>6</sup> University of the Chinese Academy of Sciences, Beijing 100049, China

functional aberrations are closely associated with many neurodegenerative diseases [8–11], such as Parkinson's disease [12, 13], Alzheimer's disease [14] and Huntington's disease [15]. Thus, it is critical to develop efficient tools for anatomical mapping and the functional decoding of neuronal circuit connections.

Retrograde tracers, owing to their unique properties of entry at axon terminals and then being transported to the cell bodies, are useful tools for targeting the long-projecting neuronal circuit assemblies [16, 17]. Compared with the classical chemical tracers [18–22], viral vectors are able to deliver genetic elements to neuronal populations with specific projection properties or molecular features, and hence are superior in morphological visualization, activity monitoring, and functional modulation in neuroscience studies. Nowadays, viral tools are drawing close attention from the field of neuroscience. The rabies virus (RABV) [23–26], herpes simplex virus (HSV) [27–31], canine adeno virus-2 (CAV-2) [32–34], retrograde adeno-associated virus (rAAV2-retro) [35], and RABV glycoprotein-enveloped lentivirus (LV) [36–38] are among the most commonly-used recent retrograde viral vectors. They seem to have rather different infection efficacies and tropisms, although this has not yet been thoroughly explored. RABV and HSV have broader tropism for different types of neurons [29, 39], and much higher cytotoxicity than CAV-2 and rAAV2-retro. CAV-2 and rAAV2-retro are valuable due to their low toxicity and outstanding retrograde gene transduction efficiency, but are limited by the gene delivery capacity and heterogeneous tropism in different neurons [40, 41]. LV also has high retrograde gene transduction efficiency, but may induce immune responses [42] or tumorigenesis [43]. By far, RABV is reported to ensure robust gene expression, possesses the most exclusive neuro-tropism and the broadest range of host species among the above viruses, but is limited by its cytotoxicity and retrograde gene transduction efficiency. Recent studies have successfully attenuated [44] and even eliminated [40] the cytotoxicity. Moreover, RABV enveloped with the N2C glycoprotein (N2C(G)) from the Challenge Virus Strain displays increased neuro-tropism in cell culture [45] and trans-synaptic efficiency *in vivo* [46]. These improvements endow the RABV-N2C(G) with great potential in both structural and functional studies of neuronal circuits. However, since the cellular environment and receptors involved may be different, the higher *in vitro* neuro-tropism and *in vivo* trans-synaptic spread efficiency do not mean higher retrograde infection efficiency. Thus, the *in vivo* retrograde gene transduction efficiency and tropisms of the RABV enveloped by N2C(G) to long-projecting neuronal circuits and comparison with the two outstanding retrograde tracers (SAD strain RABV and rAAV2-retro) are still unknown.

To address these questions, in this study, we first enveloped the glycoprotein gene-deleted SAD-RABV with N2C(G) (SAD-RV( $\Delta$ G)-N2C(G)) or the native glycoprotein (SAD-RV( $\Delta$ G)-B19(G)), and then compared the *in vivo* retrograde infection properties of the SAD-RV( $\Delta$ G)-N2C(G) with those of SAD-RV( $\Delta$ G)-B19(G) and rAAV2-retro.

## Methods

### Animals

All surgical and experimental procedures were conducted in accordance with the guidelines of the Animal Care and Use Committees (20170712015) at the Wuhan Institute of Physics and Mathematics, Chinese Academy of Sciences. Adult male C57BL/6 mice were purchased from Hunan SJA Laboratory Animal Company. Glutamate decarboxylase 67 (GAD67)-GFP transgenic mice [47] were gifts from Professor Shumin Duan (Zhejiang University), and bred with adult female C57BL/6 mice. All animals were fed *ad libitum* with food and water. A dedicated room with a 12/12 h light/dark cycle was used to house the animals.

### Virus Information

The viral vectors SAD-RV( $\Delta$ G)-B19(G)-EGFP, SAD-RV( $\Delta$ G)-N2C(G)-EGFP, SAD-RV( $\Delta$ G)-N2C(G)-mCherry, rAAV2-retro-EF1 $\alpha$ -EYFP, and rAAV2-retro-EF1 $\alpha$ -mCherry were all packaged by BrainVTA Co., Ltd. (Wuhan, China) and aliquots were stored at  $-80^{\circ}\text{C}$ .

### Production of BHK-N2C(G) Cells

For the baby hamster kidney (BHK)-N2C(G) cell lines, FUGW-H2B-GFP-P2A-N2C(G) was created by inserting the N2C-glycoprotein gene (Addgene, #73476) with histone GFP into the lentivirus expression vector FUGW (Addgene, #14883), then transfection into lentiviral packaging cells. After filtration, FUGW-H2B-GFP-P2A-N2C(G) was used to infect BHK cells.

### Packaging of the SAD-RV( $\Delta$ G)-N2C(G)-EGFP

The SAD-RV( $\Delta$ G)-B19(G)-EGFP was packaged using standard methods as described in previous reports [48]. BHK-N2C(G) cells were used to stably express N2C(G) for packaging SAD-RV( $\Delta$ G)-N2C(G)-EGFP. The SAD-RV( $\Delta$ G)-B19(G)-EGFP was used to infect BHK-N2C(G) cells for 48 h. Then, after collecting viral supernatant, the BHK-N2C(G) cells were washed with PBS, digested with pancreatin, and amplified. After 48 h,

the viral supernatant of SAD-RV( $\Delta$ G)-N2C(G)-EGFP was collected, filtered (0.45  $\mu$ m) and stored at  $-80^{\circ}\text{C}$ . The concentration procedure of SAD-RV( $\Delta$ G)-N2C(G)-EGFP was as previously reported [48].

SAD-RV( $\Delta$ G)-N2C(G)-mCherry was obtained using the same procedures as for SAD-RV( $\Delta$ G)-N2C(G)-EGFP. HEK 293T cells were used to assay the titer of all rabies viruses using limiting dilution analysis. Then the rabies viruses were stored at  $-80^{\circ}\text{C}$ . The rAAV2-retro-EF1 $\alpha$ -EYFP and rAAV2-retro-EF1 $\alpha$ -mCherry were titrated using QPCR.

### Stereotaxic Surgery

The animals were anesthetized with chloral hydrate (400 mg/kg), and placed in a stereotaxic apparatus (RWD, 68030, Shenzhen, China). The skull above the targeted areas was thinned with a dental drill (STRONG, Guangdong, China) and removed carefully with a curved needle. A mixture of virus and Alexa Fluor 594 conjugated-cholera toxin B subunit (CTB594, Thermo Fisher Scientific, C34777; final concentration, 0.02 mg/mL) was injected into the target brain regions (ventral tegmental area (VTA): A-P,  $-3.10$  mm; M-L,  $\pm 0.50$  mm, D-V,  $-4.50$  mm, 200 nL; or dentate gyrus (DG): A-P,  $-1.70$  mm; M-L,  $-0.90$  mm; D-V,  $-1.95$  mm, 100 nL) using an injector connected to a glass micropipette (WPI, 4878, Sarasota, FL), and driven by a syringe pump (Stoelting, Quintessential Stereotaxic Injector, 53311, Wood Dale, IL). After injection, the micropipette was left in place for 10 min to minimize diffusion and then slowly withdrawn.

Finally, after suturing and applying lidocaine hydrochloride to the wound, the animals were returned to the housing room.

### Slice Preparation and Confocal Imaging

Mice were anesthetized with an overdose of chloral hydrate (600 mg/kg), and perfused transcardially with phosphate-buffered saline (PBS) followed by 4% paraformaldehyde (PFA, Sigma, 158127MSDS, St. Louis, MO). The brain was removed and post-fixed overnight in 4% PFA at  $4^{\circ}\text{C}$ , then coronal sections were cut at 40  $\mu$ m on a cryostat microtome (Thermo Fisher, NX50, Waltham, MA).

Every sixth section was stained with 4',6-diamidino-2-phenylindole (DAPI), mounted in 70% glycerol, and imaged under a confocal microscope (Leica, TCS SP8, Buffalo Grove, IL) or a virtual microscopy slide-scanning system (Olympus, VS 120, Tokyo, Japan).

### Immunohistochemistry

The sections were washed with PBS (3 times, 5 min each), then incubated in blocking solution (10% normal goat serum and 0.3% Triton x-100 in PBS) for 1 h at  $37^{\circ}\text{C}$ , followed by the primary antibody rabbit anti-Ca<sup>2+</sup>/calmodulin-dependent protein kinase II (CaMKII, Abcam, ab5683, 1:500) and incubated for 72 h at  $4^{\circ}\text{C}$ . Sections were washed with PBS (3 times, 10 min each), incubated with the secondary antibody goat anti-rabbit cy3 (Jackson ImmunoResearch, 94600, 1:400) for 1 h at  $37^{\circ}\text{C}$ , then washed with PBS (3 times, 10 min each), stained with DAPI, and mounted with 70% glycerol.

### Data Analysis

#### Cell Counting

To count the labeled neurons in the whole brain using SAD-RV( $\Delta$ G)-B19(G), SAD-RV( $\Delta$ G)-N2C(G), or rAAV2-retro, images were segmented and delineated to different brain regions with Photoshop based on the Allen Brain Atlas (<http://www.brain-map.org/>). The labeled neurons were quantified with ImageJ (National Institutes of Health, Bethesda, MD), but those around the injection sites were not counted.

To count CaMKII and EYFP/GFP co-labeled cells,  $1024 \times 1024$  pixel ( $1183 \mu\text{m} \times 1183 \mu\text{m}$ ) images within the target regions were randomly selected, while to count GAD 67 or GAD 67-GFP co-labeled cells, the images were segmented and assigned to different brain regions with Photoshop based on the Allen Brain Atlas. The co-labeled neurons were quantified with ImageJ.

#### Analysis of Viral Diffusion Range

To analyze the diffusion ranges of rAAV2-retro and SAD-RV( $\Delta$ G)-N2C(G), we selected samples from around the VTA injection site containing a large enough ( $2235 \mu\text{m} \times 2235 \mu\text{m}$ ) area (referred to as cholera toxin B subunit signals). Since viral diffusion is concentric, the diffusion range was defined as an irregular circle centered on the CTB signals and containing concentric EYFP/GFP+ soma distributions. Only the EYFP/GFP+ signals within the circle were assessed. The circular range was equidistantly segmented into 57.5- $\mu\text{m}$  stripes centered on the CTB signals along the lateral-medial and dorsal-ventral axes using MatLab R (2014a). The EYFP/GFP+ signals within each square were counted and calculated separately.

## Statistical Analyses

To illustrate the input intensity from different brain regions, only those >1% were included in Fig. 3D and Fig. S2. For statistical analysis of the input intensity for the whole brain, all regions were included. For diffusion area analysis, the percentage of signal in each square was calculated, fitted to a Gaussian curve, and the  $W_{h/2}$  (peak width at half-height) was analyzed using MatLab R (2014a).

Informations on the sections included in each statistical analysis are listed below. About 36 sections from each mouse were included in Figs. 1D, 2B, 3D–E, and S2A–B; ~33 in Fig. 4E and F; 5 in Fig. 5B; 4 in Fig. 5H–K; 11 in Fig. S4C and D; and one slice closest to the injection site in Fig. 2C and D.

Independent sample *t*-tests, one-way ANOVA followed by the LSD multiple comparison test, a two-sided non-parametric test (Mann-Whitney U-test) and Spearman rank

correlation analysis were used to determine statistical differences using SPSS (22.0, International Business Machines Corporation, New York, NY). Statistical significance was set at  $***P < 0.001$ ,  $**P < 0.01$  and  $*P < 0.05$ . All values are presented as the mean  $\pm$  SEM. Graphs were drawn using Sigma Plot (version 10.0, Systat Software Inc, San Jose, CA).

## Results

### SAD-RV( $\Delta$ G)-N2C(G) Showed a Higher Retrograde Gene Transduction Efficiency but a Similar Labeled Pattern Compared with SAD-RV( $\Delta$ G)-B19(G)

First, we packaged SAD-RV( $\Delta$ G)-N2C(G)-EGFP and SAD-RV( $\Delta$ G)-B19(G)-EGFP (Fig. 1A). To compare their retrograde infection efficiencies *in vivo*, the two pseudotyped viruses were mixed with Alexa Fluor 594

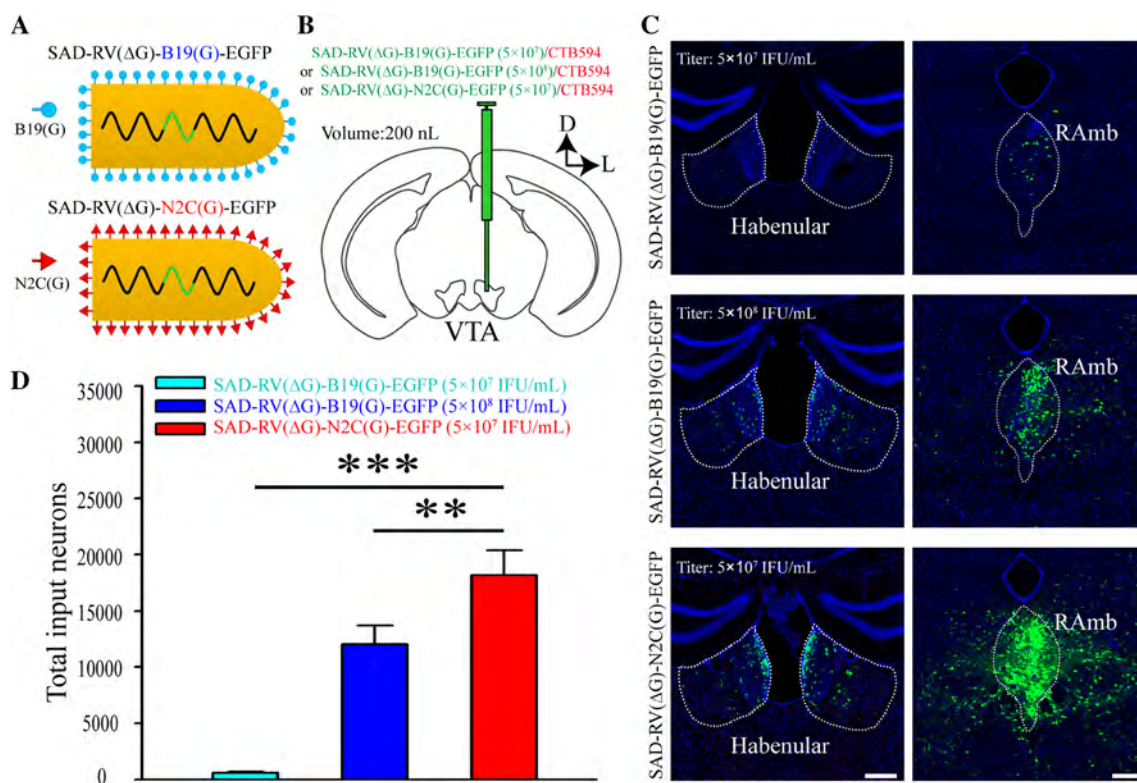


**Fig. 1** The retrograde gene transduction efficiency of SAD-RV( $\Delta$ G)-N2C(G)-EGFP is higher than that of SAD-RV( $\Delta$ G)-B19(G)-EGFP. **A** Schematics of the virion structures of SAD-RV( $\Delta$ G)-B19(G)-EGFP (upper panel) and SAD-RV( $\Delta$ G)-N2C(G)-EGFP (lower panel). **B** Schematic of the *in vivo* tracing study. A low dose of CTB594 was co-injected with either a low titer of SAD-RV( $\Delta$ G)-B19(G)-EGFP ( $5 \times 10^7$  infectious units (IFU)/mL), a high titer of SAD-RV( $\Delta$ G)-B19(G)-EGFP ( $5 \times 10^8$  IFU/mL), or SAD-RV( $\Delta$ G)-N2C(G)-EGFP ( $5 \times 10^7$  IFU/mL) into the VTA of C57 mice. **C** Many regions upstream of the VTA, such as the habenular nucleus

(left panels) and the midbrain raphe nuclei (RAmb, right panels), were retrogradely labeled by SAD-RV( $\Delta$ G)-N2C(G)-EGFP (lower panels) or SAD-RV( $\Delta$ G)-B19(G)-EGFP with different titers (upper and middle panels). **D** Numbers of neurons in the whole brain retrogradely infected by a low ( $5 \times 10^7$  IFU/mL) or a high ( $5 \times 10^8$  IFU/mL) titer of SAD-RV( $\Delta$ G)-B19(G)-EGFP, or SAD-RV( $\Delta$ G)-N2C(G)-EGFP ( $5 \times 10^7$  IFU/mL). Scale bars, 200  $\mu$ m;  $n = 4$  mice/group;  $*P < 0.05$ ,  $**P < 0.01$ ,  $***P < 0.001$ . n.s., no significant difference; one-way ANOVA followed by the LSD multiple comparison test. The nuclei were stained blue by DAPI.

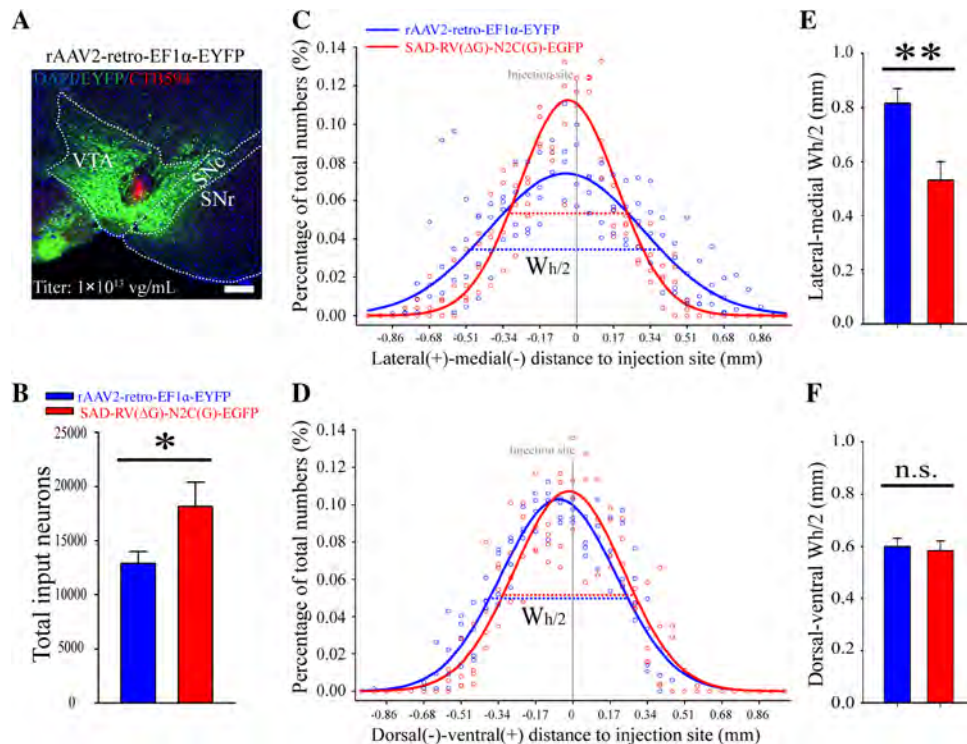


**Fig. 2** Retrograde gene transduction efficiency and diffusion range of SAD-RV( $\Delta$ G)-N2C(G) and rAAV2-retro. **A** Representative image of the injection site of rAAV2-retro-EF1 $\alpha$ -EYFP in the VTA. CTB594 was co-injected to delineate the injection site. SNc: Substantia nigra, compact part; SNr: Substantia nigra, reticular part; VTA: Ventral tegmental area. **B** Numbers of neurons in the whole brain retrogradely infected by SAD-RV( $\Delta$ G)-N2C(G)-EGFP ( $5 \times 10^7$  IFU/mL) and rAAV2-retro-EF1 $\alpha$ -EYFP ( $10^{13}$  IFU/mL). **C**, **D** The lateral-medial (**C**) and dorsal-ventral (**D**) diffusion patterns of rAAV2-retro-EF1 $\alpha$ -EYFP (blue dots and line) and SAD-RV( $\Delta$ G)-N2C(G)-EGFP (red

dots and line) around the injection sites. The signal percentages distributed along the lateral-medial and dorsal-ventral axes of all animals were fitted to Gaussian curves.  $W_{h/2}$ , peak width at half-height. **E**, **F** Statistical analysis of the lateral-medial (**E**) and dorsal-ventral (**F**) diffusion of rAAV2-retro-EF1 $\alpha$ -EYFP and SAD-RV( $\Delta$ G)-N2C(G)-EGFP. The  $W_{h/2}$  of each animal ( $n = 4$  mice/virus) was compared between the two viral groups. \* $P < 0.05$ , \*\* $P < 0.01$ , \*\*\* $P < 0.001$ . n.s., no significant difference,  $t$ -test. Scale bar, 200  $\mu$ m.

conjugated-cholera toxin B subunit (CTB594, red fluorescent signal to mark the injection sites), and injected into the VTA of different mice (Fig. 1B, Table 1). The sections were checked carefully to guarantee that the injection sites were restricted to the VTA (Fig. S1). Otherwise, the samples were excluded. In most of the GFP-labeled regions [midbrain raphe nuclei and the habenular nucleus (Fig. 1C)], SAD-RV( $\Delta$ G)-N2C(G)-EGFP clearly infected more neurons than SAD-RV( $\Delta$ G)-B19(G)-EGFP, even when the titer of the latter was ten times higher. The whole-brain GFP-positive neuron numbers were also consistent with this result (Fig. 1D,  $P = 5.72 \times 10^{-7}$  for viruses at the same titer,  $P = 0.0059$  for viruses with tenfold different titers).

The retrograde gene transduction efficiency of the SAD strain RABV was increased by pseudotyping with N2C(G), however, whether the retrograde tropism for neurons in different brain regions was also altered remained unclear. To answer this, GFP-positive neurons within each upstream region were counted and normalized by dividing

the total number of retrogradely-labeled neurons in each animal. We found that none of the analyzed regions showed significant differences in input percentage between the SAD-RV( $\Delta$ G)-N2C(G)-EGFP and SAD-RV( $\Delta$ G)-B19(G)-EGFP groups (Fig. S2A). The percentages of retrogradely-labeled neurons in different regions in the two groups were strongly correlated (Fig. S2B).

These results demonstrated that the RABV with the glycoprotein gene deleted and enveloped with N2C(G) has improved retrograde gene transduction efficiency without affecting the retrograde tropism bias.

### SAD-RV( $\Delta$ G)-N2C(G) Showed Higher Retrograde Gene Transduction Efficiency and More Restricted Diffusion Range than rAAV2-retro

rAAV2-retro is an outstanding retrograde viral vector mainly due to its high efficiency, and has been broadly used in various functional studies of neuronal circuits [35, 49]. In order to compare the retrograde efficiency of rAAV2-retro

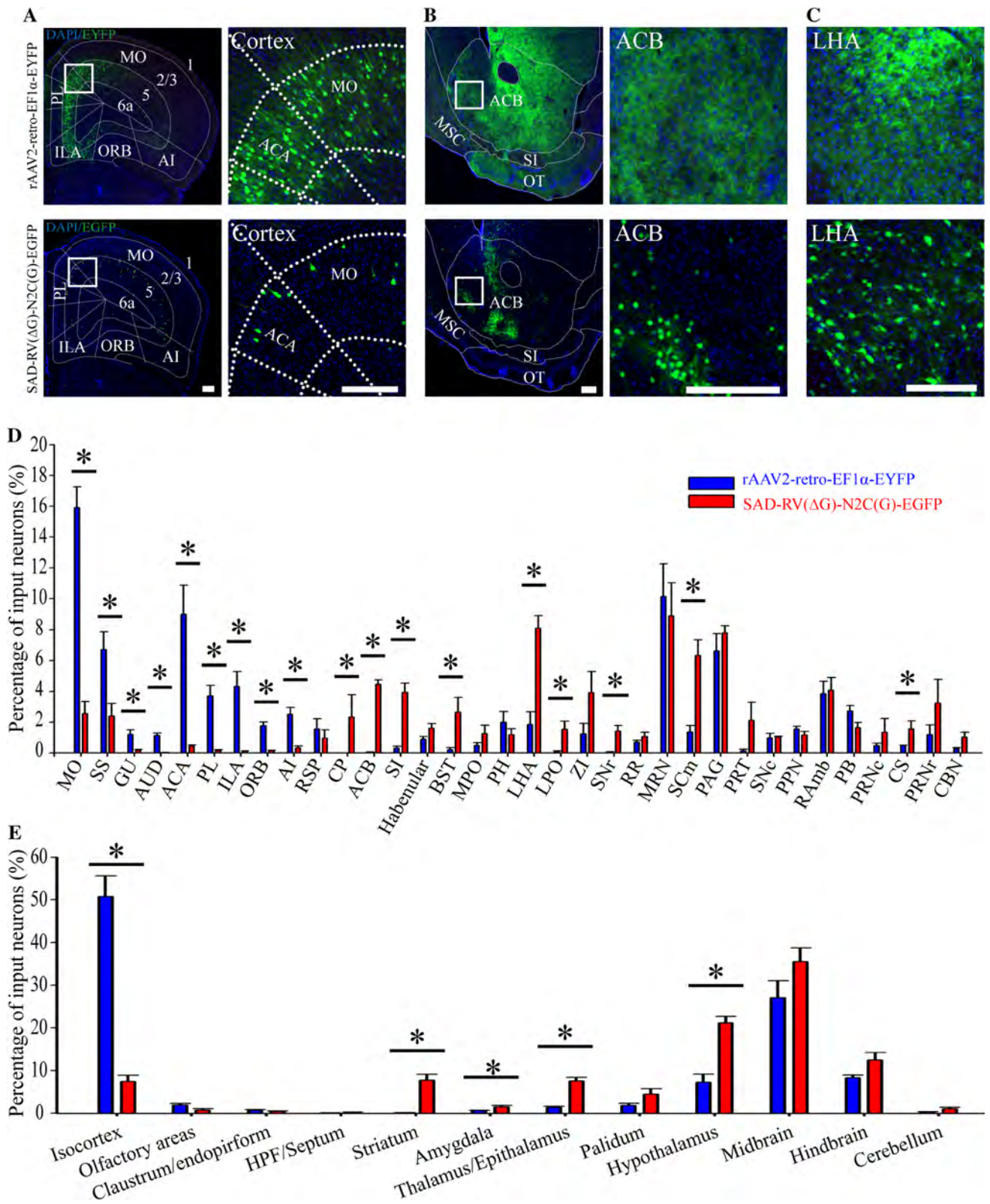


**Fig. 3** Retrograde infection tropism biases of SAD-RV( $\Delta$ G)-N2C(G) and rAAV2-retro injected into the VTA. **A–C** Representative images showing the different retrograde labeling patterns with rAAV2-retro-EF1 $\alpha$ -EYFP (upper panels) and SAD-RV( $\Delta$ G)-N2C(G)-EGFP (lower panels) in the cortex (**A**), striatum (**B**), and LHA (**C**). **D** Analysis of the input proportions of different nuclei labeled with SAD-RV( $\Delta$ G)-N2C(G)-EGFP and rAAV2-retro-EF1 $\alpha$ -EYFP. In most nuclei, the input proportions of the neurons labeled with the two viruses were dramatically different. **E** Input proportions of intact brain areas pooled from the discrete nuclei in **D**. Compared with SAD-RV( $\Delta$ G)-N2C(G)-EGFP, rAAV2-retro-EF1 $\alpha$ -EYFP preferentially infected the isocortex, but rarely infected the striatum, amygdala, pallidum, and hypothalamus.  $n = 4$  mice/group; \* $P < 0.05$ , \*\* $P < 0.01$ , \*\*\* $P < 0.001$ . Mann-Whitney U-test. Scale bars, 200  $\mu$ m. ACB: Nucleus accumbens; ACA: Anterior cingulate area; AI: Agranular insular area; AUD: Auditory areas; BST: Bed nuclei of the stria terminalis; CBN: Cerebellar nuclei; CP: Caudoputamen; CS: Superior central nucleus raphe; GU: Gustatory areas; Habenular: Habenular nucleus; HPF: hippocampal formation; ILA: Infralimbic area; LHA: Lateral hypothalamic area; LPO: Lateral preoptic area; MPO: Medial preoptic area; MO: Somatomotor areas; MRN: Midbrain reticular nucleus; MSC: Medial septal complex; ORB: Orbital area; OT: Olfactory tubercle; PAG: Periaqueductal gray; PB: Parabrachial nucleus; PL: Prelimbic area; PH: Posterior hypothalamic nucleus; PPN: Pedunculopontine nucleus; PRNc: Pontine reticular nucleus, caudal part; PRNr: Pontine reticular nucleus; PRT: Pretectal region; RAmb: Midbrain raphe nuclei; RR: Midbrain reticular nucleus, retrorubral area; RSP: Retrosplenial area; SCm: Superior colliculus, motor related; SI: Substantia innominate; SNC: Substantia nigra, compact part; SNr: Substantia nigra, reticular part; SS: Somatosensory areas; ZI: Zona incerta.

and SAD-RV( $\Delta$ G)-N2C(G), rAAV2-retro-EF1 $\alpha$ -EYFP was mixed with CTB594 and injected into the VTA (Fig. 2A, Table 1). We found that, compared to the rAAV2-retro-EF1 $\alpha$ -EYFP at a titer of  $10^{13}$  viral genomes (vg)/mL, SAD-RV( $\Delta$ G)-N2C(G)-EYFP at  $5 \times 10^7$  IFU/mL retrogradely infected more neurons ( $12,891 \pm 1,080$  for rAAV2-retro-EF1 $\alpha$ -EYFP,  $18,173 \pm 2,232$  for SAD-RV( $\Delta$ G)-N2C(G)-EGFP),  $P = 0.014$ ; Fig. 2B).

Given that the two viruses were titered using different methods based on their individual properties, and that the number of retrogradely-labeled neurons was positively correlated with the titer, it was difficult to directly compare their retrograde efficiency using different titer units. However, the increased titer could consequently increase the diffusion. Therefore, we further calculated the diffusion patterns of EYFP/GFP+ neuronal somata near the VTA. The rates of virus-labeled neurons were binned every 57.5  $\mu$ m along the lateral-medial and dorsal-ventral axes and fitted to Gaussian curves. The  $W_{h/2}$  was calculated to estimate the diffusion range of the two viruses. We found that, compared with the rAAV2-retro-EF1 $\alpha$ -EYFP ( $10^{13}$  vg/mL), the  $W_{h/2}$  of SAD-RV( $\Delta$ G)-N2C(G)-EGFP ( $5 \times 10^7$  IFU/mL) was much smaller along the lateral-medial axis (Fig. 2C, E), but showed no significant difference along the dorsal-ventral axis (Fig. 2D, F).

Together, these results suggest that SAD-RV( $\Delta$ G)-N2C(G)-EGFP has a much higher retrograde gene transduction efficiency and a more limited diffusion range than rAAV2-retro-EF1 $\alpha$ -EYFP.

### SAD-RV( $\Delta$ G)-N2C(G) and rAAV2-retro Exhibited Different Retrograde Infection Tropism in Different Brain Regions

Certain projection neurons have been reported to be refractory to rAAV2-retro infection [35, 40], so we then compared the retrograde infection tropisms of rAAV2-retro and SAD-RV( $\Delta$ G)-N2C(G).

To achieve this, we first analyzed the distribution patterns and proportions of EYFP/GFP+ neurons in different brain regions of rAAV2-retro-EF1 $\alpha$ -EYFP- and SAD-RV( $\Delta$ G)-N2C(G)-EGFP-injected samples. We found that, compared with the SAD-RV( $\Delta$ G)-N2C(G)-EGFP, rAAV2-retro-EF1 $\alpha$ -EYFP preferentially labeled neurons in the somatomotor, somatosensory, gustatory, auditor, anterior cingulate, prelimbic, infralimbic, orbital, and agranular insular areas (Fig. 3A, D). Whereas, in many of the other regions, such as the caudoputamen (CP), nucleus accumbens (ACB), substantia innominate, bed nuclei of the stria terminalis, lateral hypothalamic area (LHA), lateral preoptic area, substantia nigra, pars reticulata, motor-related superior colliculus, and superior central raphe nucleus, the rAAV2-retro-EF1 $\alpha$ -EYFP showed a modest infection efficiency (Fig. 3B–D). It should be noted that, in the CP and ACB, which are greatly enriched with GABAergic neurons and directly connected to the VTA [50–52], very few cell bodies were labeled by rAAV2-retro-EF1 $\alpha$ -EYFP. In the periaqueductal gray (PAG), midbrain reticular nucleus, midbrain raphe nuclei and a few other regions, there was no significant difference in the neuronal labeling rate between the two kinds of virus (Fig. 3D).

We further pooled the EYFP/GFP+ neuron signals of every individual brain region into several intact brain areas (Fig. 3E) according to the Allen Brain Atlas (<http://www.brain-map.org/>). The data showed that in the isocortex, the retrograde neuronal labeling rate of rAAV2-retro-EF1 $\alpha$ -EYFP was  $\sim 7$ -fold higher than that of SAD-RV( $\Delta$ G)-N2C(G)-EGFP. On the contrary, SAD-RV( $\Delta$ G)-N2C(G)-EGFP had a higher percentage of labeled neurons in many non-cortical areas, including the striatum, amygdala, pallidum, and hypothalamus. There was no significant difference in the neuronal labeling rate between the two viruses in the olfactory area, hippocampal formation/septum, claustrum/endopiriform, thalamus/epithalamus, midbrain, hindbrain, and cerebellum (Fig. 3E, Table 2).

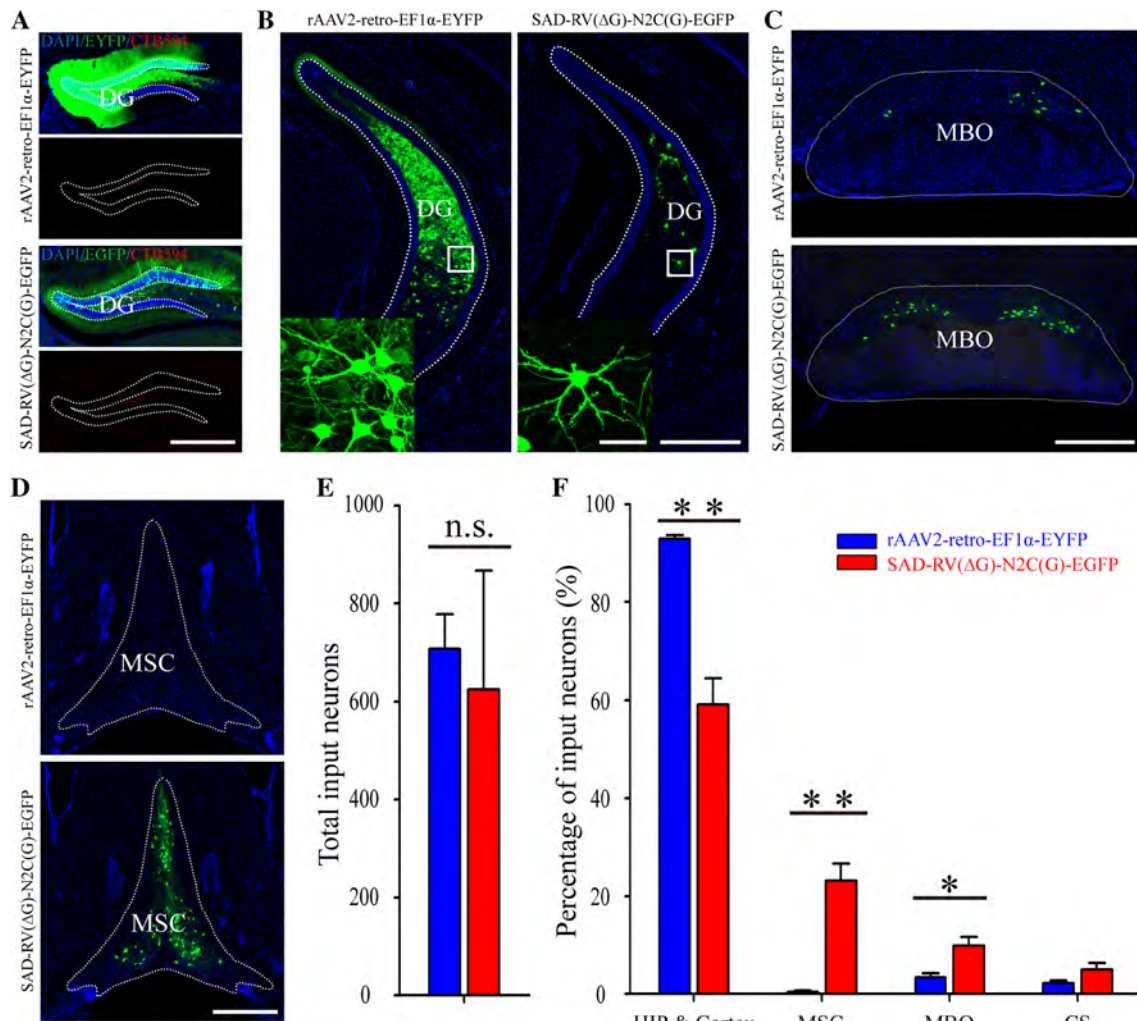


**Fig. 4** Different retrograde labeling patterns of SAD-RV( $\Delta$ G)-N2C(G)-EGFP and rAAV2-retro-EF1 $\alpha$ -EYFP injected into the hippocampus. **A** Coronal sections near the injection sites (indicated by the red signals of CTB594) in the DG by the two viruses (upper panels, rAAV2-retro-EF1 $\alpha$ -EYFP; lower panels, SAD-RV( $\Delta$ G)-N2C(G)-EGFP). **B–D**: Representative images reveal that the retrograde labeling patterns with SAD-RV( $\Delta$ G)-N2C(G)-EGFP and rAAV2-retro-EF1 $\alpha$ -EYFP are quite different in many regions, such as the hippocampus (**B**), MBO (**C**), and MSC (**D**). **E** Numbers of

neurons retrogradely infected with SAD-RV( $\Delta$ G)-N2C(G)-EGFP and rAAV2-retro-EF1 $\alpha$ -EYFP in the whole brain. **F** Proportions of input from different areas.  $n = 3$  mice for rAAV2-retro-EF1 $\alpha$ -EYFP;  $n = 4$  mice for SAD-RV( $\Delta$ G)-N2C(G)-EGFP. \* $P < 0.05$ , \*\* $P < 0.01$ , \*\*\* $P < 0.001$ ,  $t$ -test. Scale bars, 50  $\mu$ m for insets in **B**, 200  $\mu$ m for **A–D**. CS: Superior central nucleus raphe; DG: Dentate gyrus; HIP: Hippocampal region; MBO: Mammillary body; MSC: Medial septal complex.

To exclude the influence of individual variation and directly compare the retrograde infection tropisms, rAAV2-retro-EF1 $\alpha$ -EYFP and SAD-RV( $\Delta$ G)-N2C(G)-mCherry were injected separately into the bilateral VTA in the same animal (Fig. S3A and B; Table 1). The differences in the labeling patterns of the two viruses were still observed in these mice (Fig. S3C), consistent with the above results (Fig. 3A–D).

Since the retrograde gene transduction efficiency or tropism biases in different brain regions may differ with the injection site, the two viruses were additionally injected into the dentate gyrus (DG), another region that receives a

considerable amount of input from cortical areas (Fig. 4A, Table 1). The images near the injection site showed that the fluorescent signal of rAAV2-retro-EF1 $\alpha$ -EYFP was much denser and diffused more widely than SAD-RV( $\Delta$ G)-N2C(G)-EGFP (Fig. 4A). Quantitative analysis of the whole-brain GFP/EYFP+ neurons excluding the DG region revealed that SAD-RV( $\Delta$ G)-N2C(G)-EGFP at a titer of  $5 \times 10^7$  IFU/mL had a retrograde gene transduction efficiency comparable to rAAV2-retro-EF1 $\alpha$ -EYFP at  $10^{13}$  vg/mL (Fig. 4E,  $707 \pm 70$  for rAAV2-retro-EF1 $\alpha$ -EYFP;  $625 \pm 241$  for SAD-RV( $\Delta$ G)-N2C(G)-EGFP,  $P = 0.40$ ). We further analyzed the retrogradely-labeled

patterns of the two viruses. Since the hippocampus is a macroscopically defined cortical structure [53, 54], the hippocampus and the cortical areas were collectively referred to as an intact brain area, the hippocampal region (HIP) & Cortex. We found that rAAV2-retro-EF1 $\alpha$ -EYFP labeled a greater proportion of projection neurons in the HIP & Cortex (Fig. 4B and F, 92.91%  $\pm$  0.74% for rAAV2-retro-EF1 $\alpha$ -EYFP; 59.15%  $\pm$  5.28% for SAD-RV( $\Delta$ G)-N2C(G)-EGFP;  $P = 0.0015$ ) than SAD-RV( $\Delta$ G)-N2C(G)-EGFP. However, in the mammillary body (3.39%  $\pm$  0.89%, 9.75%  $\pm$  1.81%;  $P = 0.023$ ) (Fig. 4C and F) and medial septal complex (MSC, 0.39%  $\pm$  0.29%, 23.13%  $\pm$  3.54%;  $P = 0.0015$ ) (Fig. 4D and F), the neuronal labeling rate of rAAV2-retro-EF1 $\alpha$ -EYFP was  $\sim$ 3- and  $\sim$ 60-folds lower, respectively, despite substantial reports that the DG is densely connected to the MSC [55, 56].

The DG has also been reported to receive abundant contralateral hippocampal inputs [57, 58]. To investigate the retrograde infection tropism in more detail, we further compared the labeling patterns of the two viruses in the contralateral hippocampus. The proportion of EYFP/GFP+ neurons in each contralateral subregion was normalized to all contralateral hippocampal inputs. We found that the retrograde labeling patterns in the contralateral subregions were significantly different. The rAAV2-retro-EF1 $\alpha$ -EYFP-labeled neurons were highly enriched in the contralateral DG (99.35%  $\pm$  0.41% for rAAV2-retro-EF1 $\alpha$ -EYFP and 27.02%  $\pm$  6.81% for SAD-RV( $\Delta$ G)-N2C(G)-EGFP;  $P = 0.00014$ ), especially in the dorsal DG (Fig. S4A and C), but only sparsely distributed in CA3, CA2, and CA1. However, neurons labeled with SAD-RV( $\Delta$ G)-N2C(G)-EGFP were mainly found in the contralateral CA3 (0.33%  $\pm$  0.20% for rAAV2-retro-EF1 $\alpha$ -EYFP and 60.51%  $\pm$  5.83% for SAD-RV( $\Delta$ G)-N2C(G)-EGFP;  $P = 0.00016$ ), while also scattered throughout the DG, CA2, and CA1 (Fig. S4A and C). Since the contralateral DG neurons labeled with rAAV2-retro-EF1 $\alpha$ -EYFP were predominant in the posterior ventral rather than the anterior dorsal part, we then analyzed the rostral-caudal distribution of the contralateral hippocampal EYFP/GFP+ neurons. We found that the rAAV2-retro-EF1 $\alpha$ -EYFP mainly infected the caudal but not the rostral hippocampus. On the contrary, the SAD-RV( $\Delta$ G)-N2C(G)-EGFP mainly targeted neurons in the rostral hippocampus, which was close to the injection site, while also slightly labeled every part of the contralateral hippocampus along the rostral-caudal axis (Fig. S4B and D).

We also established that after the virus was injected into the VTA or the DG, neurons in several regions (ACB for the VTA and MSC, and contralateral CA1, CA2 and CA3 for the DG) were resistant to retrograde infection with

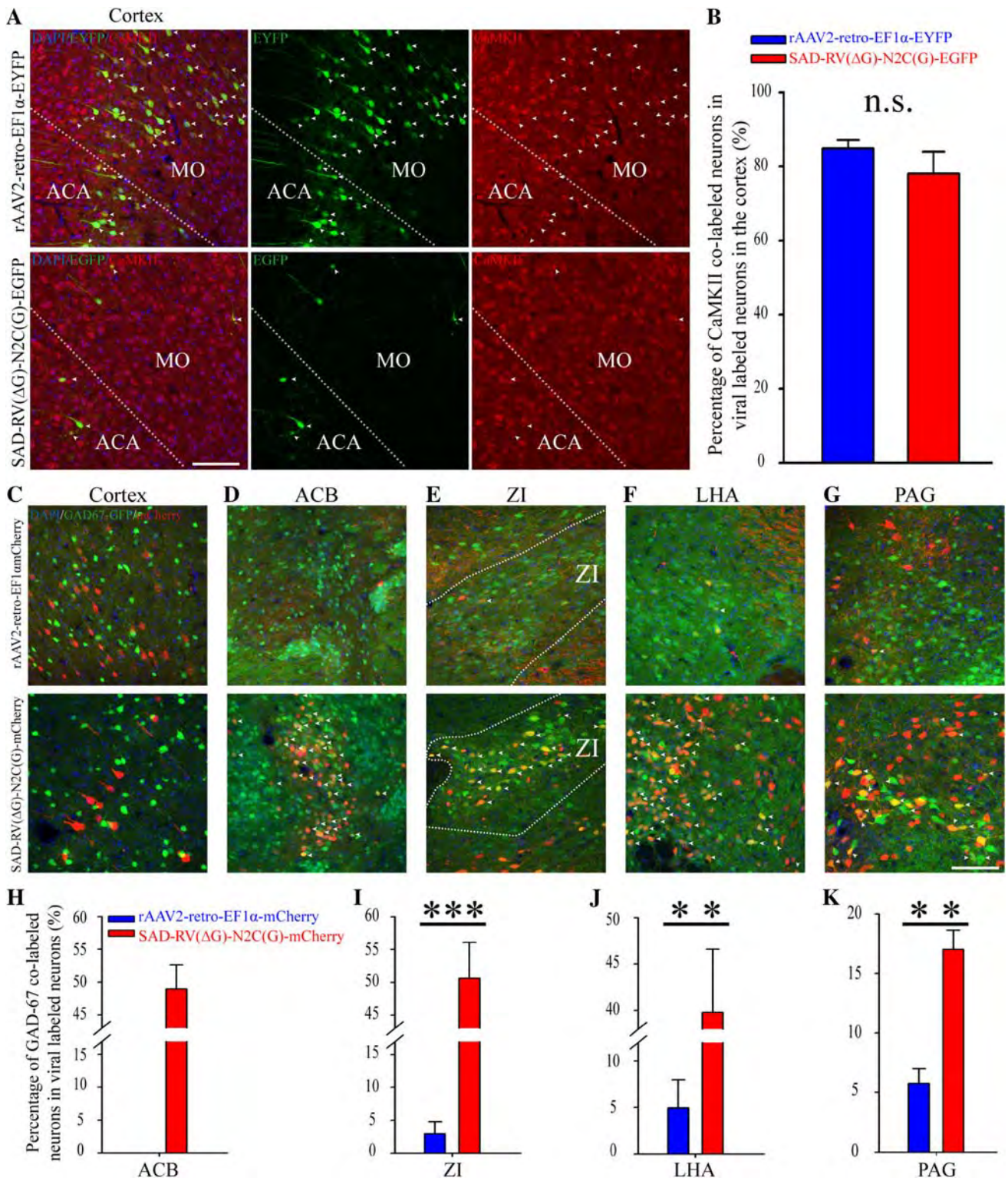
rAAV2-retro-EF1 $\alpha$ -EYFP, while the SAD-RV( $\Delta$ G)-N2C(G)-EGFP was able to infect all of these regions. These results suggest that the retrograde infection biases in rAAV2-retro-EF1 $\alpha$ -EYFP and SAD-RV( $\Delta$ G)-N2C(G)-EGFP are quite different. The rAAV2-retro-EF1 $\alpha$ -EYFP prefers to infect cortical more than subcortical neurons, while SAD-RV( $\Delta$ G)-N2C(G)-EGFP showed a less biased retrograde infection tropism for neurons in different regions.

### SAD-RV( $\Delta$ G)-N2C(G) and rAAV2-retro Exhibited Different Efficiencies in Retrogradely Labeling Long-Projection Inhibitory Neurons

rAAV2-retro-EF1 $\alpha$ -EYFP exhibited highly biased labeling patterns among different regions; that is, there was a strong preference for retrograde labeling in the long-projection cortical and hippocampal neurons, which mainly consist of excitatory subtypes [59–61], and a markedly lower tendency to label regions where GABAergic neurons are dominant. Therefore, we speculated as to whether the different retrograde infection patterns of rAAV2-retro-EF1 $\alpha$ -EYFP and SAD-RV( $\Delta$ G)-N2C(G)-EGFP were due to their tropisms toward different neuronal subtypes. To test this hypothesis, VTA-injected cortical samples were selected and immunohistochemically stained for Ca<sup>2+</sup>/calmodulin-dependent protein kinase II (CaMKII), a marker for excitatory neurons in the cortex [62, 63] (Fig. 5A). The results showed that the neurons retrogradely labeled by both rAAV2-retro-EF1 $\alpha$ -EYFP and SAD-RV( $\Delta$ G)-N2C(G)-EGFP were highly co-labeled with CaMKII, showing no significant difference, although the rAAV2-retro-EF1 $\alpha$ -EYFP group exhibited a slightly tendency to higher co-labeling (Fig. 5B). Thus, we further investigated the retrograde infection properties of the two viruses for long-projection inhibitory neurons.

To achieve this, rAAV2-retro-EF1 $\alpha$ -mCherry and SAD-RV( $\Delta$ G)-N2C(G)-mCherry were separately injected into the VTA of GAD67-GFP mice (Table 1). We found that neither of the viruses labeled inhibitory neurons in the cortex (Fig. 5C). In the ACB, which was refractory to infection, rAAV2-retro showed that about half of the SAD-RV( $\Delta$ G)-N2C(G)-mCherry-labeled neurons were inhibitory (Fig. 5D and H). In the zona incerta, LHA, and PAG, SAD-RV( $\Delta$ G)-N2C(G)-mCherry labeled a significantly higher proportion of GAD67-GFP neurons than rAAV2-retro-EF1 $\alpha$ -EYFP (Fig. 5E–G, and I–K).

These results indicate that rAAV2-retro is less efficient in retrogradely infecting long-projection inhibitory neurons than SAD-RV( $\Delta$ G)-N2C(G), which may contribute to the different retrograde infection patterns of the two viruses.



◀ **Fig. 5** rAAV2-retro and SAD-RV( $\Delta$ G)-N2C(G) exhibited different efficiencies in retrograde labeling of long-projection inhibitory neurons. **A** Representative cortical images displaying the co-localization (merged, left) of virus-labeled neurons (green, middle), and immunofluorescent CaMKII staining (red, right). **B** The CaMKII-positive rates of EYFP/GFP+ labeled neurons with SAD-RV( $\Delta$ G)-N2C(G)-EGFP and rAAV2-retro-EF1 $\alpha$ -EYFP in cortical regions. n.s., no significant difference, Mann-Whitney U-test. **C–G** Representative images showing the co-localization of GAD67-GFP (green, GAD67-GFP mice) and neurons labeled with rAAV2-retro-EF1 $\alpha$ -mCherry (red, upper panels) and SAD-RV( $\Delta$ G)-N2C(G)-mCherry (red, lower panels) in cortex (**C**), ACB (**D**), ZI (**E**), LHA (**F**), and PAG (**G**). **H–K** Analysis of co-labeling rates of GAD67-GFP with virus-labeled (red) neurons. SAD-RV( $\Delta$ G)-N2C(G)-mCherry labeled more GAD67-GFP-positive neurons than rAAV2-retro-EF1 $\alpha$ -mCherry in the ACB (**H**), ZI (**I**), LHA (**J**), and PAG (**K**).  $n = 3$  mice for rAAV2-retro-EF1 $\alpha$ -mCherry;  $n = 4$  mice for SAD-RV( $\Delta$ G)-N2C(G)-mCherry. \* $P < 0.05$ , \*\* $P < 0.01$ , \*\*\* $P < 0.001$ ,  $t$ -test; scale bars, 200  $\mu$ m. ACA: Anterior cingulate area; ACB: Nucleus accumbens; MO: Somatomotor areas; LHA: Lateral hypothalamic area; ZI: Zona incerta; PAG: Periaqueductal gray.

## Discussion

RABV has been widely used to target long-projecting neuronal networks by either the trans-monosynaptic spread or direct retrograde infection at the terminals. When used as a retrograde tracer, RABV is largely limited by its low efficiency. Here, we found that the N2C glycoprotein derived from the RABV CVS strain was able to increase the *in vivo* retrograde gene transduction efficiency of the SAD strain more than tenfold. Furthermore, the pseudotyped virus SAD-RV( $\Delta$ G)-N2C(G) showed a comparable retrograde efficiency, but a more localized diffusion range and a broader tropism to different types and regions of long-projecting neuronal populations than rAAV2-retro.

## SAD-RV( $\Delta$ G)-N2C(G) is Highly Efficient for Retrograde Tracing

It has been reported that CVS-RV( $\Delta$ G)-N2C(G) possesses higher neuronal invasiveness [64] and greater retrograde trans-synaptic spread [46] than the vaccine strain SAD-RV( $\Delta$ G)-B19(G). When pseudotyped with N2C(G), SAD-RV( $\Delta$ G)-N2C(G) also exhibits greater neuro-tropism in cell culture than SAD-RV( $\Delta$ G)-B19(G) [45]. However, a recent study [65] found that complementing SAD-RV( $\Delta$ G) with N2C(G) showed less or similar retrograde trans-synaptic efficiency than with B19(G). Besides, the mechanisms of retrograde trans-synaptic spread and retrograde infection at axon terminals could be different. Thus, comparison of the retrograde gene transduction efficiency between SAD-RV( $\Delta$ G)-B19(G) and SAD-RV( $\Delta$ G)-N2C(G) still remained obscure. We addressed this conundrum in the present work and found that, after injecting virus into the VTA, the *in vivo* retrograde gene transduction efficiency of SAD-RV( $\Delta$ G)-N2C(G) was much higher than that of SAD-RV( $\Delta$ G)-B19(G) (Fig. 1D). Our results are consistent with findings reported in earlier studies. Other than the enhanced neuronal invasiveness, the retrograde labeling patterns in SAD-RV( $\Delta$ G)-N2C(G) and SAD-RV( $\Delta$ G)-B19(G) were not significantly different (Fig. S2). A possible explanation for the similar labeling patterns is that N2C(G) might infect long-projecting neurons *via* the same receptors but with a much higher affinity than B19(G).

rAAV2-retro is also an outstanding viral tool to efficiently target long-projecting neurons. In this study, we found that the retrograde gene transduction efficiency of SAD-RV( $\Delta$ G)-N2C(G) was no less than that of rAAV2-retro (Fig. 2B and 4E), but had a more restricted diffusion

**Table 1** Experimental parameters for retrograde tracing.

Animal	Number	Nucleus	Virus	Dose (IFU/mL or viral genomes/mL)	Volume ( $\mu$ L)	Injection (Day)	Perfusion (Day)
C57BL/6	4	VTA	SAD-RV( $\Delta$ G)-B19(G)-EGFP	$5 \times 10^7$	0.2	Day1	Day7
C57BL/6	4	VTA	SAD-RV( $\Delta$ G)-B19(G)-EGFP	$5 \times 10^8$	0.2	Day1	Day7
C57BL/6	4	VTA	SAD-RV( $\Delta$ G)-N2C(G)-EGFP	$5 \times 10^7$	0.2	Day1	Day7
C57BL/6	4	VTA	rAAV2-retro-Ef1 $\alpha$ -EYFP	$1 \times 10^{13}$	0.2	Day1	Day21
C57BL/6	4	VTA(Right)	rAAV2-retro-Ef1 $\alpha$ -EYFP	$1 \times 10^{13}$	0.2	Day1	Day21
		VTA(Left)	SAD-RV( $\Delta$ G)-N2C(G)-mCherry	$1.1 \times 10^8$	0.2	Day14	
C57BL/6	4	DG	SAD-RV( $\Delta$ G)-N2C(G)-EGFP	$5 \times 10^7$	0.1	Day1	Day7
C57BL/6	3	DG	rAAV2-retro-Ef1 $\alpha$ -EYFP	$1 \times 10^{13}$	0.1	Day1	Day21
GAD67-GFP	4	VTA	SAD-RV( $\Delta$ G)-N2C(G)-mCherry	$1.1 \times 10^8$	0.2	Day1	Day7
GAD67-GFP	3	VTA	rAAV2-retro-Ef1 $\alpha$ -mCherry	$1.68 \times 10^{13}$	0.2	Day1	Day21

**Table 2** Retrograde neuronal labeling rate in brain regions.

Brain regions	Values (Mean $\pm$ SEM)		<i>P</i>
	rAAV2-retro-EF1 $\alpha$ -EYFP	SAD-RV( $\Delta$ G)-N2C(G)-EGFP	
Isocortex	50.72% $\pm$ 4.85%	7.42% $\pm$ 1.47%	0.029
Striatum	0.08% $\pm$ 0.05%	7.76% $\pm$ 1.37%	0.029
Amygdala	0.62% $\pm$ 0.05%	1.44% $\pm$ 0.38%	0.029
Pallidum	1.30% $\pm$ 0.27%	7.57% $\pm$ 0.86%	0.029
Hypothalamus	7.27% $\pm$ 1.87%	21.14% $\pm$ 1.56%	0.029
Olfactory area	1.90% $\pm$ 0.33%	0.69% $\pm$ 0.38%	0.057
Hippocampal formation (HPF)/septum	0.64% $\pm$ 0.19%	0.37% $\pm$ 0.16%	0.34
Clastrum/endopiriform	0.04% $\pm$ 0.05%	0.20% $\pm$ 0.07%	0.11
Thalamus/epithalamus	1.81% $\pm$ 0.48%	4.44% $\pm$ 1.25%	0.11
Midbrain	27.00% $\pm$ 4.07%	35.50% $\pm$ 3.26%	0.20
Hindbrain	8.34% $\pm$ 0.59%	12.43% $\pm$ 1.79%	0.057
Cerebellum	0.28% $\pm$ 0.08%	1.03% $\pm$ 0.34%	0.057

range (Fig 2C, E and 4A). This may be due to the different virion sizes [6, 26, 66, 67]. Although the number of retrogradely-labeled neurons further increased with the titer of rAAV2-retro, this could lead to a larger range of viral diffusion, which subsequently raises the risk of non-specific infection of neurons upstream from the regions adjacent to the injection site. With retrograde efficiency comparable to rAAV2-retro, the more localized diffusion range of SAD-RV( $\Delta$ G)-N2C(G) could make it more suitable to target the neuronal inputs to small nuclei.

The recently-developed receptor complementation strategy for CAV-2 has also extensively improved its retrograde transport efficiency and overcome the limitation of biased tropism [34]. However, this strategy needs an additional viral injection prior to the CAV-2-Cre, which complicates animal surgery, and makes it hard to access difficult-to-inject areas or target a large volume or even whole-brain upstream tissues. SAD-RV( $\Delta$ G)-N2C(G), with its intrinsic high efficiency and broad tropism, should be able to overcome these limitations. However, further studies analyzing the efficiency of CAV-2 and SAD-RV( $\Delta$ G)-N2C(G) in different neuronal circuits will also be valuable in guiding the applications of these viral tools.

### The Retrograde Neuronal Tropism Biases of rAAV2-retro and SAD-RV( $\Delta$ G)-N2C(G) are Different

In the present study, we showed that AAV2-retro and SAD-RV( $\Delta$ G)-N2C(G), when injected either into the VTA or DG, displayed different retrograde labeling patterns. Some regions, especially the striatum and basal forebrain, were largely resistant to retrograde infection by rAAV2-

retro, but susceptible to SAD-RV( $\Delta$ G)-N2C(G) (Fig. 3B and 4D), showing that SAD-RV( $\Delta$ G)-N2C(G) has a broader retrograde tropism for long-projecting neurons.

Our experimental data on the selectivity of SAD-RV( $\Delta$ G)-N2C(G) and rAAV2-retro for the two most dominant neuron types, CaMKII+ and GAD67+, showed that few neurons labeled with rAAV2-retro were long-projecting GABAergic, while a significant percentage of the SAD-RV( $\Delta$ G)-N2C(G)-labeled neurons (from 17 to 50 in subcortical regions) were long-projecting GABAergic neurons (Fig. 5D–K). However, it should be noted that most of the long-projecting neurons in the cortex are excitatory [59, 60, 68] (Fig. 5A, B). Therefore, the distinct retrograde infection preference of the two viruses over excitatory and inhibitory long-projection neurons generated different input patterns for a given region. The VTA receives extensive subcortical neuronal innervation [69, 70], while the major inputs to the DG are from cortical and hippocampal subregions [57, 58]. In the present study, we found that rAAV2-retro with the EF1 $\alpha$  promoter was much more efficient in labeling long-projecting cortical and hippocampal excitatory neurons. This is partially consistent with previous reports that compared the properties of SAD-RV( $\Delta$ G)-B19(G) and rAAV2-retro with the CMV promoter [44]. However, we still cannot exclude the possibility that the observed differences in retrograde tropism between RABV (viral endogenous promoter) and rAAV2-retro (EF1 $\alpha$  promoter) could be affected by the different promoters used here.

Indeed, the input patterns of the VTA and the DG revealed by the two viruses are rather different (Fig. 3D, E, 4F, S4C, D). The significantly different neuronal tropisms shown by these results suggest that when tracing

data are interpreted, the viral tools should be considered carefully. In fact, RABV may also exhibit tropism biases in some cases [71]. Thus, the best selection of viral tools depends on the specific circuit being studied, and the combined use of multiple viral tracers should get us closer to the actual facts.

Although we demonstrated that SAD-RV( $\Delta$ G)-N2C(G) has high efficiency and broad tropism for retrograde labeling of neuronal circuits, further work is still required to overcome the viral cytotoxicity for achieving long-term functional studies or transgenic expression. Fortunately, recently-developed strategies which delete certain genes [40] or introduce a self-inactivating vector [44] of SAD-RV( $\Delta$ G) have successfully overcome this limitation. One might argue that CVS-RV( $\Delta$ G)-N2C(G) is less toxic than SAD-RV( $\Delta$ G)-N2C(G) and hence is superior. However, since the virus production is much easier for SAD-RV( $\Delta$ G) than for CVS-RV( $\Delta$ G), and the most potent designs [40, 44] to reduce the toxicity of RABV to date are based on the SAD-RV( $\Delta$ G) vector, our introduction of SAD-RV( $\Delta$ G)-N2C(G) and our ongoing research to integrate these systems could provide more easily accessible and promising retrograde tools for the community.

In summary, we have provided experimental evidence for a powerful viral tool, N2C(G)-enveloped SAD-RV( $\Delta$ G)-N2C(G), which has high retrograde gene transduction efficiency and broad neuro-tropism to target the inputs to neuronal circuits. The comparison of the infection efficiency and neuro-tropism of SAD-RV( $\Delta$ G)-N2C(G) and rAAV2-retro provides valuable information for the selection of these viruses for individual research designs.

**Acknowledgements** We thank Yue Liu and Aolin Cai from Wuhan Institute of Physics and Mathematics for help with data analysis; Yanqiu Li, Yuanli Liao, and Pingping An from Wuhan Institute of Physics and Mathematics for maintaining and genotyping the GAD 67-GFP mice, and Lingling Xu from Wuhan Institute of Physics and Mathematics for capturing confocal images. This work was supported by the National Basic Research Program (973 Program) of China (2015CB755601), the Strategic Priority Research Program of the Chinese Academy of Sciences (XDB32030200), the National Natural Science Foundation of China (31771156, 81661148053, 91632303, 31800885, 31500868, 31671120 and 91732304), and the China Postdoctoral Science Foundation (2019M653118 and 2018M632946).

**Conflict of interest** The authors declare that they have no competing interests.

## References

1. Abeles M. *Corticonics: Neural Circuits of the Cerebral Cortex*. Cambridge University Press, 1991.
2. Tomioka R, Okamoto K, Furuta T, Fujiyama F, Iwasato T, Yanagawa Y, *et al.* Demonstration of long-range GABAergic connections distributed throughout the mouse neocortex. *Eur J Neurosci* 2005, 21: 1587–1600.
3. Gayoso J, Castro A, Anadon R, Manso MJ. Crypt cells of the zebrafish *Danio rerio* mainly project to the dorsomedial glomerular field of the olfactory bulb. *Chem Senses* 2012, 37: 357–369.
4. Huang ZJ. Toward a genetic dissection of cortical circuits in the mouse. *Neuron* 2014, 83: 1284–1302.
5. Miller MW, Vogt BA. Direct connections of rat visual cortex with sensory, motor, and association cortices. *J Comp Neurol* 1984, 226: 184–202.
6. Osakada F, Callaway EM. Design and generation of recombinant rabies virus vectors. *Nat Protoc* 2013, 8: 1583–1601.
7. Su YT, Gu MY, Chu X, Feng X, Yu YQ. Whole-brain mapping of direct inputs to and axonal projections from GABAergic neurons in the parafacial zone. *Neurosci Bull* 2018, 34: 485–496.
8. Roselli F, Caroni P. A circuit mechanism for neurodegeneration. *Cell* 2012, 151: 250–252.
9. Rubinov M, Bullmore E. Fledgling pathoconnectomics of psychiatric disorders. *Trends Cogn Sci* 2013, 17: 641–647.
10. Zhai S, Tanimura A, Graves SM, Shen W, Surmeier DJ. Striatal synapses, circuits, and Parkinson's disease. *Curr Opin Neurobiol* 2017, 48: 9–16.
11. Fullard ME, Morley JF, Duda JE. Olfactory dysfunction as an early biomarker in Parkinson's disease. *Neurosci Bull* 2017, 33: 515–525.
12. Gratwicke J, Jahanshahi M, Foltynie T. Parkinson's disease dementia: a neural networks perspective. *Brain* 2015, 138: 1454–1476.
13. Taverna S, Ilijic E, Surmeier DJ. Recurrent collateral connections of striatal medium spiny neurons are disrupted in models of Parkinson's disease. *J Neurosci* 2008, 28: 5504–5512.
14. Verret L, Mann EO, Hang GB, Barth AM, Cobos I, Ho K, *et al.* Inhibitory interneuron deficit links altered network activity and cognitive dysfunction in Alzheimer model. *Cell* 2012, 149: 708–721.
15. Milnerwood AJ, Raymond LA. Early synaptic pathophysiology in neurodegeneration: insights from Huntington's disease. *Trends Neurosci* 2010, 33: 513–523.
16. Vercelli A, Repici M, Garbossa D, Grimaldi A. Recent techniques for tracing pathways in the central nervous system of developing and adult mammals. *Brain Res Bull* 2000, 51: 11–28.
17. Katz LC. Local circuitry of identified projection neurons in cat visual cortex brain slices. *J Neurosci* 1987, 7: 1223–1249.
18. Stoeckel K, Schwab M, Thoenen H. Role of gangliosides in the uptake and retrograde axonal transport of cholera and tetanus toxin as compared to nerve growth factor and wheat germ agglutinin. *Brain Res* 1977, 132: 273–285.
19. Conte WL, Kamishina H, Reep RL. Multiple neuroanatomical tract-tracing using fluorescent Alexa Fluor conjugates of cholera toxin subunit B in rats. *Nat Protoc* 2009, 4: 1157–1166.
20. Katz L, Burkhalter A, Dreyer W. Fluorescent latex microspheres as a retrograde neuronal marker for *in vivo* and *in vitro* studies of visual cortex. *Nature* 1984, 310: 498.
21. Ni RJ, Luo PH, Shu YM, Chen JT, Zhou JN. Whole-brain mapping of afferent projections to the bed nucleus of the stria terminalis in tree shrews. *Neuroscience* 2016, 333: 162–180.
22. Gabriele ML, Smoot JE, Jiang H, Stein BE, McHaffie JG. Early establishment of adult-like nigroreticular architecture in the neonatal cat: a double-labeling study using carbocyanine dyes. *Neuroscience* 2006, 137: 1309–1319.
23. Ugolini G. Rabies virus as a transneuronal tracer of neuronal connections. *Adv Virus Res* 2011, 79: 165–202.
24. Callaway EM, Luo L. Monosynaptic circuit tracing with glycoprotein-deleted rabies viruses. *J Neurosci* 2015, 35: 8979–8985.
25. Wickersham IR, Finke S, Conzelmann KK, Callaway EM. Retrograde neuronal tracing with a deletion-mutant rabies virus. *Nat Methods* 2007, 4: 47–49.

26. Kelly RM, Strick PL. Rabies as a transneuronal tracer of circuits in the central nervous system. *J Neurosci Methods* 2000, 103: 63–71.
27. Ugolini G, Kuypers H, Simmons A. Retrograde transneuronal transfer of herpes simplex virus type 1 (HSV 1) from motoneurons. *Brain Res* 1987, 422: 242–256.
28. Xu C, Krabbe S, Grundemann J, Botta P, Fadok JP, Osakada F, *et al.* Distinct hippocampal pathways mediate dissociable roles of context in memory retrieval. *Cell* 2016, 167: 961–972 e916.
29. Cuchet D, Potel C, Thomas J, Epstein AL. HSV-1 amplicon vectors: a promising and versatile tool for gene delivery. *Expert Opin Biol Ther* 2007, 7: 975–995.
30. Lilley CE, Groutsi F, Han Z, Palmer JA, Anderson PN, Latchman DS, *et al.* Multiple immediate-early gene-deficient herpes simplex virus vectors allowing efficient gene delivery to neurons in culture and widespread gene delivery to the central nervous system *in vivo*. *J Virol* 2001, 75: 4343–4356.
31. Frampton AR, Jr., Goins WF, Nakano K, Burton EA, Glorioso JC. HSV trafficking and development of gene therapy vectors with applications in the nervous system. *Gene Ther* 2005, 12: 891–901.
32. Soudais C, Laplace-Builhe C, Kissa K, Kremer EJ. Preferential transduction of neurons by canine adenovirus vectors and their efficient retrograde transport *in vivo*. *FASEB J* 2001, 15: 2283–2285.
33. Junyent F, Kremer EJ. CAV-2—why a canine virus is a neurobiologist’s best friend. *Curr Opin Pharmacol* 2015, 24: 86–93.
34. Li SJ, Vaughan A, Sturgill JF, Kepecs A. A viral receptor complementation strategy to overcome CAV-2 tropism for efficient retrograde targeting of neurons. *Neuron* 2018, 98: 905–917 e905.
35. Tervo DG, Hwang BY, Viswanathan S, Gaj T, Lavzin M, Ritola KD, *et al.* A designer AAV variant permits efficient retrograde access to projection neurons. *Neuron* 2016, 92: 372–382.
36. Cronin J, Zhang XY, Reiser J. Altering the tropism of lentiviral vectors through pseudotyping. *Curr Gene Ther* 2005, 5: 387–398.
37. Kato S, Kobayashi K, Inoue K, Kuramochi M, Okada T, Yaginuma H, *et al.* A lentiviral strategy for highly efficient retrograde gene transfer by pseudotyping with fusion envelope glycoprotein. *Hum Gene Ther* 2011, 22: 197–206.
38. Hirano M, Kato S, Kobayashi K, Okada T, Yaginuma H, Kobayashi K. Highly efficient retrograde gene transfer into motor neurons by a lentiviral vector pseudotyped with fusion glycoprotein. *PLoS One* 2013, 8: e75896.
39. Coulon P, Derbin C, Kucera P, Lafay F, Prehaud C, Flamand A. Invasion of the peripheral nervous systems of adult mice by the CVS strain of rabies virus and its avirulent derivative AvO1. *J Virol* 1989, 63: 3550–3554.
40. Chatterjee S, Sullivan HA, MacLennan BJ, Xu R, Hou Y, Lavin TK, *et al.* Nontoxic, double-deletion-mutant rabies viral vectors for retrograde targeting of projection neurons. *Nat Neurosci* 2018, 21: 638–646.
41. Senn V, Wolff SB, Herry C, Grenier F, Ehrlich I, Grundemann J, *et al.* Long-range connectivity defines behavioral specificity of amygdala neurons. *Neuron* 2014, 81: 428–437.
42. Follenzi A, Santambrogio L, Annoni A. Immune responses to lentiviral vectors. *Curr Gene Ther* 2007, 7: 306–315.
43. Themis M, Waddington SN, Schmidt M, Von Kalle C, Wang Y, Al-Allaf F, *et al.* Oncogenesis following delivery of a nonprimate lentiviral gene therapy vector to fetal and neonatal mice. *Mol Ther* 2005, 12: 763–771.
44. Ciabatti E, Gonzalez-Rueda A, Mariotti L, Morgese F, Tripodi M. Life-long genetic and functional access to neural circuits using self-inactivating rabies virus. *Cell* 2017, 170: 382–392 e314.
45. Hagendorf N, Conzelmann KK. Pseudotyping of G-gene-deficient rabies virus. *Cold Spring Harb Protoc* 2015, 2015: pdb prot089417.
46. Reardon TR, Murray AJ, Turi GF, Wirblich C, Croce KR, Schnell MJ, *et al.* Rabies virus CVS-N2c(DeltaG) strain enhances retrograde synaptic transfer and neuronal viability. *Neuron* 2016, 89: 711–724.
47. Tamamaki N, Yanagawa Y, Tomioka R, Miyazaki J, Obata K, Kaneko T. Green fluorescent protein expression and colocalization with calretinin, parvalbumin, and somatostatin in the GAD67-GFP knock-in mouse. *J Comp Neurol* 2003, 467: 60–79.
48. Osakada F, Mori T, Cetin AH, Marshel JH, Virgen B, Callaway EM. New rabies virus variants for monitoring and manipulating activity and gene expression in defined neural circuits. *Neuron* 2011, 71: 617–631.
49. Capelli P, Pivetta C, Soledad Esposito M, Arber S. Locomotor speed control circuits in the caudal brainstem. *Nature* 2017, 551: 373–377.
50. Yang H, de Jong JW, Tak Y, Peck J, Bateup HS, Lammel S. Nucleus accumbens subnuclei regulate motivated behavior *via* direct inhibition and disinhibition of VTA dopamine subpopulations. *Neuron* 2018, 97: 434–449 e434.
51. Watabe-Uchida M, Zhu L, Ogawa SK, Vamanrao A, Uchida N. Whole-brain mapping of direct inputs to midbrain dopamine neurons. *Neuron* 2012, 74: 858–873.
52. Ogawa SK, Cohen JY, Hwang D, Uchida N, Watabe-Uchida M. Organization of monosynaptic inputs to the serotonin and dopamine neuromodulatory systems. *Cell Rep* 2014, 8: 1105–1118.
53. Watson C, Paxinos G, Puelles L. The mouse nervous system. Academic Press, 2012.
54. Isaacson R. The Hippocampus: Volume 1: Structure and Development. Springer Science & Business Media, 2012.
55. Vivar C, Potter MC, Choi J, Lee JY, Stringer TP, Callaway EM, *et al.* Monosynaptic inputs to new neurons in the dentate gyrus. *Nat Commun* 2012, 3: 1107.
56. Semba K. Multiple output pathways of the basal forebrain: organization, chemical heterogeneity, and roles in vigilance. *Behav Brain Res* 2000, 115: 117–141.
57. Sun Y, Grieco SF, Holmes TC, Xu X. Local and long-range circuit connections to hilar mossy cells in the dentate gyrus. *eNeuro* 2017, 4.
58. Bui AD, Nguyen TM, Limouse C, Kim HK, Szabo GG, Felong S, *et al.* Dentate gyrus mossy cells control spontaneous convulsive seizures and spatial memory. *Science* 2018, 359: 787–790.
59. Molyneux BJ, Arlotta P, Menezes JR, Macklis JD. Neuronal subtype specification in the cerebral cortex. *Nat Rev Neurosci* 2007, 8: 427.
60. Lodato S, Rouaux C, Quast KB, Jantrachotechatchawan C, Studer M, Hensch TK, *et al.* Excitatory projection neuron subtypes control the distribution of local inhibitory interneurons in the cerebral cortex. *Neuron* 2011, 69: 763–779.
61. Bezaire MJ, Soltesz I. Quantitative assessment of CA1 local circuits: knowledge base for interneuron-pyramidal cell connectivity. *Hippocampus* 2013, 23: 751–785.
62. Hayashi Y, Shi SH, Esteban JA, Piccini A, Poncer JC, Malinow R. Driving AMPA receptors into synapses by LTP and CaMKII: requirement for GluR1 and PDZ domain interaction. *Science* 2000, 287: 2262–2267.
63. Miller SG, Kennedy MB. Distinct forebrain and cerebellar isozymes of type II Ca<sup>2+</sup>/calmodulin-dependent protein kinase associate differently with the postsynaptic density fraction. *J Biol Chem* 1985, 260: 9039–9046.
64. Morimoto K, Hooper DC, Carbaugh H, Fu ZF, Koprowski H, Dietzschold B. Rabies virus quasispecies: implications for pathogenesis. *Proc Natl Acad Sci U S A* 1998, 95: 3152–3156.

65. Kim EJ, Jacobs MW, Ito-Cole T, Callaway EM. Improved monosynaptic neural circuit tracing using engineered rabies virus glycoproteins. *Cell Rep* 2016, 15: 692–699.
66. Daya S, Berns KI. Gene therapy using adeno-associated virus vectors. *Clin Microbiol Rev* 2008, 21: 583–593.
67. Ayuso E, Mingozzi F, Bosch F. Production, purification and characterization of adeno-associated vectors. *Curr Gene Ther* 2010, 10: 423–436.
68. Bezaire MJ, Soltesz I. Quantitative assessment of CA1 local circuits: knowledge base for interneuron-pyramidal cell connectivity. *Hippocampus* 2013, 23: 751–785.
69. Beier KT, Steinberg EE, DeLoach KE, Xie S, Miyamichi K, Schwarz L, *et al.* Circuit architecture of VTA dopamine neurons revealed by systematic input-output mapping. *Cell* 2015, 162: 622–634.
70. Ogawa SK, Watabe-Uchida M. Organization of dopamine and serotonin system: Anatomical and functional mapping of monosynaptic inputs using rabies virus. *Pharmacol Biochem Behav* 2018, 174: 9–22.
71. Albigetti GW, Ghanem A, Foster E, Conzelmann KK, Zeilhofer HU, Wildner H. Identification of two classes of somatosensory neurons that display resistance to retrograde infection by rabies virus. *J Neurosci* 2017, 37: 10358–10371.



# Projection from the Anterior Cingulate Cortex to the Lateral Part of Mediodorsal Thalamus Modulates Vicarious Freezing Behavior

Chaowen Zheng<sup>1,2</sup> · Yanwang Huang<sup>1,2</sup> · Binshi Bo<sup>1</sup> · Lei Wei<sup>1</sup> · Zhifeng Liang<sup>1</sup> · Zuoren Wang<sup>1,2,3</sup>

Received: 11 March 2019 / Accepted: 26 May 2019 / Published online: 17 September 2019  
© Shanghai Institutes for Biological Sciences, CAS 2019

**Abstract** Emotional contagion, a primary form of empathy, is present in rodents. Among emotional contagion behaviors, social transmission of fear is the most studied. Here, we modified a paradigm used in previous studies to more robustly assess the social transmission of fear in rats that experienced foot-shock. We used resting-state functional magnetic resonance imaging to show that foot-shock experience enhances the regional connectivity of the anterior cingulate cortex (ACC). We found that lesioning the ACC specifically attenuated the vicarious freezing behavior of foot-shock-experienced observer rats. Furthermore, ablation of projections from the ACC to the mediodorsal thalamus (MDL) bilaterally delayed the vicarious freezing responses, and activation of these projections decreased the vicarious freezing responses. Overall, our results demonstrate that, in rats, the ACC modulates vicarious freezing behavior *via* a projection to the MDL and provide clues to understanding the mechanisms underlying empathic behavior in humans.

**Keywords** Rat · Empathy · Vicarious freezing · Neuronal circuit

## Introduction

Empathy refers to the capability of a subject to stand in another individual's situation and experience the feelings of the latter [1]. It is a sophisticated psychological process vital for individuals to live in society. In addition, abnormalities in this ability are closely associated with mental diseases, such as autism spectrum disorder [2, 3] and schizophrenia [4–6]. Thus, defining the neuronal mechanisms underlying empathy could enable understanding and lead to cures for psychiatric disorders. Currently, these mechanisms in humans remain unknown, in part due to limited research methods.

Initially, researchers defined empathy as unique to humans and apes [7, 8]. Now, increasing evidence has shown that empathy is evolutionarily conserved from rodents to humans [1, 9]. Although advanced empathic behaviors such as perspective-taking have not been defined in rodents, many studies support the idea that rodents exhibit emotional contagion [10, 11], a primary form of empathic behavior. In the hierarchy of empathic behaviors, emotional contagion refers to an individual's ability to unconsciously mimic the emotional state of a conspecific [7] and is thought to be a fundamental component of advanced empathy [12, 13]. Examples of emotional contagion include the contagion of a baby's cry [14] and the social transmission of fear [15, 16]. Thus, understanding the mechanisms of emotional contagion in simpler animals could shed light on the neuronal basis of advanced empathy in humans.

To date, behavioral studies have revealed a variety of primary empathy behaviors in rodents, such as social buffering [17], social analgesia [18], and social transmission of fear. Among these, the last has been most studied in rodents, mainly using the paradigm of observational fear

✉ Zuoren Wang  
zuorenwang@ion.ac.cn

<sup>1</sup> Institute of Neuroscience, State Key Laboratory of Neuroscience, CAS Center for Excellence in Brain Science and Intelligence Technology, Chinese Academy of Sciences, Shanghai 200031, China

<sup>2</sup> University of Chinese Academy of Sciences, Beijing 100049, China

<sup>3</sup> School of Future Technology, University of Chinese Academy of Sciences, Beijing 100049, China

established by Shin and colleagues [11]. Observational fear tasks evaluate the social transmission of fear by detecting the vicarious behavior of an observer (OS) when a demonstrator (DS) suffers distress (such as foot-shock, a mild electric shock administered to the feet of rats), but some studies have reported that since the OS must observe the foot-shock response of the DS in real time, the resulting vicarious behavior likely includes a startle-induced component [19]. However, in another paradigm reported by Kim *et al.* [20], the OS performs a vicarious response simply by observing the emotional state of the DS, without a startle-induced component. Thus, in the present study, we used Kim's behavioral paradigm to further explore the potential mechanisms.

The neuronal substrates underlying the social transmission of fear remain largely unknown. Previous studies have shown that the anterior cingulate cortex (ACC) modulates vicarious freezing behavior in a paradigm of observational fear [15], since current-injection stimulation or lesion of the ACC respectively increased or decreased vicarious freezing. Shin's lab also found that optogenetic activation or inhibition of somatostatin-positive neurons in the ACC respectively decreased or increased observational fear [21]. Several studies have also reported that the neuropeptide oxytocin modulates empathy-related behaviors in humans [22–24] as well as social behavior-like observational fear in rodents [25]. In particular, intranasal administration of oxytocin increases ACC neuronal activity and vicarious freezing behavior in mice [25]. Since the ACC appears to be closely associated with vicarious freezing behavior, and the capacity for empathy is strongly associated with personal experience, especially unpleasant experience, in humans [26], it is important to determine whether foot-shock experience enhances vicarious freezing behavior by increasing ACC activity. If so, this would be conducive to further understanding the potential neuronal mechanism underlying unpleasant-experience-induced empathy disorder.

Among the structures downstream of the ACC, the lateral part of the mediodorsal thalamus (MDL) has been reported to participate in observational fear learning [15]. In addition, since the ACC is close to and partially overlaps with the medial prefrontal cortex (mPFC), and disconnection of the mPFC from the MD is associated with dysfunction of working memory [27–29], reduced cognitive flexibility [30–32], and especially schizophrenia [33–36] (which is accompanied by abnormal empathy [4–6]), it is of great interest to explore the function of the neuronal projection between the ACC and the MD in the process of vicarious freezing behavior.

We therefore set out to determine which brain region was activated after footshock-experience and its role in footshock-experienced vicarious freezing behavior. We

also want to explore function of ACC and the projection from ACC to MDL in vicarious freezing behavior.

## Experimental Procedures

### Animals

We used a total of 346 wild-type male Sprague–Dawley rats weighing 300 g–450 g each. Among them, 164 were used for behavioral tests, 15 for fMRI scanning, 60 for the chemical lesion study, 2 for neuronal circuit-tracing, 41 for the caspase3 apoptosis study, 2 for patch-clamp recording, and 62 for optogenetic manipulation. All rats were reared in pairs in exhaust-ventilated cages under a 12 h/12 h light/dark cycle. Water and food were supplied *ad libitum*. The use of animals bred for and manipulated in this study was approved by the Animal Care and Use Committee of the Institute of Neuroscience, Chinese Academy of Sciences, and experiments were performed in accordance with the guidelines of the Ministry of Science and Technology of the People's Republic of China for the Care and Use of Laboratory Animals.

### Establishment of the Paradigm

#### *Social Transmission of Fear Under Kim's Paradigm*

Under Kim's paradigm, rats paired in the same cage served as respective DS and OS. On day 1, the DS underwent 10 trials of classical fear conditioning training in a closed electrical shock box: in each trial, a conditioned stimulus (sound cue, 5 kHz) was presented persistently for 20 s, accompanied in the last second by an unconditioned foot shock (1 s, 2 mA). Both stimuli ended simultaneously. The intertrial interval was 1 min and the session ended 2 min after the last foot shock. OSs were divided into naïve and foot-shock-experienced groups. The latter underwent the following foot-shock paradigm before the test day. After 3 min of adaption to the shock cage, one foot shock was delivered (1 s, 2 mA), followed by another 3 min later. By contrast, naïve OSs did not experience a foot shock prior to the test day. On day 2, DSs and OSs were placed in a new open box, and after 1 min, the conditioned stimulus (5 kHz tone) was presented persistently for 7 min to test the responses of DSs and OSs.

Fear conditioning learning was established in a stainless-steel shock box measuring  $27 \times 28 \times 30 \text{ cm}^3$ . The floor consisted of 18 stainless-steel tubes (outer diameter, 5 mm) and the ceiling was a transparent acrylic plate. The open box used to test the social transmission of fear was  $35 \times 36 \times 40 \text{ cm}^3$  and made of white acrylic plates. The sound cue was played using a full-frequency-range

loudspeaker (FR89EX; Fountek Electronics Co., Ltd, Jiaxing, China), and an electric shock was delivered by a constant current stimulator (Anilab Software and Instruments Co., Ltd, Ningbo, China). Both the sound cue and foot shock stimuli were controlled by Anilab software.

### *Social Transmission of Fear Under an Optimized Paradigm*

In our modified paradigm, DSs underwent fear-conditioning training on days 1 and 2 (10 trials on each day), while OSs received foot shocks twice on day 2 only, and the social transmission of fear was tested on day 3. Other conditions were the same as in Kim's paradigm. All the behavioral tests of social transmission shown in Figs. 3, 4 and 5 used this modified paradigm.

### **Pharmacological Lesioning**

In the lesion studies, general anesthesia was maintained by pentobarbital sodium (80 mg/kg, i.p.). Atropine sulfate (0.05 mg/kg, i.p.) was administered to inhibit mucus secretion, which hinders breathing. Glass electrodes for ibotenic acid (IBO) injection (5 mg/mL, Sigma, St. Louis, MO) were pulled on a P97 system (Sutter Instrument Co., Novato, USA). The Pico III system (Parker Hannifin, Mayfield Heights, OH) was used to pump IBO (1  $\mu$ L) bilaterally into the ACC (AP, +1.35 mm; ML, 0.60 mm; DV, 2.4 mm). After suturing, gentamycin (5 mg/kg, i.p.) was administered for one week to minimize infection. After 1 week of recovery, the social transmission of fear was tested using our optimized paradigm. The retrieval test occurred on the second day after fear conditioning training in the same box used for the social transmission of fear. The experimental settings and procedures were the same as in the social transmission of fear test on day 3.

### **Caspase 3 Ablation**

For virus injection, the procedures followed the same sequence as for stereotactic injection in the pharmacological experiment. After 3 weeks of virus expression, the social transmission of fear was tested using our optimized paradigm.

### **Optogenetic Activation**

For virus injection, the procedures followed the same sequence as for the stereotactic injection in the pharmacological experiment. Before implantation of the optical fibers into the MDL (AP, - 2.55 mm; ML, 1.00 mm; DV, 4.50 mm), three bone screws were fixed to the rat's skull and acrylic dental cement was used to stabilize the fibers.

Gentamycin was administered as above. Three weeks after virus injection, the rats underwent behavioral tests. The social transmission of fear test was the same as before. Blue light was delivered to the MDL of the virus-injected rats throughout the test period. The lasers used to deliver blue light (473 nm, BL473T3-050FC) were from Shanghai Laser & Optics Century Co., Ltd. The power intensity was set to 5 mW at the tips of the fibers and confirmed using a Fiber Optic Power Meter (Thorlabs, Inc., Newton, NJ). The frequency of laser stimulation (controlled by Anilab software) in the behavioral tests was set to 20 Hz with a 25-ms pulse-width.

To establish fear conditioning and for the fear memory retrieval test, the procedure was the same as in the pharmacological experiment. Locomotion was recorded. The frequency, duration, and intensity of the blue light stimuli were the same as above. An optical fiber commutator was used to prevent twisting of the cable.

### **Open Field Test**

For virus injection and implantation of the optical fibers, the procedures were the same as for stereotactic injection in the pharmacological experiment and social transmission of fear with optogenetic activation part.

In the open field test, rats were placed in a box measuring 54  $\times$  40  $\times$  38 cm<sup>3</sup>. On day 1, locomotion was recorded for 30 min using the Cineplex (Plexon Inc., Hong Kong, China) system in the absence of laser stimulation with the fiber cable attached. However, on day 2 the light pulses and locomotion were recorded. The light frequency, duration, and intensity were set the same as the parameters in optogenetic activation part.

### **Video Tracking and Analysis**

Rats were marked with different colors, and their locomotion was tracked as above and saved in text files. Freezing behavior was defined as when an animal did not move (except for spontaneous respiration) for at least 2 s. Huddling time was defined as the period when two rats were within huddling distance. Statistics relevant to freezing and huddling times and locomotor velocity were processed in MATLAB (MathWorks, Natick, MA).

### **Resting-State Functional Magnetic Resonance Scanning (rs-fMRI) and Image Processing**

Ten male Sprague-Dawley rats in the footshock-experienced group and 5 in the control group were anesthetized with isoflurane (5% for induction, 0.5% for maintenance) and paralyzed with dexmedetomidine (0.03 mg/kg bolus, 0.015 mg/kg per hour continuous subcutaneous infusion).

Respiration rate, rectal temperature, O<sub>2</sub> saturation, and heart rate were maintained within the following ranges: 40–60 breaths/min, 36 °C–37 °C, 98%–100%, and 200–300 beats/min. MRI data were acquired using a small-animal 9.4T MR system (Bruker BioSpec 94/30, Ettlingen, Germany) equipped with a 2 × 2 phased array surface receiver coil. T2 RARE anatomical images were acquired with a repetition time/echo time = 3735 ms/33 ms, field of view = 30 × 30 mm<sup>2</sup>, matrix size = 256 × 256, slice thickness 0.6 mm, number of slices 35, and number of averages 1. Gradient-echo echo-planar imaging (GE-EPI) data were acquired with a repetition time/echo time/flip angle = 1000 ms/13 ms/55°, 600 repetitions, matrix dimensions = 80 × 67, in-plane voxel dimensions of 375 × 373 μm<sup>2</sup>, and slice thickness 0.6 mm.

Functional images were processed using scripts custom-written in MatLab and SPM12 (<http://www.fil.ion.ucl.ac.uk/spm/>). The preprocessing included the following main steps. (1) EPI images were converted from Bruker format to NIFTI format (nominal voxel size enlarged 10 times to facilitate image processing in SPM). (2) Realignment: the first 5 volumes were discarded to minimize relaxation-related signal changes and then realigned for motion correction. (3) Spatial normalization: the realigned EPI images were co-registered to the rat's own T2 anatomical images, which were normalized to a rat brain template [37]. (4) The normalized images were band-pass filtered (0.001 Hz–0.1 Hz) and the whole brain signal and the six motion parameters were regressed. (5) Regional homogeneity (ReHo) calculation: Kendall's coefficient was calculated to determine the degree of regional synchronization, including the 27 pixels of the fMRI time courses [38]. Individual ReHo maps were generated voxel-wise for all groups. (6) Smoothing: spatial smoothing was applied with a 0.8-mm full-width at half-maximum Gaussian kernel.

## Virus

Recombinant adeno-associated virus (AAV) vectors of serotype 9 were packaged by Shanghai Taitool Bioscience Co. Ltd. Viral titers were  $1.32 \times 10^{13}$  particles/mL for AAV-hSyn-hChR2-EGFP-ER2-WPRE-PolyA,  $1.61 \times 10^{13}$  particles/mL for AAV-hSyn-eGFP-3Flag-WPRE-SV40pA,  $1.16 \times 10^{13}$  particles/mL for AAV-hSyn-FLEX-tdTomato-WPRE-bGHPA,  $2.03 \times 10^{13}$  particles/mL for AAV-CAG-DIO-taCasp3-TEVp,  $1.60 \times 10^{13}$  particles/mL, and  $1.82 \times 10^{13}$  particles/mL for AAV-CMV\_bGI-Cre-EGFP. The viruses were injected in a volume of 1 μL on each side.

## Perfusion and Histology

After the rats were deeply anesthetized (as above), they were perfused transcardially with phosphate-buffered

saline (PBS) until the liver began to turn yellow, and then the PBS was replaced by 4% formaldehyde. After the tail became stiff, the brain was removed and post-fixed in 4% formaldehyde for 12 h, followed by incubation in 30% sucrose. When the brain sank, 50 μm coronal sections were cut on a freezing microtome.

For histology, we performed 4',6-diamidino-2-phenylindole (DAPI, Sigma) staining. Sections were washed 3 times in PBS for 5 min and then incubated for 5 min with DAPI. After two 5-min PBS washes, sections were mounted with 75% glycerin. Images were acquired using an Olympus VS120 High Throughput fluorescent imaging system (Shinjuku, Tokyo, Japan) with a 10 × air objective.

## Statistics

Two-way repeated measures analysis of variance (ANOVA) was used to analyze the differences in ReHo values between two groups, and the interaction effects (time and condition) F map calculated in SPM12 was used to analyze the differences in ReHo values between two groups. Multiple comparison correction was done using the AlphaSim function (corrected  $P < 0.05$ ) in REST software [39]. Student's *t*-test was used to further analyze the interaction type in brain areas showing significant interaction effects.

## Results

### Behavioral Paradigm

To define the neuronal mechanisms underlying the social transmission of fear in rats, the overall experimental design is shown in Fig. 1. We first applied a paradigm based on that of Kim *et al.* [20] (Fig. 2A). Cage-mates were randomly divided into DS and OS groups. On day 1, the DS underwent classical fear conditioning training, in which a foot-shock (unconditioned stimulus) was associated with

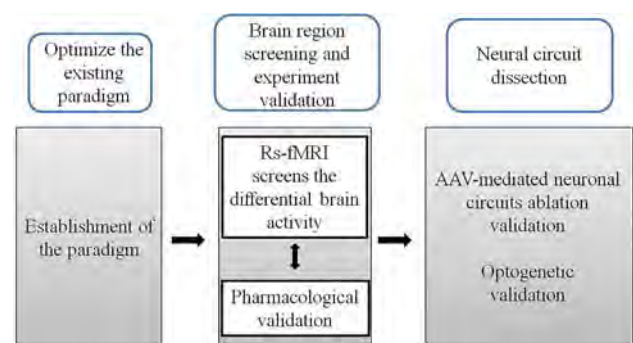


**Fig. 1** Experimental design. Schematic of the experimental design of the present study.

a sound cue (conditioned stimulus). OS rats either experienced foot-shock twice (2 mA, 1 s, as the experience group (EP)) or were left untreated (naïve, NA). The behavioral responses of OSs were tested on day 2, when both DSs and OSs were placed together in pairs and continuously exposed to the conditioned stimulus in a new

context. To confirm that the behavioral response of OSs was indeed caused by DSs, the control group (Ctrl) was set to test the behavioral response of EP OSs to the naïve DSs. Compared with the NA and Ctrl groups, the huddling time of DSs and OSs of the EP group was significantly increased (Fig. 2B;  $n = 12$  pairs/group,  $P < 0.05$  EP vs NA, and

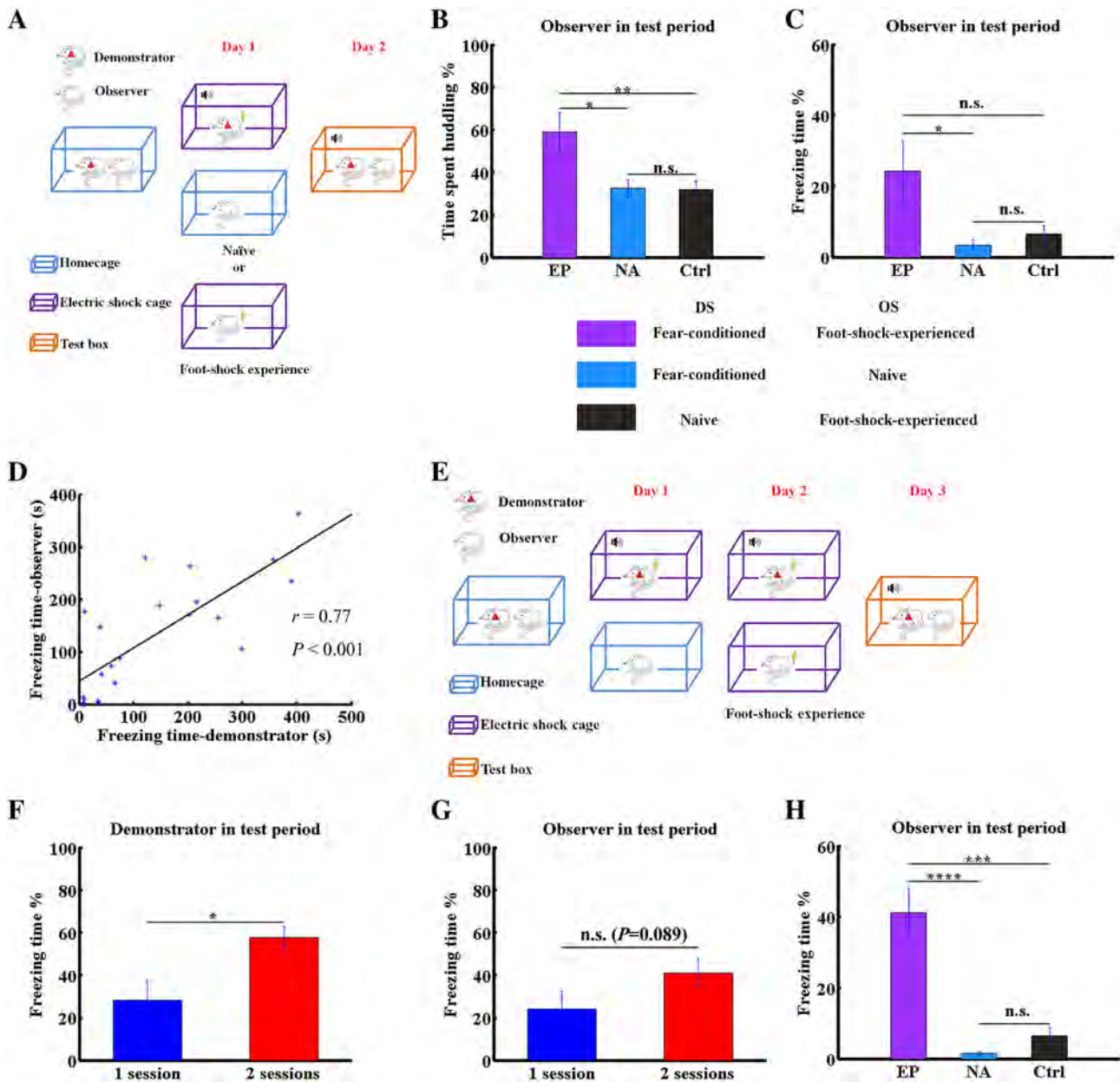


**Fig. 2** Behavioral paradigm modification. **A** Schematic of the paradigm adapted from Kim *et al.* [20]. Different colored boxes represent different experimental contexts. **B**, **C** Percentage of huddling (**B**) and freezing (**C**) times of OSs in the indicated groups. **D** Correlation of freezing times between fear conditioned DSs and foot-shock-experienced OS cage-mates ( $n = 22$ ,  $P < 0.001$ , Student's *t*-test). **E** Schematic showing our modified paradigm. **F** Percentage freezing time of DSs in the EP group in Kim's (1 session) and our modified paradigm (2 sessions) on the test day ( $n = 12$ ,  $P < 0.05$ ,

non-parametric rank-sum test). **G** Percentage freezing time of OSs in the EP group in Kim's (1 session) and our modified paradigm (2 sessions) on the test day ( $n = 12$ ,  $P = 0.089$ , non-parametric rank-sum test). **H** Percentage freezing time of OSs in the EP, NA, and Ctrl groups ( $n = 12$ ,  $P < 0.0001$  for EP vs NA and  $P < 0.001$  for EP vs Ctrl). Data are shown as the mean  $\pm$  SEM; asterisks represent the level of significance: \* $P < 0.05$ , \*\* $P < 0.01$ , \*\*\* $P < 0.001$ , n.s., not significant, non-parametric rank-sum test.

$P < 0.01$  EP vs Ctrl, non-parametric rank-sum test), indicating that foot-shock experience by the OS enhanced the social transmission of fear. However, unlike the findings of Kim *et al.* [20], we found that under our experimental conditions, the level of vicarious freezing of OSs tended to increase relative to the Ctrl group (Fig. 2C), but this apparent increase was not statistically significant ( $n = 12$  pairs/group,  $P = 0.13$ , non-parametric rank-sum test). To find the reason for the inconsistency between our and Kim's results, we performed correlation analysis of total freezing time between fear-conditioned DSs and their foot-shock-experienced OS cage-mates in the test period. The results revealed a positive correlation between the freezing time of DSs and OSs (Fig. 2D;  $n = 22$ ,  $r = 0.77$ ,  $P < 0.001$ , Student's *t*-test). This indicated that the low vicarious freezing level of OSs was probably due to the low freezing level of DSs. As expected, only 5 out of 12 DSs in the EP group exhibited obvious freezing behavior ( $> 100$  s) in the test period on day 2 under the conditions of Kim's paradigm. These results suggested that unstable performance by DSs may explain why we did not find significant vicarious freezing responses in OSs.

To achieve more robust vicarious freezing behavior, we modified the paradigm by increasing the number of sessions of fear conditioning training of DSs to two and then moving the OS foot-shock experience to day 2 (Fig. 2E vs Fig. 2A). Using this paradigm, we found that the freezing level of DSs in the EP group in the test period was significantly greater than that under Kim's paradigm (Fig. 2F;  $n = 12$  pairs for each of the 1-session and 2-sessions groups,  $P < 0.05$ , non-parametric rank-sum test), and 10 out of 12 DSs in our modified paradigm exhibited obvious freezing behavior ( $> 100$  s). In our modified paradigm, the level of vicarious freezing behavior of OSs in the EP group showed a tendency to increase compared with that under Kim's paradigm (Fig. 2G;  $n = 12$  pairs for each of the 1-session and 2-sessions groups,  $P = 0.089$ , non-parametric rank-sum test). Furthermore, under the modified paradigm, the level of vicarious freezing in OSs in the EP group was significantly higher than those in the NA and Ctrl groups (Fig. 2H;  $n = 12$  pairs/group,  $P < 0.0001$  for EP vs NA and  $P < 0.001$  for EP vs Ctrl, non-parametric rank-sum test). These results support the conclusion that our optimized paradigm is more stable for studies of the potential neuronal mechanisms of experience-dependent vicarious freezing behavior.

### Foot-Shock Experience Elevates Basic ACC Activity

We next asked whether foot-shock experience modulates the activity of a specific brain region. To do so, we performed rs-fMRI and computed which brain region exhibited significant changes after foot-shock experience.

The control and foot-shock-experienced groups underwent fMRI scanning on days 1 and 2, although the latter underwent foot-shock on the night of day 1 (Fig. 3A). We used the ReHo algorithm, as it reflects intra-regional synchronization [40, 41], to compute regional connectivity. To identify regions whose regional connectivity changed significantly after foot-shock experience, we used two-way ANOVA to analyze interaction effects in the results acquired from ReHo. This analysis revealed the ACC to be the region showing the strongest interaction effect among all scanned brain regions in thresholded maps (Fig. 3B) ( $n = 10$  for the foot-shock experienced group,  $n = 5$  for the naïve group;  $P < 0.05$ , Student's *t*-test). Further simple effect analysis confirmed that foot-shock experience enhanced the intra-regional connectivity of the ACC (Fig. 3C, D;  $P < 0.05$ ,  $n = 10$  for the foot-shock experienced group,  $n = 5$  for the NA group, non-parametric rank-sum test). Since altered ReHo is linked with altered neuronal activity [42], these results suggested that the increased social transmission of fear seen in OSs in the EP group may be associated with enhanced neuronal activity in the ACC.

### Effects of ACC Lesions on Freezing and Huddling Behavior

To confirm ACC involvement in the social transmission of fear, we asked whether decreasing ACC activity reverses the behavioral phenotypes induced by foot-shock-experience. So, we lesioned the ACC by bilateral delivery of IBO and found a significant decrease in vicarious freezing levels (Fig. 4A, B;  $n = 12$  pairs/group,  $P < 0.01$ , non-parametric rank-sum test), consistent with previous studies [15]. Interestingly, unlike the impaired freezing behavior seen following ACC lesioning, the huddling behavior between DSs and OSs was unaffected (Fig. 4C;  $n = 12$  pairs/group,  $P = 0.10$ , non-parametric rank-sum test). To exclude the possibility that ACC lesioning decreased the expression of fear, we evaluated freezing levels in the classical fear conditioning retrieval period and found no significant difference in primary fear responses between lesioned and control groups (Fig. 4D;  $n = 6$ /group,  $P = 0.4848$ , non-parametric rank-sum test). These results indicated that ACC activity specifically affects vicarious freezing but not huddling behaviors during the social transmission of fear.

### Ablating the ACC-to-MDL Projection Delays the Onset of Vicarious Behavior

Since the ACC contributes to experience-dependent vicarious freezing, we asked which ACC projections specifically modulate this behavior. To identify regions connected to the ACC, we injected neuron-labeling AAV-hSyn-EGFP

**Fig. 3** Foot-shock experience is associated with enhanced regional connectivity in the ACC. **A** Schema of fMRI experimental design. **B** Thresholded maps of interaction effects based on a two-way repeated measures ANOVA. Yellow voxels indicate region with significant interaction effects (corrected  $P < 0.05$ ). **C** The ACC was selected for simple effect analysis; purple voxels indicate the selected regions. **D** Simple effect analysis of the ReHo values in foot-shock-experienced and naïve rats on days 1 and 2. Data are presented as the mean  $\pm$  SEM;  $*P < 0.05$ , non-parametric rank-sum test.

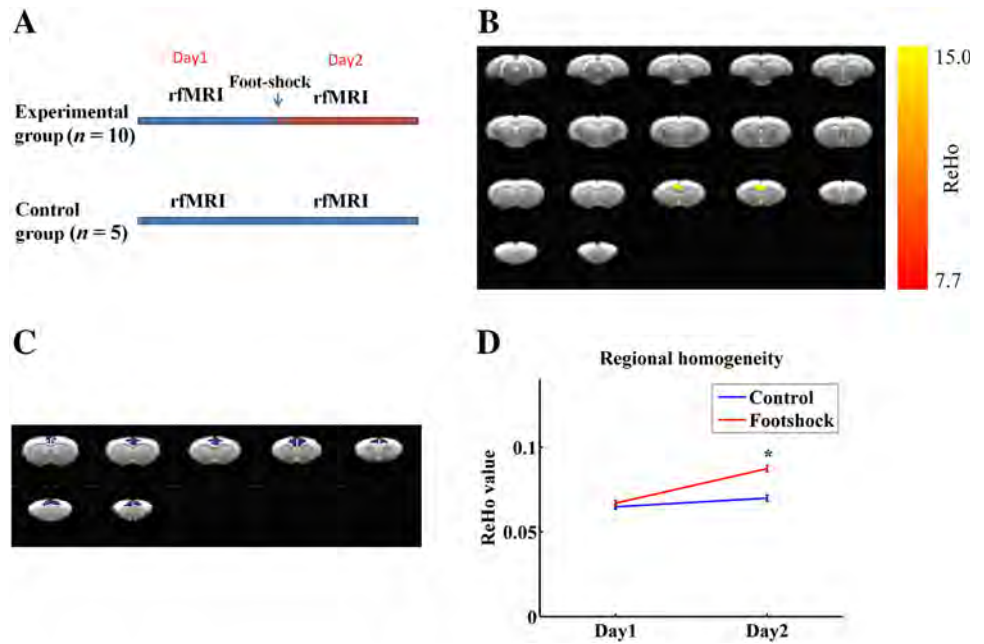
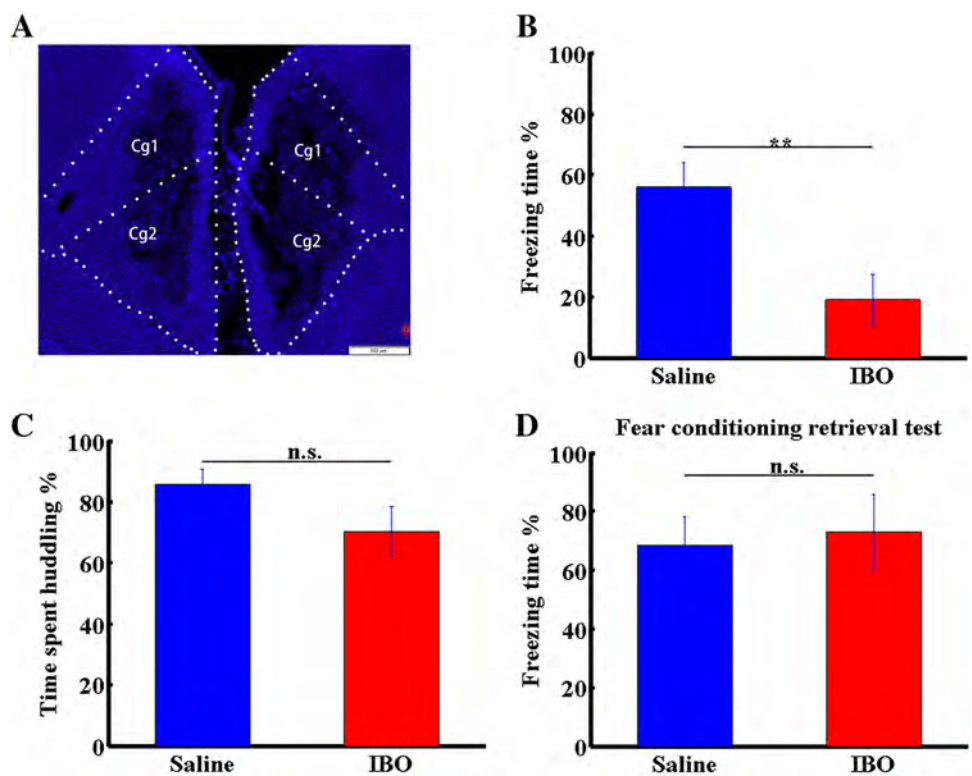


**Fig. 4** ACC lesioning impairs vicarious freezing but not huddling behaviors following foot-shock experience. **A** Effects of IBO. Blue represent the nuclei stained with DAPI. Cg1, 2, cingulate cortex 1 and 2. **B**, **C** Percentage freezing (**B**) and huddling (**C**) times of OS rats in IBO- and saline-treated groups. **D** Percentage freezing times of OS rats in IBO- or saline-treated groups in the retrieval period after fear conditioning. Data are presented as the mean  $\pm$  SEM;  $**P < 0.01$ , non-parametric rank-sum test, n.s., not significant.



virus into the ACC and observed that the MDL received dense fiber terminal input from the ACC (Fig. 5A). We also injected cholera toxin B into the MDL to retrogradely trace projections and observed dense labeling of ACC cell bodies (Fig. 5B). These results, which are consistent with those of others [15], showed that the MDL receives ACC

input. However, the function of these projections remained unclear.

We next investigated the function of the ACC-to-MDL projection using an ablation strategy. We first performed control experiments by injecting retroAAV-Cre into the MDL and AAV-FLEX-tdTomato into the ACC (Fig. 5C),

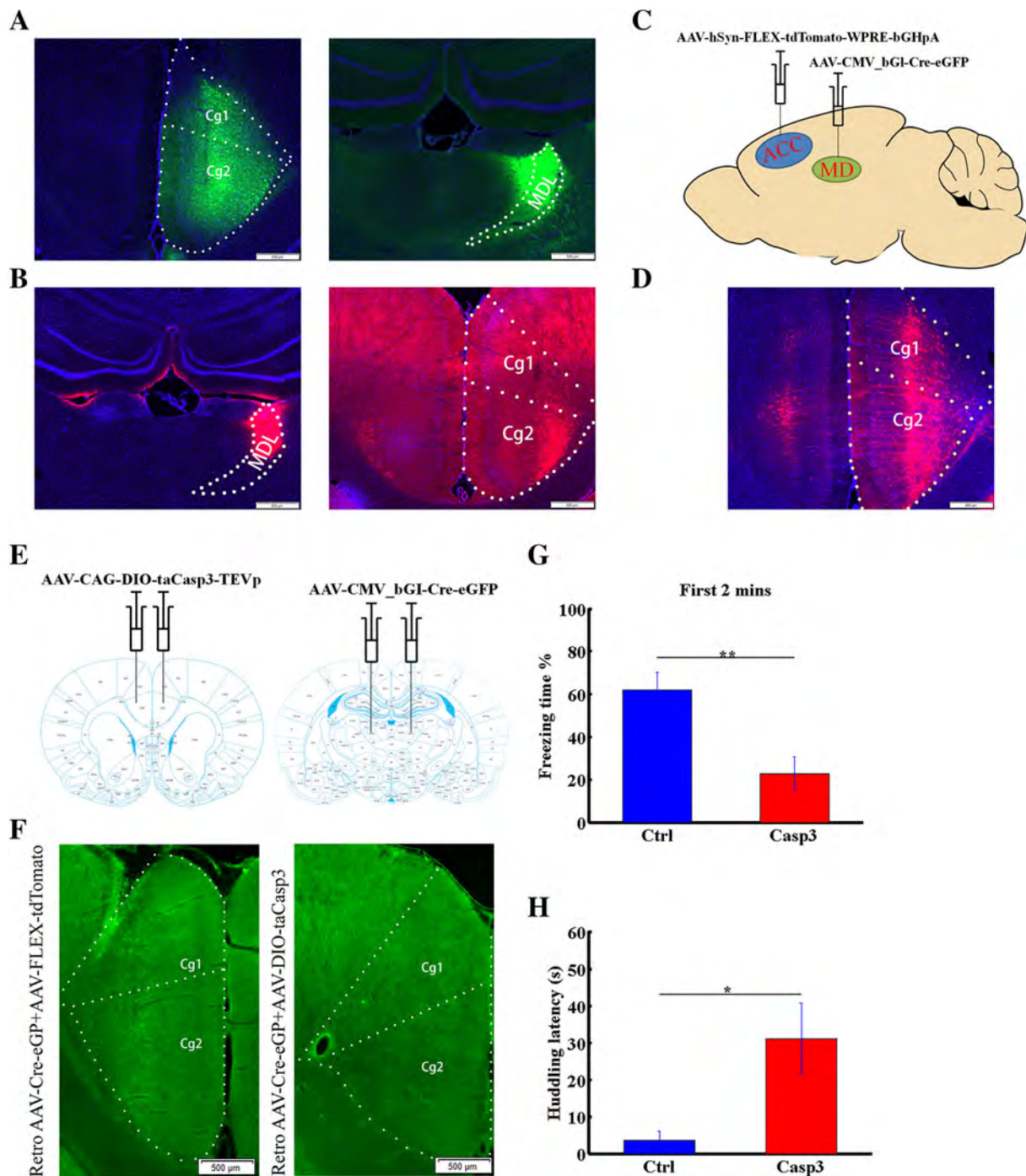


**Fig. 5** Ablating ACC neurons projecting to the MDL delays the onset of vicarious behaviors. **A** Left panel, AAV-hSyn-EGFP injection target in the ACC; right panel, labeled projection terminals in the MDL. **B** Left panel, Cholera toxin B injection target in the MDL; right panel, ACC cell bodies. Cg1, 2, cingulate cortex 1 and 2. **C** Diagram of virus-injection strategy used to label MDL-projecting ACC neurons. AAV-hSyn-FLEX-tdTomato-WPRE-bGHpA was injected into the right ACC and AAV-CMV\_bGI-Cre-EGFP into the right MDL. **D** ACC neurons projecting to the MDL labeled by the strategy shown in **A**. **E** Diagram of virus-injection strategy used to

ablate MDL-projecting ACC neurons. AAV-CAG-DIO-taCasp3-TEVp was injected into the ACC on both sides and AAV-CMV\_bGI-Cre-EGFP into the MDL on both sides. **F** Examples of eGFP-labeled neurons in the ACC of control (left) and caspase3 (right) groups. **G** Percentage freezing time in the first 2 min of the test in caspase-3-expressing and control groups. **H** Huddling behavior latency in caspase-3-expressing and control groups. Data are presented as the mean  $\pm$  SEM; \* $P < 0.05$ , \*\* $P < 0.01$ , non-parametric rank-sum test.

and found that MDL-projecting ACC neurons were effectively labeled by this strategy (Fig. 5D). These results demonstrated that our strategy effectively targeted the ACC-to-MDL projection. We then bilaterally injected a retrograde-labeling virus (retroAAV-CMV\_bG1-Cre-eGFP), which carries Cre recombinase, into the MDL and then injected a Cre-dependent anterograde-labeling virus (AAV-CAG-DIO-taCasp3-TEVp), which carries the double-floxed inverted open reading frame (as a substitute for FLEX) and caspase-3 (to induce apoptotic ablation), into the ACC on both sides (Fig. 5E). As the example shows, retroAAV-Cre + AAV-DIO-taCasp3 decreased the number of retro-AAV-Cre-labeled GFP<sup>+</sup> neurons in the ACC (Fig. 5F).

Behavioral tests showed that, for the time of freezing and huddling behaviors throughout the test period, rats in the experimental and control groups performed comparably (data not shown). However, further analysis revealed that ablation of ACC neurons projecting to the MDL decreased the vicarious freezing behavior in OSs in the first 2 min of behavioral testing (Fig. 5G;  $n = 8$  pairs for the Casp3 group,  $n = 12$  pairs for the control group,  $P < 0.01$ , non-parametric rank-sum test) and increased the latency of huddling onset (Fig. 5H;  $n = 8$  pairs for the Casp3 group,  $n = 12$  pairs for the control group,  $P < 0.05$ , non-parametric rank-sum test). These results demonstrated that ablating the ACC projection to the MDL delays the onset of vicarious behavior.

### Activation of the ACC-to-MDL Projection Decreases Vicarious Freezing Behavior

To further assess the role of the ACC-to-MDL projection in the social transmission of fear, we injected AAV virus carrying channelrhodopsin (ChR2) into the right ACC and implanted an optical fiber into the right MDL (Fig. 6A, B). As a control, we injected AAV virus carrying EGFP into the right ACC and implanted an optical fiber into the right MDL (Fig. 6C). To confirm the activation of neurons expressing ChR2 by light, we delivered blue light pulses at two frequencies (1 or 5 Hz) to a brain slice expressing ChR2 and found that ChR2-expressing neurons effectively followed the light pulse stimuli (Fig. 6D), while slices from a control group expressing AAV-EGFP in the ACC did not.

We then asked whether activation of the ACC–MDL projection alters the social transmission of fear. Following application of a continuous train of blue light pulses (473 nm, 20 Hz, 5 mW) to axon terminals in the MDL in the test period, we observed a significant decrease in vicarious freezing behavior in OSs (Fig. 6E). However, the huddling time of DSs and OSs in the EP group was unaffected (Fig. 6F;  $n = 8$  pairs for the ChR2 group,

$n = 11$  pairs for the control group,  $P < 0.01$ , non-parametric rank-sum test). To exclude the possibility that these outcomes were due to impaired expression of fear, we measured fear-expression time in the retrieval period after fear conditioning of ChR2- or EGFP-expressing rats and found that the values were comparable (Fig. 6G;  $n = 6$  for each EGFP- and ChR2-delivered group, non-parametric rank-sum test). We also asked whether the decreased vicarious freezing was due to enhanced locomotion by monitoring the average locomotor velocity in open field tests. This analysis showed that activation of the ACC–MDL projection did not alter the movement of OSs in the EP group (Fig. 6H;  $n = 6$  for each EGFP- and ChR2-delivered group, non-parametric rank-sum test). We concluded that activation of the ACC-to-MDL projection specifically decreases vicarious freezing behavior.

## Discussion

In this study, we focused on foot-shock-experienced vicarious freezing behavior and defined the neuronal substrates underlying this behavior. As in humans, experience can modulate the social transmission of fear in rodents (Fig. 2B, C) [43]. Using a paradigm modified from a study by Kim *et al.* [20], we found that an elevated fear state in the DS significantly enhanced the OS fear state, especially vicarious freezing behavior. Using rs-fMRI analysis, we found that ACC regional connectivity was significantly enhanced after foot-shock experience (Fig. 3D). ACC lesioning decreased the vicarious freezing behavior in foot-shock-experienced OSs (Fig. 4B). Given that a previous study reported that an altered ReHo is linked to altered spontaneous neuronal activity [42], and that Zhuo [44] showed that the plasticity of ACC neurons is altered by pain experience in rats and mice, we propose that foot-shock experience alters neuronal plasticity of the ACC, in turn modulating vicarious social behavior. Recent studies have identified a projection from the ACC to the MDL [15, 45], but its function remained unclear. Interestingly, we found that ablation of this projection delayed and its activation decreased vicarious freezing behavior (Figs. 5G, H, and 6E), demonstrating that the ACC modulates vicarious freezing behavior through this projection.

The social transmission of fear, defined as the transfer of fear emotion between individuals, is a primary form of empathy behavior and has been demonstrated in rodents [11]. This ability has been proposed to assist species to cooperatively achieve a common goal [1]. Previous studies have suggested that the transfer of fear is modulated by factors as varied as gender, age, familiarity, experience, and genetic background [10, 11, 25, 46]. In laboratory-bred

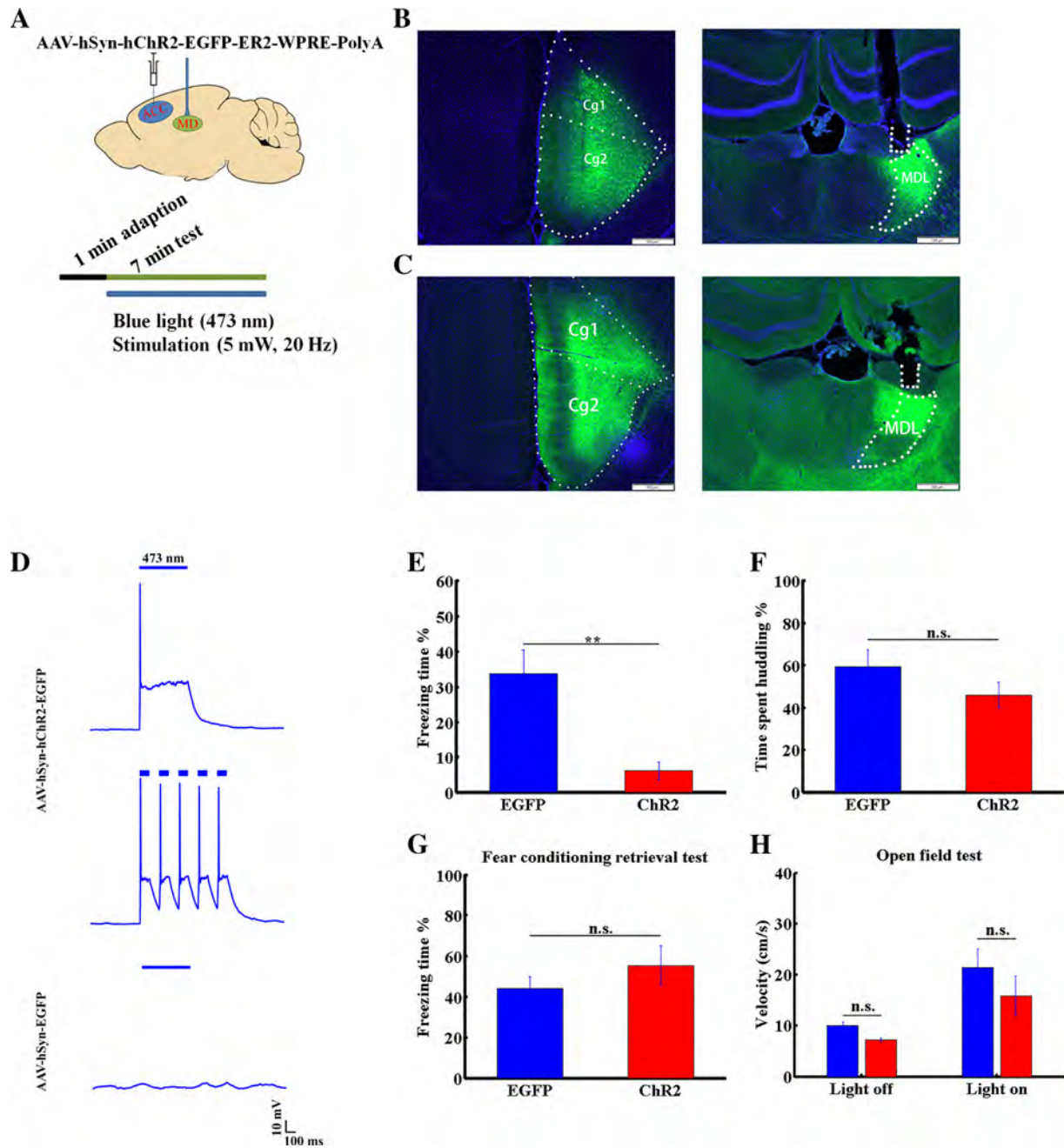


**Fig. 6** Activation of the ACC-to-MDL projection decreases vicarious freezing behavior. **A** Diagram showing optogenetic manipulation. **B** Tracing of projection from the ACC to the MDL. Left panel, AAV-hSyn-EGFP virus injection target in the ACC. Cg1, 2, cingulate cortex 1 and 2; right panel, projection terminals and optical fiber position in the MDL. **C** Left panel, AAV-hSyn-hChr2-EGFP virus injection target in the ACC; right panel, projection terminals and optical fiber position in the MDL. Nuclei stained with DAPI. **D** Light pulse-induced response of Chr2-expressing (upper and middle, 10

mW, 1 Hz and 5 Hz, respectively) and EGFP-expressing (lower, 10 mW, 1 Hz) ACC neurons in brain slice. **E**, **F** Freezing (**E**) and huddling (**F**) times of OSs in AAV-hSyn-EGFP (blue) or AAV-hSyn-ChR2 (red) groups. **G** Percentage freezing time of OSs in AAV-hSyn-EGFP- and AAV-hSyn-ChR2-injected groups in the retrieval period after fear conditioning. **H** Locomotor velocity of OSs in AAV-hSyn-EGFP (blue) and AAV-hSyn-ChR2 (red) groups, before and after light stimulation. Data are presented as the mean  $\pm$  SEM;  $**P < 0.01$ , non-parametric rank-sum test, n.s., not significant.

rodents, the lack of predators or challenging environments may be associated with lower levels of empathy in response to the distress of conspecifics. For example, when we applied the paradigm of Kim *et al.* [20], we observed

unstable performance of OSs (Fig. 2C), possibly due to different breeding or experimental environments. We then determined that this outcome was likely due to the low expression of fear by DSs in the retrieval period, as only 5

of 12 DSs exhibited a freezing response. Thus, we added an extra fear conditioning training session for DSs and allowed OSs to experience foot-shock before the test session. These modifications resulted in more robust vicarious freezing behavior by OSs (Fig. 2H) and allowed us to evaluate the social transmission of fear. Our modified paradigm can serve as a useful tool for future studies of the mechanisms underlying emotion contagion.

Observational fear studies [11] have reported that naïve OS mice show vicarious freezing behavior in response to behavior by DSs. However, we did not observe such behavior by OS rats in the NA group. Similarly, in some mouse studies, naïve OSs display significant observational fear [11], while in others, investigators have searched for but not found these behaviors [19]. Such differences may be due to variable breeding or test environments. Activation or inactivation of the ACC or of somatostatin-positive neurons found in that region [21] bidirectionally modulates the vicarious freezing behavior of OSs. Pain experience can change ACC neuronal plasticity [44], and using ReHo analysis we also found that ACC regional connectivity significantly increased after foot-shock experience (Fig. 3D). These findings suggest overall that vicarious freezing behavior is likely modified by the baseline ACC activity. Moreover, we found that lesioning of the ACC decreased vicarious freezing behavior due to foot-shock experience (Fig. 4B). However, the mechanisms underlying these outcomes need to be examined in greater detail at the neuronal and circuit levels.

Previous studies have shown that the MD participates in the processes of observational fear learning [15] and fear memory retrieval [47]. In addition, the functional connection between the mPFC (which is close to the ACC and overlaps with the dorsal ACC) and the MD is vital for working memory [27], cognitive flexibility [29, 30, 32], attentional control [48], goal-directed behavior [49], and schizophrenia [34, 35]. Recent studies of neuronal circuit-tracing have reported a projection from the ACC to the MDL in mice [45]. Here, we confirmed the existence of this projection in rats and investigated its function. Ablation of ACC neurons projecting to the MDL delayed the onset of vicarious behaviors (Fig. 5G, H). Moreover, activation of ACC projections to the MDL during the test period (Fig. 6E) specifically decreased the vicarious freezing behavior of OSs but not huddling (Fig. 6F) or conditioned fear (Fig. 6G). Based on the results that the mPFC-to-MD circuit is crucial for cognitive flexibility [29, 30, 32], and the MD is involved in fear memory retrieval [47], we propose that ACC neurons projecting to the MDL detect the emotional states of conspecifics and fire in a specific pattern to retrieve the foot-shock-experience-induced fear memory of OSs in the context of DS freezing. Using the Yerkes–Dodson law [50] as

reference, in which both hypo- and hyperarousal states in animals can compromise the normal behavioral response, the degree of activation of ACC neurons projecting to the MDL may have an inverted-U influence [51] on vicarious freezing performance. An inverted-U influence in regard to working memory has been reported in another study [52]. In addition, a previous study [53] also found that either activation or inhibition of a specific cell type in the mPFC has an inhibitory effect on performance in a working memory task. Thus, in our experiment, both ablation and over-activation of MDL-projecting ACC neurons probably perturbed the appropriate reaction of downstream neurons in the physiological state, and then resulted in an impairment of vicarious freezing behavior.

Recent studies have reported that the brain oxytocin system modulates empathy in humans and rodents [25, 54, 55], and specifically, intranasal oxytocin administration enhances observational fear in mice [25]. Interestingly, the oxytocin receptor is expressed in what are likely to be interneurons of the ACC [56, 57]. Future studies are needed to address whether neurons expressing oxytocin receptors and ACC projection neurons function together to modulate vicarious behavior.

### Limitations

In the present study, we used rs-fMRI to screen the brain regions that are correlated with experience-dependent vicarious freezing behavior. We performed rs-fMRI screening on anesthetized rats, and behavioral assays on freely-moving rats. We found that foot-shock not only increased the regional connectivity of the ACC, but also the performance of vicarious freezing. However, we did not provide sufficient evidence to support a causal relation between the changes in the regional connectivity of the ACC and the increased vicarious freezing behavior. In terms of the pharmacological lesion, caspase3 ablation, and optogenetic manipulation experiments, we just tested limited behavioral tasks. In addition, the ACC is a sophisticated brain region associated with various functions. Thus, we cannot exclude the possibility that other behaviors could have been affected by these manipulations.

### Conclusions

In summary, we modified a previous paradigm of social transmission of fear and found that foot-shock experience enhanced vicarious behavior and was associated with enhanced regional connectivity of the ACC. Activation or ablation of the ACC-to-MDL projection specifically decreased the vicarious freezing behavior, suggesting that these neurons fire in a specific pattern to modulate these

behaviors. Our findings provide a mechanistic understanding of foot-shock-experienced vicarious freezing behavior and new clues for future studies of the mechanisms underlying more advanced empathy behaviors.

**Acknowledgements** We thank Dr. Dingcheng Wu for help in data analysis. We are also grateful for technical support from the Optical Imaging Facility and the Animal Facility of the Institute of Neuroscience, Chinese Academy of Sciences. This work was supported in part by The National Key Research and Development Program of China (2017YFB1300200, 2017YFB1300203) and the National Natural Science Foundation of China (61627808).

**Conflict of interest** The authors declare that the research was conducted in the absence of any commercial or financial relationship that could be construed as a potential conflict of interest.

## References

- de Waal FBM, Preston SD. Mammalian empathy: behavioural manifestations and neural basis. *Nat Rev Neurosci* 2017, 18: 498–509.
- Frith U, Happe F. Autism spectrum disorder. *Curr Biol* 2005, 15: R786–790.
- Baron-Cohen S, Ashwin E, Ashwin C, Tavassoli T, Chakrabarti B. Talent in autism: hyper-systemizing, hyper-attention to detail and sensory hypersensitivity. *Philos Trans R Soc Lond B Biol Sci* 2009, 364: 1377–1383.
- Achim AM, Ouellet R, Roy MA, Jackson PL. Assessment of empathy in first-episode psychosis and meta-analytic comparison with previous studies in schizophrenia. *Psychiatry Res* 2011, 190: 3–8.
- Horan WP, Reise SP, Kern RS, Lee J, Penn DL, Green MF. Structure and correlates of self-reported empathy in schizophrenia. *J Psychiatr Res* 2015, 66-67: 60–66.
- Derntl B, Finkelmeyer A, Toygar TK, Hulsmann A, Schneider F, Falkenberg DI, *et al.* Generalized deficit in all core components of empathy in schizophrenia. *Schizophrenia Res* 2009, 108: 197–206.
- de Waal FBM. Putting the altruism back into altruism: The evolution of empathy. *Annu Rev Psychol* 2008, 59: 279–300.
- Zaki J, Ochsner K. The neuroscience of empathy: progress, pitfalls and promise. *Nat Neurosci* 2012, 15: 675–680.
- Decety J. The neuroevolution of empathy. *Ann N Y Acad Sci* 2011, 1231: 35–45.
- Chen Q, Panksepp JB, Lahvis GP. Empathy is moderated by genetic background in mice. *PLoS One* 2009, 4: e4387.
- Jeon D, Kim S, Chetana M, Jo D, Ruley HE, Lin SY, *et al.* Observational fear learning involves affective pain system and Cav1.2 Ca<sup>2+</sup> channels in ACC. *Nat Neurosci* 2010, 13: 482–488.
- Sivaselvachandran S, Acland EL, Abdallah S, Martin LJ. Behavioral and mechanistic insight into rodent empathy. *Neurosci Biobehav Rev* 2018, 91: 130–137.
- Chen J. Empathy for distress in humans and rodents. *Neurosci Bull* 2018, 34: 216–236.
- Liddle MJ, Bradley BS, McGrath A. Baby empathy: infant distress and peer prosocial responses. *Infant Ment Health J* 2015, 36: 446–458.
- Kim S, Matyas F, Lee S, Acsady L, Shin HS. Lateralization of observational fear learning at the cortical but not thalamic level in mice. *Proc Natl Acad Sci U S A* 2012, 109: 15497–15501.
- Twining RC, Vantrease JE, Love S, Padival M, Rosenkranz JA. An intra-amygdala circuit specifically regulates social fear learning. *Nat Neurosci* 2017, 20: 459–469.
- Guzman YF, Tronson NC, Guedea A, Huh KH, Gao C, Radulovic J. Social modeling of conditioned fear in mice by non-fearful conspecifics. *Behav Brain Res* 2009, 201: 173–178.
- D'Amato FR. Kin interaction enhances morphine analgesia in male mice. *Behav Pharmacol* 1998, 9: 369–373.
- Allsop SA, Wichmann R, Mills F, Burgos-Robles A, Chang CJ, Felix-Ortiz AC, *et al.* Corticoamygdala transfer of socially derived information gates observational learning. *Cell* 2018, 173: 1329–1342 e1318.
- Kim EJ, Kim ES, Covey E, Kim JJ. Social transmission of fear in rats: the role of 22-kHz ultrasonic distress vocalization. *PLoS One* 2010, 5: e15077.
- Keum S, Kim A, Shin JJ, Kim JH, Park J, Shin HS. A missense variant at the *Nrxn3* locus enhances empathy fear in the mouse. *Neuron* 2018, 98: 588–601.e585.
- Hurlmann R, Patin A, Onur OA, Cohen MX, Baumgartner T, Metzler S, *et al.* Oxytocin enhances amygdala-dependent, socially reinforced learning and emotional empathy in humans. *J Neurosci* 2010, 30: 4999–5007.
- Kovacs B, Keri S. Off-label intranasal oxytocin use in adults is associated with increased amygdala-cingulate resting-state connectivity. *Eur Psychiatry* 2015, 30: 542–547.
- Meyer-Lindenberg A, Domes G, Kirsch P, Heinrichs M. Oxytocin and vasopressin in the human brain: social neuropeptides for translational medicine. *Nat Rev Neurosci* 2011, 12: 524–538.
- Pisansky MT, Hanson LR, Gottesman, II, Gewirtz JC. Oxytocin enhances observational fear in mice. *Nat Commun* 2017, 8: 2102.
- Bernhardt BC, Singer T. The neural basis of empathy. *Annu Rev Neurosci* 2012, 35: 1–23.
- Bolkan SS, Stujenske JM, Parnaudeau S, Spellman TJ, Rauffenbart C, Abbas AI, *et al.* Thalamic projections sustain prefrontal activity during working memory maintenance. *Nat Neurosci* 2017, 20: 987–996.
- Cardoso-Cruz H, Sousa M, Vieira JB, Lima D, Galhardo V. Prefrontal cortex and mediodorsal thalamus reduced connectivity is associated with spatial working memory impairment in rats with inflammatory pain. *Pain* 2013, 154: 2397–2406.
- Rikhye RV, Gilra A, Halassa MM. Thalamic regulation of switching between cortical representations enables cognitive flexibility. *Nat Neurosci* 2018, 21: 1753–1763.
- Marton TF, Seifkar H, Luongo FJ, Lee AT, Sohal VS. Roles of prefrontal cortex and mediodorsal thalamus in task engagement and behavioral flexibility. *J Neurosci* 2018, 38: 2569–2578.
- Jett JD, Bulin SE, Hatherall LC, McCartney CM, Morilak DA. Deficits in cognitive flexibility induced by chronic unpredictable stress are associated with impaired glutamate neurotransmission in the rat medial prefrontal cortex. *Neuroscience* 2017, 346: 284–297.
- Parnaudeau S, Taylor K, Bolkan SS, Ward RD, Balsam PD, Kellendonk C. Mediodorsal thalamus hypofunction impairs flexible goal-directed behavior. *Biol Psychiatry* 2015, 77: 445–453.
- Anticevic A, Cole MW, Repovs G, Murray JD, Brumbaugh MS, Winkler AM, *et al.* Characterizing thalamo-cortical disturbances in schizophrenia and bipolar illness. *Cereb Cortex* 2014, 24: 3116–3130.
- Woodward ND, Karbasforoushan H, Heckers S. Thalamocortical dysconnectivity in schizophrenia. *Am J Psychiatry* 2012, 169: 1092–1099.
- Anticevic A, Haut K, Murray JD, Repovs G, Yang GJ, Diehl C, *et al.* Association of thalamic dysconnectivity and conversion to psychosis in youth and young adults at elevated clinical risk. *JAMA Psychiatry* 2015, 72: 882–891.

36. Zhou Y, Fan L, Qiu C, Jiang T. Prefrontal cortex and the dysconnectivity hypothesis of schizophrenia. *Neurosci Bull* 2015, 31: 207–219.
37. Valdes-Hernandez PA, Sumiyoshi A, Nonaka H, Haga R, Aubert-Vasquez E, Ogawa T, *et al.* An *in vivo* MRI template set for morphometry, tissue segmentation, and fMRI localization in rats. *Front Neuroinform* 2011, 5: 26.
38. Zang Y, Jiang T, Lu Y, He Y, Tian L. Regional homogeneity approach to fMRI data analysis. *Neuroimage* 2004, 22: 394–400.
39. Song XW, Dong ZY, Long XY, Li SF, Zuo XN, Zhu CZ, *et al.* REST: a toolkit for resting-state functional magnetic resonance imaging data processing. *PLoS One* 2011, 6: e25031.
40. Wu T, Grandjean J, Bosshard SC, Rudin M, Reutens D, Jiang T. Altered regional connectivity reflecting effects of different anaesthesia protocols in the mouse brain. *Neuroimage* 2017, 149: 190–199.
41. Yin Y, Jin CF, Eyler LT, Jin H, Hu XL, Duan L, *et al.* Altered regional homogeneity in post-traumatic stress disorder: a resting-state functional magnetic resonance imaging study. *Neurosci Bull* 2012, 28: 541–549.
42. Peng CY, Chen YC, Cui Y, Zhao DL, Jiao Y, Tang TY, *et al.* Regional coherence alterations revealed by resting-state fMRI in post-stroke patients with cognitive dysfunction. *PLoS One* 2016, 11: e0159574.
43. Atsak P, Orre M, Bakker P, Cerliani L, Roozendaal B, Gazzola V, *et al.* Experience modulates vicarious freezing in rats: a model for empathy. *PLoS One* 2011, 6: e21855.
44. Zhuo M. Long-term potentiation in the anterior cingulate cortex and chronic pain. *Philos Trans R Soc Lond B Biol Sci* 2014, 369: 20130146.
45. Matyas F, Lee J, Shin HS, Acsady L. The fear circuit of the mouse forebrain: connections between the mediodorsal thalamus, frontal cortices and basolateral amygdala. *Eur J Neurosci* 2014, 39: 1810–1823.
46. Sanders J, Mayford M, Jeste D. Empathic fear responses in mice are triggered by recognition of a shared experience. *PLoS One* 2013, 8: e74609.
47. Padilla-Coreano N, Do-Monte FH, Quirk GJ. A time-dependent role of midline thalamic nuclei in the retrieval of fear memory. *Neuropharmacology* 2012, 62: 457–463.
48. Schmitt LI, Wimmer RD, Nakajima M, Happ M, Mofakham S, Halassa MM. Thalamic amplification of cortical connectivity sustains attentional control. *Nature* 2017, 545: 219–223.
49. Alcaraz F, Fresno V, Marchand AR, Kremer EJ, Coutureau E, Wolff M. Thalamocortical and corticothalamic pathways differentially contribute to goal-directed behaviors in the rat. *Elife* 2018, 7.
50. Yerkes RM, Dodson JD. The relation of strength of stimulus to rapidity of habit-formation. *J Comp Neurol Psychol* 1908, 18: 459–482.
51. Arnsten AF, Wang MJ, Paspalas CD. Neuromodulation of thought: flexibilities and vulnerabilities in prefrontal cortical network synapses. *Neuron* 2012, 76: 223–239.
52. Arnsten AF, Cai JX, Murphy BL, Goldman-Rakic PS. Dopamine D1 receptor mechanisms in the cognitive performance of young adult and aged monkeys. *Psychopharmacology (Berl)* 1994, 116: 143–151.
53. Liu D, Gu XW, Zhu J, Zhang XX, Han Z, Yan WJ, *et al.* Medial prefrontal activity during delay period contributes to learning of a working memory task. *Science* 2014, 346: 458–463.
54. Barraza JA, Zak PJ. Empathy toward strangers triggers oxytocin release and subsequent generosity. *Ann N Y Acad Sci* 2009, 1167: 182–189.
55. Riem MM, Bakermans-Kranenburg MJ, Pieper S, Tops M, Boksem MA, Vermeiren RR, *et al.* Oxytocin modulates amygdala, insula, and inferior frontal gyrus responses to infant crying: a randomized controlled trial. *Biol Psychiatry* 2011, 70: 291–297.
56. Mitre M, Marlin BJ, Schiavo JK, Morina E, Norden SE, Hackett TA, *et al.* A distributed network for social cognition enriched for oxytocin receptors. *J Neurosci* 2016, 36: 2517–2535.
57. Li K, Nakajima M, Ibanez-Tallon I, Heintz N. A cortical circuit for sexually dimorphic oxytocin-dependent anxiety behaviors. *Cell* 2016, 167: 60–72 e11.



# Dopamine D2 Receptor-Mediated Modulation of Rat Retinal Ganglion Cell Excitability

Ning Yin<sup>1</sup> · Yu-Long Yang<sup>1</sup> · Shuo Cheng<sup>1</sup> · Hong-Ning Wang<sup>1</sup> · Xin Hu<sup>1</sup> ·  
Yanying Miao<sup>1</sup> · Fang Li<sup>1</sup> · Zhongfeng Wang<sup>1</sup>

Received: 7 April 2019 / Accepted: 9 June 2019 / Published online: 12 October 2019  
© Shanghai Institutes for Biological Sciences, CAS 2019

**Abstract** Ganglion cells (RGCs) are the sole output neurons of the retinal circuitry. Here, we investigated whether and how dopamine D2 receptors modulate the excitability of dissociated rat RGCs. Application of the selective D2 receptor agonist quinpirole inhibited outward  $K^+$  currents, which were mainly mediated by glybenclamide- and 4-aminopyridine-sensitive channels, but not the tetraethylammonium-sensitive channel. In addition, quinpirole selectively enhanced Nav1.6 voltage-gated  $Na^+$  currents. The intracellular cAMP/protein kinase A,  $Ca^{2+}$ /calmodulin-dependent protein kinase II, and mitogen-activated protein kinase/extracellular signal-regulated kinase signaling pathways were responsible for the effects of quinpirole on  $K^+$  and  $Na^+$  currents, while phospholipase C/protein kinase C signaling was not involved. Under current-clamp conditions, the number of action potentials evoked by positive current injection was increased by quinpirole. Our results suggest that D2 receptor activation increases RGC excitability by suppressing outward  $K^+$  currents and enhancing Nav1.6 currents, which may affect retinal visual information processing.

**Keywords** Retinal ganglion cell · Dopamine D2 receptor · Outward  $K^+$  current · Nav1.6 voltage-gated  $Na^+$  current · Excitability

## Introduction

By activating distinct G-protein-coupled receptors, dopamine (DA) has been demonstrated to be involved in diverse functions in the central nervous system [1–6]. Five DA receptor (DAR) subtypes (D1–D5) have been identified according to their biochemical and pharmacological characteristics. On the basis of their effects on adenylate cyclase activity, DARs are further classified into D1 (subtypes D1 and D5) and D2 receptors (subtypes D2, D3, and D4). Activation of D1 receptors positively regulates adenylate cyclase activity by coupling with the  $G_s$  protein, while activation of D2 receptors negatively regulates adenylate cyclase activity through the  $G_{i/o}$  protein [3, 7, 8].

DA, released mainly from dopaminergic amacrine cells in retina, plays an important role in modulating retinal neuronal functions [9–12]. As the sole output neurons of the retina, ganglion cells (RGCs) integrate retinal visual signals. Therefore, changes in the excitability of RGCs may modulate visual information processing in the retina. It has been reported that DA might change RGC spiking by regulating retinal neuronal circuits [13–16]. In addition, DA might also modulate RGC activity directly. For example, DA inhibits the discharges of dissociated RGCs by modulating voltage-dependent  $Na^+$  channels [17–20]. RGCs express DARs [18, 21, 22], while also expressing various voltage-gated ion channels [23–27]. There is evidence that stimulation of D1 receptors reduces outward  $K^+$  current amplitudes in rat RGC preparations and

Ning Yin and Yu-Long Yang have contributed equally to this work.

**Electronic supplementary material** The online version of this article (<https://doi.org/10.1007/s12264-019-00431-3>) contains supplementary material, which is available to authorized users.

✉ Zhongfeng Wang  
zfwang@fudan.edu.cn

<sup>1</sup> Department of Neurology, State Key Laboratory of Medical Neurobiology and MOE Frontiers Center for Brain Science, Institutes of Brain Science, Zhongshan Hospital, Fudan University, Shanghai 200032, China

hyperpolarization-activated cation currents in retinal slices [28, 29]. Our recent study showed that temporal summation of excitatory postsynaptic potentials in rat RGCs is enhanced by D1 receptor activation, mainly by affecting inward-rectifier  $K^+$  (Kir) currents [30]. These studies indicate that RGC excitability is influenced by D1 receptor stimulation. Moreover, activation of D2 receptors modulates neuronal excitability and synaptic integration in different brain regions, thereby participating in the regulation of reward-related behaviors, working memory, and locomotion [2]. D2 receptor-induced modulation of neuronal excitability is largely a result of changes in the functions of voltage-gated ion channels [31–35]. In the present study, we investigated the effects of D2 receptors on RGC excitability and the underlying mechanisms by whole-cell patch-clamp recording in acutely-dissociated rat RGCs.

## Materials and Methods

### Animals

All experimental procedures were performed in compliance with the National Institutes of Health guidelines for the Care and Use of Laboratory Animals. The experimental protocol was approved by the Animal Care Committee of the Institutes of Brain Science, Fudan University. Male Sprague-Dawley rats (70 g–100 g, 4 weeks–5 weeks old) were purchased from the SLAC Laboratory Animal Co., Ltd (Shanghai, China). Animals were housed on a 12-h light/dark cycle. To the best of our ability, we minimized the number of animals used in this study, and ameliorated their suffering.

### Retrograde Labeling of RGCs

RGCs were retrogradely labeled following the procedures previously described in detail [29, 37]. RGCs were labeled with 1% cholera toxin B subunit (CTB; List Biological Laboratories, Campbell, CA) or 4% rhodamine-B-isothiocyanate (RITC; List Biological Laboratories).

### Preparation of Isolated RGCs

Isolated RGCs were obtained by digesting retinal tissue with papain and mechanically dissociated as previously described [29, 38].

### Immunohistochemistry and Immunocytochemistry

Immunohistochemistry was performed in vertical retinal slices and immunocytochemistry in isolated RGCs,

following the procedures described previously [29, 36, 39]. The primary antibodies used were anti-dopamine D2 receptor antibody (1:200 dilution; AB1558, Chemicon International Inc., Temecula, CA) and polyclonal goat anti-CTB (1:4000, List Biological Laboratories). Images were captured using a Leica SP2 confocal laser-scanning microscope (Nussloch, Germany).

### Whole-Cell Patch-Clamp Recordings

Standard whole-cell patch-clamp techniques were applied to record membrane currents and potentials in RITC-labeled RGCs using a patch amplifier (Axopatch700B; Molecular Devices, Novato, CA) with a Digidata 1440A data acquisition board and pClamp 10.2 software [37, 38, 40]. The sampling rate was set at 10 kHz, and signals were filtered at 1 kHz. The recording pipettes (3 M $\Omega$ –6 M $\Omega$ ) were filled with internal solutions. The bath solution used for  $K^+$  current recordings consisted of (in mmol/L) NaCl 140, KCl 5, CaCl<sub>2</sub> 2, MgCl<sub>2</sub> 1, HEPES 10, and glucose 20, with 0.5  $\mu$ mol/L tetrodotoxin (TTX) and 100  $\mu$ mol/L CdCl<sub>2</sub> (pH 7.4 with NaOH, 300 mOsm/L–310 mOsm/L with sucrose); the pipette solution contained (in mmol/L) KCl 140, NaCl 9, MgCl<sub>2</sub> 1, EGTA 0.2, ATP-Mg 2, GTP-Na 0.25, and HEPES 10 (pH 7.2 with KOH, 290 mOsm/L–300 mOsm/L with sucrose). To record Na<sup>+</sup> currents, the bath solution contained (in mmol/L) NaCl 130, CaCl<sub>2</sub> 2, MgCl<sub>2</sub> 1, HEPES 10, tetraethylammonium (TEA)-Cl 15, 4-aminopyridine (4-AP) 10, and glucose 10 (pH 7.4 with NaOH, 300 mOsm/L–310 mOsm/L with sucrose); the pipette solution contained (in mmol/L) CsCl 130, NaCl 10, HEPES 5, EGTA 8, TEA-Cl 10, ATP-Mg 2, and GTP-Na 1 (pH 7.2 adjusted with CsOH, 290 mOsm/L–300 mOsm/L with sucrose). To record evoked action potentials, the bath solution consisted of (in mmol/L) NaCl 135, KCl 3, CaCl<sub>2</sub> 2, MgCl<sub>2</sub> 1, HEPES 10, glucose 11, and sucrose 10 (pH 7.4 with NaOH, 300 mOsm/L–310 mOsm/L with sucrose), while the pipettes were filled with an internal solution containing (in mmol/L) potassium D-glucuronate 120, EGTA 1, HEPES 10, ATP-Mg 4, GTP-Na 0.3, phosphocreatine 10, CaCl<sub>2</sub> 0.1, and MgCl<sub>2</sub> 1 (pH 7.2 with KOH, 280 mOsm/L–290 mOsm/L with sucrose). All experiments were performed at room temperature (22 °C–25 °C).

### Reagents and Drug Application

Quinpirole, sulpiride, 4-AP, TEA, Rp-cAMP, bisindolylmaleimide IV (Bis IV), KN-62, ICA121431, 4-diamino-2,3-dicyano-1,4-bis[2-aminophenylthio]butadiene (U0126), 4,9-anhydrotetrodotoxin (AHTTX), phrixotoxin-3, and TTX were from Tocris (Tocris Bioscience, Ellisville, MO), while others were from Sigma (Sigma-

**Fig. 1** Suppression of outward  $K^+$  currents by activating D2 receptors in rat RGCs. **A** Representative outward  $K^+$  currents recorded from an RGC, showing that extracellular application of quinpirole (10  $\mu\text{mol/L}$ ), a selective D2 receptor agonist, significantly suppressed the current amplitudes. The cell was held at  $-70$  mV and the currents were evoked by a series of voltage pulses (from  $-70$  mV to  $+30$  mV in increments of 10 mV). **B, C**  $I$ - $V$  curves showing that quinpirole voltage-dependently suppressed average peak (**B**) and steady-state (**C**) current amplitudes ( $n = 12$ ).  $**P < 0.01$ ,  $***P < 0.001$  vs control. **D** Time course of quinpirole-induced suppression of  $K^+$  currents at  $+30$  mV. Note that the current amplitudes were almost unchanged during a period of 8 min without quinpirole (Control), while quinpirole significantly reduced the current amplitudes. **E, F** Concentration-dependent suppression of peak (**E**) and steady-state (**F**) current amplitudes by quinpirole ( $n = 7$ – $11$  for each quinpirole concentration). **G** Sample current traces showing that sulpiride (10  $\mu\text{mol/L}$ ), a selective D2 receptor antagonist, blocked the quinpirole-induced suppression of  $K^+$  currents recorded in a rat RGC. Bar chart summarizing the changes of  $K^+$  current amplitudes at  $+30$  mV under different conditions ( $n = 11$ ). All data are normalized to control and presented as the mean  $\pm$  SEM.

Aldrich, Inc., St. Louis, MO). The drug-containing solution was delivered by a stepper motor-based rapid solution exchanger (RSC-160, Bio-Logic, Claix, France) [29, 38].

### Data Analysis

Data were analyzed using Clampfit 10.2 (Molecular Devices, Foster City, CA), SigmaPlot 10.0 (version 10.0, Systat Software Inc., San Jose, CA), and Igor 4.0 software (WaveMetrics, Lake Oswego, OR). A Boltzmann function was used to fit the activation and inactivation curves. Data are shown as the mean  $\pm$  SEM. Statistical analysis was performed by either one-way ANOVA with Bonferroni's *post-hoc* test (multiple comparisons) or the paired *t* test. A *P* value  $< 0.05$  was considered significant.

## Results

### Activation of D2 Receptors Selectively Suppresses Glybenclamide- and 4-AP-Sensitive Outward $K^+$ Currents

It has been shown that D2 receptors are expressed in cells of the retinal ganglion cell layer [22] and D2 receptor agonists and antagonists modulate the responses of rat RGCs [19, 41], suggesting that D2 receptors are expressed in rat RGCs. We first detected the expression of D2 receptors on isolated RGCs labelled retrogradely with CTB using double immunofluorescent labeling (Fig. S1A). We further confirmed the expression of D2 receptors on RGCs in retinal vertical slices in which labeled D2 receptors colocalized with RGCs retrogradely labeled by CTB

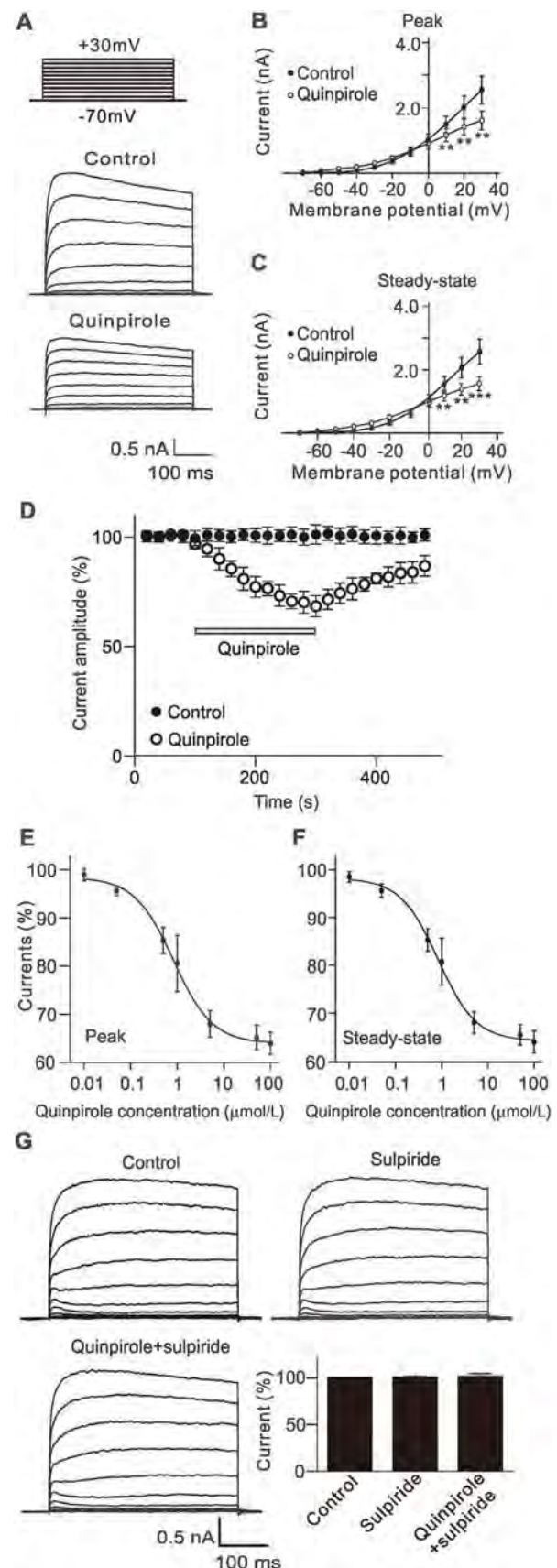


(Fig. S1B). To avoid possible non-specific binding of the D2 receptor antibody, we did negative control experiment by replacing the D2 receptor antibody with phosphate-buffered saline. This experiment demonstrated the specificity of the D2 receptor antibody used in the present study (Fig. S1B). These results confirmed that D2 receptors are indeed expressed in rat retinal RGCs.

Outward  $K^+$  currents in rat RGCs were recorded and the effects of D2 receptor activation on these currents were examined. The protocol for inducing the  $K^+$  currents is shown in Fig. 1A. RGCs were held at  $-70$  mV and stepped to  $+30$  mV in increments of  $10$  mV. Bath application of quinpirole ( $10$   $\mu$ mol/L), a selective D2 receptor agonist, markedly reduced the  $K^+$  current amplitudes (Fig. 1A). The current-voltage curves showed that quinpirole inhibited the  $K^+$  currents in a voltage-dependent manner (Fig. 1B, C). The time course of changes in  $K^+$  current amplitudes at  $+30$  mV with or without quinpirole clearly showed that stable recordings could be obtained in the control group (Fig. 1D). Extracellular application of quinpirole ( $10$   $\mu$ mol/L) progressively reduced the current amplitudes and washout with normal solution brought the currents to the control level. Moreover, the suppressive effect of quinpirole on the  $K^+$  currents was dose-dependent (Fig. 1E, F). To confirm the quinpirole effect was through activating D2 receptors, sulpiride ( $10$   $\mu$ mol/L), a selective D2 receptor antagonist, was first applied to RGCs, which did not change the  $K^+$  currents ( $100.4\% \pm 1.4\%$  of control,  $n = 11$ ,  $P = 0.803$ ); then, co-application of quinpirole failed to suppress the  $K^+$  currents ( $101.4\% \pm 3.2\%$  of control,  $n = 11$ ,  $P = 0.684$ ) (Fig. 1G). These results indicated that the effect of quinpirole is indeed through activating D2 receptors.

RGCs are known to express various  $K^+$  channels, including large-conductance  $Ca^{2+}$ -activated  $K^+$  channels ( $BK_{Ca}$ ) that are sensitive to TEA, delayed rectifying  $K^+$  channels that are blocked by 4-AP, and ATP-sensitive  $K^+$  channels ( $K_{ATP}$ ) that are sensitive to glybenclamide (Gb) [24, 26, 29]. We then set out to identify which  $K^+$  channels were modulated by activating D2 receptors. Fig. 2A shows that the outward  $K^+$  currents recorded from RGCs pretreated with 4-AP ( $5$  mmol/L) and TEA ( $10$  mmol/L) were still clearly reduced by perfusion with quinpirole. At  $+30$  mV, the average current amplitude was reduced to  $68.8\% \pm 5.2\%$  of control ( $n = 8$ ,  $P = 0.002$ ; Fig. 2B). Similarly, when TEA- and Gb-sensitive currents were blocked by pretreatment with TEA ( $10$  mmol/L) and Gb ( $10$   $\mu$ mol/L), the quinpirole-induced suppression of  $K^+$  currents still occurred ( $80.2\% \pm 3.8\%$  of control,  $n = 10$ ,  $P = 0.002$ ) (Fig. 2C, D). In contrast, after blockade of Gb- and 4-AP-sensitive  $K^+$  currents, the remaining currents were not influenced by quinpirole application ( $97.6\% \pm 1.3\%$  of control,  $n = 9$ ,  $P = 0.099$ ; Fig. 2E, F), suggesting that D2

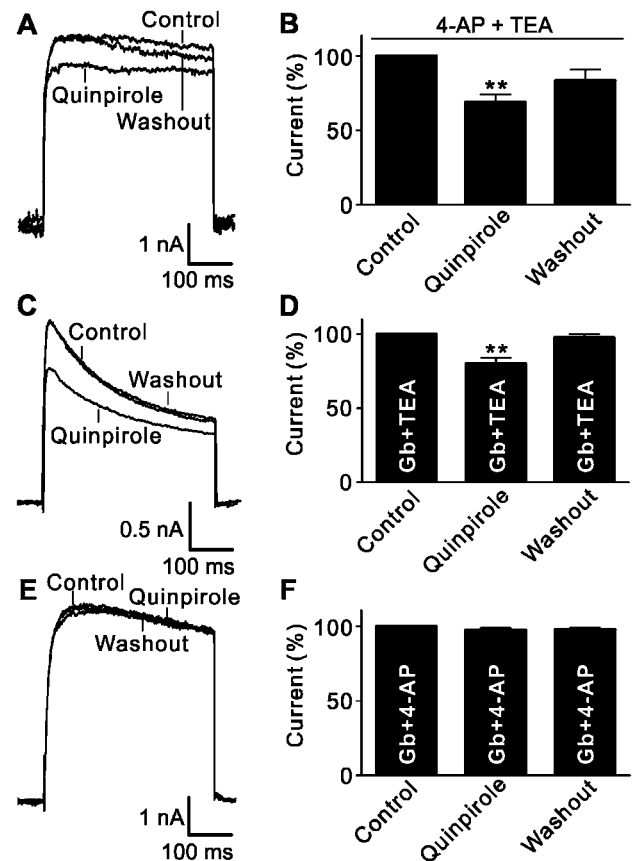


**Fig. 2** Quinpirole selectively suppresses Gb- and 4-AP-sensitive  $K^+$  current components. **A** Representative current traces recorded from an RGC, showing that extracellular application of  $10$   $\mu$ mol/L quinpirole still suppressed the current amplitude after the 4-AP- and TEA-sensitive current components were blocked. **B** Bar chart summarizing the changes of  $K^+$  current amplitudes at  $+30$  mV ( $n = 8$ ,  $**P < 0.01$  vs control). **C** Representative current recordings from an RGC, showing that extracellular application of quinpirole ( $10$   $\mu$ mol/L) significantly reduced the current amplitude in the presence of Gb ( $10$   $\mu$ mol/L) and TEA ( $10$  mmol/L). **D** Bar chart summarizing the changes of  $K^+$  current amplitudes at  $+30$  mV under different conditions ( $n = 10$ ,  $**P < 0.01$  vs control). **E** Sample current traces from an RGC showing that quinpirole ( $10$   $\mu$ mol/L) did not further reduce the current amplitude after the Gb- and 4-AP-sensitive components were blocked. **F** Bar chart summarizing the changes of  $K^+$  current amplitudes at  $+30$  mV ( $n = 9$ ).

receptors selectively modulate the Gb- and 4-AP-sensitive  $K^+$  channels.

#### cAMP/PKA, CaMKII, and MAPK/ERK Signaling Pathways are Involved in D2 Receptor-Mediated Effects

We then further investigated the possible signaling pathways involved in the D2 receptor-mediated effect on  $K^+$  currents. There is evidence showing that D2 receptors are linked to many intracellular signaling pathways [32, 42, 43]. We first examined the possible involvement

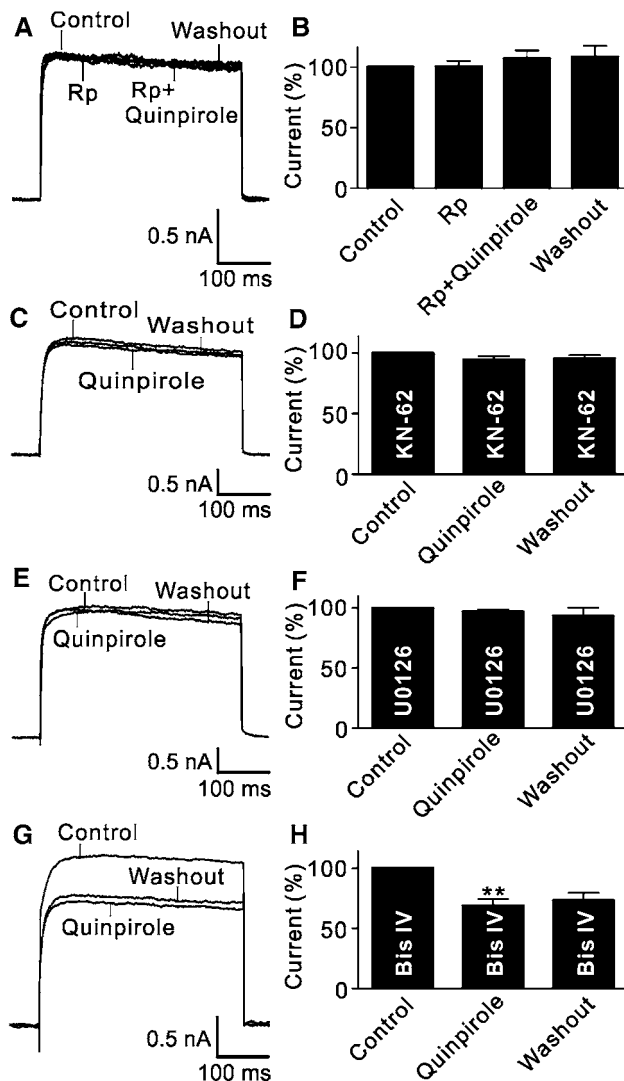


**Fig. 3** Signaling pathways involved in the quinpirole-induced suppression of outward  $K^+$  channels. **A** Representative current traces recorded from an RGC, showing that quinpirole did not change the outward  $K^+$  current amplitude when the cell was perfused with Rp-cAMP (2  $\mu\text{mol/L}$ ). **B** Bar chart summarizing the changes in  $K^+$  current amplitudes at +30 mV under different conditions ( $n = 13$ ). **C**, **D** Sample current traces showing that the CaMKII signaling inhibitor KN-62 (10  $\mu\text{mol/L}$ ) blocked the quinpirole-induced suppression of outward  $K^+$  currents (**C**), and summary data are shown in (**D**) ( $n = 11$ ). **E** Sample current traces showing that U0126 (10  $\mu\text{mol/L}$ ), a MAPK/ERK signaling inhibitor, blocked the quinpirole-induced suppression of outward  $K^+$  currents. **F** Bar chart summarizing the changes of outward  $K^+$  current amplitudes at +30 mV ( $n = 12$ ). **G** Representative current traces recorded from an RGC, showing that the PKC inhibitor Bis IV (10  $\mu\text{mol/L}$ ) failed to block the quinpirole-induced suppression of outward  $K^+$  currents. **H** Summary bar graphs for the effect of Bis IV on the quinpirole-induced suppression of outward  $K^+$  currents ( $n = 14$ ,  $^{**}P < 0.01$  vs control).

of the forskolin-stimulated cAMP/protein kinase A (PKA) signaling pathway. Perfusion with Rp-cAMP (2  $\mu\text{mol/L}$ ), a cAMP/PKA pathway inhibitor [29, 38], for at least 3 min did not change the  $K^+$  current amplitude recorded from

RGCs ( $100.7\% \pm 4.6\%$  of control,  $n = 13$ ,  $P = 0.926$ ; Fig. 3A), and the current remained unchanged when quinpirole was added ( $107.3\% \pm 6.7\%$  of control,  $n = 13$ ,  $P = 0.403$ ; Fig. 3B). Similarly, when RGCs were intracellularly dialyzed with KN-62 (10  $\mu\text{mol/L}$ ), a  $\text{Ca}^{2+}$ -calmodulin-dependent protein kinase II (CaMKII) pathway blocker, or U0126 (10  $\mu\text{mol/L}$ ), a specific inhibitor of the mitogen-activated protein kinase (MAPK)/extracellular signal-regulated kinase (ERK) pathway, through the recording pipette [38], extracellular perfusion with quinpirole no longer suppressed outward  $K^+$  currents ( $94.5\% \pm 3.1\%$  of control for KN-62,  $n = 11$ ,  $P = 0.247$ ;  $96.8\% \pm 2.1\%$  of control for U0126,  $n = 12$ ,  $P = 0.06$ ; Fig. 3C–F). Although activation of D2 receptors may also be coupled to the phospholipase C (PLC)/protein kinase C (PKC) pathway, experiments involving this pathway presented different results. After blocking PKC by intracellular dialysis with the PKC inhibitor Bis IV (10  $\mu\text{mol/L}$ ) [29, 38], the  $K^+$  currents recorded from RGCs were still reduced by quinpirole ( $68.9\% \pm 5.7\%$  of control,  $n = 14$ ,  $P = 0.004$ ; Fig. 3G, H).

#### Activation of D2 Receptors Selectively Increases Nav1.6 Channel Currents

RGCs express voltage-gated  $\text{Na}^+$  channels [27, 44, 45], so we further investigated whether activation of D2 receptors modulates  $\text{Na}^+$  currents in acutely isolated rat RGCs.  $\text{Na}^+$  currents were induced by 50-ms depolarizing voltage pulses from a holding potential of  $-70$  mV to  $+30$  mV in steps of 10 mV. Bath application of quinpirole remarkably enhanced the current amplitudes (Fig. 4A, B). The current-voltage curves showed that quinpirole voltage-dependently enhanced the current amplitudes (Fig. 4C). For example, the current amplitude at  $-20$  mV was significantly increased to  $130.2\% \pm 5.2\%$  of control by quinpirole ( $n = 12$ ,  $P < 0.001$ ). The time course of quinpirole-induced changes in  $\text{Na}^+$  current amplitudes at  $-20$  mV showed that they remained unchanged during 8 min of recording; extracellular application of quinpirole (10  $\mu\text{mol/L}$ ) significantly enhanced the current amplitudes; and the currents returned to the control level after washout (Fig. 4D). The quinpirole effect on  $\text{Na}^+$  currents was through activating D2 receptors. In the presence of sulpiride, addition of quinpirole failed to change the  $\text{Na}^+$  current amplitude ( $104.5\% \pm 2.6\%$  of control,  $n = 6$ ,  $P = 0.129$ ; Fig. 4E, F).

We also studied changes in the activation and inactivation curves of  $\text{Na}^+$  channels. The steady-state activation curve of  $\text{Na}^+$  channels was not significantly shifted after quinpirole application; the  $V_h$  value obtained from Boltzmann function fitting was  $-31.4$  mV  $\pm$  0.98 mV ( $n = 10$ ), which was comparable to that of control ( $-29.2$  mV  $\pm$

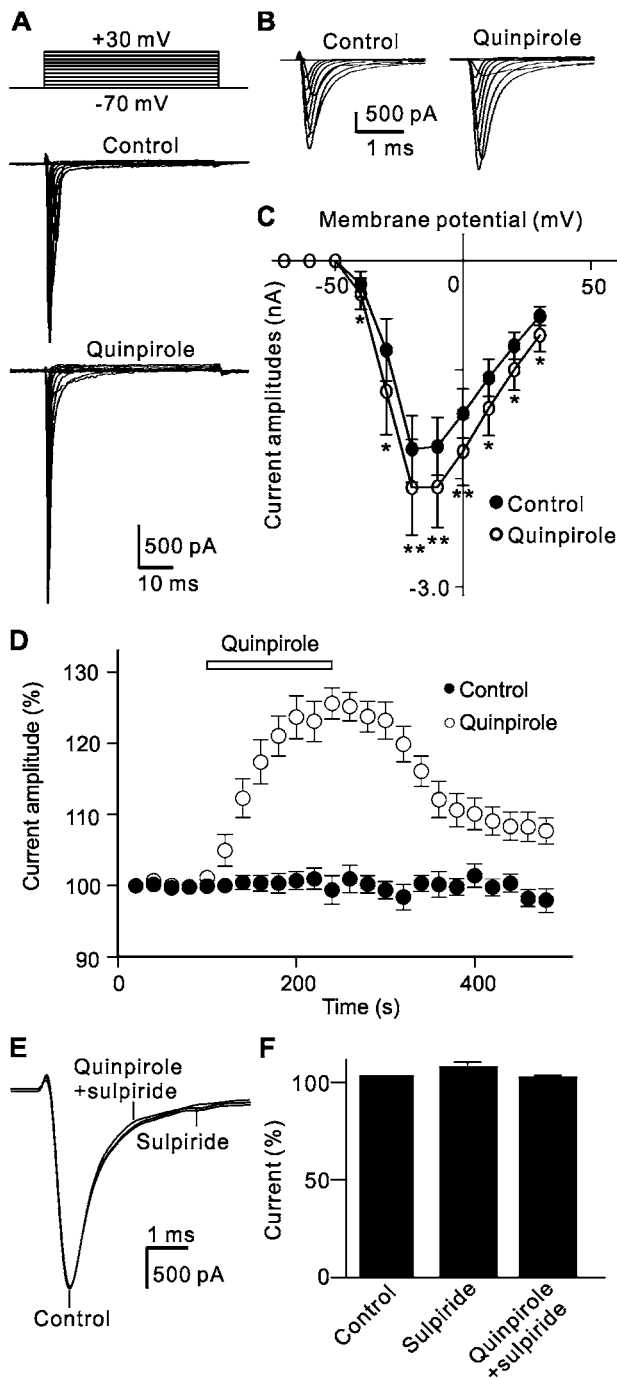


**Fig. 4** D2 receptor activation-induced enhancement of Na<sup>+</sup> channel currents in rat RGCs. **A** Representative Na<sup>+</sup> currents recorded from an RGC showing that extracellular application of quinpirole (10 μmol/L) significantly increased the current amplitudes. The cell was held at -70 mV and the currents were induced by a series of depolarizing voltage pulses from -70 mV to +30 mV at steps of 10 mV. **B** Expanded peak current traces before and after quinpirole application as in **A**. **C** I-V curves showing that quinpirole voltage-dependently enhanced Na<sup>+</sup> currents (n = 12; \*P < 0.05, \*\*P < 0.01 vs control). **D** Time course of quinpirole-induced enhancement of Na<sup>+</sup> currents at -20 mV. Note that the current amplitudes were almost unchanged during a period of 8 min without quinpirole (Control), while quinpirole significantly increased the current amplitudes. **E** Sample current traces showing that the quinpirole-induced increase in Na<sup>+</sup> currents was blocked by sulpiride (10 μmol/L). **F** Bar chart summarizing the changes of Na<sup>+</sup> current amplitudes at -20 mV under different conditions (n = 6).

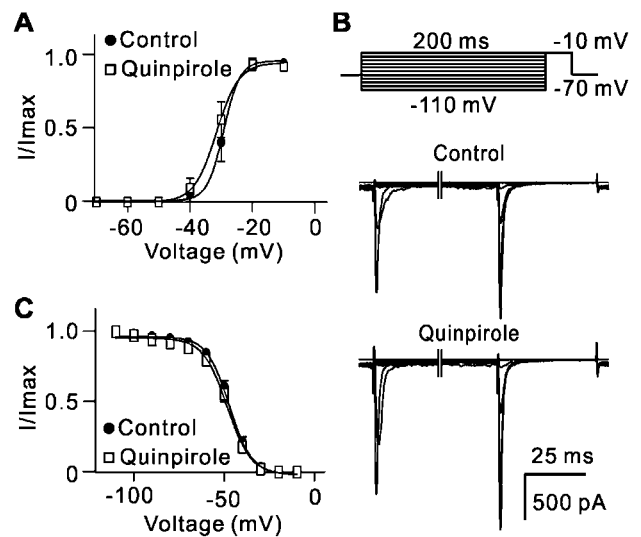


**Fig. 5** Activation of D2 receptors has no effect on activation and inactivation curves of Na<sup>+</sup> currents. **A** Activation curves of Na<sup>+</sup> currents before and after quinpirole (10 μmol/L) application. Normalized points are fitted with a Boltzmann function (n = 12). **B** Representative Na<sup>+</sup> currents in an RGC evoked when the cells were first hyperpolarized to different potentials from a holding potential of -70 mV and then depolarized to -10 mV before and after application of quinpirole (10 μmol/L). **C** Inactivation curves of Na<sup>+</sup> currents before and after application of quinpirole. Normalized points are fitted with a Boltzmann function (n = 12).

0.89 mV) (n = 10, P = 0.521; Fig. 5A). The inactivation curves also fitted a Boltzmann function. The cells were first given a 200-ms pre-pulse from a holding potential of -70 mV to different potentials, and then depolarized to -10 mV. The inactivation curves of the channels before and after quinpirole application were almost same (V<sub>h</sub> values: -47.1 ± 0.57 mV in control; -48.3 ± 0.63 mV in quinpirole group, n = 12, P = 0.881; Fig. 5B, C).

There are two components in Na<sup>+</sup> channel currents, TTX-sensitive and TTX-resistant, both of which are expressed in sensory neurons of the mammalian nervous system [23]. Perfusion with 500 nmol/L TTX almost completely inhibited Na<sup>+</sup> currents in isolated RGCs (Fig. 6A), suggesting that only TTX-sensitive Na<sup>+</sup> channels are expressed in rat RGCs. Several Na<sup>+</sup> channel subunits, including Nav1.1, Nav1.2, and Nav1.6, are expressed in RGCs [25, 27]. Our results showed that bath application of 10 nmol/L phrixotoxin-3 (Ph3), a Nav1.2

blocker, reduced the Na<sup>+</sup> current amplitude to  $96.5\% \pm 0.7\%$  of control ( $n = 6$ ,  $P = 0.007$ ), and addition of  $1 \mu\text{mol/L}$  ICA121431 (ICA), a Nav1.1 blocker, reduced the currents to  $78.0\% \pm 2.9\%$  of control ( $n = 6$ ,  $P = 0.005$ ), and further to  $13.6\% \pm 2.4\%$  of control ( $n = 6$ ,  $P = 0.002$ ) when  $100 \text{ nmol/L}$  4,9-anhydrotetrodotoxin (AHTTX), a Nav1.6 blocker [46, 47], was added (Fig. 6B, C). These results demonstrated that Nav1.6 is the dominant Na<sup>+</sup> channel in rat RGCs although other subunits are also expressed.

We further determined which subunit(s) of the Na<sup>+</sup> channels are modulated by activation of D2 receptors. In the presence of ICA and Ph3, bath application of quinpirole still enhanced the Na<sup>+</sup> currents ( $125.6\% \pm 4.3\%$  of control,  $n = 10$ ,  $P < 0.001$ ) (Fig. 6D, E). The increase was comparable to that of quinpirole in the absence of ICA and Ph3 ( $130.2\% \pm 5.2\%$  of control,  $P = 0.351$ ; Fig. 5A–C). In contrast, bath application of quinpirole had no effect on the currents when the cells were pretreated with AHTTX ( $102.5\% \pm 5.4\%$  of control,  $n = 11$ ,  $P = 0.567$ ; Fig. 6F, G), suggesting that activation of D2 receptors selectively enhances Na<sup>+</sup> currents mediated by the Nav1.6 subunit in rat RGCs.

### Involvement of Signaling Pathways in the Quinpirole-Induced Enhancement of Na<sup>+</sup> Currents

The intracellular signaling pathways mediating the effect of D2 receptor activation on Nav1.6 currents were similar to those on outward K<sup>+</sup> currents. Quinpirole failed to enhance the current amplitude when the cells were pretreated with Rp-cAMP ( $110.1\% \pm 5.7\%$  of control,  $n = 9$ ,  $P = 0.121$ ; Fig. 7A, B). Moreover, when the CaMKII and MAPK/ERK pathways were blocked by intracellular dialysis with KN-62 or U0126 through the recording pipette, quinpirole perfusion had no significant effect on the current amplitudes ( $106.6\% \pm 4.9\%$  of control for KN-62,  $n = 12$ ,  $P = 0.25$ ;  $102.4\% \pm 2.5\%$  of control for U0126,  $n = 11$ ,  $P = 0.447$ ; Fig. 7C–F). In addition, when PKC was inhibited by Bis IV, quinpirole continued to enhance the currents ( $117.8\% \pm 3.1\%$  of control,  $n = 10$ ,  $P < 0.01$ ; Fig. 7G, H).

### D2 Receptor Activation Increases the Number of Evoked Action Potentials in RGCs

DA may modulate voltage-gated ion channels, thereby influencing the excitability of RGCs [17, 18, 28, 30]. The above results showed that activation of D2 receptors suppressed outward K<sup>+</sup> current and enhanced Na<sup>+</sup> current. We then tested whether D2 receptor activation changes RGC excitability by recording the numbers of action potentials induced by current injection before (control) and

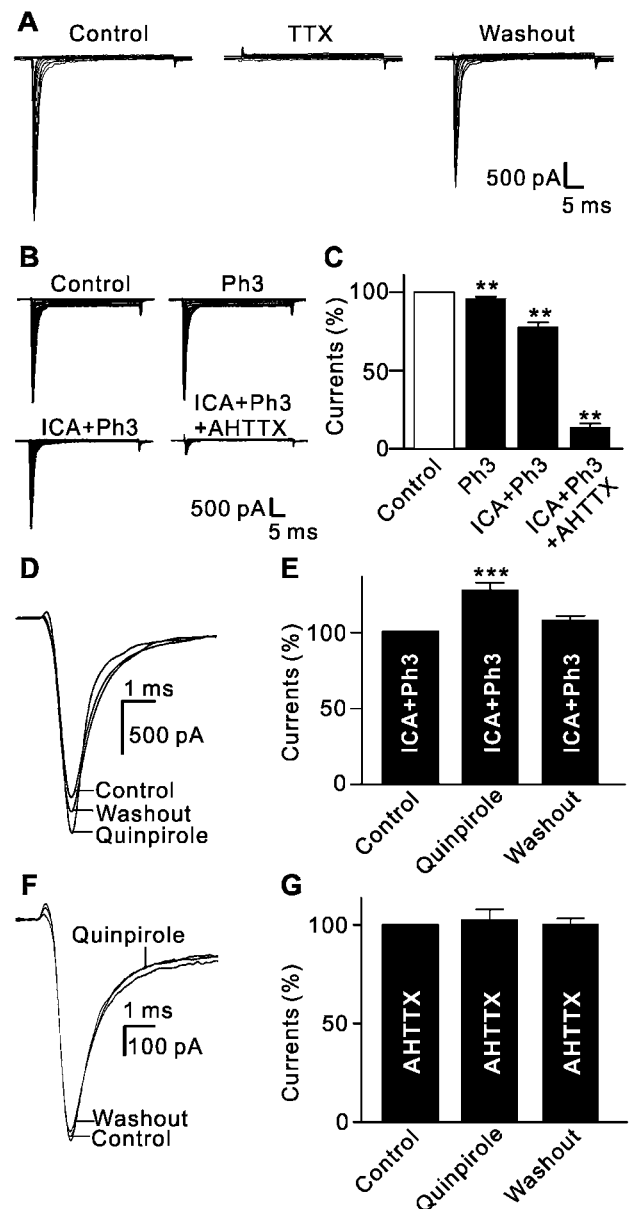


**Fig. 6** Activation of D2 receptors selectively enhances Nav1.6 voltage-gated Na<sup>+</sup> currents. **A** Representative current recordings from an RGC, showing that TTX ( $500 \text{ nmol/L}$ ) completely and reversibly suppressed Na<sup>+</sup> currents. **B** Representative Na<sup>+</sup> currents recorded from an RGC, showing the effects of successive addition of the Nav1.2 blocker phrixotoxin-3 (Ph3,  $10 \text{ nmol/L}$ ), the Nav1.1 blocker ICA121431 (ICA,  $1 \mu\text{mol/L}$ ), and the Nav1.6 blocker 4,9-anhydrotetrodotoxin (4,9-AHTTX,  $100 \text{ nmol/L}$ ). **C** Bar chart summarizing the changes in Na<sup>+</sup> current amplitudes at  $-20 \text{ mV}$  under different conditions ( $n = 6/\text{group}$ ,  $**P < 0.01$  vs control). **D** Sample current traces showing that extracellular application of quinpirole ( $10 \mu\text{mol/L}$ ) still enhanced current amplitudes after blocking the Nav1.1 and Nav1.2 channels. **E** Bar chart summarizing the changes in the Na<sup>+</sup> current amplitudes at  $-20 \text{ mV}$  ( $n = 10$ ,  $***P < 0.001$  vs control). **F** Sample current traces showing that extracellular application of quinpirole ( $10 \mu\text{mol/L}$ ) failed to change Na<sup>+</sup> currents after blocking the Nav1.6 channels. **G** Bar chart summarizing the changes in the Na<sup>+</sup> current amplitudes at  $-20 \text{ mV}$  ( $n = 11$ ).

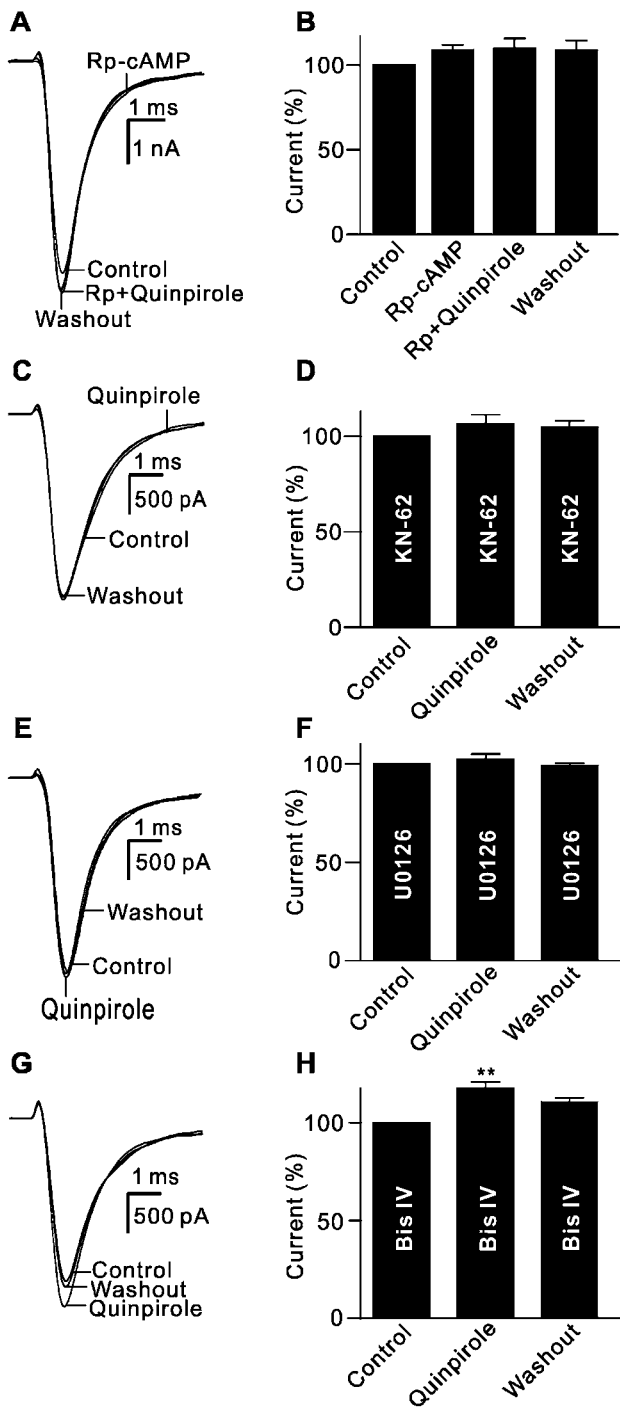


**Fig. 7** Signaling pathways involved in the quinpirole-induced enhancement of Na<sup>+</sup> channels. **A** Sample current traces showing that Rp-cAMP (2 μmol/L) blocked the quinpirole-induced enhancement of Na<sup>+</sup> currents. **B** Bar chart summarizing the changes in Na<sup>+</sup> current amplitudes at -20 mV under different conditions (*n* = 9). **C**, **D** Sample current traces showing that extracellular application of quinpirole (10 μmol/L) failed to change Na<sup>+</sup> currents when the cell was pre-treated with 10 μmol/L KN-62 (**C**), and summary data are shown in (**D**) (*n* = 10). **E**, **F** Sample current traces showing that U0126 (10 μmol/L) blocked the quinpirole-induced enhancement of Na<sup>+</sup> currents (**E**), and cumulative data are shown in (**F**) (*n* = 11). **G** Sample current traces showing that extracellular application of quinpirole (10 μmol/L) enhanced Na<sup>+</sup> currents when the cell was pre-treated by 10 μmol/L Bis IV. **H** Bar chart summarizing the changes of the Na<sup>+</sup> current amplitudes at -20 mV under different conditions (*n* = 10, \*\**P* < 0.01 vs control).

**Discussion**

**Modulation of K<sup>+</sup> Channels in RGCs by D2 Receptors**

Although previous studies have shown that specific staining for D2 receptors is observed in cells of the ganglion cell layer in rat retinas [22], and that pharmacological interference with D2 receptors modulates the responses of RGCs [19, 41], our present work clearly showed that D2 receptors are indeed expressed in rat RGCs, as evidenced by double immunofluorescent labeling in RGCs retrogradely labeled with CTB (Fig. S1).

In the present study we found that one of the major effects of D2 receptor stimulation in rat RGCs is to significantly suppress the Gb-sensitive K<sub>ATP</sub> and the transient outward K<sup>+</sup> channels (KA) and delayed rectifying K<sup>+</sup> channels [48, 49], but not the TEA-sensitive BK<sub>Ca</sub> channel (Fig. 2). Consistently, previous studies have shown

after perfusion of quinpirole (Fig. 8A). The numbers of action potentials increased with increasing positive current injection (Fig. 8B). On average, the firing frequency gradually increased from 0 Hz to 10.5 Hz ± 1.5 Hz with 0 pA to +100 pA current injections in controls (*n* = 15). After quinpirole application, the firing frequency at 0 pA current injection was 2.0 Hz ± 1.5 Hz (*n* = 15, *P* = 0.178), and 6.5 Hz ± 1.5 Hz to 15.5 Hz ± 1.7 Hz at 10 pA to 100 pA current injection (*n* = 15, *P* < 0.05 for all; Fig. 8B).

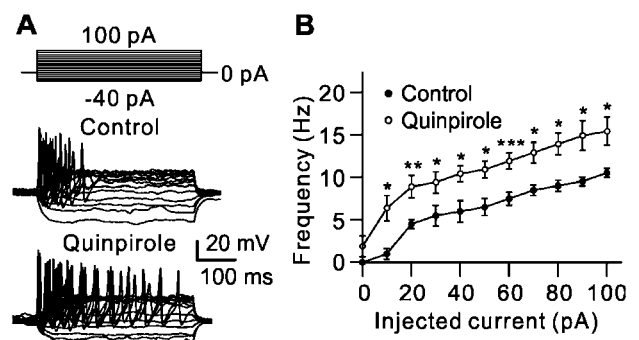


**Fig. 8** Activation of D2 receptors increases the numbers of action potential evoked by current injection in RGCs. **A** Representative recordings from an RGC, showing that extracellular application of quinpirole (10 μmol/L) increased the numbers of action potentials evoked by a series of 400-ms current injections from -40 pA to +100 pA in increments of 10 pA. **B** Plot of average firing frequency of evoked action potentials versus different injected currents (*n* = 15, \**P* < 0.05, \*\**P* < 0.01, \*\*\**P* < 0.001 vs control).

that activation of the D4 subtype of D2-class receptors reversibly inhibits  $K^+$  currents in the neurohypophysial nerve terminals of rats [50]. In addition, D2 receptor activation reduces small-conductance  $Ca^{2+}$ -activated  $K^+$  channel currents in subthalamic nucleus neurons [34]. In contrast to the data presented here, extensive evidence has shown that activation of D2 receptors increases the activity of several  $K^+$  channels in neurons of different brain regions [51–54]. For example, D2 receptor-modulated changes in the excitability of nucleus accumbens neurons are dynamically regulated and integrated by  $K_A$ ,  $K_{ir}$ , and leak  $K^+$  currents [52]. In B5 neurons of the buccal ganglion in the freshwater pond snail *Helisoma trivolvis*, DA increases 4-AP- and TEA-sensitive  $K^+$  currents through D2 receptors, resulting in a strong hyperpolarization of membrane potential [54]. Activation of D2 receptors increases the activity of slowly inactivating  $K^+$  channels and enhances the action potential discharge in neurons of the ventrobasal thalamus [51], and decreases the spontaneous firing of rat substantia nigra pars compacta (SNc) dopaminergic neurons by directly activating G protein-dependent inward rectifying  $K^+$  channels [53].

It is of interest that modulation of  $K_{ATP}$  due to D2 receptor stimulation revealed a contradictory situation. Rather than a reduction in  $K_{ATP}$  currents in rat RGCs (Fig. 2), an increase in  $K_{ATP}$  currents has been reported in isolated rat striatal neurons and in primary rat lactotrophs [55, 56]. The absence of an effect on  $K_{ATP}$  has also been reported in neurons of the rat SNc. DA acting on D2 receptors activates  $K^+$  currents and this is not mediated by  $K_{ATP}$  [57]. In addition, it is noteworthy that the outward current components inhibited by D4 receptor activation are  $K_A$  and  $BK_{Ca}$  channels in the neurohypophysial nerve terminals of rats [50]. A possible explanation is that the distinct  $K^+$  channel subtypes may be affected by different subtypes of D2 receptor. Which subtype(s) of D2 receptors are expressed in rat RGCs remains to be explored.

It should be noted that activation of both D1 and D2 receptors suppresses similar subtypes of outward  $K^+$  channel in rat RGCs [29] (and this study). We speculate that outward  $K^+$  currents in rat RGCs are modulated by a variety of signaling pathways coupled to distinct G protein subunits (see below).

### D2 Receptor-Mediated Modulation of $Na^+$ Currents in RGCs

Voltage-gated  $Na^+$  channels ignite neuronal action potentials. Nine distinct  $Na^+$  channels (Nav1.1–Nav1.9) have been identified, among which Nav1.1–Nav1.3 are expressed in neurons and play roles in electrogenesis [58–61]. Although the Nav1.1, Nav1.2, and Nav1.6  $Na^+$  channel proteins have been identified in RGCs by

immunohistochemistry [25, 27, 45], our data demonstrated that these  $Na^+$  channel subtypes indeed functionally exist in rat RGCs, and that the Nav1.6 channel predominates (Fig. 6). Furthermore, TTX completely blocked these  $Na^+$  currents, which is consistent with all these  $Na^+$  channels being TTX-sensitive.

An important finding in this study was that activation of D2 receptors enhanced  $Na^+$  currents in rat RGCs. We further demonstrated that Nav1.6 channels were selectively modulated by D2 receptors. Although previous studies have demonstrated that DA acting on D2 receptors modulates  $Na^+$  channels in various neurons [32, 33, 36, 62, 63], the present work is the first to show the selective modulation of Nav1.6 channels due to D2 receptor stimulation. In agreement with our findings, quinpirole induces a robust increase of TTX-sensitive  $Na^+$  influx in primary cultures of striatal neurons, and the effect is abolished by sulpiride, suggestive of involvement of D2 receptors [31]. Enhancement of  $Na^+$  currents by D2 receptor stimulation has also been reported in freshly-dissociated rat nucleus accumbens neurons [32] and in neurons of layer V entorhinal cortex in slice preparations [63]. However, it should be emphasized that a reduction in  $Na^+$  current amplitudes by D2 receptors has been reported in cochlear spiral ganglion neurons [36], and in striatal cholinergic interneurons [33]. One possibility for this inconformity is that D2 receptors are coupled to different subunits of G proteins in different neurons. For example, this is  $G_{i/o}$  in nucleus accumbens neurons [32], but  $G_{\beta\gamma}$  in striatal cholinergic interneuron [33]. On the other hand,  $Na^+$  channels are composed of  $\alpha$  and  $\beta$  subunits [60, 61]. It has been reported that Nav1.6 and  $\beta 1$  or  $\beta 2$  are clustered in RGCs [64, 65]. Whether activation of D2 receptors modulates either  $\alpha$  or  $\beta$  subunit in different cells remains to be addressed.

Since D2 receptor activation did not significantly shift the activation and inactivation curves, the enhancement of  $Na^+$  currents due to D2 receptor stimulation may be mediated through changing the  $Na^+$  channel conductance, but not through changing the activation and inactivation probability. In other words, D2 receptor stimulation did not change the activation and inactivation gates of the channels.

### Mechanisms Underlying D2 Receptor-Mediated Effects on $K^+$ and $Na^+$ Channels in RGCs

It has been reported that activation of D2 receptors may be coupled to several signaling pathways [32, 42, 43, 66]. The data presented in this study demonstrated that similar signaling pathways (cAMP/PKA, CaMKII, and MAPK/ERK) mediated the modulation of outward  $K^+$  currents and  $Na^+$  currents in rat RGCs. Since D2 receptors negatively

modulate the activity of adenylate cyclase, application of quinpirole should suppress cAMP/PKA signaling activity, then affect the outward  $K^+$  and  $Na^+$  currents. Consistently, the enhancement of  $Na^+$  currents or modulation of  $K^+$  channels in nucleus accumbens neurons due to D2 receptor stimulation results from suppressing tonic activity of cAMP/PKA signaling *via* the activation of  $G_{i/o}$  proteins; blockade of PKA activity mimics the D2 receptor-mediated effects [32, 52]. It has also been reported that  $Ca^{2+}$  influx through N-methyl-D-aspartate (NMDA) receptors is modulated by PKA; this process is inhibited by D2 receptors, thus reducing corticostriatal glutamate release. These results further demonstrate the suppression of tonic activity of cAMP/PKA signaling by D2 receptors [67].

Activation of D2 receptors may modulate the activity of CaMKII and MAPK/ERK signaling in cell lines and neurons [42, 43, 66, 68]. In this study, we found that the CaMKII and MAPK/ERK pathways were indeed involved in the quinpirole effects on  $K^+$  and  $Na^+$  channels because quinpirole no longer changed the current amplitudes when these two signaling pathways were blocked. How CaMKII and MAPK/ERK modulate outward  $K^+$  and  $Na^+$  currents remains to be explored.

Regulation of PLC/PKC is another classical signaling pathway due to D2 receptor stimulation [33, 69]. However, our results clearly showed that the PLC/PKC pathway did not participate in the quinpirole-induced modulation of  $K^+$  and  $Na^+$  currents (Figs. 3 and 7). In agreement with our data, the effects of D2 receptor activation in the rat striatum are not mediated by the PLC/PKC pathway since quinpirole does not affect the basal level of PLC or the levels of phosphoinositols (inositol monophosphate, inositol biphosphate, and inositol triphosphate), which are well characterized consequence of PLC stimulation [70]. On the other hand, the PLC/PKC pathway has been demonstrated to be involved in the effects of D2 receptor activation. For example, D2 receptor agonists reduce L-type  $Ca^{2+}$  currents and excitability in striatal medium spiny neurons through the PLC $\beta$ 1/IP $_3$ /calcineurin pathway [69]. Inhibition of  $Na^+$  channels by D2 receptors in striatal cholinergic interneurons is mediated by PLC/PKC signaling [33]. The reason for this inconformity may be that D2 receptors are linked to different subunits of G proteins in different cells. In striatal cholinergic interneurons,  $G_{\beta\gamma}$  signaling that activates the PLC/PKC cascade mediates the D2 receptor-induced inhibition of  $Na^+$  currents [33], whereas the enhancement of  $Na^+$  currents in the present study was not mediated by this signaling.

### Modulation of RGC Excitability by D2 Receptors

RGC excitability can be modulated by two elements, synaptic inputs and the intrinsic properties of the ion

channels.  $K^+$  channels play a critical role in setting up the membrane potential [71], while neuronal voltage-gated  $Na^+$  channels ignite action potentials and determine the firing frequency of the cells. D2 receptor-induced inhibition of outward  $K^+$  currents and enhancement of  $Na^+$  currents would increase RGC excitability. In line with this, quinpirole indeed increased the numbers of action potential discharges evoked by current injection (Fig. 8). It is noteworthy that both increases and decreases of cell excitability due to D2 receptor activation have been reported. Activation of D2 receptors causes increased firing in thalamocortical relay neurons [51], and enhances hippocampal-accumbens neuron excitability [72]. In contrast, stimulation of D2 receptors decreases evoked firing in medium spiny neurons of the nucleus accumbens [52], and decreases the spontaneous firing activity in rat SNc neurons [53] and in the striatal cholinergic interneurons of mice [33]. We speculate that different subunits of G protein mediate these effects as noted above.

Increasing evidence shows that the modulatory effect of D2 receptors on cell excitability is mediated by increasing or inhibiting Kir currents [51–53]. However, we previously showed that Kir channels are mainly expressed in RGC dendrites [73]. In this study, we could not record Kir channels since most of the RGC dendrites were lost during cell dissociation. Whether D2 receptor activation also affects Kir channels in RGCs remains to be further explored.

Since both D1 and D2 receptors are extensively expressed in retinal cells, in the intact retina, intrinsic DA may regulate the activity of RGCs through two pathways. First, DA acts on the D1/D2 receptors expressed in bipolar and amacrine cells to regulate the balance of inhibitory and excitatory inputs to RGCs, thus affecting RGC activity [13–16]. Second, DA activates D1/D2 receptors expressed in RGCs, directly influencing RGC excitability. It is of interest that both increased and reduced RGC excitability induced by DA have been reported, although the effects of DA are all mediated by activating D1 receptors [18, 28]. In retinal slices, DA enhances RGC excitability through inhibiting  $I_h$  [28], while in dissociated RGCs DA reduces RGC excitability through inhibiting voltage-gated  $Na^+$  current [18]. In addition, in a previous study, we showed that the temporal summation of excitatory postsynaptic potentials in rat RGCs is enhanced by D1 receptor activation and that this is mediated by affecting Kir currents [30]. The reason for this inconsistency may be that the dissociated RGCs lost their intact dendrites. Therefore, the net effect of DA on RGC activity in the intact retina depends on the integration of presynaptic and postsynaptic effects. On the other hand, the density and affinity of D1 and D2 receptors in RGCs are also important factors. We speculate that DA may enhance visual contrast

sensitivity by changing the center/surround balance of RGCs in the intact retina [12, 16]. The detailed mechanisms need to be explored.

In conclusion, we provide compelling evidence that activation of D2 receptors increases rat RGC excitability through suppressing outward  $K^+$  currents and selectively enhancing Nav1.6 currents, and subsequently modulating visual integrative processing. In addition, DA and its receptors have been shown to associate with retinal disorders such as diabetic retinopathy, retinitis pigmentosa, and NMDA-induced retinal injury [41, 74–76]. Modulation of RGC excitability by D2 receptors may provide a potential strategy for RGC neuroprotection.

**Acknowledgements** We thank Dr. Xiong-Li Yang for helpful discussion and critical comments on the manuscript. This work was supported by grants from the National Natural Science Foundation of China (31671078, 81790642, and 31872765), the Shanghai Municipal Science and Technology Major Project (No.2018SHZDZX01) and ZJ Lab.

**Conflict of interest** The authors declare no potential conflict of interest.

## References

- Barros M, Mello EL, Huston JP, Tomaz C. Behavioral effects of buspirone in the marmoset employing a predator confrontation test of fear and anxiety. *Pharmacol Biochem Behav* 2001, 68: 255–262.
- Bissiere S, Humeau Y, Luthi A. Dopamine gates LTP induction in lateral amygdala by suppressing feedforward inhibition. *Nat Neurosci* 2003, 6: 587–592.
- Missale C, Nash SR, Robinson SW, Jaber M, Caron MG. Dopamine receptors: From structure to function. *Physiol Rev* 1998, 78: 189–225.
- Paspalas CD, Goldman-Rakic PS. Presynaptic D1 dopamine receptors in primate prefrontal cortex: Target-specific expression in the glutamatergic synapse. *J Neurosci* 2005, 25: 1260–1267.
- Yang CR, Seamans JK. Dopamine D1 receptor actions in layers V-VI rat prefrontal cortex neurons in vitro: Modulation of dendritic-somatic signal integration. *J Neurosci* 1996, 16: 1922–1935.
- Wang ZY, Liang SX, Yu SS, Xie T, Wang BC, Wang JK, *et al.* Distinct roles of dopamine receptors in the lateral thalamus in a rat model of decisional impulsivity. *Neurosci Bull* 2017, 33: 413–422.
- Enjalbert A, Bockaert J. Pharmacological characterization of the D2 dopamine receptor negatively coupled with adenylate-cyclase in rat anterior pituitary. *Mol Pharmacol* 1983, 23: 576–584.
- Sibley DR, Monsma FJ Jr. Molecular-biology of dopamine-receptors. *Trends Pharmacol Sci* 1992, 13: 61–69.
- Beaulieu JM, Espinoza S, Gainetdinov RR. Dopamine receptors - IUPHAR Review 13. *Br J Pharmacol* 2015, 172: 1–23.
- Jackson CR, Ruan GX, Aseem F, Abey J, Gamble K, Stanwood G, *et al.* Retinal dopamine mediates multiple dimensions of light-adapted vision. *J Neurosci* 2012, 32: 9359–9368.
- Lavoie J, Illiano P, Sotnikova TD, Gainetdinov RR, Beaulieu JM, Hebert M. The electroretinogram as a biomarker of central dopamine and serotonin: Potential relevance to psychiatric disorders. *Biol Psychiat* 2014, 75: 479–486.
- Witkovsky P. Dopamine and retinal function. *Doc Ophthalmol* 2004, 108: 17–40.
- Gustincich S, Feigenspan A, Wu DK, Koopman LJ, Raviola E. Control of dopamine release in the retina: A transgenic approach to neural networks. *Neuron* 1997, 18: 723–736.
- Hokoc JN, Mariani AP. Tyrosine-hydroxylase immunoreactivity in the rhesus-monkey retina reveals synapses from bipolar cells to dopaminergic amacrine cells. *J Neurosci* 1987, 7: 2785–2793.
- Pourcho RG. Dopaminergic amacrine cells in the cat retina. *Brain Res* 1982, 252: 101–109.
- Thier P, Alder V. Action of iontophoretically applied dopamine on cat retinal ganglion cells. *Brain Res* 1984, 292: 109–121.
- Hayashida Y, Ishida AT. Dopamine receptor activation can reduce voltage-gated  $Na^+$  current by modulating both entry into and recovery from inactivation. *J Neurophysiol* 2004, 92: 3134–3141.
- Hayashida Y, Rodriguez CV, Ogata G, Partida GJ, Oi H, Stradleigh TW, *et al.* Inhibition of adult rat retinal ganglion cells by D-1-type dopamine receptor activation. *J Neurosci* 2009, 29: 15001–15016.
- Ogata G, Stradleigh TW, Partida GJ, Ishida AT. Dopamine and full-field illumination activate D1 and D2-D5-type receptors in adult rat retinal ganglion cells. *J Comp Neurol* 2012, 520: 4032–4049.
- Vaquero CF, Pignatelli A, Partida GJ, Ishida AT. A dopamine- and protein kinase A-dependent mechanism for network adaptation in retinal ganglion cells. *J Neurosci* 2001, 21: 8624–8635.
- Tran VT, Dickman M. Differential localization of dopamine D1-receptors and D2 receptors in rat retina. *Invest Ophthalmol Vis Sci* 1992, 33: 1620–1626.
- Wagner HJ, Luo BG, Ariano MA, Sibley DR, Stell WK. Localization of D2 dopamine-receptors in vertebrate retinæ with anti-peptide antibodies. *J Comp Neurol* 1993, 331: 469–481.
- Akopian AN, Sivilotti L, Wood JN. A tetrodotoxin-resistant voltage-gated sodium channel expressed by sensory neurons. *Nature* 1996, 379: 257–262.
- Ettaihe M, Heurteaux C, Blondeau N, Borsotto M, Tinel N, Lazdunski M. ATP-sensitive potassium channels (K-ATP) in retina: a key role for delayed ischemic tolerance. *Brain Res* 2001, 890: 118–129.
- Fjell J, DibHajj S, Fried K, Black JA, Waxman SG. Differential expression of sodium channel genes in retinal ganglion cells. *Mol Brain Res* 1997, 50: 197–204.
- Koeberle PD, Wang Y, Schlichter LC. Kv1.1 and Kv1.3 channels contribute to the degeneration of retinal ganglion cells after optic nerve transection in vivo. *Cell Death Differ* 2010, 17: 134–144.
- Van Wart A, Matthews G. Expression of sodium channels Na(v)1.2 and Na(v)1.6 during postnatal development of the retina. *Neurosci Lett* 2006, 403: 315–317.
- Chen L, Yang XL. Hyperpolarization-activated cation current is involved in modulation of the excitability of rat retinal ganglion cells by dopamine. *Neuroscience* 2007, 150: 299–308.
- Li Q, Wu N, Cui P, Gao F, Qian WJ, Miao Y, *et al.* Suppression of outward  $K^+$  currents by activating dopamine D1 receptors in rat retinal ganglion cells through PKA and CaMKII signaling pathways. *Brain Res* 2016, 1635: 95–104.
- Cui P, Li XY, Zhao Y, Li Q, Gao F, Li LZ, *et al.* Activation of dopamine D1 receptors enhances the temporal summation and excitability of rat retinal ganglion cells. *Neuroscience* 2017, 355: 71–83.
- Aizman O, Brismar H, Uhlen P, Zettergren E, Levey AI, Forsberg H, *et al.* Anatomical and physiological evidence for D1 and D2 dopamine receptor colocalization in neostriatal neurons. *Nat Neurosci* 2000, 3: 226–230.

32. Hu XT, Dong Y, Zhang XF, White FJ. Dopamine D2 receptor-activated  $\text{Ca}^{2+}$  signaling modulates voltage-sensitive sodium currents in rat nucleus accumbens neurons. *J Neurophysiol* 2005, 93: 1406–1417.
33. Maurice N, Mercer J, Chan CS, Hernandez-Lopez S, Held J, Tkatch T, *et al.* D2 dopamine receptor-mediated modulation of voltage-dependent  $\text{Na}^{+}$  channels reduces autonomous activity in striatal cholinergic interneurons. *J Neurosci* 2004, 24: 10289–10301.
34. Ramanathan S, Tkatch T, Atherton JF, Wilson CJ, Bevan MD. D2-like dopamine receptors modulate SKCa channel function in subthalamic nucleus neurons through inhibition of Cav2.2 channels. *J Neurophysiol* 2008, 99: 442–459.
35. Chen XY, Xue B, Wang J, Liu HX, Shi LM, Xie JX. Potassium channels: a potential therapeutic target for Parkinson's disease. *Neurosci Bull* 2018, 34: 341–348.
36. Valdes-Baizabal C, Soto E, Vega R. Dopaminergic modulation of the voltage-gated sodium current in the cochlear afferent neurons of the rat. *PLoS One* 2015, 10: e0120808.
37. Dong LD, Gao F, Wang XH, Miao Y, Wang SY, Wu Y, *et al.* GluA2 trafficking is involved in apoptosis of retinal ganglion cells induced by activation of EphB/EphrinB reverse signaling in a rat chronic ocular hypertension model. *J Neurosci* 2015, 35: 5409–5421.
38. Qian WJ, Yin N, Gao F, Miao Y, Li Q, Li F, *et al.* Cannabinoid CB1 and CB2 receptors differentially modulate L- and T-type  $\text{Ca}^{2+}$  channels in rat retinal ganglion cells. *Neuropharmacology* 2017, 124: 143–156.
39. Gao F, Li F, Miao Y, Xu LJ, Zhao Y, Li Q, *et al.* Involvement of the MEK-ERK/p38-CREB/c-fos signaling pathway in Kir channel inhibition-induced rat retinal Müller cell gliosis. *Sci Rep* 2017, 7: 1480.
40. Li LZ, Yin N, Li XY, Miao Y, Cheng S, Li F, *et al.* Rac1 modulates excitatory synaptic transmission in mouse retinal ganglion cells. *Neurosci Bull* 2019, 35: 673–687.
41. Jensen R. Effects of dopamine d2-like receptor antagonists on light responses of ganglion cells in wild-type and P23H rat retinas. *PLoS One* 2015, 10: e0146154.
42. Bofill-Cardona E, Kudlacek O, Yang Q, Ahorn H, Freissmuth M, Nanoff C. Binding of calmodulin to the D-2-dopamine receptor reduces receptor signaling by arresting the G protein activation switch. *J Biol Chem* 2000, 275: 32672–32680.
43. Liu XY, Chu XP, Mao LM, Wang M, Lan HX, Li MH, *et al.* Modulation of D2R-NR2B interactions in response to cocaine. *Neuron* 2006, 52: 897–909.
44. Fohlmeister JF. Voltage gating by molecular subunits of  $\text{Na}^{+}$  and  $\text{K}^{+}$  ion channels: higher-dimensional cubic kinetics, rate constants, and temperature. *J Neurophysiol* 2015, 113: 3759–3777.
45. Mojumder DK, Frishman LJ, Otteson DC, Sherry DM. Voltage-gated sodium channel alpha-subunits Na(v)1.1, Na(v)1.2, and Na(v)1.6 in the distal mammalian retina. *Mol Vis* 2007, 13: 2163–2182.
46. Bosmans F, Rash L, Zhu SY, Diochot S, Lazdunski M, Escoubas P, *et al.* Four novel tarantula toxins as selective modulators of voltage-gated sodium channel subtypes. *Mol Pharmacol* 2006, 69: 419–429.
47. Rosker C, Lohberger B, Hofer D, Steinecker B, Quasthoff S, Schreibleyner W. The TTX metabolite 4,9-anhydro-TTX is a highly specific blocker of the Na-v1.6 voltage-dependent sodium channel. *Am J Physiol Cell Physiol* 2007, 293: C783–C789.
48. Saito M, Murai Y, Sato H, Bae YC, Akaike T, Takada M, *et al.* Two opposing roles of 4-AP-sensitive  $\text{K}^{+}$  current in initiation and invasion of spikes in rat mesencephalic trigeminal neurons. *J Neurophysiol* 2006, 96: 1887–1901.
49. Wu RL, Barish ME. Modulation of a slowly inactivating potassium current, I-D, by metabotropic glutamate receptor activation in cultured hippocampal pyramidal neurons. *J Neurosci* 1999, 19: 6825–6837.
50. Wilke RA, Hsu SF, Jackson MB. Dopamine D4 receptor mediated inhibition of potassium current in neurohypophysial nerve terminals. *J Pharmacol Exp Ther* 1998, 284: 542–548.
51. Govindaiah G, Wang Y, Cox CL. Dopamine enhances the excitability of somatosensory thalamocortical neurons. *Neuroscience* 2010, 170: 981–991.
52. Perez MF, White FJ, Hu XT. Dopamine D2 receptor modulation of  $\text{K}^{+}$  channel activity regulates excitability of nucleus accumbens neurons at different membrane potentials. *J Neurophysiol* 2006, 96: 2217–2228.
53. Uchida S, Akaike N, Nabekura J. Dopamine activates inward rectifier  $\text{K}^{+}$  channel in acutely dissociated rat substantia nigra neurones. *Neuropharmacology* 2000, 39: 191–201.
54. Zhong LR, Artinian L, Rehder V. Dopamine suppresses neuronal activity of helisoma B5 neurons via a D2-Like receptor, activating PLC and K channels. *Neuroscience* 2013, 228: 109–119.
55. Lin YJ, Greif GJ, Freedman JE. Multiple sulfonylurea-sensitive potassium channels - a novel subtype modulated by dopamine. *Mol Pharmacol* 1993, 44: 907–910.
56. Einhorn LC, Gregerson KA, Oxford GS. D2 dopamine receptor activation of potassium channels in identified rat lactotrophs - whole-cell and single-channel recording. *J Neurosci* 1991, 11: 3727–3737.
57. Hicks GA, Henderson G. Lack of evidence for coupling of the dopamine D2 receptor to an adenosine triphosphate-sensitive potassium ( $\text{ATP-K}^{+}$ ) channel in dopaminergic neurones of the rat substantia nigra. *Neurosci Lett* 1992, 141: 213–217.
58. Catterall WA, Goldin AL, Waxman SG. International union of pharmacology. XLVII. nomenclature and structure-function relationships of voltage-gated sodium channels. *Pharmacol Rev* 2005, 57: 397–409.
59. Black JA, Waxman SG. Noncanonical roles of voltage-gated sodium channels. *Neuron* 2013, 80: 280–291.
60. Catterall WA. From ionic currents to molecular mechanisms: The structure and function of voltage-gated sodium channels. *Neuron* 2000, 26: 13–25.
61. Catterall WA. Forty years of sodium channels: structure, function, pharmacology, and epilepsy. *Neurochem Res* 2017, 42: 2495–2504.
62. Centonze D, Bracci E, Pisani A, Gubellini P, Bernardi G, Calabresi P. Activation of dopamine D1-like receptors excites LTS interneurons of the striatum. *Eur J Neurosci* 2002, 15: 2049–2052.
63. Rosenkranz JA, Johnston D. State-dependent modulation of amygdala inputs by dopamine-induced enhancement of sodium currents in layer V entorhinal cortex. *J Neurosci* 2007, 27: 7054–7069.
64. Fein AJ, Meadows LS, Chen C, Slat EA, Isom LL. Cloning and expression of a zebrafish SCN1B ortholog and identification of a species-specific splice variant. *BMC Genomics* 2007, 8: 226.
65. Kaplan MR, Cho MH, Ullian EM, Isom LL, Levinson SR, Barres BA. Differential control of clustering of the sodium channels Na(v)1.2 and Na(v)1.6 at developing CNS nodes of Ranvier. *Neuron* 2001, 30: 105–119.
66. Cho DI, Zheng M, Kim KM. Current perspectives on the selective regulation of dopamine D2 and D3 receptors. *Arch Pharm Res* 2010, 33: 1521–1538.
67. Higley MJ, Sabatini BL. Competitive regulation of synaptic  $\text{Ca}^{2+}$  influx by D2 dopamine and A2A adenosine receptors. *Nat Neurosci* 2010, 13: 958–966.
68. Cussac D, Newman-Tancredi A, Pasteau V, Millan MJ. Human dopamine D3 receptors mediate mitogen-activated protein kinase activation via a phosphatidylinositol 3-kinase and an atypical

- protein kinase C-dependent mechanism. *Mol Pharmacol* 1999, 56: 1025–1030.
69. Hernandez-Lopez S, Tkatch T, Perez-Garci E, Galarraga E, Bargas J, Hamm H, *et al.* D2 dopamine receptors in striatal medium spiny neurons reduce L-type  $\text{Ca}^{2+}$  currents and excitability via a novel PLC[ $\beta$ 1]-IP3-calcineurin-signaling cascade. *J Neurosci* 2000, 20: 8987–8995.
  70. Gupta SK, Mishra RK. The effect of dopamine-D1 and dopamine-D2 receptor agonists on inositol phosphate turnover in rat striatal slices. *Biochem Int* 1990, 22: 887–894.
  71. Hille B. Potassium channels and chloride channels. In: Hille B (Ed.). *Ion Channels of Excitable Membrane*. Sunderland: Sinauer Associates, Inc. 2001: 131–167.
  72. Yang CR, Mogenson GJ. Dopamine enhances terminal excitability of hippocampal accumbens neurons via D2 receptor: role of dopamine in presynaptic inhibition. *J Neurosci* 1986, 6: 2470–2478.
  73. Li Q, Cui P, Miao Y, Gao F, Li XY, Qian WJ, *et al.* Activation of group I metabotropic glutamate receptors regulates the excitability of rat retinal ganglion cells by suppressing Kir and I (h). *Brain Struct Funct* 2017, 222: 813–830.
  74. Aung MH, Park HN, Han MK, Obertone TS, Abey J, Aseem F, *et al.* Dopamine deficiency contributes to early visual dysfunction in a rodent model of type 1 diabetes. *J Neurosci* 2014, 34: 726–736.
  75. Kitaoka Y, Kumai T. Modulation of retinal dopaminergic cells by nitric oxide. A protective effect on NMDA-induced retinal injury. *In Vivo* 2004, 18: 311–315.
  76. Nishimura C, Kuriyama K. Alterations in the retinal dopaminergic neuronal system in rats with streptozotocin-induced diabetes. *J Neurochem* 1985, 45: 448–455.



# Scorpion Venom Heat-Resistant Peptide is Neuroprotective against Cerebral Ischemia-Reperfusion Injury in Association with the NMDA-MAPK Pathway

Xu-Gang Wang<sup>1,2,3</sup> · Dan-Dan Zhu<sup>1,3</sup> · Na Li<sup>2</sup> · Yue-Lin Huang<sup>1</sup> · Ying-Zi Wang<sup>1,3</sup> · Ting Zhang<sup>1</sup> · Chen-Mei Wang<sup>1</sup> · Bin Wang<sup>1</sup> · Yan Peng<sup>1</sup> · Bi-Ying Ge<sup>1</sup> · Shao Li<sup>1,2</sup> · Jie Zhao<sup>1,2</sup>

Received: 1 March 2019 / Accepted: 3 June 2019 / Published online: 9 September 2019  
© Shanghai Institutes for Biological Sciences, CAS 2019

**Abstract** Scorpion venom heat-resistant peptide (SVHRP) is a component purified from *Buthus martensii* Karsch scorpion venom. Our previous studies have shown that SVHRP is neuroprotective in models of Alzheimer's disease and Parkinson's disease. The present study aimed to explore the potential neuroprotective effects of SVHRP on cerebral ischemia/reperfusion (I/R) injury, using a mouse model of middle cerebral artery occlusion/reperfusion (MCAO/R) and a cellular model of oxygen-glucose deprivation/reoxygenation (OGD/R). Our results showed that SVHRP treatment decreased the neurological deficit scores, edema formation, infarct volume and neuronal loss in the MCAO/R mice, and protected primary neurons against OGD/R insult. SVHRP pretreatment suppressed the alterations in protein levels of N-methyl-D-aspartate receptors (NMDARs) and phosphorylated p38 MAPK as well as some proinflammatory factors in both the animal and cellular models. These results suggest that SVHRP has neuroprotective effects against cerebral I/R injury, which

might be associated with inhibition of the NMDA-MAPK-mediated excitotoxicity.

**Keywords** Scorpion venom heat-resistant peptide · Cerebral ischemia/reperfusion injury · Neuroprotection · NMDARs · p38 MAPK

## Introduction

Ischemic cerebrovascular disease is a common brain disorder characterized by high incidence, high disability, and high mortality worldwide. Each year, ~6 million people die of acute ischemia [1–3]. Thrombolytic therapy is often used in the treatment of ischemic disease in clinical practice. However, it has strict indications and certain risks such as post-perfusion lesions and bleeding [4]. The molecular mechanisms of cerebral ischemia and reperfusion (I/R) injury are complicated and not fully understood. Increasing evidence has suggested that excitatory amino acid toxicity and inflammation are the predominant mechanisms underlying cerebral I/R injury [5–7]. These complex processes involve interactions among many factors that slow cerebral healing and even aggravate cerebral damage.

Scorpion venom heat-resistant peptide (SVHRP, National Invention Patent No. ZL011061669) was isolated from *Buthus martensii* Karsch (BmK) venom in our laboratory. Our previous studies have shown that SVHRP regulates gene expression in astrocytes, promotes neurogenesis in mice, protects dopamine neurons in a 6-hydroxydopamine rat model and protects *Caenorhabditis elegans* from  $\beta$ -amyloid toxicity [8–11]. However, it is unknown whether SVHRP is protective against cerebral I/R insult. In this study, we investigated the neuroprotective

Xu-Gang Wang, Dan-Dan Zhu and Na Li have contributed equally to this work.

✉ Shao Li  
lishao89@hotmail.com; lishao89@dmu.edu.cn

✉ Jie Zhao  
dlzhaoj@163.com

<sup>1</sup> Liaoning Provincial Key Laboratory of Cerebral Diseases, Department of Physiology, College of Basic Medical Sciences, Dalian Medical University, Dalian 116044, China

<sup>2</sup> National-Local Joint Engineering Research Center for Drug-Research and Development of Neurodegenerative Diseases, Dalian Medical University, Dalian 116000, China

<sup>3</sup> The Second Hospital of Dalian Medical University, Dalian 116023, China

effects of SVHRP in a mouse model of middle cerebral artery occlusion/reperfusion (MCAO/R) and a cellular model of oxygen-glucose deprivation/reoxygenation (OGD/R).

## Materials and Methods

### Isolation of Scorpion Venom Heat-Resistant Peptide

The isolation of SVHRP from BmK venom was reported in our previous publication [8] with a patented method in our laboratory (No. 011061669). First, the crude venom was collected by electrical stimulation of the telson of BmK scorpions from Henan Province, China, and the lyophilized crude venom was dissolved in ddH<sub>2</sub>O and maintained at 100 °C for 4 h followed by centrifugation. Then the supernatant was loaded onto a Superdex Peptide 10/300GL Column (ÅKTA avant 25) and separated by fast protein liquid chromatography. Fraction I (P1) from the Superdex Peptide 10/300GL Column was collected and used for cell treatment. The results from reverse-phase HPLC using a C18 column (Zorbax SB-C18 250 x 4.6 mm, 5 μm) demonstrated that the purity of SVHRP was > 99.5%.

### Experimental Animals and Drug Administration

Male C57BL/6 mice (6–8 weeks old and weighing 16–25 g) were provided by Dalian Medical University. The animals were housed under international standards. Forty-eight mice were divided randomly into four groups: normal saline (NS) + sham, SVHRP + sham, NS + MCAO/R, and SVHRP + MCAO/R groups. The mice were pretreated with SVHRP (20 μg/kg, i.p.) or NS (5 mL/kg, i.p.) 48 h and 1 h before MCAO/R [9]. The dose of SVHRP was chosen based on previous animal studies [9, 10] showing that 20–50 μg/kg of SVHRP promotes neurogenesis in mouse hippocampus and olfactory bulb and protects dopamine neurons challenged by oxidative stress.

### Establishment of the MCAO/R Model

C57BL/6 mice were anaesthetized by intraperitoneal injection of 1% pentobarbital (50 mg/kg, i.p.). The MCAO/R model was established according to a published method [12] with minor modifications. Briefly, a ventral midline neck incision was made to expose the right common carotid artery, and right internal and external carotid arteries. After ligation at the proximal end of the common carotid artery, an MCAO suture (Southern Medical University, China) was inserted and positioned at the origin of the middle cerebral artery to occlude it. The same surgical procedure was performed in sham-operated animals except for occlusion of the artery. After occlusion

for 2 h, the suture was removed and blood flow was restored (reperfusion) [13].

### Evaluation of Neurological Deficit

The mice were returned to their cages after the suture was withdrawn and were given free access to food and water. The neurological behavior of the mice was scored 24 h after MCAO/R. A 28-point scale of neurological deficit was used to evaluate neurological behavior [14]. The scale was based on the following seven tests, each of which was scored as 0–4 points: (1) body symmetry, (2) gait, (3) climbing, (4) circling behavior, (5) forelimb symmetry, (6) compulsory circling, and (7) whisker response.

### Measurement of Cerebral Infarct Volume

After neurological evaluation, the mice were euthanized with isoflurane and brains were collected for measurement of infarct volume [15]. In brief, each brain was first frozen for 20 min before being cut into 2-mm-thick coronal sections, and stained with 2% triphenyltetrazolium chloride (TTC) (Solarbio, Beijing, China) for 15 min at 37 °C followed by overnight immersion in 4% paraformaldehyde. The infarct area of each slice was demarcated and analyzed using Image Pro plus software.

### Quantification of Brain Water Content

After neurological measurement, we used the wet-dry method to determine the brain water content [16]. Each hemisphere was weighed (wet weight) and left in a desiccating oven at 105 °C overnight, then the dried hemispheres were weighed again (dry weight) and the brain water content was calculated.

### Nissl Staining

For this staining protocol, brain samples were collected 24 h after reperfusion. After transcardial perfusion with 50 mL of 4% paraformaldehyde under anesthesia (50 mg/kg pentobarbital, i.p.), each brain was removed and post-fixed for 24 h. The tissue was embedded in paraffin and sectioned at 10 μm. The sections were stained with 2% cresyl violet, cleaned in graded ethanols and xylene, and coverslipped with Permount mounting medium (Sigma, Markham, ON, Canada).

### Cortical Neuron Culture and Establishment of the OGD/R Model

Primary cortical neurons were cultured from newborn C57BL/6 mice anesthetized with diethyl ether inhalation

within 24 h using the procedures described below [17]. The cerebral cortices were isolated and digested in 0.125% trypsin for 30 min at 37 °C. Then, 500 µL of suspension was added to each well of a 24-well plate pre-coated with poly-*L*-lysine and cultured in Dulbecco's modified Eagle's medium with 10% FBS, 1% *L*-glutamate, and 1% penicillin-streptomycin in an incubator at 37 °C with 5% CO<sub>2</sub> for 4 h. Then, the supernatant was replaced with 500 µL Neurobasal medium containing 1% *L*-glutamate, 1% penicillin-streptomycin, 1% N2, and 2% B27 and maintained for 12 days. Half of the medium was changed every other day. The purity of mature neurons (> 95%) was confirmed by microtubule-associated protein-2 staining.

OGD/R was performed using a combination of chemical hypoxia and glucose deprivation according to published methods [18, 19] with modifications. Mature cortical neurons were transiently deprived of both oxygen and glucose through incubation with a glucose-free Earle's balanced salt solution (EBSS) containing 1 mmol/L azide (Sigma, St. Louis, MO), a deoxygenating reagent, for 3 h. Reoxygenation was induced by quickly replacing the deoxygenated and glucose-free EBSS with the pre-OGD culture medium to return the cells to normoxic conditions. The cortical neurons were divided into four groups: vehicle + control, SVHRP + control, vehicle + OGD/R, and SVHRP + OGD/R groups. Cells were cultured in the presence or absence of SVHRP (20 µg/mL) for 24 h before OGD/R. The concentration of 20 µg/mL was selected as it is the optimal concentration within the dose range (0.2–80 µg/mL) in cell culture and *Caenorhabditis elegans* studies, according to our previous reports [8, 9].

### Assessment of Cell Viability and Cytotoxicity

Cell viability was assessed using the 3-(4,5-dimethylthiazol-2-yl)-2,5-diphenyl tetrazolium bromide (MTT) assay. The cortical neurons were pretreated with SVHRP (20 µg/mL) or vehicle before being subjected to OGD/R insult. MTT solution was added to the culture medium to a final concentration of 0.5 mg/mL 24 h after reoxygenation and incubated for 4 h at 37 °C. The supernatant was then removed, and 100 µL dimethyl sulfoxide was added. The optical density was measured at 490 nm.

Lactic dehydrogenase (LDH) released from cells was detected using a commercial LDH kit (Roche, Basel, Switzerland) to evaluate the neurotoxicity. Absorbance was measured at 490 nm, and the relative LDH release rate was calculated.

### Reverse Transcription Polymerase Chain Reaction (RT-PCR)

RT-PCR was used to analyze the mRNA levels of tumor necrosis factor- $\alpha$  (TNF- $\alpha$ ) and interleukin (IL)-6 at 24 h after reperfusion in MCAO/R mice. Total RNA was extracted using an RNA extraction kit according to the manufacturer's instructions (Takara Biotechnology, China). Reverse transcription of RNA to cDNAs was performed using TransScript One-Step gDNA Removal and cDNA Synthesis SuperMix (Transgen Biotechnology). Regular PCR was then conducted to amplify the cDNA using the following conditions: a hot start at 95 °C for 600 s, followed by 95 °C for 30 s, 58 °C for 40 s, and 72 °C for 40 s at the annealing temperature through 35 cycles for TNF- $\alpha$  and IL-6; a hot start at 95 °C for 180 s, followed by 94 °C for 15 s, 60 °C for 25 s, 72 °C for 20 s through 30 cycles, and then 72 °C for 300 s for  $\beta$ -actin. The following primers were used: for TNF- $\alpha$  forward 5'-CGT CAG CCG ATT TGC TAT CT-3', reverse 5'-CGG ACT CCG CAA AGT CTA AG -3'; for IL-6 forward 5'-TCC ATC CAG TTG CCT TCT TGG-3', reverse 5'-CCA CGA TTT CCC AGA GAA CAT G-3'; and for  $\beta$ -actin forward 5'-AGC CAT GTA CGT AGC CAT CC-3', reverse 5'-GCT GTG GTG GTG AAG CTG TA-3'.

### Western Blot Analysis

Samples from the ischemic penumbra of cerebral cortex and cortical neurons were homogenized in ice-cold lysis buffer and then centrifuged at 12,000 rpm for 15 min at 4 °C. The supernatants were collected, and the protein concentrations were determined using a bicinchoninic acid (BCA) protein assay reagent kit (Pierce Biotechnology, Waltham, MA) with bovine serum albumin (BSA, Sigma) as a standard. Equal amounts of protein samples from each group were separated by 8%–10% SDS-polyacrylamide gel electrophoresis and transferred onto polyvinylidene difluoride membranes (Chemicon, Billerica, MA) for immunoblotting using an electrophoretic transfer system (Bio-Rad, Hercules, CA). The membrane was blocked at room temperature for 1 h with 5% nonfat dry milk or 5% BSA (Sigma) in TBST (Tris-buffered saline containing 0.1% Tween-20), followed by incubation overnight at 4 °C with primary antibodies for rabbit p38 (1:1000 dilution, Cell Signaling, Beverly, MA), mouse p-p38 (1:1000, Cell Signaling), rabbit NR1 (1:1000, Abcam, Cambridge, MA), mouse NR2A (1:1000, Abcam), mouse NR2B (1:1000, Abcam), mouse GABA<sub>A</sub> (1:1000, Abcam), iNOS (1:1000, Cell Signaling),  $\beta$ -actin (1:2000, Abcam), and  $\beta$ -tubulin (1:2000, Abcam). The following day, the membranes were washed three times with TBST buffer (10 min each) and incubated with horseradish peroxidase secondary

antibodies for 1 h at room temperature. The bands corresponding to the proteins of interest were detected using an enhanced chemiluminescence detection system (Bio-Rad).

### Statistics

Data were analyzed using the Statistical Package for the Social Sciences (IBM SPSS Statistics 19.0). Values are presented as the mean  $\pm$  SEM. All data were analyzed by one-way analysis of variance (ANOVA).  $P < 0.05$  indicated statistically significant differences.

## Results

### Effects of SVHRP on Neurological Deficit Scores, Infarct Volume, and Brain Water Content

MCAO has been used extensively for modelling ischemic stroke and leads to cerebral ischemia and edema, as well as serious brain injury such as neurological impairment and even death. To test whether SVHRP has neuroprotective effect on ischemic stroke, we used MCAO in mice. After 2 h of ischemia followed by 24 h of reperfusion, MCAO/R mice showed neurologic impairment and demonstrated significantly higher neurological deficit scores compared with those in the sham group ( $P < 0.001$ , Fig. 1A). Meanwhile, in the group pretreated with SVHRP (20  $\mu\text{g}/\text{kg}$ , i.p.) 48 h before MCAO/R, the total neurological score was significantly lower than that of the MCAO/R group ( $11.07 \pm 1.14$  vs  $15.5 \pm 0.96$ ,  $P < 0.05$ ;  $n = 14$ – $16$ ). Among the seven items, the scores for circling behavior ( $1.71 \pm 0.19$  vs  $2.44 \pm 0.20$ ,  $P < 0.01$ ,  $n = 14$ – $16$ ) and whisker responses ( $1.50 \pm 0.17$  vs  $2.19 \pm 0.23$ ,  $P < 0.01$ ,  $n = 14$ – $16$ ) were significantly reduced by SVHRP pretreatment. There was no significant difference between the NS+sham group and the SVHRP+sham group (Fig. 1A).

MCAO leads to a prominent cerebral infarct. Mice pretreated with SVHRP (20  $\mu\text{g}/\text{kg}$ , i.p.) showed significantly smaller infarct volumes (Fig. 1B) than those in the MCAO/R group ( $36.53\% \pm 3.5\%$  vs  $61.37\% \pm 3.3\%$ ,  $P < 0.001$ ,  $n = 11$ – $13$ , Fig. 1C). These results indicated that SVHRP pretreatment reduces the brain damage caused by I/R injury.

Cerebral I/R injury leads to cerebral edema. Brain water content was used to assess edema in the hemispheres. The brain water content was higher in the MCAO/R group than in the sham group; however, this effect was significantly reduced by SVHRP pretreatment (20  $\mu\text{g}/\text{kg}$ , i.p.) ( $80.59\% \pm 0.23\%$  vs  $81.48\% \pm 0.29\%$ ,  $P < 0.05$ ,  $n = 6$ – $10$ , Fig. 1D). No infarction or edema formation occurred in the sham operation group.

### Effects of SVHRP on the Survival of Neurons after I/R Injury

A Nissl body is a large granular body found in neurons. The Nissl staining method is used to localize the cell body—the stain can be seen in the soma and dendrites. Nissl staining was performed here to determine the numbers of neurons in the ischemic penumbra (Fig. 2Aa). Dramatic decreases in staining density and numbers of cells stained were induced in the MCAO/R group, and these were ameliorated by SVHRP pretreatment ( $292 \pm 34.26$  vs  $470 \pm 62.29$ ,  $P < 0.05$ ,  $n = 5$ , Fig. 2Ab;  $276 \pm 30.59$  vs  $416 \pm 69.4$ ,  $P < 0.05$ ,  $n = 5$ , Fig. 2Ac). Our results revealed dramatic neuronal loss in the MCAO/R group, while SVHRP pretreatment partially prevented the neuronal loss, suggesting that SVHRP protected neurons against the I/R insult and contributed to the improved functional outcome after I/R.

OGD/R is used to study I/R injury *in vitro*. In order to investigate the effects of SVHRP on OGD/R-induced neuronal injury, the viability/injury of neurons was assessed by the MTT assay and by measuring LDH. Studies have shown that the amount of LDH leakage is correlated with cell membrane damage [20, 21]. Viability by the MTT assay was lower and the LDH release rate was higher in the OGD/R group ( $P < 0.001$ , Fig. 2B). This indicated that OGD/R treatment led to neuronal damage and impaired cell viability. However, pretreatment with SVHRP (20  $\mu\text{g}/\text{mL}$ ) raised the cell viability and reduced the LDH release rate under OGD/R conditions ( $P < 0.001$ , Fig. 2B), reconfirming the neuroprotective effect of SVHRP on I/R injury ( $F = 261.00$ , Fig. 2Ba;  $F = 185.90$ , Fig. 2Bb).

### Effects of SVHRP on the Expression Levels of NMDA and $\gamma$ -Aminobutyric Acid (GABA) Receptors in the MCAO/R and OGD/R Models

Excitatory toxicity, referring to the over-activation of NMDA receptors (NMDARs) (such as subunits NR1 and NR2B) and the consequent increase in intracellular levels of  $\text{Ca}^{2+}$ , activates noxious signaling cascades and promotes neuronal cell death [22, 23]. To explore whether SVHRP pretreatment has a neuroprotective effect against this excitotoxicity pattern, we investigated the protein expression of NR1 and NR2B in the MCAO/R and OGD/R models by Western blotting. Compared with the sham operation groups, the protein expression levels of NR1 and NR2B were up-regulated in the MCAO/R group ( $P < 0.01$ , Fig. 3Aa, b). However, pretreatment with SVHRP inhibited the increment of expression levels for NR1 ( $P < 0.05$ , Fig. 3Aa) and NR2B ( $P < 0.01$ , Fig. 3Ab).

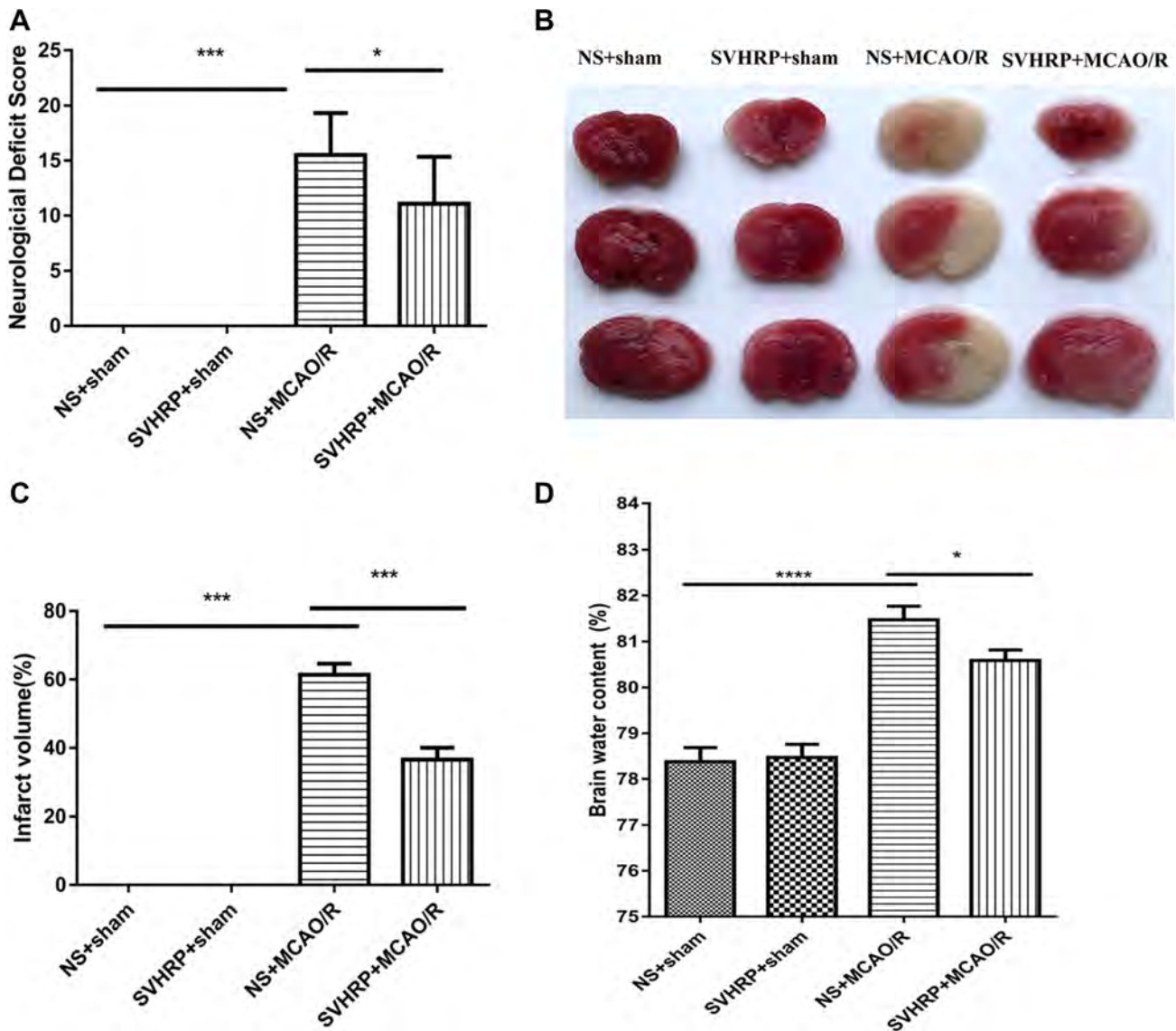


**Fig. 1** Effects of SVHRP (20  $\mu\text{g}/\text{kg}$ , i.p.) on neurological deficit score, infarct volume, and water content in mice after MCAO/R. **A** Neurological deficit scores 24 h after MCAO/R. Pretreatment with SVHRP significantly reduced the scores. **B** Representative coronal brain slices stained with TTC. Red, healthy tissue; white, infarcted

tissue. Pretreatment with SVHRP significantly reduced the infarct size. **C, D** Quantitative analyses of infarct volume (**C**) and brain water content (**D**). Pretreatment with SVHRP reduced brain water content after MCAO/R (mean  $\pm$  SEM;  $n = 6\text{--}16$  mice/group; \* $P < 0.05$ , \*\*\* $P < 0.001$ , one-way ANOVA followed by the LSD *post-hoc* test).

The NR2A and NR2B subunits play different roles in mediating excitotoxic neuronal ischemic tolerance and cell death; increased synaptic expression of the NR2A subunit promotes the survival of neurons, whereas increased expression of NR2B promotes neuronal apoptosis [24, 25]. Here, our results showed lower expression of NR2A in the MCAO/R group than in the sham operation groups ( $P < 0.05$ , Fig. 3Ac). GABA is the principal inhibitory neurotransmitter that binds to GABA<sub>A</sub>, GABA<sub>B</sub>, and GABA<sub>C</sub> receptors. The GABA<sub>A</sub> receptor plays a major role in inhibiting excitotoxicity and ischemia-induced neuronal cell death in the central nervous system

[26, 27]. Compared with the sham operation groups, MCAO/R mice also showed decreased expression of GABA<sub>A</sub> ( $P < 0.05$ , Fig. 3Ad). Moreover, compared with the MCAO/R mice, the SVHRP pretreatment group showed significantly increased expression levels of NR2A and GABA<sub>A</sub> ( $P < 0.05$ , Fig. 3Ac, d). No differences were found in the expression of NMDARs and GABA<sub>A</sub> between the NS + sham and SVHRP + sham groups ( $P > 0.05$ ) ( $F = 14.67$ , Fig. 3Aa;  $F = 14.16$ , Fig. 3Ab;  $F = 7.39$ , Fig. 3Ac;  $F = 4.445$ , Fig. 3Ad).

A similar pattern of protein expression of the above receptors was detected with OGD/R. The results in the

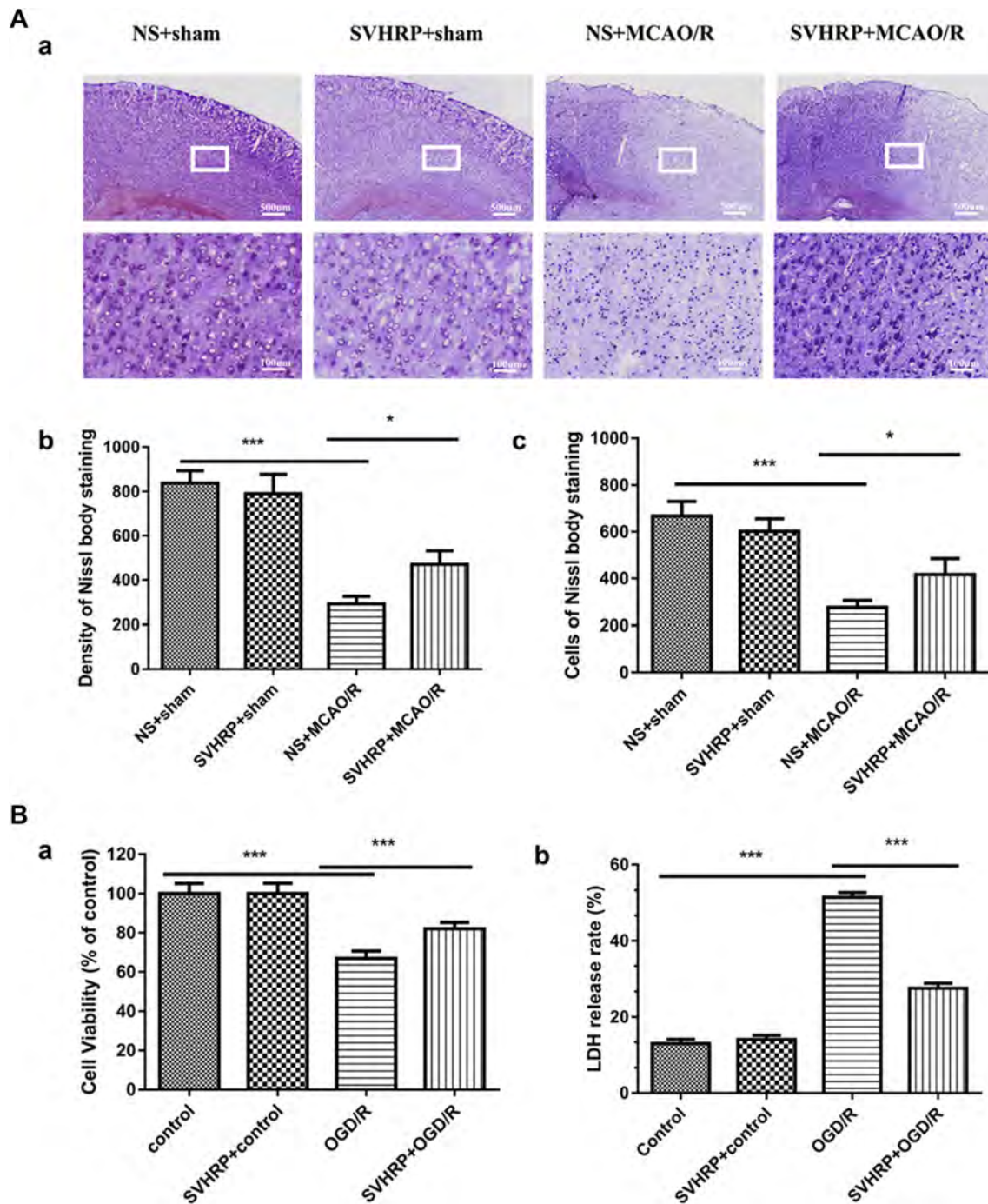


**Fig. 2** Effects of SVHRP on the survival of neurons after I/R injury. **A** Effects of SVHRP (20  $\mu\text{g}/\text{kg}$ , i.p.) on neuronal survival in the ischemic penumbra after MCAO/R. (a) Representative image of Nissl staining in cortex 24 h after MCAO/R (scale bars, 500  $\mu\text{m}$  for upper panel, 100  $\mu\text{m}$  for lower panel). (b, c) Density (b) and cell number (c) analyzed by quantitative imaging (Proplus). SVHRP pretreatment attenuated the neuronal loss caused by MCAO/R and SVHRP alone

had no effect on these histological changes (mean  $\pm$  SEM;  $n = 5$  mice/group;  $*P < 0.05$ ,  $**P < 0.01$ , one-way ANOVA followed by Turkey's test). **B** Effects of SVHRP (20  $\mu\text{g}/\text{mL}$ ) on survival of primary cortical neurons after OGD/R. (a, b) Cell viability (a) by MTT assay and LDH release rate (b) from cultured cortical neurons (mean  $\pm$  SEM; data from 3 separate experiments;  $***P < 0.001$ , one-way ANOVA followed by the LSD *post-hoc* test).

OGD/R model were consistent with those in the MCAO/R mice (Fig. 3Ba-d) ( $F = 11.43$ , Fig. 3Ba;  $F = 14.16$ , Fig. 3Bb;  $F = 12.33$ , Fig. 3Bc;  $F = 5.524$ , Fig. 3Bd). In

summary, these results demonstrated that SVHRP had neuroprotective effects by inhibiting glutamate excitotoxicity.

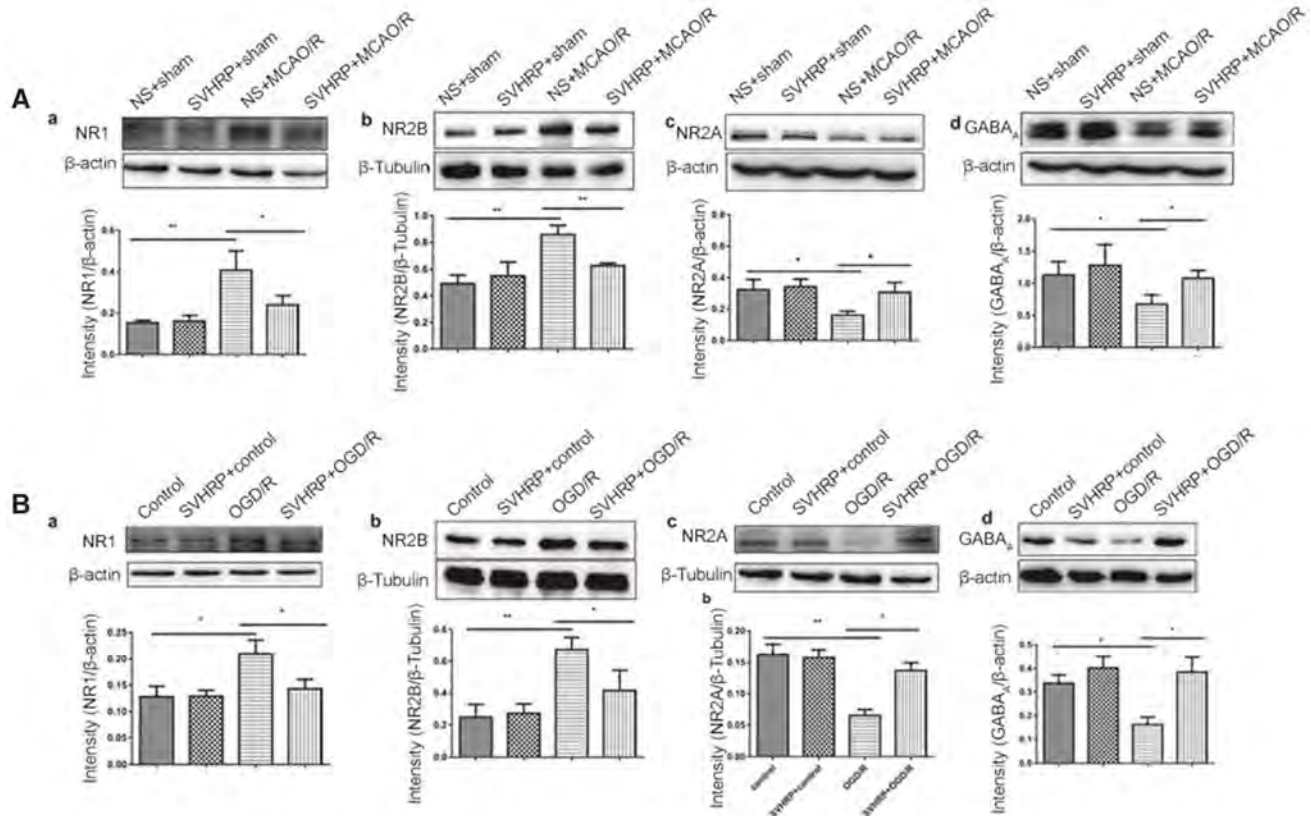


**Fig. 3** Effects of SVHRP on the expressions of NR1, NR2B, NR2A and GABA<sub>A</sub> receptors in the ischemic penumbra after MCAO/R and in cultured cortical neurons under OGD/R. **A** Pretreatment with SVHRP (20 μg/kg, i.p.) significantly decreased the protein levels of NR1 (a) and NR2B (b), and increased the NR2A (c) and GABA<sub>A</sub> (d) levels compared with the MCAO/R group. **B** Primary cortical

neurons subjected to OGD/R injury and the effects of SVHRP (20 μg/mL) pretreatment on the protein levels of NR1 (a), NR2B (b), NR2A (c), and GABA<sub>A</sub> (d) corresponded with those in the MCAO/R mice. Data are presented as the mean ± SEM;  $n = 3$  mice/group; \* $P < 0.05$ , \*\* $P < 0.01$ , one-way ANOVA followed by Turkey's test.

### Effects of SVHRP on the Expression of Components of the p38 MAPK Pathway in MCAO/R Mice and the OGD/R Model

Reports have shown that the MAPK pathways are involved in NMDA-induced excitotoxicity. In addition, p38 kinases in MAPK systems are well known to be activated after several types of ischemia [28, 29]. In our study, 24 h after reperfusion, western blot analysis showed significantly higher expression of active p-p38 MAPK in the MCAO/R group than in the sham operation group (Fig. 4A). Compared with the MCAO/R group, SVHRP pretreatment significantly attenuated the increase in p-p38 MAPK expression induced by MCAO/R ( $P < 0.01$ , Fig. 4A).

Consistent with the results *in vivo*, p-p38 MAPK was up-regulated in the *in vitro* OGD/R group ( $P < 0.01$ , Fig. 4B), and this was suppressed by SVHRP pretreatment ( $P < 0.05$ , Fig. 4B). No significant difference was found

between the control and SVHRP groups (Fig. 4B) ( $F = 18.20$ , Fig. 4A;  $F = 23.16$ , Fig. 4B).

### SVHRP Inhibits Pro-inflammatory Cytokines in the Ischemic Penumbra after MCAO/R

p38 MAPKs are known to play a critical role in the signaling pathways that induce a series of pro-inflammatory cytokines and iNOS in glial cells. To further elucidate the mechanisms underlying the neuroprotection by SVHRP against I/R injury, we assessed the protein expression of iNOS after I/R, and found that pretreatment with SVHRP inhibited the increment of iNOS expression ( $P < 0.05$ , Fig. 5A). In addition, we investigated the mRNA levels of TNF-α and IL-6 in the ischemic penumbra after 24 h of reperfusion using RT-PCR. We found that the mRNA levels of both were dramatically higher in the MCAO/R group than in the sham groups, and this was suppressed by SVHRP pretreatment ( $0.89 \pm 0.11$  vs  $0.37 \pm 0.08$ ,  $P <$

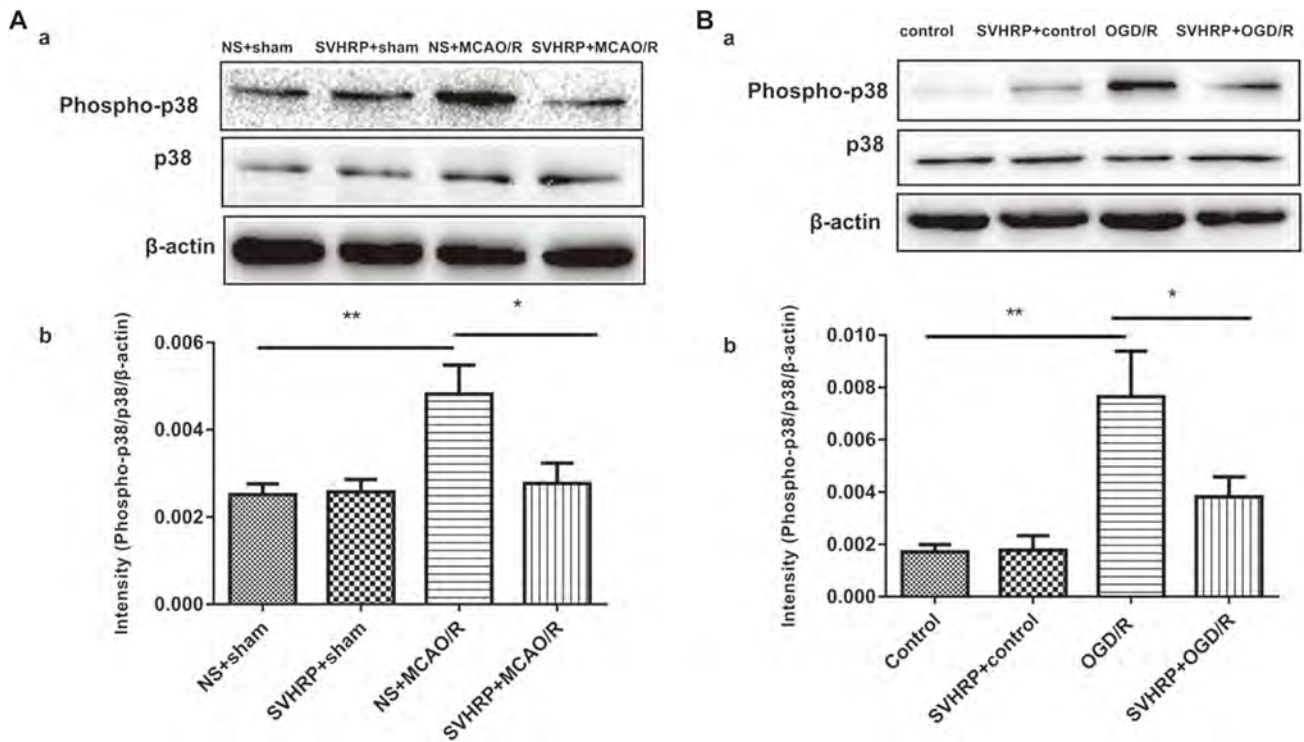


**Fig. 4** Effect of SVHRP on the expression of p-p38 MAPK in MCAO/R and OGD/R models. **A** Representative immunoblots (a) and densitometric analysis (b) of the immunoblots demonstrated that SVHRP (20 μg/kg, i.p.) decreased the expression of p-p38 MAPK in the ischemic penumbra after MCAO/R. **B** SVHRP (20 μg/mL)

remarkably down-regulated p-p38 MAPK expression in OGD/R-treated cortical neurons, corresponding with the effect *in vivo* (mean ± SEM;  $n = 3$  mice/group;  $*P < 0.05$ ,  $**P < 0.01$ , one-way ANOVA followed by Tukey's test).

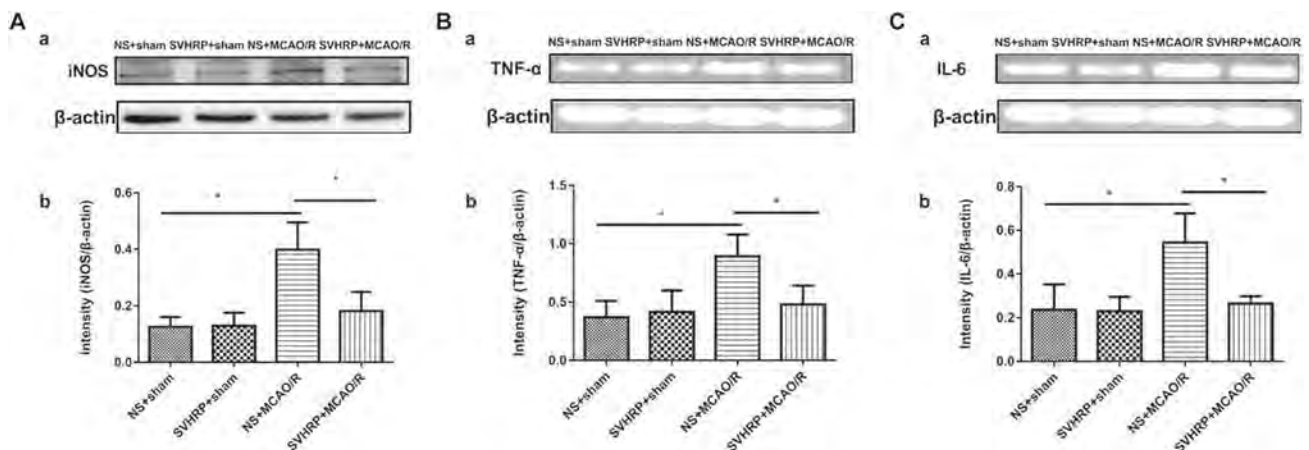


**Fig. 5** Effects of SVHRP (20 μg/kg, i.p.) on the expression of iNOS protein and TNF-α and IL-6 mRNA in the ischemic penumbra after MCAO/R. The MCAO/R group had significantly higher expression of iNOS protein (A) and TNF-α (B), IL-6 mRNA (C) than that of the

sham operation groups, and SVHRP pretreatment significantly reduced their levels. There were no significant differences between the NS+sham and SVHRP+sham groups (mean ± SEM;  $n = 3$  mice/group;  $*P < 0.05$ , one-way ANOVA followed by Tukey's test).

0.05,  $n = 3$ , Fig. 5B;  $0.54 \pm 0.08$  vs  $0.24 \pm 0.07$ ,  $P < 0.05$ ,  $n = 3$ , Fig. 5C). There were no significant differences between the NS + sham and SVHRP + sham groups ( $F = 6.02$ ,  $F = 6.80$ , Fig. 5B, C). These results indicated that SVHRP inhibited the activation of pro-inflammatory cytokines in the ischemic penumbra after MCAO/R.

## Discussion

Ischemic stroke greatly affects health, but its mortality is still at a high level, with few medications available [30, 31]. Reperfusion therapy is an important medical treatment following stroke; however, for a certain period of

time, the recovery of blood flow frequently causes reperfusion injury. It is believed that cerebral I/R injury involves many complicated pathological mechanisms and induces multiple cell signaling pathways in the brain [32, 33]. Among these, excitotoxicity and inflammation are both important events [34, 35].

BmK and its venom, as well as many other natural product-based therapies, are used to treat neurological diseases [36–39]. SVHRP is isolated from BmK venom, which is highly biologically active [40–43]. Our previous studies have shown that SVHRP is neuroprotective in animal models of Alzheimer's disease and Parkinson's disease [10, 11]. In this study, we used models of MCAO/R in mice and OGD/R in primary cultured neurons to further investigate the neuroprotection of SVHRP against cerebral I/R injury and the potential underlying mechanisms, focusing on NMDAR-mediated p38 MAPK signaling pathways.

First, our MCAO/R *in vivo* study showed that SVHRP had neuroprotective effects by reducing the neurological deficit score, infarct volume, edema formation, and neuronal loss. *In vitro*, pretreatment with SVHRP reduced the damage to primary cultured neurons subjected to OGD/R, further suggesting the neuroprotective effects of SVHRP.

Excitotoxicity, i.e., increased extracellular glutamate concentration, is an essential etiology associated with I/R injury [44]. NMDARs, ligand-gated ion channels with a high permeability to  $\text{Ca}^{2+}$ , are activated by glutamate [45–47]. After cerebral ischemia, excess glutamate accumulates in synapses and activates NMDARs, leading to an excessive influx of  $\text{Ca}^{2+}$  and thereby resulting in excitotoxicity [48]. Functional NMDARs associated with cerebral I/R injury mainly consist of the NR1 and the NR2A-D subunits [49]. The NR2A and NR2B subunits play different roles in mediating excitotoxic neuronal death and ischemic tolerance. Increased expression of synaptic NR2A promotes the survival of neurons, whereas elevated expression of NR2B promotes neuronal apoptosis and increases the sensitivity to excitotoxicity [24, 25, 50]. In the central nervous system,  $\text{GABA}_A$  plays a major role in inhibiting excitotoxicity and ischemia-induced neuronal death [26, 27]. The level of  $\text{GABA}_A$  on neuronal cell membranes decreases with exposure to OGD/R [51]. Here, we provide the first evidence showing that the neuroprotection conferred by SVHRP is mediated by inhibiting the expression of NR1 and NR2B and preventing the reduction in expression of NR2A and  $\text{GABA}_A$  in the cortex of MCAO/R mice and in OGD/R neurons, suggesting the anti-neurotoxic action of SVHRP.

Reports have shown that the MAPK pathways are involved in NMDA-induced excitotoxicity. p38 MAPK plays an important role in pathophysiological processes, such as cell growth, cell injury, apoptosis, inflammation,

and the stress response. Activated MAPK signaling cascade reactions play roles in neuronal damage [52, 53]. p38 kinase is one of the best-known MAPK effectors that is activated after various types of ischemia [28, 29]. In cerebral I/R injury, cellular stress mediated by activated p38 MAPKs is linked to inflammatory cytokine production and apoptosis *via* transcription factors, phosphorylating intracellular enzymes, and cytosolic proteins [54]. Inhibition of p38 MAPK activation can provide protection against brain injury. As many investigations have shown that activation of the p38 MAPK participates in the process of I/R injury, therapy with p38 MAPK inhibitors could reduce the inflammatory cytokine protein expression induced by ischemia. The suppression of p38 MAPK phosphorylation would reduce neuronal death by inhibiting NMDA-induced excitotoxicity and inflammatory mediator production [55–57]. Our results demonstrated that the phosphorylation of p38 MAPK proteins was significantly increased in the MCAO/R and OGD/R models, and this was remarkably suppressed by SVHRP. Intriguingly, SVHRP also inhibited the pro-inflammatory factors iNOS,  $\text{TNF-}\alpha$ , and IL-6 at the protein and mRNA levels. This indicated that SVHRP inhibited the neuroinflammation induced by p38 MAPK phosphorylation. Taken together, our findings supported the hypothesis that the NMDA-mediated p38 MAPK pathways are involved in the neuroprotective and anti-inflammatory effects of SVHRP.

Traditional Chinese medicines and their active components have been widely used for thousands of years in many Asian countries, including China, Korea, and Japan. Scorpions were used as a source of medicinal material as early as the Han Dynasty (206 BC–220 AD) and are recorded in the *Compendium of Materia Medica (Bencao Gangmu)*. However, due to the complexity of the active components and lack of scientific study, the effectiveness and safety of these natural materials have not been determined in modern medicine. Our study shows that SVHRP might be an important component that is responsible for the therapeutic effects of scorpion products in traditional Chinese medicine.

In conclusion, this study demonstrated that SVHRP, derived from scorpion venom, is neuroprotective against cerebral I/R injury both *in vivo* and *in vitro*, which might be due to a reduction of neurotoxicity. This finding suggests that natural products used in traditional medicinal practices are a good source for finding potential therapeutic agents for diseases that need more effective treatments.

**Acknowledgements** This work was supported by grants from National Natural Science Foundation of China (81571061 and 81671061), the Scientific Study Project for Institutes of Higher Learning, Ministry of Education, Liaoning Province, China (LZ2017001), Liaoning Provincial Key R&D Program (2019JH2/

10300043) and the Liaoning Revitalization Talents Program (XLYC1808031).

**Conflict of interest** All authors claim that there are no conflicts of interest.

## References

- Go AS, Mozaffarian D, Roger VL, Benjamin EJ, Berry JD, Baha MJ, *et al.* Heart disease and stroke statistics–2014 update: a report from the American Heart Association. *Circulation* 2014, 129: e28–e292.
- Jauch EC, Saver JL, Adams HP, Jr, Bruno A, Connors JJ, Demaerschalk BM, *et al.* American Heart Association Stroke Council; Council on Cardiovascular Nursing; Council on Peripheral Vascular Disease; Council on Clinical Cardiology: Guidelines for the early management of patients with acute ischemic stroke: a guideline for healthcare professionals from the American Heart Association/American Stroke Association. *Stroke* 2013, 44: 870–947.
- Yang Z, Zhu L, Li F, Wang J, Wan H, Pan Y. Bone marrow stromal cells as a therapeutic treatment for ischemic stroke. *Neurosci Bull* 2014, 30: 524–534.
- Eltzschig HK, Eckle T. Ischemia and reperfusion—from mechanism to translation. *Nat Med* 2011, 17: 1391–1401.
- Aromugam TV, Woodruff TM, Lathia JD, Selvaraj PK, Mattson MP, Taylor SM. Neuroprotection in stroke by complement inhibition and immunoglobulin therapy. *Neuroscience* 2009, 158: 1074–1089.
- Doyle KP, Simon RP, Stenzel-Poore MP. Mechanisms of ischemic brain damage. *Neuropharmacology* 2008, 55: 310–318.
- Lee JM, Zjpfel GJ, Choi DW. The changing landscape of ischemic brain injury mechanisms. *Nature* 1999, 399: A7–14.
- Cao Z, Wu XF, Peng Y, Zhang R, Li N, Yang JY, *et al.* Scorpion venom heat-resistant peptide attenuates glial fibrillary acidic protein expression via c-jun/ap-1. *Cell Mol Neurobiol* 2015, 35: 1073–1079.
- Wang T, Wang SW, Zhang Y, Wu XF, Peng Y, Cao Z, *et al.* Scorpion venom heat-resistant peptide (SVHRP) enhances neurogenesis and neurite outgrowth of immature neurons in adult mice by up-regulating brain-derived neurotrophic factor (BDNF). *PLoS One* 2014, 9: e109977.
- Yin SM, Zhao D, Yu DQ, Li SL, An D, Peng Y, *et al.* Neuroprotection by scorpion venom heat resistant peptide in 6-hydroxydopamine rat model of early-stage Parkinson's disease. *Sheng Li Xue Bao* 2014, 66: 658–666.
- Zhang XG, Wang X, Zhou TT, Wu XF, Peng Y, Zhang WQ, *et al.* Scorpion venom heat-resistant peptide protects transgenic *Caenorhabditis elegans* from  $\beta$ -amyloid toxicity. *Front Pharmacol* 2016, 7: 227.
- Sun J, Tong L, Luan Q, Deng J, Li Y, Li Z, *et al.* Protective effect of delayed remote limb ischemic postconditioning: role of mitochondrial K (ATP) channels in a rat model of focal cerebral ischemic reperfusion injury. *J Cereb Blood Flow Metab* 2012, 32: 851–859.
- Hossmann KA. Cerebral ischemia: models, methods and outcomes. *Neuropharmacology* 2008, 55: 257–270.
- Clark WM, Lessov NS, Dixon MP, Eckenstein F. Monofilament intraluminal middle cerebral artery occlusion in the mouse. *Neurol Res* 1997, 19: 641–648.
- Tsubokawa T, Jadhav V, Solaroglu I, Shiokawa Y, Konishi Y, Zhang JH. Lecithinized superoxide dismutase improves outcomes and attenuates focal cerebral ischemic injury via antiapoptotic mechanisms in rats. *Stroke* 2007, 38: 1057–1062.
- Mdzinarishvili A, Kiewert C, Kumar V, Hillert M, Klein J. Bilobalide prevents ischemia-induced edema formation *in vitro* and *in vivo*. *Neuroscience* 2007, 144: 217–222.
- Stumm R, Kolodziej A, Prinz V, Endres M, Wu DF, Holtt V. Pituitary adenylate cyclase-activating polypeptide is up-regulated in cortical pyramidal cells after focal ischemia and protects neurons from mild hypoxic/ischemic damage. *J Neurochem* 2007, 103: 1666–1681.
- Shu JC, Bradley ME, Lee TC. Chemical hypoxia triggers apoptosis of cultured neonatal rat cardiac myocytes: Modulation by calcium-regulated proteases and protein kinases. *Mol Cell Biochem* 1998, 178: 141–149.
- Goldberg MP, Choi DW. Oxygen and glucose deprivation in cortical cell culture: calcium-dependent and calcium-independent mechanisms of neuronal injury. *J Neurosci* 1993, 13: 3510–3524.
- Wu JB, Song NN, Wei XB, Guan HS, Zhang XM. Protective effects of paeonol on cultured rat hippocampal neurons against oxygen-glucose deprivation induced injury. *J Neurol Sci* 2008, 264: 50–55.
- Xu W, Zha RP, Wang WY, Wang YP. Effects of scutellarin on PKC $\gamma$  in PC12 cell injury induced by oxygen and glucose deprivation. *Acta Pharmacol Sin* 2007, 28: 1573–1579.
- Schinder AF, Olson EC, Spitzer NC, Montal M. Mitochondrial dysfunction is a primary event in glutamate neurotoxicity. *J Neurosci* 1996, 16: 6125–6133.
- Sgambato-Faure V, Cenci MA. Glutamatergic mechanisms in the dyskinesias induced by pharmacological dopamine replacement and deep brain stimulation for the treatment of Parkinson's disease. *Prog Neurobiol* 2012, 96: 69–86.
- Ankarcrona M, Dypbukt JM, Bonfoco E, Zhivotovsky B, Orrenius S, Lipton SA, *et al.* Glutamate-induced neuronal death: a succession of necrosis or apoptosis depending on mitochondrial function. *Neuron* 1995, 15: 961–973.
- Chen M, Lu TJ, Chen XJ, Zhou Y, Chen Q, Feng XY, *et al.* Differential roles of NMDA receptor subtypes in ischemic neuronal cell death and ischemic tolerance. *Stroke* 2008, 39: 3042–3048.
- Liu, B, Li L, Zhang Q, Chang N, Wang D, Shan Y, *et al.* Preservation of GABAA receptor function by PTEN inhibition protects against neuronal death in ischemic stroke. *Stroke* 2010, 41: 1018–1026.
- Lyden PD, Jackson-Friedman C, Shin C, Hassid S. Synergistic combinatorial stroke therapy: A quantal bioassay of a GABA agonist and a glutamate antagonist. *Exp Neurol* 2000, 163: 477–489.
- Krupinski J, Slevin M, Marti E, Catena E, Rubio F, Gaffney J. Time-course phosphorylation of the mitogen activated protein (MAP) kinase group of signalling proteins and related molecules following middle cerebral artery occlusion (MCAO) in rats. *Neuropathol Appl Neurobiol* 2003, 29: 144–158.
- Piao CS, Che Y, Han PL, Lee JK. Delayed and differential induction of p38 MAPK isoforms in microglia and astrocytes in the brain after transient global ischemia. *Mol Brain Res* 2002, 107: 137–144.
- Ginsberg MD. Neuroprotection for ischemic stroke: past, present and future. *Neuropharmacology* 2008, 55: 363–389.
- Moussaddy A, Demchuk AM, Hill MD. Thrombolytic therapies for ischemic stroke: Triumphs and future challenges. *Neuropharmacology* 2018, 134: 272–279.
- Mehta SL, Manhas N, Raghuram R. Molecular targets in cerebral ischemia for developing novel therapeutics. *Brain Res Rev* 2007, 54: 34–66.
- Nakka VP, Gusain A, Mehta SL, Raghuram R. Molecular mechanisms of apoptosis in cerebral ischemia: multiple neuroprotective opportunities. *Mol Neurobiol* 2008, 37: 7–38.

34. Aromugam TV, Woodruff TM, Lathia JD, Selvaraj PK, Mattson MP, Taylor SM. Neuroprotection in stroke by complement inhibition and immunoglobulin therapy. *Neuroscience* 2009, 158: 1074–1089.
35. Burd I, Welling J, Kannan G, Johnston MV. Excitotoxicity as a common mechanism for fetal neuronal injury with hypoxia and intrauterine inflammation. *Adv Pharmacol* 2016, 76: 85–101.
36. Howes MJ, Houghton PJ. Plants used in Chinese and Indian traditional medicine for improvement of memory and cognitive function. *Pharmacol Biochem Behav* 2003, 75: 513–527.
37. Jiang H, Luo X, Bai D. Progress in clinical, pharmacological, chemical and structural biological studies of huperzine A: a drug of traditional Chinese medicine origin for the treatment of Alzheimer's disease. *Curr Med Chem* 2003, 10: 2231–2252.
38. Yan H, Li L, Tang XC. Treating senile dementia with traditional Chinese medicine. *Clin Interv Aging* 2007, 2: 201–208.
39. Wang Z, Wang W, Shao Z, Gao B, Li J, Ma J, *et al.* Eukaryotic expression and purification of anti-epilepsy peptide of *Buthus martensii* Karsch and its protein interactions. *Mol Cell Biochem* 2009, 330: 97–104.
40. Gong JP, Gwee MC, Gopalakrishnakone P. *Buthus martensii* karsch venom: prejunctional adrenergic activity in the rat isolated anococcygeus muscle. *Toxicon* 1995, 33: 1133–1139.
41. Srinivasan KN, Nirthanan S, Sasaki T, Sato K, Cheng B, Gwee MC, *et al.* Functional site of bukatoxin, an alpha-type sodium channel neurotoxin from the Chinese scorpion (*Buthus martensii* Karsch) venom: probable role of the (52) PDKVP (56) loop. *FEBS Lett* 2001, 494: 145–149.
42. Ye P, Jiao Y, Li Z, Hua L, Fu J, Jiang F, *et al.* Scorpion toxin BmK I directly activates Nav1.8 in primary sensory neurons to induce neuronal hyperexcitability in rats. *Protein Cell* 2015, 6: 443–452.
43. Zhu H, Wang Z, Jin J, Pei X, Zhao Y, Wu H, *et al.* Parkinson's disease-like forelimb akinesia induced by BmK I, a sodium channel modulator. *Behav Brain Res* 2016, 308: 166–176.
44. Mitani A, Kataoka K. Critical levels of extracellular glutamate mediating gerbil hippocampal delayed neuronal death during hypothermia: Brain microdialysis study. *Neuroscience* 1991, 42: 661–670.
45. Cull-Candy S, Brickley S, Farrant M. NMDA receptor subunits: diversity, development and disease. *Curr Opin Neurobiol* 2001, 11: 327–335.
46. Lau CG, Zukin RS. NMDA receptor trafficking in synaptic plasticity and neuropsychiatric disorders. *Nat Rev Neurosci* 2007, 8: 413–426.
47. Prybylowski K, Wenthold RJ. N-methyl-D-aspartate receptors: subunit assembly and trafficking to the synapse. *J Biol Chem* 2004, 279: 9673–9676.
48. Su F, Guo AC, Li WW, Zhao YL, Qu ZY, Wang YJ, *et al.* Low-dose ethanol preconditioning protects against oxygen-glucose deprivation/reoxygenation-induced neuronal injury by activating large conductance, Ca<sup>2+</sup>-activated K<sup>+</sup> channels in vitro. *Neurosci Bull* 2017, 33: 28–40.
49. Prybylowski K, Wenthold RJ. N-methyl-D-aspartate receptors: subunit assembly and trafficking to the synapse. *J Biol Chem* 2004, 279: 9673–9676.
50. Chang YY, Gong XW, Gong HQ, Liang PJ, Zhang PM, Lu QC. GABA<sub>A</sub> receptor activity suppresses the transition from interictal to ictal epileptiform discharges in juvenile mouse hippocampus. *Neurosci Bull* 2018, 34:1007–1016.
51. Mele M, Aspromonte MC, Duarte CB. Downregulation of GABA<sub>A</sub> receptor recycling mediated by HAP1 contributes to neuronal death in in vitro brain ischemia. *Mol Neurobiol* 2017, 54: 45–57.
52. Kovalska M, Kovalska L, Pavlikova M, Janickova M, Mikuskova K, Adamkov M, *et al.* Intracellular signaling MAPK pathway after cerebral ischemia-reperfusion injury. *Neurochem Res* 2012, 37:1568–1577.
53. Chen L, Liu X, Wang H, Qu M. Gastrodin attenuates pentylentetrazole-induced seizures by modulating the mitogen-activated protein kinase-associated inflammatory responses in mice. *Neurosci Bull* 2017, 33: 264–272.
54. Irving EA, Bamford M. Role of mitogen- and stress-activated kinases in ischemic injury. *J Cereb Blood Flow Metab* 2002, 22: 631–647.
55. Barone FC, Irving EA, Ray AM, Lee JC, Kassis S, Kumar S, *et al.* Inhibition of p38 mitogen-activated protein kinase provides neuroprotection in cerebral focal ischemia. *Med Res Rev* 2001, 21: 129–145.
56. Jiang M, Li J, Peng Q, Liu Y, Liu W, Peng J, *et al.* Neuroprotective effects of bilobalide on cerebral ischemia and reperfusion injury are associated with inhibition of pro-inflammatory mediator production and down-regulation of JNK1/2 and p38 MAPK activation. *J Neuroinflammation* 2014, 11: 167.
57. Strassburger M, Braun H, Reymann KG. Anti-inflammatory treatment with the p38 mitogen-activated protein kinase inhibitor SB239063 is neuroprotective, decreases the number of activated microglia and facilitates neurogenesis in oxygen-glucose-deprived hippocampal slice cultures. *Eur J Pharmacol* 2008, 592: 55–61.



ORIGINAL ARTICLE

# AVP(4-8) Improves Cognitive Behaviors and Hippocampal Synaptic Plasticity in the APP/PS1 Mouse Model of Alzheimer's Disease

Xiumin Zhang<sup>1,2</sup> · Fang Zhao<sup>2</sup> · Chenfang Wang<sup>2</sup> · Jun Zhang<sup>2</sup> · Yu Bai<sup>2</sup> · Fang Zhou<sup>2</sup> · Zhaojun Wang<sup>2</sup> · Meina Wu<sup>2</sup> · Wei Yang<sup>2</sup> · Junhong Guo<sup>1</sup> · Jinshun Qi<sup>2</sup>

Received: 9 January 2019 / Accepted: 12 July 2019 / Published online: 12 October 2019  
© Shanghai Institutes for Biological Sciences, CAS 2019

**Abstract** Memory deficits with aging are related to the neurodegeneration in the brain, including a reduction in arginine vasopressin (AVP) in the brain of patients with Alzheimer's disease (AD). AVP(4-8), different from its precursor AVP, plays memory enhancement roles in the CNS without peripheral side-effects. However, it is not clear whether AVP(4-8) can improve cognitive behaviors and synaptic plasticity in the APP/PS1 mouse model of AD. Here, we investigated for the first time the neuroprotective effects of AVP(4-8) on memory behaviors and *in vivo* long-term potentiation (LTP) in APP/PS1-AD mice. The results showed that: (1) APP/PS1-AD mice had lower spontaneous alternation in the Y-maze than wild-type (WT) mice, and this was significantly reversed by AVP(4-8); (2) the prolonged escape latency of APP/PS1-AD mice in the Morris water maze was significantly decreased by AVP(4-8), and the decreased swimming time in target quadrant recovered significantly after AVP(4-8) treatment; (3) *in vivo* hippocampal LTP induced by high-frequency stimulation had a significant deficit in the AD mice, and this was partly rescued by AVP(4-8); (4) AVP(4-8) significantly up-regulated the expression levels of postsynaptic density 95 (PSD95) and nerve growth factor (NGF) in the hippocampus of AD mice. These results reveal the

beneficial effects of AVP(4-8) in APP/PS1-AD mice, showing that the intranasal administration of AVP(4-8) effectively improved the working memory and long-term spatial memory of APP/PS1-AD mice, which may be associated with the elevation of PSD95 and NGF levels in the brain and the maintenance of hippocampal synaptic plasticity.

**Keywords** AVP(4-8) · APP/PS1 transgenic mice · Cognitive behavior · Synaptic plasticity · *In vivo* hippocampal LTP

## Introduction

Alzheimer's disease (AD) is an insidious degenerative disease of the brain characterized by progressive cognitive deficits, memory loss, and specific neuropsychiatric anomalies [1]. Multiple pathological characteristics of AD have been identified in the brain, including amyloid-beta ( $A\beta$ ) deposits, tau hyperphosphorylation, neurotrophic factor dysregulation, and synaptic deficits [2–4]. Interestingly, a significant decrease in arginine vasopressin (AVP) has been found in the cerebrospinal fluid and many brain regions, especially in the hippocampus [5, 6] of AD patients.

AVP, traditionally associated with the regulation of water balance and blood pressure in the periphery [7], has been considered as a neurotransmitter and/or neuromodulator in the central neural system (CNS) and affects diverse aspects of cognitive ability such as the consolidation and retrieval of memory [8]. Previous research has shown that AVP-deficient rats have poor social discrimination, object discrimination, and conditioned learning [2, 9]; mice with V1a and V1b receptor knockout have deficits in mnemonic

✉ Junhong Guo  
neuroguo@163.com

✉ Jinshun Qi  
jinshunqi2009@163.com

<sup>1</sup> Department of Neurology, First Hospital, Shanxi Medical University, Taiyuan 030001, China

<sup>2</sup> Department of Physiology, Key laboratory of Cellular Physiology, Ministry of Education, Shanxi Medical University, Taiyuan 030001, China

function [10–12]; and administration of AVP receptor antagonists leads to memory impairment in rats [13]. On the contrary, administration of AVP has been reported to facilitate learning and memory [14–16], and enhance synaptic plasticity and the expression of synapse-related protein in the hippocampus [15]. We have reported that AVP rescues A $\beta$ -induced impairments of spatial memory [17], hippocampal long-term potentiation (LTP) [18], and spontaneous discharges [17] in rats.

Unfortunately, the effects of systemic administration of AVP are more complicated [19–21] due to the widely distributed receptors and more peripheral side-effects. AVP(4-8), a major metabolic fragment of AVP, differs from its precursor and has specific receptors and distribution in the CNS including the hippocampus [22] and cortex [23]. There is evidence that the hippocampus may be an important target site for the effect of AVP(4-8), and its receptor may be a link between AVP and cognitive behavior [24]. More importantly, AVP(4-8) has a 1000-times more potent effect on memory processes than AVP in a passive avoidance experience [25, 26]. Besides, another advantage of AVP(4-8) in the CNS is that it lacks the peripheral side-effects of its parent hormone AVP, like pressor and/or antidiuretic activity [25, 26].

However, it is not clear whether AVP(4-8) can improve the cognitive behaviors and synaptic plasticity in the APP/PS1 mouse model of AD. We supposed that the decreased AVP, especially its intermediate product AVP(4-8), in the brain may contribute to the cognitive impairment of AD, and exogenous application of AVP(4-8) might be beneficial for improving synaptic plasticity and cognitive behaviors in AD. Therefore, we investigated for the first time the neuroprotective effects of AVP(4-8) on the cognitive behaviors in APP/PS1-AD mice using several behavioral techniques. We also examined memory-related activity (*in vivo* hippocampal LTP) and proteins [post-synaptic density-95 (PSD95) and nerve growth factor (NGF)] in the hippocampus to clarify the possible electrophysiological and molecular mechanisms.

## Material and Methods

### Animals and Grouping

Male heterozygous APP/PS1 transgenic mice (APP<sup>swe</sup>/PS1<sup>dE9</sup>, Beijing Huafukang Bioscience Co., Inc.) and wild-type (WT) mice (C57BL/6J, Beijing Vital River Laboratory Animal Technology Co., Ltd.) were maintained in an animal room (20 °C  $\pm$  2 °C, 12 h light/dark cycle) with enough food and water. All operations on mice were approved by the Ethical Committee of Shanxi Medical University. At 8 months of age, the mice were randomly divided into 4 groups

( $n = 10$ – $13$ /group): WT+Saline, WT+AVP(4-8), APP/PS1+Saline, and APP/PS1+AVP(4-8).

### Drug Administration

Before behavioral tests, vasopressin metabolite neuropeptide [pGlu4, Cystine6]-AVP(4-8) (2  $\mu$ g/kg, Phoenix Pharmaceuticals, Inc., USA) or an equivalent volume of saline was administered intranasally three times a day for 4 weeks. The application of AVP(4-8) or saline was continued throughout the behavioral test period. Fig. 1 shows the timeline of the experimental procedures.

### Y-Maze Test

After 4 weeks of drug administration (Fig. 1), the Y-maze was first used to measure short-term working memory in mice. This was a three-arm equiangular maze, and the arms were 30 cm long, 7 cm high, and 15 cm wide. Each animal ( $n = 9$ /group) was placed in the central triangular region and allowed to travel freely in the maze for 8 min. The Smart 3.0 software system was used to record the number and order of arm entries. A correct spontaneous alternation was identified as a set of three different arm entries. The percentage of correct spontaneous alternation was calculated as (number of correct alternations)/(total arm entries  $- 2$ )  $\times 100\%$ . A higher percentage of correct spontaneous alternation indicates better working memory.

### Morris Water Maze (MWM) Test

Hippocampus-dependent spatial learning and reference memory were assessed with the MWM test, as performed previously in our lab. The pool (diameter, 120 cm; height, 50 cm) filled with opaque water (temperature 20 °C  $\pm$  2 °C), was conceptually divided into four equal quadrants with the escape platform submerged in the center of the first quadrant (target quadrant) (1 cm below the water surface). Different-shaped black marks were displayed at the perimeter of each quadrant. During the acquisition phase, mice ( $n = 9$ – $10$ /group) were trained in 4 sessions (60 s per session) per day over 5 consecutive days in searching for the underwater platform. The escape latency and swimming trials were recorded by a video-tracking system (Ethovision 3.0, Noldus Information Technology, Wageningen, Netherlands). In probe trials (day 6), mice were allowed to swim freely for 1 min without the platform. The swimming time in the target quadrant and the swimming speed were recorded. After that, a visible platform test was performed to assess the visual and motor ability of mice by recording the time when they arrived at the escape platform.

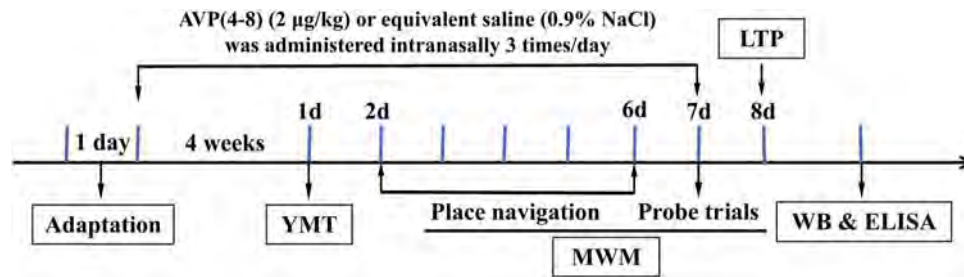


**Fig. 1** Timeline of the experimental procedures. After 1 day of adaptation to the lab setting and 4 weeks of treatment with AVP(4-8) (2 µg/kg) or equivalent saline, the Y-maze test (YMT), Morris water

maze (MWM) test, *in vivo* hippocampal long-term potentiation (LTP) recording, Western blotting, and ELISA were performed sequentially.

### **In Vivo Hippocampal LTP Recording**

Hippocampal LTP is a synaptic model of memory with the closest connection to long-term memory due to its long duration. Therefore, field excitatory postsynaptic potentials (fEPSPs) in the hippocampal CA1 region were recorded after the MWM test was finished. Mice were anesthetized with chloral hydrate (5%, i.p., 0.08 mL/kg) and placed in a stereotaxic apparatus (RWD Life Science, Shenzhen, China). Then, a hole (2.0 mm posterior to bregma and 1.5 mm from midline) was drilled through the skull for a self-made bound stimulating/recording electrode (FHC, USA) inserted into the Schaffer collateral/CA1 region and recording fEPSPs. The distance between the tips of the recording and stimulating electrodes was 0.5 mm horizontally, with a 0.3 mm of vertical difference. The tips of the stimulating and recording electrodes were located in the Schaffer collateral/commissural pathway and the stratum radiatum of the hippocampal CA1 region. The orientation of the tips was determined by electrophysiological criteria (appearance of an evoked fEPSP) and final histological verification. Test stimuli from Master-9 stimulator (AMPI, Jerusalem, Israel) were delivered to the Schaffer-collateral/commissural pathway at 0.033 Hz and an intensity that induced 40%–50% of the maximum fEPSP response. Baseline synaptic transmission was recorded for 30 min to ensure stability. Paired pulse facilitation (PPF) was initiated by paired stimuli at an interval of 50 ms, and calculated as fEPSP2/fEPSP1. Then, LTP was induced by high-frequency stimulation (HFS) (three trains of 20 pulses at 200 Hz with an interval of 30 s) at an intensity that evoked 80% of the maximum fEPSP. After that, fEPSPs were evoked and recorded again for at least 60 min with the same intensity as the test stimuli. The voltage signals were acquired at 40 kHz and filtered with a 1-kHz cutoff frequency and a 1-s time constant. The slopes of the raw fEPSP traces were obtained automatically by the system software (RM-6240 Biological Signal Collecting and Processing System, Chengdu Instruments Ltd, China), and every four fEPSPs were averaged.

### **Western Blotting**

Mice ( $n = 6/\text{group}$ ) were sacrificed to obtain whole brains and the hippocampus was quickly dissected on ice to determine the level of PSD95. All samples were snap-frozen in liquid nitrogen and stored at  $-80\text{ }^{\circ}\text{C}$  until use. The hippocampal tissue was homogenized in the tissue protein extraction reagent and phenylmethylsulfonyl fluoride (PMSF). After centrifugation (13,000 rpm, 15 min,  $4\text{ }^{\circ}\text{C}$ ), protein in the supernatant was quantified using a BCA Protein Assay Kit. Each sample (20 µg) was separated by 10% sodium dodecyl sulfate-polyacrylamide gel electrophoresis for detecting  $\beta$ -actin, PSD95, and NGF. Separated proteins were then transferred onto polyvinylidene difluoride membranes, which were blocked with 5% bovine serum albumin (BSA) for 2 h and then incubated with primary rabbit antibodies against  $\beta$ -actin (1:5,000, ZSGB-BIO, Beijing), PSD95 (1:500, Abcam), or mouse antibody against NGF (1:200, Santa Cruz Biotechnology) in TBST containing 5% BSA at  $4\text{ }^{\circ}\text{C}$  overnight. After washing with TBST 3 times for 15 min, 10 min, and 5 min, the blots were incubated with horseradish peroxidase-conjugated goat anti-rabbit IgG (1:5,000, Abcam) and goat anti-mouse IgG (1:5,000, Abcam) for 2 h at  $4\text{ }^{\circ}\text{C}$ . After washing as above, the blots were assessed by an ECL assay system. Densitometric analysis of the Western blots was performed using Alpha View software.

### **Enzyme-Linked Immunosorbent Assay (ELISA)**

To further verify the result of hippocampal NGF measurement in Western blots, we used a pre-coated Mouse NGF/NGF Beta ELISA Kit (Boster Biological Technology, Wuhan, China. Catalog #EK0470) ( $n = 4\text{--}5/\text{group}$ ) to measure the NGF content in the hippocampus according to the manufacturer's instructions. The absorbance was measured at 450 nm using an Enspire<sup>TM</sup> multilabel reader 2300 (Perkin Elmer, Turku, Finland).

## Statistical Analysis

All data are reported as the mean  $\pm$  SEM, and analyzed with SPSS 16.0 and SigmaPlot 12.3 statistical packages. Three-way repeated measure analysis of variance (ANOVA) with time, genotype, and treatment as within-subject factors was used to analyze the escape latency in MWM acquisition and the fEPSP slopes from *in vivo* hippocampal LTP. The other data were analyzed with two-way ANOVA followed by Tukey's *post hoc* test. Statistical significance was considered to be  $P < 0.05$ .

## Results

### AVP(4-8) Improves Working Memory of Both WT and APP/PS1 Mice in the Y-Maze Test

The total arm entries did not show any significant difference among the four groups ( $P > 0.05$ ), which revealed that genotype and AVP(4-8) had no influence on the locomotor activity and motor function (Fig. 2A). In contrast, a significantly less spontaneous alternation was seen in the APP/PS1+Saline group ( $59.67\% \pm 4.98\%$ ) than in the WT+Saline group ( $76.56\% \pm 2.01\%$ ,  $P < 0.001$ ). AVP(4-8) treatment caused significantly more spontaneous alternation in the WT+AVP(4-8) ( $81.44\% \pm 1.16\%$ ,  $P < 0.05$ ) and APP/PS1+AVP(4-8) groups ( $71.78\% \pm 1.14\%$ ,  $P < 0.001$ ) than in their respective saline control groups (Fig. 2B; two-way ANOVA: genotype:  $F_{(1,32)} = 74.449$ ,  $P < 0.001$ ; AVP(4-8):  $F_{(1,32)} = 30.510$ ,  $P < 0.001$ ; genotype  $\times$  AVP(4-8):  $F_{(1,32)} = 5.507$ ,  $P < 0.05$ ), indicating a working memory enhancement in normal mice by AVP(4-8), an impairment in APP/PS1 mice, and its reversal by AVP(4-8).

### AVP(4-8) Rescued Spatial Learning and Reference Memory Impairments of APP/PS1 Mice in MWM

The MWM test was used to assess the spatial learning and memory of mice. The three-way repeated measure ANOVA showed no interaction among the three within-subject factors (time  $\times$  genotype  $\times$  treatment:  $F_{(4,32)} = 1.015$ ,  $P > 0.05$ ), but genotype and treatment had significant main effects and an interaction on the escape latency (genotype:  $F_{(1,8)} = 112.694$ ,  $P < 0.001$ ; treatment:  $F_{(1,8)} = 5.755$ ,  $P < 0.05$ ; genotype  $\times$  treatment:  $F_{(1,8)} = 448.594$ ,  $P < 0.05$ ). Throughout the acquisition session there was an overall gradual decrease in escape latency (day:  $F_{(4,32)} = 45.195$ ,  $P < 0.001$ ; Table 1, Fig. 3A). What is more, the APP/PS1+Saline group spent more time on finding the hidden platform than the WT+Saline group on days 3–5 ( $P < 0.001$ ), while treatment with AVP(4-8) decreased the escape latency in the APP/PS1+AVP(4-8) group on days 4–5 ( $P < 0.05$ ). Representative swimming traces of mice on navigation training day 5 are shown in Fig. 3B. This result indicated a spatial learning impairment in APP/PS1 mice, which was partly rescued by AVP(4-8) treatment. In the probe test (Fig. 3C, D), a reference memory deficit also occurred in the APP/PS1+Saline group, with a lower percentage of swimming time in the target quadrant than its WT control ( $P < 0.001$ ). After treatment with AVP(4-8), the APP/PS1+AVP(4-8) group showed a significantly higher percentage of swimming time ( $P < 0.05$ ) than the APP/PS1+Saline group (two-way ANOVA: genotype:  $F_{(1,35)} = 31.43$ ,  $P < 0.001$ ; AVP(4-8):  $F_{(1,35)} = 6.62$ ,  $P < 0.05$ ; genotype  $\times$  AVP(4-8):  $F_{(1,35)} = 0.586$ ,  $P = 0.450$ ). Meantime, all mice in the four groups showed similar swimming speeds in the probe test (Fig. 3E) and similar swimming times to the visible platform (Fig. 3F). These results suggested that the differences in spatial learning and memory did not result from alterations of motor ability and visual acuity.

**Fig. 2** AVP(4-8) improved the working memory of APP/PS1 mice in the Y-maze test. **A** Total arm entries during 8 min, with no significant difference between groups ( $n = 9/\text{group}$ ). **B** Percentage of correct spontaneous alternation, with a significant decrease in the APP/PS1 mice compared with controls, and a significant reversal after AVP(4-8) treatment ( $*P < 0.05$ ,  $***P < 0.001$ ).

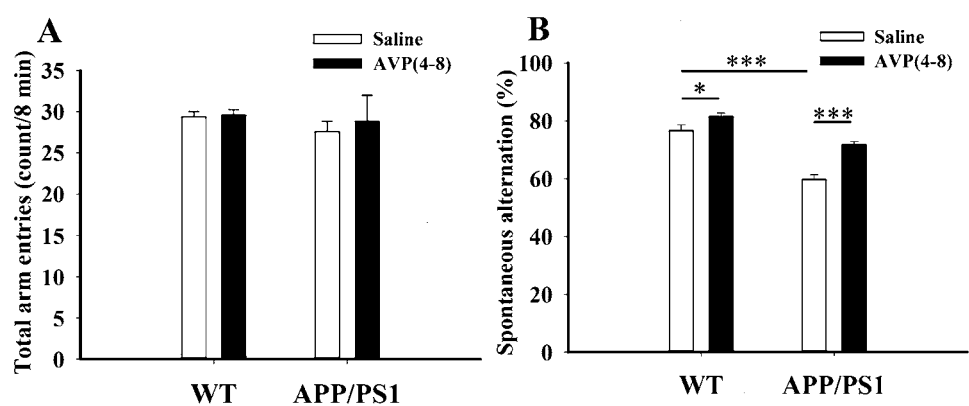


**Table 1** The escape latency (s) of mice in the four groups during acquisition phase.

	WT+Saline ( <i>n</i> = 9)	WT+AVP (4-8) ( <i>n</i> = 9)	APP/PS1+Saline ( <i>n</i> = 9)	APP/PS1+AVP (4-8) ( <i>n</i> = 9)
Day 1	50.58 ± 3.14	50.06 ± 3.69	55.60 ± 2.56	57.34 ± 1.31
Day 2	42.37 ± 3.92	44.74 ± 3.82	54.22 ± 2.50	46.78 ± 3.08
Day 3	36.18 ± 2.48	38.78 ± 4.75	50.46 ± 3.26***	54.92 ± 1.48
Day 4	20.82 ± 2.07	20.24 ± 2.33	46.19 ± 5.00***	32.10 ± 3.37 <sup>#</sup>
Day 5	20.71 ± 2.15	15.54 ± 1.42	45.38 ± 4.11***	32.99 ± 4.40 <sup>#</sup>

\*\*\**P* < 0.001 versus WT+Saline mice; <sup>#</sup>*P* < 0.05 versus APP/PS1 + Saline mice.

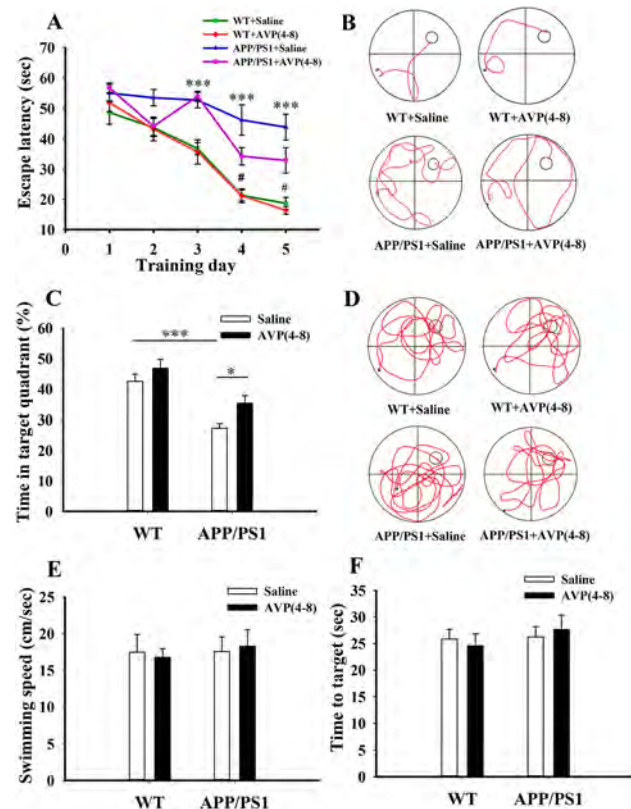


**Fig. 3** AVP(4-8) rescued the spatial learning and memory of APP/PS1 mice in MWM tests. **A** Average escape latencies of mice in the place navigation test during 5 training days (\*\*\**P* < 0.001 vs WT+Saline mice, <sup>#</sup>*P* < 0.05 vs APP/PS1+Saline mice). **B** Representative swimming traces of mice on navigation training day 5. **C** Percentages of swimming time spent in the target quadrant in the spatial probe test (\**P* < 0.05, \*\*\**P* < 0.001). **D** Representative swimming traces in the probe test. **E, F** Average swimming speed in the probe test (**E**) and swimming time to the visible platform (**F**) (*n* = 9).

### AVP(4-8) Partly Reversed the Suppression of Hippocampal Synaptic Plasticity in APP/PS1 Mice

The hippocampal fEPSP slope differed before and after HFS (Fig. 4A, B). During 30 min of fEPSP recording before HFS, the basic synaptic transmission was stable in each group. After HFS, LTP was induced successfully with

a rapid increase in the fEPSP slope and then gradual attenuation with time in the four groups (time:  $F_{(44, 176)} = 293.464$ ,  $P < 0.001$ ). At 30 and 60 min after HFS, the fEPSP slope in the APP/PS1+Saline group was significantly lower ( $n = 6$ ; 30 min:  $139.09\% \pm 2.69\%$ ,  $P < 0.01$ ; 60 min:  $116.69\% \pm 5.09\%$ ,  $P < 0.001$ ) than in the WT+Saline group ( $n = 8$ ; 30 min:  $176.19\% \pm 8.86\%$ ; 60 min:  $166.72\% \pm 3.68\%$ ). After treatment with AVP(4-8), the fEPSP slopes in the APP/PS1+AVP(4-8) group significantly increased compared to that in the APP/PS1+Saline group ( $n = 7$ ; 30 min:  $157.19\% \pm 3.52\%$ ,  $P < 0.05$ ; 60 min:  $145.06\% \pm 3.38\%$ ,  $P < 0.001$ ) (genotype:  $F_{(1,24)} = 23.604$ ,  $P < 0.01$ , AVP(4-8):  $F_{(1,24)} = 4.204$ ,  $P < 0.05$ ; genotype  $\times$  AVP(4-8):  $F_{(1,24)} = 0.507$ ,  $P < 0.05$ ). Representative fEPSP traces before and 60 min after HFS in different groups are shown in Fig. 4C. Besides, we did not find any significant difference in the PPF ratio among the four groups. These results demonstrated that AVP(4-8) partly rescued the LTP maintenance in APP/PS1 mice, and this could involve a postsynaptic mechanism.

### AVP(4-8) Up-Regulated the Levels of PSD95 and NGF in the Hippocampus of APP/PS1 Mice

To further clarify the molecular mechanisms underlying the improving effects of AVP(4-8) on behaviors and LTP in APP/PS1 mice, the expression levels of PSD95 and NGF were measured using Western blot ( $n = 6$ /group). The data (Fig. 5A) showed that the level of PSD95 in the APP/PS1+Saline group was significantly lower ( $P < 0.001$ ) than in the WT+Saline group, while AVP(4-8) application significantly up-regulated the level of PSD95 in the APP/PS1+AVP(4-8) group ( $P < 0.001$ ). Two-way ANOVA showed significant main effects and an interaction (genotype:  $F_{(1,23)} = 128.605$ ,  $P < 0.001$ , AVP(4-8):  $F_{(1,23)} = 32.890$ ,  $P < 0.001$ ; genotype  $\times$  AVP(4-8):  $F_{(1,23)} = 7.319$ ,  $P < 0.05$ ). In addition, the NGF data (Fig. 5B) showed a distinct increase in the NGF level in the WT+AVP(4-8) ( $P < 0.05$ ) and APP/PS1+AVP(4-8) ( $P < 0.05$ ) groups compared to their respective saline controls (two-way

**Fig. 4** AVP(4-8) partly reversed the suppression of synaptic plasticity in the hippocampus of APP/PS1 mice. **A** Changes in the slope of fEPSPs before and after high-frequency stimulation (HFS) in the CA1 region. **B** fEPSP slopes before HFS, and 1, 30, and 60 min after HFS in the four groups ( $*P < 0.05$ ,  $**P < 0.01$ ,  $***P < 0.001$ ). **C** Representative fEPSP traces before (black) and 60 min after (red) HFS in the different groups. **D** Paired-pulse facilitation (PPF) in the different groups. Inset: a sample PPF trace.

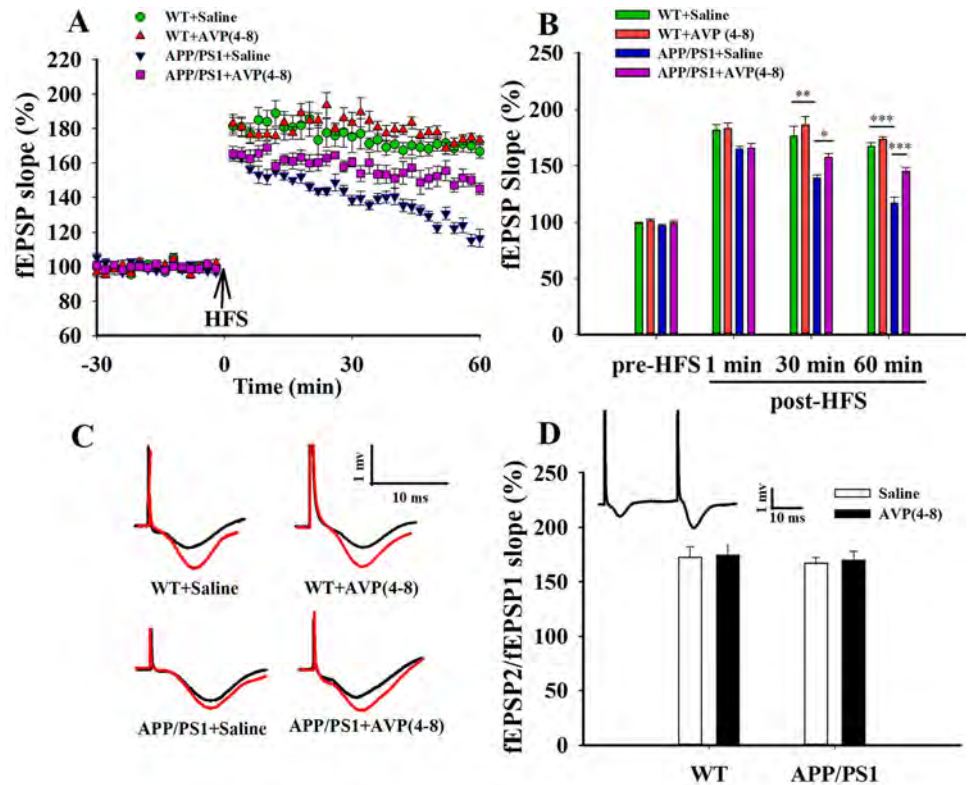
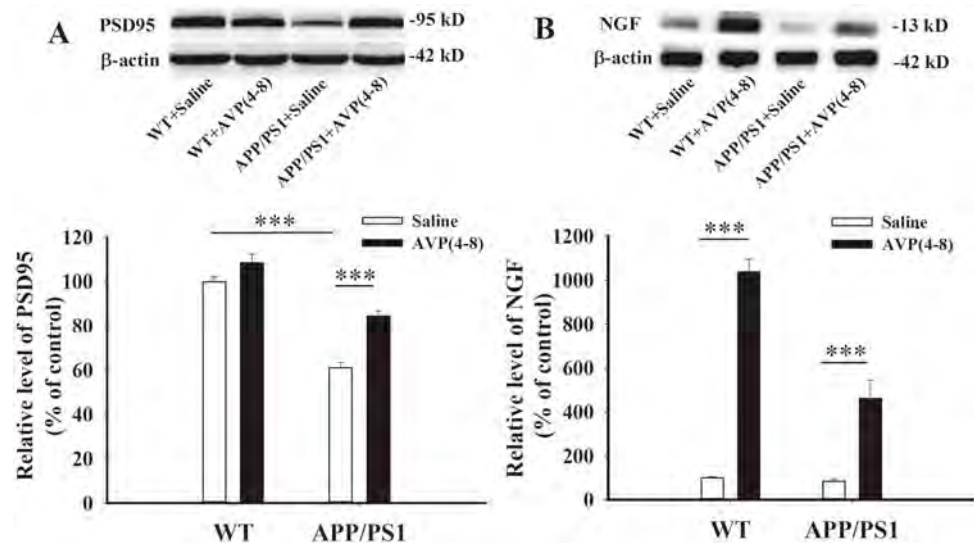


**Fig. 5** AVP(4-8) up-regulated the levels of PSD95 and NGF in the hippocampus of APP/PS1 mice. **A** Representative Western blots of PSD95 (upper) and their quantitative plots (lower) in the different groups, showing that the decreased level of PSD95 in the hippocampus of APP/PS1 mice was partially reversed in the APP/PS1+AVP(4-8) group. **B** Representative Western blots of NGF (upper) and corresponding quantitative plots (lower), showing significantly increased levels of NGF in both the AVP(4-8)-treated groups ( $***P < 0.001$ ).



ANOVA: genotype:  $F_{(1,17)} = 2.937$ ,  $P = 0.109$ ; AVP(4-8):  $F_{(1,17)} = 12.116$ ,  $P < 0.01$ ; genotype  $\times$  AVP(4-8):  $F_{(1,17)} = 0.117$ ,  $P = 0.738$ ), but without any significant difference between the WT+Saline and APP/PS1+Saline groups. Similarly, the result of ELISA measurement of NGF (data not shown) was in accord with that from the Western blots. These together indicated that the neuroprotection of AVP(4-8) on the cognitive behavior and synaptic plasticity

in APP/PS1 mice is closely associated with the up-regulation of PSD95 and NGF levels in the hippocampus.

## Discussion

AD brings about a number of neurophysiological and neurochemical dysfunctions, like decreased AVP in the rat hippocampus [6], which partly accounts for the impairment

of learning and memory. AVP exerts complicated effects in the periphery and CNS, such as a classical neuroendocrine role, and neurotransmitter or neuromodulator functions. Interestingly, the central behavioral effects of AVP are dissociated from its traditional peripheral effects [26]. AVP(4-8), a more potent peptide than its parent molecule, is considered to be a mediator of the central behavioral effects of AVP [24]. Moreover, it has been established that there are specific receptors for AVP(4-8) in regions such as the hippocampus, cerebral cortex, and amygdaloid nucleus [22]. These regions are closely associated with learning and memory. Thus, AVP(4-8) receptors have been thought to link AVP with cognitive behaviors.

In the present study, we investigated for the first time the effects of AVP(4-8) on learning and memory in the APP/PS1 mouse model of AD. Because the hippocampus is essential for place learning and cognitive mapping, we first used the Y maze and MWM to study spatial reference memory. The behavioral tests showed that intranasal administration of AVP(4-8) for > 4 weeks improved the deficits in learning and memory of APP/PS1 mice. In the Y-maze test, AVP(4-8) increased the percentage of correct spontaneous alternation in both WT and APP/PS1 mice. This suggested that AVP(4-8) not only facilitated working memory in WT mice but also rescued the working memory impairment due to the gene mutation in APP/PS1 mice. Afterwards, the classical MWM test showed that the APP/PS1+AVP(4-8) group had a decreased escape latency in the acquisition phase and an increased swimming time in the target quadrant compared with the APP/PS1+saline group. These results indicated that AVP(4-8) partly improved the long-term spatial learning and memory in APP/PS1 mice. We noted that the escape latency of the APP/PS1+AVP(4-8) group on training day 3 had an unexpected increase over that on training day 2. We suppose this resulted from internal or external influences. The acquisition phase involves many complex memory processes, including collecting visual information about spatial location, and processing and remembering it to find the hidden platform. In the AD model treatment group, the drug effect might be another influencing factor. So, the escape latency is vulnerable to many internal or external factors. Maybe environmental disturbances on training day 3 affected the learning behaviors.

The mechanisms underlying the neuroprotective effects of AVP(4-8) are uncertain. It is known that hippocampal synaptic failure is the best correlate of cognitive decline in AD patients and in animal models of the disease. Hippocampal LTP, defined as long-lasting modifications of synaptic potentiation, is believed to be the basis of memory processes in the mammalian brain [27]. Thus, the improvement of cognitive behavior in APP/PS1 mice might be due to the recovery of hippocampal synaptic function [28].

Similar to our *in vivo* results for PPF and LTP, a recent *in vitro* brain slice study showed that APP/PS1 mice (8–10 months old) exhibit reduced basal synaptic transmission and LTP in the CA1 area of the hippocampus [29]. It has been reported that AVP and AVP(4-8) potentiate the excitatory postsynaptic potential and elicit the LTP of synaptic transmission of CA1/subiculum neurons in rat hippocampal slices [30]; AVP potentiates or rescues LTP in the hippocampal DG region of rats [18, 31, 32]. The present study further showed that AVP(4-8) treatment effectively rescued the hippocampal LTP in the CA1 region of APP/PS1 mice, adding to the research on AVP(4-8). The electrophysiological results were also consistent with and supported our findings in the cognitive behavioral tests, further clarifying the relevance of hippocampal LTP to spatial learning and memory.

Similar to our results, Gelman *et al.* also found that the reduction of basal synaptic transmission and LTP in the CA1 area is accompanied by invariant PPF [29]. This suggests that the impairments in basal synaptic transmission and LTP may result from a postsynaptic mechanism. It has been reported that hippocampal mutant APP and A $\beta$  significantly reduce the level of PSD [33]. Moreover, AD patients with mild cognitive impairment already demonstrate a decline of PSD95 [34]. Thus, a dysfunction of PSD95 may be the beginning of the process of synaptic damage prior to synaptic loss in the pathology of AD [35]. PSD95 is closely associated with synaptic plasticity because the neuronal scaffolding protein is associated with NMDA- and AMPA-type glutamate receptors and their downstream signaling molecules [36]. In accordance with previous studies, our Western blot results showed that the expression level of PSD95 in the hippocampus of APP/PS1 mice was markedly decreased. Interestingly, AVP(4-8) administration significantly up-regulated the level in APP/PS1 mice, which might partly account for the improvement of behavior and the rescue of LTP.

Previous studies [37] have confirmed the molecular basis of AVP(4-8) in cognitive protection, including: binding to and stimulating G protein-coupled receptors [38, 39], accumulating inositol 1,4,5-triphosphate, activating Ca<sup>2+</sup>/CaM-dependent kinase II [40] and protein kinase C [41], facilitating the phosphorylation of growth-associated protein and mitogen-activated protein kinase [42], enhancing the gene expression of NGF [43, 44] and brain-derived neurotrophic factor [45], and finally, strengthening synaptic plasticity and LTP [46]. In accordance with the above, our experimental results from Western blotting and ELISA showed that the expression level of NGF was greatly up-regulated in both WT and APP/PS1 mice by AVP(4-8). NGF is a neurotrophin particularly necessary for the survival, differentiation, maintenance and plasticity of forebrain cholinergic neurons. The degeneration of these

neurons has been thought to be responsible for cognitive impairments in AD patients [47, 48]. Early studies reported that anti-NGF antibody impairs cognitive behavior in rats, while NGF synthesis stimulators restore it [49]. The function of NGF has also been demonstrated in AD11 mice. These mice express recombinant anti-NGF monoclonal antibodies and thus show marked neuronal degeneration, memory impairments, and A $\beta$  accumulation in the cortex and hippocampus, while these deficits can be rescued by exogenous NGF [50, 51]. Besides, NGF stimulates nerve fiber growth in cultured spinal ganglia and increases the cell body size of septal neurons [47]. Likewise, AVP(4-8) also affects nerve growth in cultured hippocampal neurons [52]. Together, these findings imply that increased NGF content in the hippocampus plays an important role in improving learning and memory in APP/PS1 mice. It is interesting that AVP(4-8) enhanced working memory but not spatial memory in WT mice while the NGF level was dramatically increased. This probably involves the time-dependence of memory development. Correct alternation in the Y maze reflects working memory, which is a component of short-term memory. On the other hand, spatial memory in the probe test of the MWM represents long-term memory. The establishment of long-term memory needs more and longer associative learning. Four weeks of treatment with AVP(4-8) in the present study may be enough for working memory, but not enough for the long-term spatial memory in WT mice. In fact, the WT mice still expressed an increasing trend (although not significant) in spatial memory induced by AVP(4-8).

In addition, the present study also indicated that intranasal administration is a convenient and effective drug-delivery approach for central effects. De Wied *et al.* showed that central administration (intracerebroventricular; icv) of AVP(4-8) is 2,300 times more potent than peripheral administration (subcutaneous) [16, 25]. Because icv injection is impractical for patients, nasal administration may be the only drug-delivery route for easy entry into the brain. By bypassing liver metabolism and the blood-brain barrier, the half-life of AVP(4-8) in the brain may be much longer and the final concentration in the brain should be much higher. Meantime, intranasal application of AVP(4-8) also avoids peripheral side-effects.

In conclusion, our study reveals for the first time the neuroprotective effects of AVP(4-8) in APP/PS1-AD mice. These results indicate that intranasal administration of AVP(4-8) effectively improves working memory and long-term spatial memory in APP/PS1-AD mice, and this is associated with the elevation of PSD95 and NGF levels in the brain and the maintenance of hippocampal synaptic plasticity.

**Acknowledgements** This work was supported by the National Natural Science Foundation of China (31471080), the Scientific Program for “Sanjin Scholars” of Shanxi Province, Shanxi “1331 Project” Key Subjects Construction (1331KSC), and Science Foundation for Excellent Young Scholars of Shanxi Province, China (201801D211005).

**Conflict of interest** The authors claim no conflict of interest.

## References

1. Wuwongse S, Chang RC, Law AC. The putative neurodegenerative links between depression and Alzheimer’s disease. *Prog Neurobiol* 2010, 91: 362–375.
2. Varga J, Klausz B, Kálmán ÁD, Pákási M, Szucs S, Garab D, *et al.* Increase in Alzheimer’s related markers precedes memory disturbances: Studies in vasopressin-deficient Brattleboro rat. *Brain Res Bull* 2014, 100: 6–13.
3. Strac DS, Muck-Seler D, Pivac N. Neurotransmitter measures in the cerebrospinal fluid of patients with Alzheimer’s disease: a review. *Psychiatr Danub* 2015, 27: 14–24.
4. Sun BL, Li WW, Zhu C, Jin WS, Zeng F, Liu YH, *et al.* Clinical research on Alzheimer’s disease: progress and perspectives. *Neurosci Bull* 2018, 34: 1111–1118.
5. Raskind MA, Peskind ER, Lampe TH, Risse SC, Taborsky GJ, Dorsa D. Cerebrospinal fluid vasopressin, oxytocin, somatostatin, and beta-endorphin in Alzheimer’s disease. *Arch Gen Psychiatry* 1986, 43: 382–388.
6. Mazurek MF, Bed MF, Bird ED, Martin JB. Vasopressin in Alzheimer’s disease: a study of postmortem brain concentrations. *Ann Neurol* 1986, 20: 665–670.
7. Rotondo F, Butz H, Syro LV, Yousef GM, Di Ieva A, Restrepo LM. Arginine vasopressin (AVP): a review of its historical perspectives, current research and multifunctional role in the hypothalamohypophysial system. *Pituitary* 2016, 19: 345–355.
8. van Wimersma Greidanus TB, Bohus B, de Wied D. The role of vasopressin in memory processes. *Prog Brain Res* 1975, 42: 135–141.
9. Engelmann M, Landgraf R. Microdialysis administration of vasopressin into the septum improves social recognition in Brattleboro rats. *Physiol Behav* 1994, 55: 145–149.
10. Egashira N, Tanoue A, Higashihara F, Mishima K, Fukue Y, Takano Y, *et al.* V1a receptor knockout mice exhibit impairment of spatial memory in an eight-arm radial maze. *Neurosci Lett* 2004, 356: 195–198.
11. DeVito LM, Konigsberg R, Lykken C, Sauvage M, Young WS, 3rd, Eichenbaum H. Vasopressin 1b receptor knock-out impairs memory for temporal order. *J Neurosci* 2009, 29: 2676–2683.
12. Bielsky IF, Hu SB, Szegda KL, Westphal H, Young LJ. Profound impairment in social recognition and reduction in anxiety-like behavior in vasopressin V1a receptor knockout mice. *Neuropsychopharmacology* 2004, 29: 483–493.
13. Nephew BC, Bridges RS. Arginine vasopressin V1a receptor antagonist impairs maternal memory in rats. *Physiol Behav* 2008, 95: 182–186.
14. Weingartner H, Gold P, Ballenger JC, Smallberg SA, Summers R, Rubinow DR, *et al.* Effects of vasopressin on human memory functions. *Science* 1981, 211: 601–603.
15. Yang C, Zhang X, Gao J, Wang M, Yang Z. Arginine vasopressin ameliorates spatial learning impairments in chronic cerebral hypoperfusion via V1a receptor and autophagy signaling partially. *Transl Psychiatry* 2017, 7: e1174.

16. de Wied D, Gaffori O, van Ree JM, de Jong W. Central target for the behavioural effects of vasopressin neuropeptides. *Nature* 1984, 308: 276–278.
17. Pan YF, Jia XT, Wang XH, Chen XR, Li QS, Gao XP, *et al.* Arginine vasopressin remodels the spontaneous discharges disturbed by amyloid beta protein in hippocampal CA1 region of rats. *Regul Pept* 2013, 183: 7–12.
18. Jing W, Guo F, Cheng L, Zhang JF, Qi JS. Arginine vasopressin prevents amyloid beta protein-induced impairment of long-term potentiation in rat hippocampus *in vivo*. *Neurosci Lett* 2009, 450: 306–310.
19. Hicks C, Ramos L, Reekie T, Misagh GH, Narlawar R, Kassiou M, *et al.* Body temperature and cardiac changes induced by peripherally administered oxytocin, vasopressin and the non-peptide oxytocin receptor agonist WAY 267,464: a biotelemetry study in rats. *Br J Pharmacol* 2014, 171: 2868–2887.
20. Song Z, Albers HE. Cross-talk among oxytocin and arginine-vasopressin receptors: Relevance for basic and clinical studies of the brain and periphery. *Front Neuroendocrinol* 2018, 51: 14–24.
21. Alescio-Lautier B, Soumireu-Mourat B. Effects of peripherally administered arginine-vasopressin on learning, retention and forgetting in mice. *Behav Brain Res* 1990, 41: 117–128.
22. Wu JH, Du YC. Binding sites of ZNC(C)PR, a pentapeptide fragment of argipressin, in rat brain. *Acta Pharmacol Sin* 1995, 16: 141–144.
23. Du YC, Wu JH, Jiang XM, Gu YJ. Characterization of binding sites of a memoryenhancing peptide AVP(4-8) in rat cortical synaptosomal membranes. *Peptides* 1994, 15: 1273–1279.
24. Reijmers LGJE, van Ree JM, Spraijt BM, Burbach JP, De Wied D. Vasopressin metabolites: A link between vasopressin and memory? *Prog Brain Res* 1999, 119: 523–535.
25. Burbach JP, Kovacs GL, de Wied D, van Nispen JW, Greven HM. A major metabolite of arginine vasopressin in the brain is a highly potent neuropeptide. *Science* 1983, 221: 1310–1312.
26. De Wied D, Gaffori O, Van Ree JM, De Jong W. Vasopressin antagonists block peripheral as well as central vasopressin receptors. *Pharmacol Biochem Behav* 1984, 21: 393–400.
27. Peineau S, Rabiant K, Pierrefiche O, Potier B. Synaptic plasticity modulation by circulating peptides and metaplasticity: Involvement in Alzheimer's disease. *Pharmacol Res* 2018, 130: 385–401.
28. Ni B, Wu R, Yu T, Zhu H, Li Y, Liu Z. Role of the hippocampus in distinct memory traces: timing of match and mismatch enhancement revealed by intracranial recording. *Neurosci Bull* 2017, 33: 664–674.
29. Gelman S, Palma J, Tombaugh G, Ghavami A. Differences in synaptic dysfunction between rTg4510 and APP/PS1 mouse models of Alzheimer's disease. *J Alzheimers Dis* 2018, 61: 195–208.
30. Chepkova AN, French P, De Wied D, Ontskul AH, Ramakers GM, Skrebinski VG, *et al.* Long-lasting enhancement of synaptic excitability of CA1/subiculum neurons of the rat ventral hippocampus by vasopressin and vasopressin(4-8). *Brain Res* 1995, 701: 255–266.
31. Dubrovsky B, Tatarinov A, Gijsbers K, Harris J, Tsiodras A. Effects of arginine-vasopressin (AVP) on long-term potentiation in intact anesthetized rats. *Brain Res Bull* 2003, 59: 467–472.
32. Wang M, Chen JT, Ruan DY, Xu YZ. Vasopressin reverses aluminum-induced impairment of synaptic plasticity in the rat dentate gyrus *in vivo*. *Brain Res* 2001, 899: 193–200.
33. Reddy PH, Yin X, Manczak M, Kumar S, Pradeepkiran JA, Vijayan M, *et al.* Mutant APP and amyloid beta-induced defective autophagy, mitophagy, mitochondrial structural and functional changes and synaptic damage in hippocampal neurons from Alzheimer's disease. *Hum Mol Genet* 2018, 27: 2502–2516.
34. Mirza FJ, Zahid S. The role of synapsins in neurological disorders. *Neurosci Bull* 2018, 34: 349–358.
35. Pham E, Crews L, Ubhi K, Hansen L, Adame A, Cartier A, *et al.* Progressive accumulation of amyloid-beta oligomers in Alzheimer's disease and in amyloid precursor protein transgenic mice is accompanied by selective alterations in synaptic scaffold proteins. *FEBS J* 2010, 277: 3051–3067.
36. Shinohara Y. Quantification of postsynaptic density proteins: glutamate receptor subunits and scaffolding proteins. *Hippocampus* 2012, 22: 942–953.
37. Du YC, Yan QW, Qiao LY. Function and molecular basis of action of vasopressin 4-8 and its analogues in rat brain. *Prog Brain Res* 1998, 119: 163–175.
38. Qiao LY, Du YC. Involvement of a putative G-protein-coupled receptor and a branching pathway in argipressin (4-8) signal transduction in rat hippocampus. *Acta Pharmacol Sin* 1998, 19: 15–20.
39. Yan QW, Du YC. AVP(4-8) may stimulate a G protein-coupled receptor in rat hippocampal synaptosomal membranes. *Acta Biochim Biophys Sin* 1998, 30: 505–509.
40. Qiao LY, Chen XF, Gu BX, Wang TX, Du YC. Effect of AVP(4-8) administration on Ca<sup>2+</sup>/CaM-dependent protein kinase II autophosphorylation in rat brain. *Acta Physiol Sin* 1998, 50: 132–138.
41. Zhen X, Dong M, Du YC. Effect of arginine-vasopressin(4-8) on PKC and PKA activities in rat brain. *Chin J Biochem Mol Biol* 2000, 16: 529–532.
42. Zhen XG, Du YC. AVP(4-8) enhances PKC and MAPK activities in SK-N-SH cells. *Acta Biochim Biophys Sin* 2000, 32: 105–108.
43. Guo J, Zhou AW, Du YC, Chen XF. AVP(4-8) increases NGF mRNA and protein content in rat hippocampus. *Chin J Neurosci* 1996, 3: 23–27.
44. Zhou AW, Guo J, Wang HY, Gu BX, Du YC. Enhancement of NGF gene expression in rat brain by the memory-enhancing peptide AVP(4-8). *Peptides* 1995, 16: 581–586.
45. Zhou AW, Li WX, Guo J, Du YC. Facilitation of AVP(4-8) on gene expression of BDNF and NGF in rat brain. *Peptides* 1997, 18: 1179–1187.
46. Chen XF, Tang T, Zhang JW, Miao HH, Wang TX, Du YC. ZNC(C)PR affects developmental changes of P46 phosphorylation in rat hippocampus. *Mol Reprod Dev* 1993, 35: 251–256.
47. Isaev NK, Stelmashook EV, Genrikhs EE. Role of nerve growth factor in plasticity of forebrain cholinergic neurons. *Biochemistry (Mosc)* 2017, 82: 291–300.
48. Tiernan CT, Ginsberg SD, He B, Ward SM, Guillozet-Bongaarts AL, Kanaan NM, *et al.* Pretangle pathology within cholinergic nucleus basalis neurons coincides with neurotrophic and neurotransmitter receptor gene dysregulation during the progression of Alzheimer's disease. *Neurobiol Dis* 2018, 117: 125–136.
49. Yamada K, Nitta A, Hasegawa T, Fuji K, Hiramatsu M, Kameyama T, *et al.* Orally active NGF synthesis stimulators: potential therapeutic agents in Alzheimer's disease. *Behav Brain Res* 1997, 83: 117–122.
50. Berardi N, Braschi C, Capsoni S, Cattaneo A, Maffei L. Environmental enrichment delays the onset of memory deficits and reduces neuropathological hallmarks in a mouse model of Alzheimer-like neurodegeneration. *J Alzheimers Dis* 2007, 11: 359–370.
51. De Rosa R, Garcia AA, Braschi C, Capsoni S, Maffei L, Berardi N, *et al.* Intranasal administration of nerve growth factor (NGF) rescues recognition memory deficits in AD11 anti-NGF transgenic mice. *Proc Natl Acad Sci U S A* 2005, 102: 3811–3816.
52. Tarumi T, Sugimoto Y, Chen Z, Zhao Q, Kamei C. Effects of metabolic fragments of [Arg(8)]-vasopressin on nerve growth in cultured hippocampal neurons. *Brain Res Bull* 2000, 51: 407–411.



# Role of Elevated Thrombospondin-1 in Kainic Acid-Induced Status Epilepticus

Yurong Zhang<sup>1</sup> · Mengdi Zhang<sup>1</sup> · Wei Zhu<sup>2</sup> · Xiaohong Pan<sup>1</sup> · Qiaoyun Wang<sup>1</sup> ·  
Xue Gao<sup>1</sup> · Chaoyun Wang<sup>1</sup> · Xiuli Zhang<sup>1</sup> · Yuxia Liu<sup>1</sup> · Shucui Li<sup>1</sup> ·  
Hongliu Sun<sup>1</sup>

Received: 30 March 2019 / Accepted: 22 July 2019 / Published online: 29 October 2019  
© Shanghai Institutes for Biological Sciences, CAS 2019

**Abstract** Previous studies have suggested that thrombospondin-1 (TSP-1) regulates the transforming growth factor beta 1 (TGF- $\beta$ 1)/phosphorylated Smad2/3 (pSmad2/3) pathway. Moreover, TSP-1 is closely associated with epilepsy. However, the role of the TSP-1-regulated TGF- $\beta$ 1/pSmad2/3 pathway in seizures remains unclear. In this study, changes in this pathway were assessed following kainic acid (KA)-induced status epilepticus (SE) in rats. The results showed that increases in the TSP-1/TGF- $\beta$ 1/pSmad2/3 levels spatially and temporally matched the increases in glial fibrillary acidic protein (GFAP)/chondroitin sulfate (CS56) levels following KA administration. Inhibition of TSP-1 expression by small interfering RNA or inhibition of TGF- $\beta$ 1 activation with a Leu-Ser-Lys-Leu peptide significantly reduced the severity of KA-induced acute seizures. These anti-seizure effects were accompanied by decreased GFAP/CS56 expression and Smad2/3 phosphorylation. Moreover, inhibiting Smad2/3 phosphorylation with ponatinib or SIS3 also significantly reduced seizure severity, alongside reducing GFAP/CS56 immunoreactivity. These results suggest that the TSP-1-regulated TGF- $\beta$ 1/pSmad2/3 pathway plays a key role in

KA-induced SE and astrogliosis, and that inhibiting this pathway may be a potential anti-seizure strategy.

**Keywords** Astrogliosis · Status epilepticus · Ponatinib · Thrombospondin-1

## Introduction

Epilepsy is a common disease that affects approximately 0.5%–1% of the global population. Although pharmacotherapy is the most widely-used and effective treatment option, up to one-third of patients are resistant to antiepileptic drugs [1, 2]. Research on the mechanisms underlying epilepsy may identify new targets for antiepileptic drugs.

Astrocytes are associated with neuronal excitability and epileptic seizures [3–5]. Almost all prolonged seizures result in reactive gliosis or astrogliosis, characterized by severe morphological and biochemical changes in astrocytes [6]. Moreover, astrogliosis is one of the most important factors promoting neuronal hyperexcitability and epileptogenesis [7].

Astrocytes secrete thrombospondin-1 (TSP-1) and regulate its expression [8]. TSP-1 is a unique member of the TSP family in that it activates transforming growth factor beta 1 (TGF- $\beta$ 1) *via* two binding sites. TGF- $\beta$ 1 signaling controls many cellular responses and developmental processes in animals [9]. Previous studies have confirmed that enhanced TGF- $\beta$ 1 signaling contributes to epileptogenesis and epileptic seizures [10–13]. TGF- $\beta$ 1 further modulates cytokine responses and the secretion of other growth factors [14]. Among TGF- $\beta$ 1 signaling pathways, the canonical TGF- $\beta$ 1/Smad2/3 pathway plays an important epileptogenic role [10, 11, 15] and has therefore been

Yurong Zhang and Mengdi Zhang have contributed equally to this work.

**Electronic supplementary material** The online version of this article (<https://doi.org/10.1007/s12264-019-00437-x>) contains supplementary material, which is available to authorized users.

✉ Hongliu Sun  
sun\_china6@163.com

<sup>1</sup> School of Pharmaceutical Sciences, Binzhou Medical University, Yantai 264003, China

<sup>2</sup> Shandong Academy of Medical Sciences, Jinan 250062, China

identified as a therapeutic target for treating astrogliosis [6]. The Smad family includes the main downstream messenger molecules that transmit TGF- $\beta$ 1 signals from cell membrane receptors to the nucleus [16]. Smad proteins are thought to play an important role in regulating intracellular responses to TGF- $\beta$ 1 through the TGF- $\beta$ 1-regulated phosphorylation of Smad2 and Smad3 [17]. Phosphorylated Smad2 (pSmad2) and pSmad3 further combine with co-Smads before entering the nucleus and forming transcription complexes that complete the intracellular signal transduction process [17].

Consequently, we hypothesized that the TSP-1/TGF- $\beta$ 1/pSmad2/3 pathway participates in and contributes to both seizures and astrogliosis. We therefore investigated changes in the TSP-1/TGF- $\beta$ 1/pSmad2/3 pathway in a kainic acid (KA)-induced rat model of status epilepticus (SE). To this end, we used drugs and small interfering RNA (siRNA) to manipulate pathway activity in order to elucidate the role of the pathway in KA-induced SE.

## Methods

### Animals and Experimental Groups

Male Sprague-Dawley rats (280 g–320 g) were obtained from Jinan Jinfeng Experimental Animal Co. Ltd. (Certificate No. SCXK2014-0006; China). All procedures were approved by the Animal Ethics Committee of Binzhou Medical University (Approval No. 2015005) and conducted in complete compliance with Chinese law and the US National Institutes of Health *Guide for the Care and Use of Laboratory Animals* (National Institutes of Health Publication No. 80-23, revised 1996). Water and food were provided *ad libitum*. All experiments were performed between 09:00 and 17:00.

Rats were assigned to the KA-treated group ( $n = 336$ ) or the saline-treated control group ( $n = 36$ ). The KA-treated rats were further assigned to groups receiving siRNA ( $n = 36$ ) or negative control RNA ( $n = 36$ ), those receiving Leu-Ser-Lys-Leu (LSKL; Sigma-Aldrich, St. Louis, MO;  $n = 36$ ) or saline ( $n = 36$ ), those receiving SIS3 (Sigma-Aldrich;  $n = 42$ ) or saline ( $n = 42$ ), and those receiving ponatinib (MedChem Express, Princeton, NJ;  $n = 36$ ) or saline ( $n = 36$ ).

### Surgical Implantation of Electrodes and Cannulae

As we previously described [18], after intraperitoneal administration of sodium pentobarbital (50 mg/kg; CAS, 57-33-0, Xiya Reagent, Chengdu, China), each rat was secured in a stereotaxic apparatus (Stoelting, Wood Dale, IL), and an electrode was implanted into the right cortex at

a point 3.2 mm posterior and 3.0 mm lateral to bregma and at a depth of 1.8 mm. The electrode consisted of two twisted-pair stainless-steel wires 0.2 mm in diameter (A.M. Systems, Carlsborg, WA) and  $\sim 3$  cm long, soldered to a miniature socket to record electroencephalograms (EEGs) using a PowerLab device (AD Instruments, Bella Vista, New South Wales, Australia). Each rat also had a cannula (Reward Biotech, Shenzhen, China) implanted into the left ventricle at a point 1.8 mm posterior and 1 mm lateral to bregma and at a depth of 3.6 mm. The implanted electrode and cannula were fixed to the skull with dental cement. Each rat was allowed a week-long postoperative recovery period.

### Drug Interventions and siRNA

For intraventricular injections, drugs were infused into the left ventricle over a 10-min period through a needle (Reward Biotech, China) inserted 0.2 mm beyond the end of the guide cannula. The needle was left in place for 5 min before being slowly retracted.

SE was induced by a single intraventricular KA injection (1.25 mg/mL, 0.65  $\mu$ L per rat; Sigma-Aldrich, St. Louis, MO) *via* the implanted cannula. Following KA administration, almost all rats showed immediate and continuous Racine's stage 4 or 5 seizures [19]. Sixty minutes later, the seizures were terminated with an intraperitoneal diazepam injection (1 mg/mL solution at 2 mg/kg; Sigma-Aldrich). Seven rats were excluded from our study as they did not develop SE following KA administration.

To target TSP-1, siRNAs were designed, synthesized, and assessed by Tuoran Biological Technology (Shanghai, China). The siRNA sequences were as follows: TSP-1 siRNA 5'-GCCAGUAUGUUACAACGUdTdT-3' and 5'-ACGUUGUAAACAACUACUGGCdTdT-3'; negative control siRNA 5'-UUCUCCGAACGUGUCACGUTT-3' and 5'-ACGUGACACGUUCGGAGAATT-3'.

Twenty-four hours prior to KA injection, the siRNA group received a 4- $\mu$ L (0.5  $\mu$ g/ $\mu$ L) intraventricular injection of anti-TSP-1 siRNA, while the control group received 4  $\mu$ L (0.5  $\mu$ g/ $\mu$ L) of negative control RNA. The siRNA or negative control RNA injection was then repeated every 48 h. Smad3 phosphorylation was altered in both the hippocampus and cortex, so 4 h before KA injections, the SIS3 group received intraventricular SIS3 (0.085  $\mu$ g/ $\mu$ L solution at 0.85  $\mu$ g per 300 g) to selectively inhibit TGF- $\beta$ 1-regulated Smad3 phosphorylation [20], while the associated control group received the same volume of saline. Thirty minutes prior to the KA injections, the ponatinib group received an intraperitoneal ponatinib injection (1 mg/mL solution at 0.002 mg/g) to inhibit Smad2/3 phosphorylation [21], while the control group received the same volume of saline. The LSKL group received an intraventricular

injection of 10  $\mu$ L (0.2 mg) LSKL, while the associated control group received the same volume of saline. SIS3, ponatinib, LSKL, or saline was administered daily for 7 days.

### EEG Recordings and Seizure Severity Classification

After KA treatment, each rat was placed in a Plexiglas arena (50 cm  $\times$  30 cm  $\times$  30 cm). Their behaviors were observed and EEGs recorded during the following 60 min, and the power spectrum was analyzed using a Powerlab system (AD Instruments, Bella Vista, New South Wales, Australia). Seizure severity was classified according to modified Racine's stages [19]: stage 1, non-selective chewing; stage 2, head nodding; stage 3, unilateral forelimb clonus; stage 4, "wet dog" shakes with bilateral forelimb clonus and rearing; and stage 5, falling. We also recorded generalized seizure durations (GSDs), seizure durations, and seizure latencies to evaluate the severity of seizures.

### Immunohistochemistry

At 24 h, 3 days, and 7 days following KA administration, 6 rats from each group were anesthetized with intraperitoneal sodium pentobarbital (50 mg/kg; CAS, 57-33-0, Xiya Reagent, Chengdu, China). The chest was opened to expose the heart, a needle was inserted into the left ventricle, the right auricle opened, and 250 mL saline rapidly injected followed by 250 mL of 4% paraformaldehyde (PFA). Each rat was decapitated and the brain placed in 4% PFA and left for at least 24 h. After soaking in 30% sucrose, the brain was cut at 10  $\mu$ m on a cryostatic microtome (CM3050 S, Leica, Wetzlar, Germany).

For double immunofluorescent staining of glial fibrillary acidic protein (GFAP) and chondroitin sulfate (CS56) or TSP-1, the sections were first washed three times with 0.01 mol/L phosphate-buffered saline (PBS) for 15 min, and then blocked with 10% bovine serum albumin in PBS for 2 h at room temperature. Then the sections were incubated overnight at 4°C in antibody dilution buffer containing rabbit anti-GFAP immunoglobulin G (IgG; 1:100; BM0055, Boster, Wuhan, China), mouse anti-CS56 IgG (1:100; ab11570, EMD Millipore, Billerica, MA), or rabbit anti-TSP-1 IgG (1:100; ab85762, Abcam, Cambridge, UK). After 3 washes in PBS for 15 min each, the sections were sequentially incubated at 37°C for 2 h in antibody dilution buffer with fluorescein isothiocyanate-conjugated (1:200; A22110, EMD Millipore) and Cy3-conjugated (1:200; A0516, Beyotime Institute of Biotechnology, Shanghai, China) secondary antibodies. After three washes in PBS for 15 min on a shaking table, the sections were coverslipped.

Fluorescence intensities corresponding to GFAP and either CS56 or TSP-1 levels were assessed by laser

confocal microscopy (LSM880, Zeiss, Oberkochen, Germany). Six stained slices from each rat were obtained and un-collapsed confocal images from the same brain region were analyzed. The fluorescence intensities in different brain regions were comparable because the slices were stained according to the same protocol and the same exposure intensity and time were used for image acquisition. Fluorescence intensities were quantified using ImageJ 1.37 software (National Institutes of Health, Bethesda, MD) as previously described [18].

### Western Blotting

At 24 h, 3 days, and 7 days following KA administration, we decapitated six rats from each group and immediately removed their brains. The hippocampus and cortex were isolated and proteins were extracted. The protein concentrations were determined using a bicinchoninic acid assay kit (P0011, Beyotime Institute of Biotechnology) and emission at 562 nm was measured with a microplate reader (ELx800, BioTek Instruments, Winooski, VT). The proteins were separated by electrophoresis on 12% sodium dodecyl sulfate polyacrylamide gels and electroblotted to a polyvinylidene difluoride membrane. The membrane was then blocked with 5% fat-free milk for 3 h at room temperature.

The blocked membranes were incubated with rabbit anti-GFAP IgG (1:1000; BM0055, Boster), mouse anti-CS56 IgG (1:1000; ab11570, EMD Millipore) or rabbit anti-TSP-1 (1:100; ab85762, Abcam), mouse monoclonal anti-TGF- $\beta$ 1 (1:800; ab64751, Abcam), rabbit anti-Smad2/3/pSmad2/3 monoclonal antibodies (1:2000; ab47083 and ab40854, Abcam; Ser\_465/467, Cell Signaling Technology, Boston, MA, USA; ab52903, Abcam), and glyceraldehyde-3-phosphate dehydrogenase (GAPDH; 1:3000; AB-P-R001, Zhejiang Kangcheng Biotech, Jiaying, China) at room temperature for 2 h and then at 4°C overnight. We visualized immunoreactive bands after 2-h exposure to horseradish peroxidase-conjugated IgG secondary antibodies. We acquired images with the Odyssey infrared imaging system (LI-COR Biosciences, Lincoln, NE) and analyzed them with the accompanying software. TGF- $\beta$ 1, Smad2/3, and pSmad2/3 expression intensities were expressed as ratios relative to the GAPDH expression intensities and normalized to the control group values.

### Flow Cytometry

Three days after KA administration, we anesthetized and decapitated 6 rats from each group and immediately removed their brains. The hippocampus and cortex were separated and immediately immersed in PBS. Single-cell suspensions were prepared by filtration. Repetitive centrifugation was used to wash the suspension with PBS. Cell

solutions with densities of  $5\text{--}10 \times 10^6$  cells/mL were fixed in 4% PFA, and 200- $\mu$ L volumes of cell suspension, each containing  $1\text{--}5 \times 10^5$  cells, were incubated with 5% bovine serum albumin on ice for 10 min. Monoclonal rabbit anti-Smad3 antibody (1:100; ab40854, Abcam) was added to each tube, and the tubes were incubated for 20 min at 4 °C. The cells were washed three times by centrifugation. Fluorescein isothiocyanate-conjugated secondary antibodies (1:150; A22110, Beyotime, Shanghai, China) were added to each tube, and the tubes were again incubated for 15 min. The cells were again washed three times by centrifugation, and 500–550-nm fluorescence intensities produced by the samples were analyzed with a flow cytometer (BD FACSVerser, Becton Dickinson, Franklin Lakes, NJ).

### Statistical Analysis

All values are presented as the mean  $\pm$  SEM. We performed statistical analyses in SPSS 13.0 for Windows (IBM, Armonk, NY). One-way analysis of variance was used to compare seizure latencies, cumulative seizure durations, and GSDs. The nonparametric Mann–Whitney *U* test was used to compare cumulative times in each seizure stage and changes in protein expression levels. We defined statistical significance as  $P < 0.05$ .

## Results

### KA Administration Upregulates Hippocampal and Cortical Expression of GFAP, CS56, and TSP-1

We evaluated the immunoreactivity of GFAP, an astrocyte-specific marker [22, 23], and CS56, secreted by astrocytes and accordingly used as another astrocytic marker [24]. At all time points from 24 h onwards, hippocampal and cortical GFAP immunoreactivity levels in the KA-treated group were significantly higher than in the control group ( $P < 0.001$ ; Fig. 1A, D, G, J, L, M). Similarly, hippocampal and cortical CS56 immunoreactivity levels were also higher in the KA-treated group than those in the control group ( $P < 0.001$ ; Fig. 1B, E, H, K, L, N). Western blotting yielded similar results ( $P < 0.001$ ; Fig. 1L–N).

Further, TSP-1 immunoreactivity was detected. The immunohistochemistry results indicated that TSP-1 immunoreactivity was elevated in the hippocampus ( $P = 0.048$ ; Fig. 2A, C, I) and cortex ( $P = 0.02$ ; Fig. 2J) 30 min after KA administration. Western blotting revealed similar increases in hippocampal and cortical TSP-1 immunoreactivity 30 min after KA administration (Fig. S1A, B). Western blotting further confirmed that

TGF- $\beta$ 1 immunoreactivity was significantly elevated from 24 h onwards in the hippocampus ( $P < 0.001$ ; Fig. 2K, M) and cortex ( $P < 0.001$ ; Fig. 2M) in the KA-treated group.

We further found that KA significantly increased Smad2/3 protein levels in the hippocampus (Smad2,  $P < 0.001$ ; Smad3,  $P < 0.001$ ) and cortex (Smad2,  $P < 0.001$ ; Smad3,  $P < 0.001$ ) from 24 h onwards (Fig. 2K, N, P). KA administration also promoted Smad2/3 phosphorylation, as evidenced by increased pSmad2/3 levels in the hippocampus (pSmad2,  $P < 0.001$ ; pSmad3,  $P < 0.001$ ) and cortex (pSmad2,  $P < 0.001$ ; pSmad3,  $P < 0.001$ ) from 24 h onwards (Fig. 2K, O, Q).

### Inhibiting TSP-1 Expression with siRNA Attenuates KA-Evoked Seizures Accompanied by Reduced GFAP/CS56 Expression

Rats that received anti-TSP-1 siRNA in addition to KA spent more time in stages 0–3 ( $53.7 \pm 0.8$  min vs.  $12.0 \pm 0.9$  min;  $P < 0.001$ ) and less time in stage 4 ( $4.0 \pm 0.5$  min vs.  $15.6 \pm 0.7$  min;  $P < 0.001$ ) and stage 5 ( $2.3 \pm 0.4$  min vs.  $32.4 \pm 1.4$  min;  $P < 0.001$ ) than rats that received negative control RNA in addition to KA (Fig. 3A). The siRNA group also showed reduced GSDs ( $6.3 \pm 0.8$  min vs.  $48.0 \pm 0.9$  min;  $P < 0.001$ ; Fig. 3B) and seizure durations ( $9.8 \pm 0.7$  min vs.  $51.5 \pm 0.8$  min;  $P < 0.001$ ; Fig. 3C) as well as increased latencies ( $51.2 \pm 0.9$  min vs.  $2.8 \pm 0.1$  min;  $P < 0.001$ ; Fig. 3D). Representative EEGs and EEG power spectra are shown in Fig. 3N.

Immunohistochemical and western blotting experiments revealed that hippocampal ( $P < 0.001$ , Fig. 3J, L, E;  $P < 0.001$ , Fig. 4A, B) and cortical ( $P < 0.001$ ; Fig. S2A) TSP-1 immunoreactivity was significantly lower in the siRNA group than in the negative control RNA group. The siRNA group also exhibited reduced hippocampal ( $P < 0.001$  and  $0.001$ ; Fig. 3E, F–I) and cortical ( $P < 0.001$  and  $0.001$ ; Fig. S2A) immunoreactivity for GFAP and CS56.

Western blotting showed that hippocampal ( $P < 0.001$ ; Fig. 4A, C) and cortical ( $P < 0.001$ ; Fig. S2C) TGF- $\beta$ 1 expression levels were significantly greater in the siRNA group than in the control group from 24 h onwards. We found similar increases in Smad2 (Fig. 4A, D; Fig. S2D) and Smad3 expression (Fig. 4A, F; Fig. S2F) in the siRNA group from 24 h onwards, while the pSmad2/3 levels were significantly decreased (Fig. 4A, E, G; Fig. S2E, G).

These results indicated that inhibiting TSP-1 expression attenuates KA-induced seizures, along with reduced Smad2/3 phosphorylation and GFAP and CS56 expression.

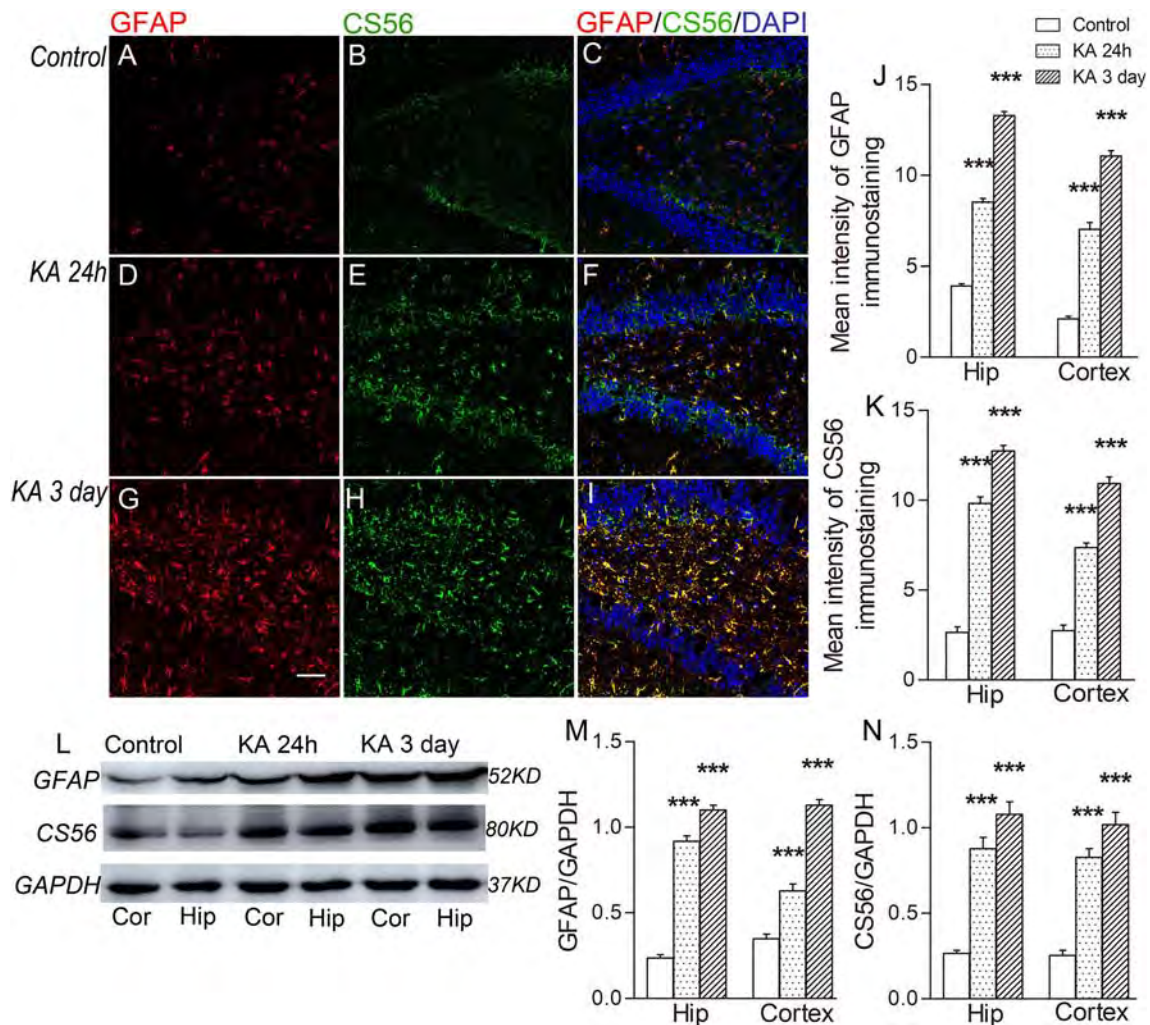


**Fig. 1** KA-induced upregulation of GFAP/CS56 expression in rat brain. **A–I** Representative images of immunoreactivity for GFAP and CS56 in the right dentate gyrus in controls and after KA treatment (scale bar, 100  $\mu$ m;  $n = 6$ /group). **J, K** Quantified GFAP and CS56 immunoreactivity levels in the hippocampus and cortex of controls

and KA-treated rats. **L–N** Western blots (**L**) and statistics for GFAP (**M**) and CS56 (**N**) immunoreactivity. Data are shown as the mean  $\pm$  SEM. \*\*\* $P < 0.001$  vs. controls. Hip, hippocampus; Cor, cortex.

### Inhibiting TGF- $\beta$ 1 Activation with LSKL Attenuates KA-Evoked Seizures Accompanied by Reduced GFAP/CS56 Expression

LSKL is a competitive antagonist that inhibits TGF- $\beta$ 1 activation by specifically blocking the binding of TSP-1 to TGF- $\beta$ 1. Our behavioral results showed that administering LSKL before KA significantly prolonged the time spent in stages 0–3 ( $52.0 \pm 0.8$  min vs.  $15.0 \pm 0.8$  min;  $P < 0.001$ ) and shortened the time spent in stage 4 ( $4.3 \pm 0.6$  min vs.  $19.1 \pm 0.8$  min;  $P < 0.001$ ) and stage 5 ( $3.7 \pm 0.5$  min vs.  $25.9 \pm 1.5$  min;  $P < 0.001$ ) (Fig. 5A). Moreover, LSKL treatment significantly reduced GSDs ( $8.0 \pm 0.8$  min vs.  $45.0 \pm 0.8$  min;  $P < 0.001$ ; Fig. 5B) and seizure durations ( $10.9 \pm 0.7$  min vs.  $46.2 \pm 0.6$  min;  $P < 0.001$ ; Fig. 5C), and increased the

latencies ( $35.3 \pm 1.8$  min vs.  $3.0 \pm 0.1$  min;  $P < 0.001$ ; Fig. 5D). Representative EEGs and their power spectra are shown in Fig. 5N.

LSKL treatment also significantly reduced the hippocampal ( $P < 0.001$  and  $0.001$ ; Fig. 5F–I, E) and cortical ( $P < 0.001$  and  $0.001$ ; Fig. S3A) levels of GFAP and CS56. No effects on TSP-1 immunoreactivity were found (Figs. 5J–M, E; 6A, B; S3A).

We also found that from 24 h onwards, LSKL significantly increased the hippocampal and cortical expression of TGF- $\beta$ 1 (hippocampus,  $P < 0.001$ ; Fig. 6A, C; cortex,  $P < 0.001$ ; Fig. S3C), and Smad2/3 ( $P < 0.001$  and  $0.001$ ; Figs. 6A, D, F; S3D, F). However, the phosphorylation levels of Smad2/3 were significantly decreased from 24 h onwards ( $P < 0.001$  and  $0.001$ ; Figs. 6A, E, G; S3E, G).

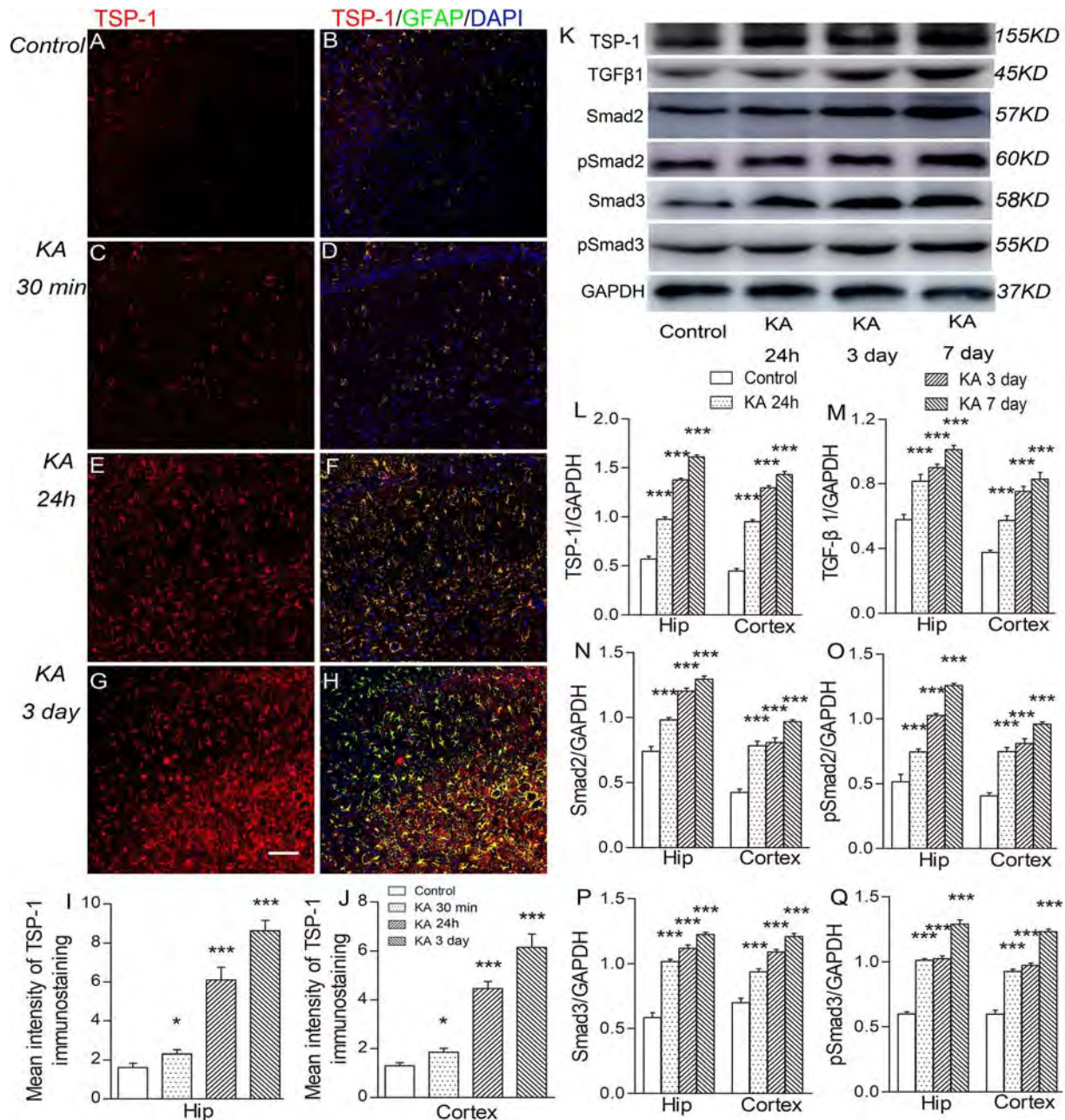


**Fig. 2** KA-induced upregulation of TSP-1, TGF- $\beta$ 1, Smad2/3, and pSmad2/3. **A–H** Representative images of immunoreactivity for TSP-1 and GFAP in CA2 in controls and after KA treatment (scale bar, 150  $\mu$ m;  $n = 6$ /group). **I, J** Quantified TSP-1 immunoreactivity in the hippocampus and cortex in controls and KA-treated rats. **K–Q**

Western blots (**K**) and statistics for hippocampal and cortical expression of TSP-1 (**L**), TGF- $\beta$ 1 (**M**), Smad2/3 (**N, P**), and pSmad2/3 (**O, Q**) ( $n = 6$ /group). Data are shown as the mean  $\pm$  SEM. \* $P < 0.05$ , \*\*\* $P < 0.001$  vs. controls. Hip, hippocampus.

These results indicated that inhibiting TGF- $\beta$ 1 activation with LSKL attenuates KA-evoked seizures, and reduces the Smad2/3 phosphorylation and the protein levels of GFAP and CS56. These effects are similar to those obtained by inhibiting TSP-1 expression by siRNA interference.

### SIS3 and Ponatinib Attenuate KA-Evoked Seizures While Reducing GFAP/CS56 Expression

As with LSKL and siRNA treatment, SIS3 (a specific inhibitor of Smad3 phosphorylation) in addition to KA prolonged the time spent in Racine's stages 0–3 ( $52.1 \pm 0.6$  min vs.  $14.1 \pm 0.8$  min;  $P < 0.001$ ), and

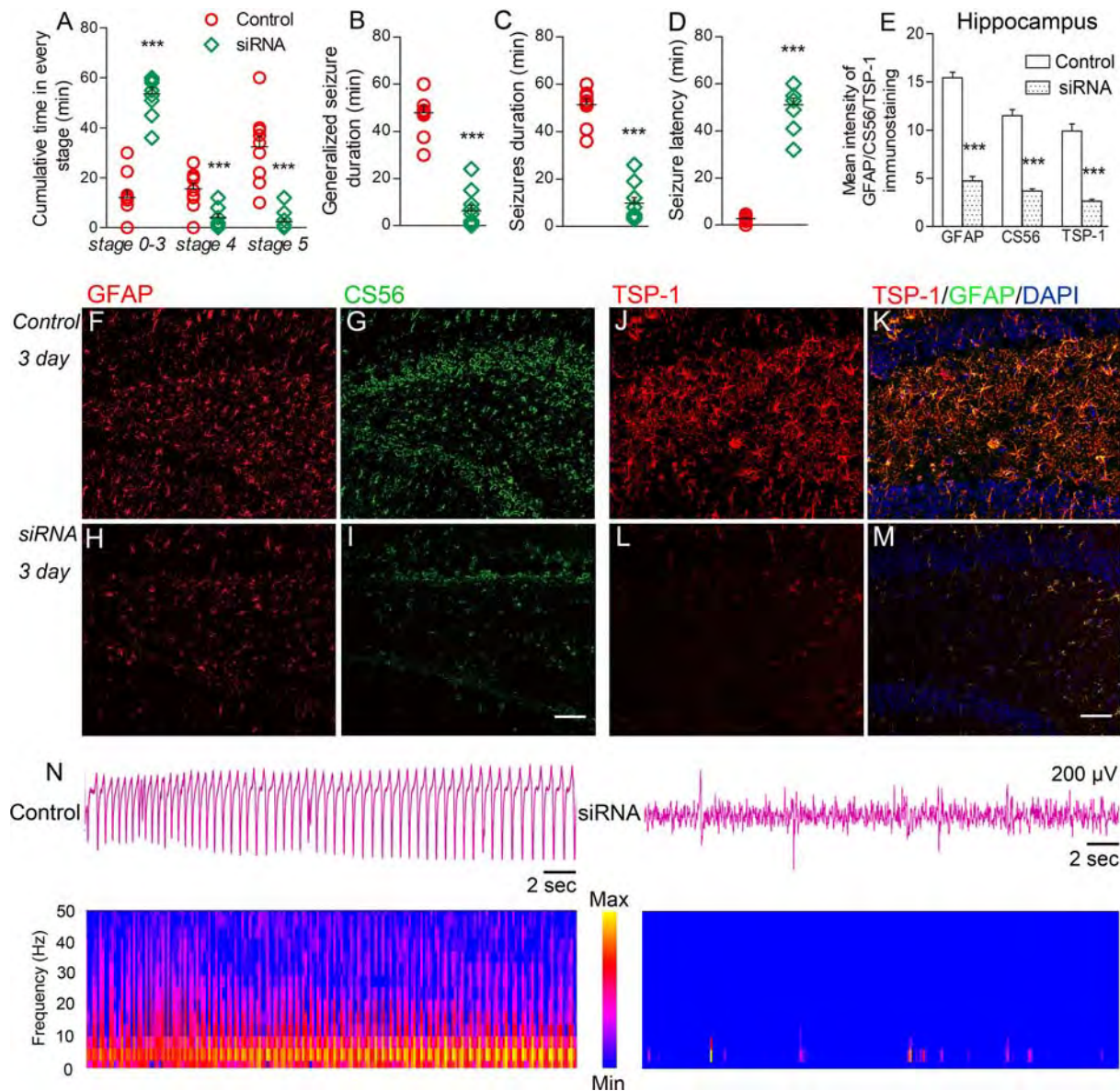


**Fig. 3** Effects of inhibiting TSP-1 expression with siRNA in KA model rats. **A–D** siRNA treatment altered the cumulative time in every stage (**A**), shortened the GSDs (**B**) and seizure durations (**C**), and increased the latencies (**D**) ( $n = 10/\text{group}$ ). **E–M** siRNA treatment reduced the KA-induced increases in immunoreactivity for

GFAP (**E**, **F**, **H**), CS56 (**E**, **G**, **I**), and TSP-1 (**E**, **J–M**) in the hippocampus ( $n = 6/\text{group}$ ; scale bars for **F–I**, 150  $\mu\text{m}$ ; **J–M**, 100  $\mu\text{m}$ ). **N** Representative EEGs (upper) and EEG power spectra (lower) in a control (left) and a siRNA-treated rat (right). Data are shown as the mean  $\pm$  SEM. \*\*\* $P < 0.001$  vs. controls.

reduced the time spent in stage 4 ( $6.4 \pm 0.5$  min vs.  $18.5 \pm 0.9$  min;  $P < 0.001$ ) and stage 5 ( $1.5 \pm 0.2$  min vs.  $25.4 \pm 1.1$  min;  $P < 0.001$ ) (Fig. 7A). Meanwhile, the seizure durations ( $10.8 \pm 0.6$  min vs.  $48.0 \pm 0.7$  min;  $P < 0.001$ ; Fig. 7C) and GSDs ( $7.9 \pm 0.6$  min vs.  $43.9 \pm 0.7$  min;  $P < 0.001$ ; Fig. 7B) were shortened and the latencies were increased ( $48.7 \pm 0.8$  min vs.  $3.0 \pm 0.1$  min;  $P < 0.001$ ; Fig. 7D). Representative EEGs and their power spectra are shown in Fig. S4D. SIS3 treatment also significantly reduced the hippocampal and

cortical expression of GFAP and CS56 ( $P < 0.001$  and  $0.001$ ; Fig. 7 E–L).

Western blotting experiments also showed that SIS3 significantly reduced hippocampal ( $P < 0.001$ ; Fig. 7M, N) and cortical ( $P < 0.001$ ; Fig. S4A) pSmad3 levels and increased hippocampal ( $P < 0.01$  and  $0.001$ ; Fig. 7M, N) and cortical ( $P < 0.001$ ; Fig. S4A) Smad3 expression from 24 h onwards. It had no significant effect on Smad2 expression or pSmad2 levels (Fig. S4B, C). Increased

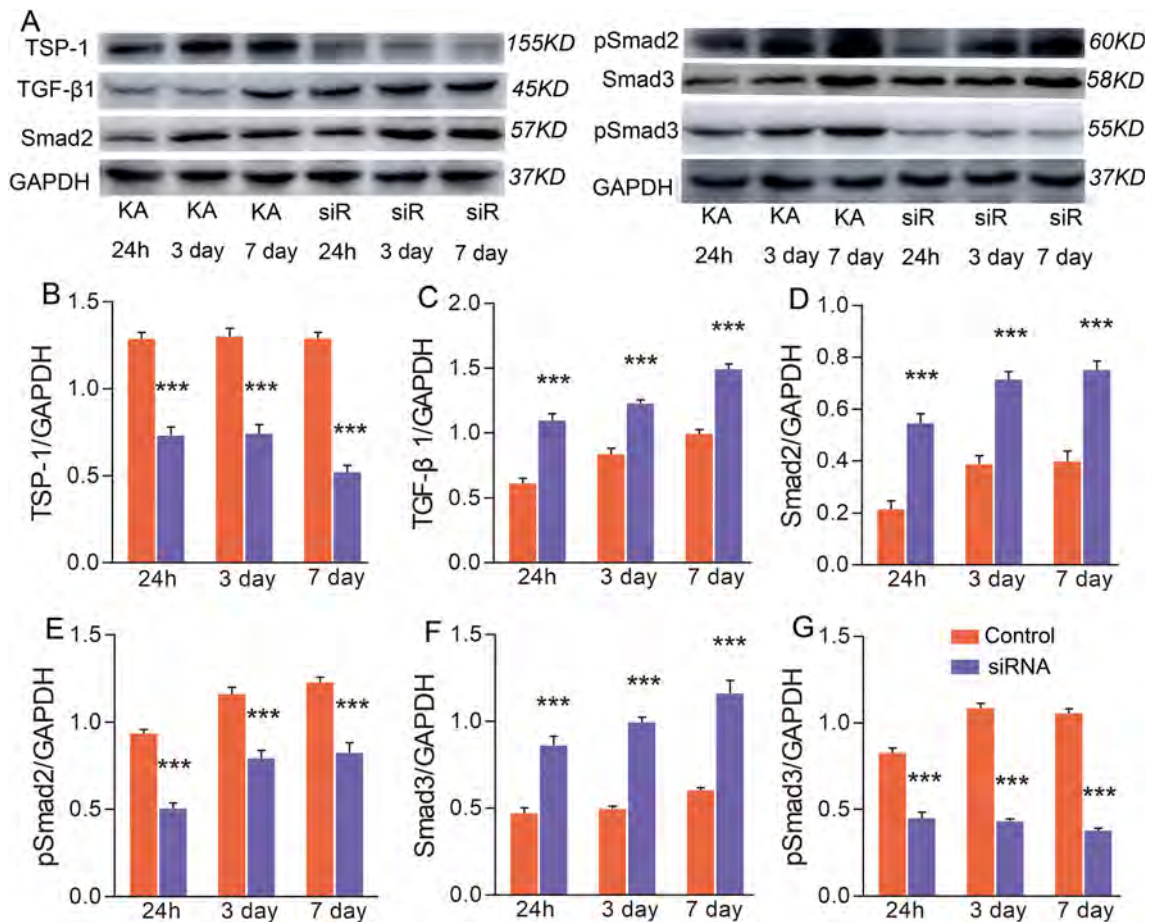


**Fig. 4** Changes in TSP-1, TGF- $\beta$ 1, Smad2/3, and pSmad2/3 levels after anti-TSP-1 siRNA treatment. Western blots (A) and statistics (B–G) for TSP-1, TGF- $\beta$ 1, Smad2/3, and pSmad2/3 ( $n = 6/\text{group}$ ). The data are shown as the mean  $\pm$  SEM. \*\*\* $P < 0.001$  vs. controls.

Smad3 immunoreactivity following SIS3 treatment was confirmed by flow cytometry (Fig. 7O).

We further found that administering the tyrosine kinase inhibitor ponatinib in addition to KA significantly prolonged the time spent in Racine's stages 0–3 ( $50.2 \pm 0.8$  min vs.  $14.8 \pm 1.0$  min;  $P < 0.001$ ), reduced the time spent in stage 4 ( $5.0 \pm 0.4$  min vs.  $19.7 \pm 1.3$  min;  $P < 0.001$ ) and stage 5 ( $4.8 \pm 0.5$  min vs.  $25.5 \pm 1.6$  min;  $P < 0.001$ ) (Fig. 8A), and shortened seizure durations ( $13.1 \pm 0.7$  min vs.  $53.4 \pm 0.6$  min;  $P < 0.001$ ; Fig. 8C) and GSDs ( $9.8 \pm 0.7$  min vs.  $45.2 \pm 1.0$  min;  $P < 0.001$ ; Fig. 8B) in addition to increasing the latencies ( $41.4 \pm 0.5$  min vs.  $2.9 \pm 0.1$  min;  $P < 0.001$ ; Fig. 8D). Ponatinib significantly reduced the hippocampal and cortical expression of GFAP and CS56 ( $P < 0.001$ ; Fig. 8E–L). It also significantly reduced the Smad2/3 and pSmad2/3 levels from 24 h onwards ( $P < 0.001$ ; Fig. 8M–O; Fig. S5A, B).

## Discussion

We hypothesized that seizures are mediated by the TSP-1/TGF- $\beta$ 1/pSmad2/3 pathway. Accordingly, as predicted, we found previously unreported increases in TSP-1 expression, TGF- $\beta$ 1 expression, and pSmad2/3 levels in a KA-induced rat model of SE. Inhibiting TSP-1 expression with siRNA and inhibiting TGF- $\beta$ 1 activation with LSKL significantly attenuated seizure severity, along with reducing GFAP/CS56 and Smad2/3 phosphorylation in this model. Inhibiting Smad3 phosphorylation with SIS3 similarly reduced seizure severity and GFAP/CS56 levels. Moreover, ponatinib significantly reduced seizure severity, Smad2/3 phosphorylation, and GFAP/CS56 levels. Since the upregulation in the TSP-1/TGF- $\beta$ 1/pSmad2/3 pathway was consistent with the KA-induced SE and GFAP/CS56 levels, these results support our initial hypothesis.

TSP-1 is secreted by astrocytes and promotes synaptogenesis, neuronal migration, and axonal growth [25–29]. Moreover, TSP-1 interacts with the  $\alpha 2\delta$ -1 subunit of the gabapentin receptor to stimulate the formation of excitatory

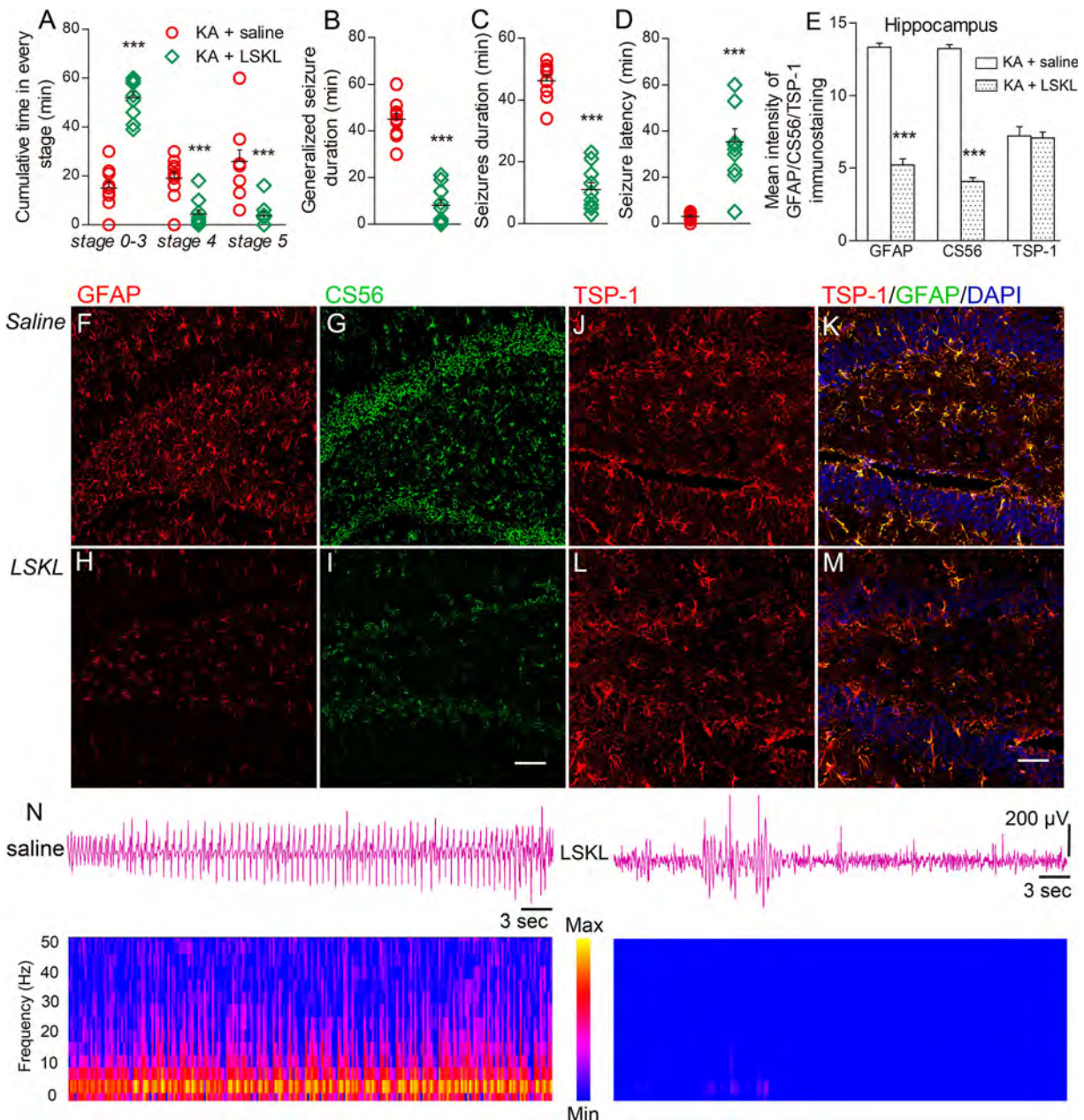


**Fig. 5** Effects of LSKL treatment in the KA-induced SE model. **A–D** LSKL altered the cumulative times for each stage (A), shortened the GSDs (B) and seizure durations (C), and increased the latencies (D) ( $n = 10$  group). **E–I** LSKL reduced the KA-induced upregulation of immunoreactivity for GFAP and CS56 in the hippocampus 3 days

after KA treatment ( $n = 6$ /group; scale bars, 100  $\mu\text{m}$ ). **J–M** The immunoreactivity of TSP-1 in the hippocampus 3 days after KA treatment (scale bars, 50  $\mu\text{m}$ ;  $n = 6$ /group). **N** Representative EEGs and EEG power spectra in saline- and LSKL-treated groups. Data are shown as the mean  $\pm$  SEM. \*\*\* $P < 0.001$  vs. controls.

synapses [30]. Consistent with these reports, we found dynamically increased TSP-1 levels in the brains of rats that experienced KA-induced SE and amygdaloid-kindling [18]. Together, these results suggest a contribution of TSP-1 in the early phase of seizures and epilepsy development, such as *via* the formation of an excitatory seizure network. In contrast, however, a reduction in TSP-1 expression has been reported in the ventrobasal thalamus in a rat model of

spontaneous absence epilepsy and in patients with generalized epilepsy [31]. Increased sensitivity to pentylenetetrazol-induced kindling has been reported in mice lacking TSP-1 [32]. Previous reports have suggested that TSP-1 levels are closely linked to epilepsy development and seizures, with both elevated and reduced TSP-1 levels aggravating seizures. Further, these results indicate that TSP-1 plays different roles in different phases of epilepsy

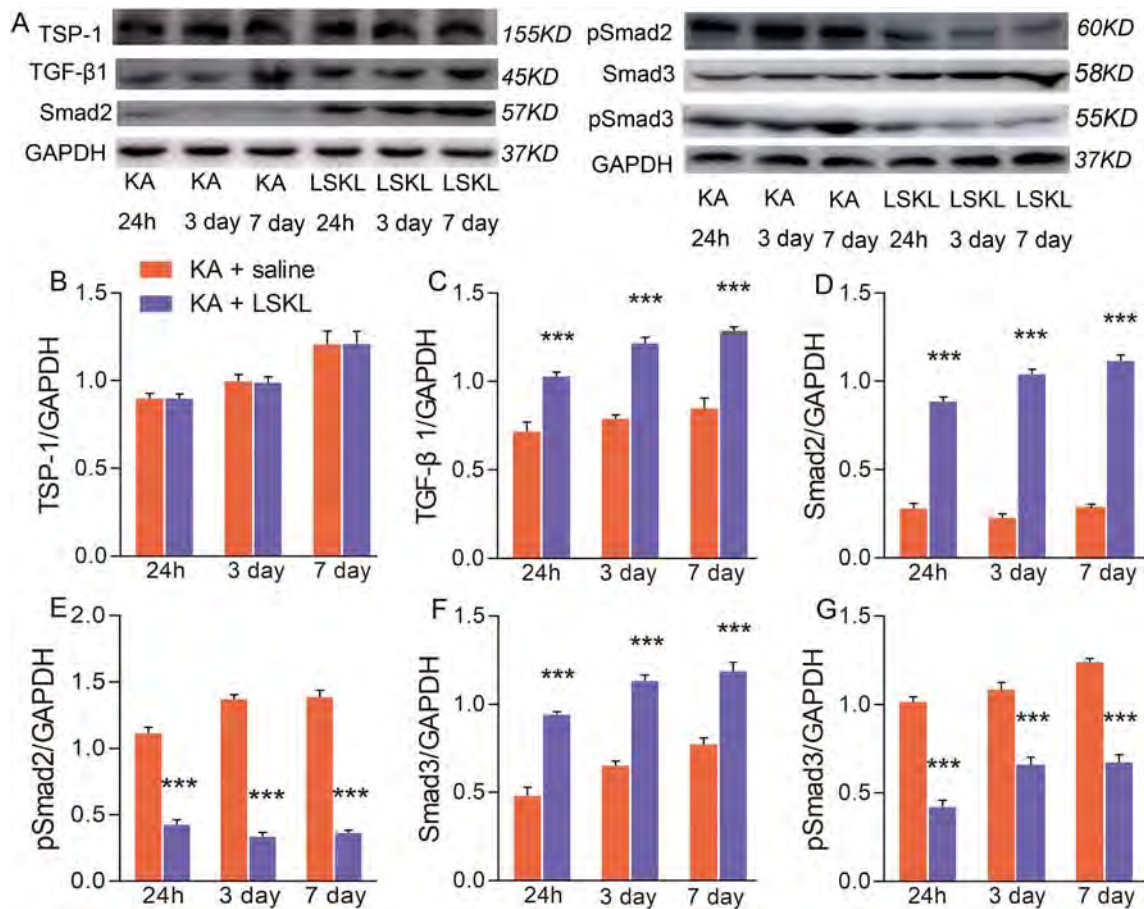


**Fig. 6** LSKL-induced changes in hippocampal levels of TSP-1, TGF- $\beta$ 1, Smad2/3, and pSmad2/3. Western blots (A) and statistics (B–G) for TSP-1 (B), TGF- $\beta$ 1 (C), Smad2/3 (D, F), and pSmad2/3

(E, G) in hippocampus ( $n = 6$ /group). The data are shown as the mean  $\pm$  SEM. \*\*\* $P < 0.001$  vs. controls.

and seizures. For example, in the early phases of epilepsy, levels of TSP-1, which plays a vital role in synaptogenesis, are increased and may be responsible for synaptogenesis and the development of an excitatory epileptic network [18]. However, kindled animals and patients with generalized epilepsy display significantly reduced concentrations of PSD-95 [33], in addition to neuronal injury and even neuronal loss [33, 34]. The reduced number of synapses [35] may be partly due to the reduced TSP-1 levels.

Upstream regulation of TGF- $\beta$ 1 activation is provided by TSP-1, an important astrocytic secretion [36, 37]. TGF- $\beta$ 1 is stored in the extracellular matrix bound to latency-associated peptide (LAP) [38, 39]. TSP-1 converts latent TGF- $\beta$ 1 to its active form by binding to LAP and thereby releases active TGF- $\beta$ 1, which then binds to the TGF- $\beta$ 1 receptor to induce signal transduction [40]. TGF- $\beta$ 1 exerts its downstream effects on target cells, with Smad proteins playing a pivotal role in relaying signals from cell-surface receptors to the nucleus [41, 42]. The best-described intracellular pathway for TGF- $\beta$ 1 is the canonical cascade, which involves the upregulation and phosphorylation of

Smad2/3 [42]. TGF- $\beta$ 1 promotes Smad2/3 phosphorylation and TGF- $\beta$ 1/Smad signaling has therefore been recognized as a therapeutic target for the treatment of astrogliosis [43].

TGF- $\beta$ 1 is associated with astrogliosis and epilepsy [43, 44]. TGF- $\beta$ 1 levels and Smad2/3 phosphorylation, which are increased in activated astrocytes and microglia [6, 45, 46], are elevated in animals and patients with epilepsy [48–49]. Cacheaux *et al.* [10] reported that direct activation of the TGF- $\beta$ 1 pathway by TGF- $\beta$ 1 results in epileptiform activity. Importantly, TGF- $\beta$  pathway blockers prevent the generation of epileptiform activity [10], and an antagonist to the TGF- $\beta$  receptor prevents the development of spontaneous seizures [11]. These studies point to a contributory role of the TGF- $\beta$ 1 pathway to the generation of epileptic seizures.

We found that inhibiting TSP-1 activity with siRNA or inhibiting TGF- $\beta$ 1 activity with LSKL alleviated the seizures induced by KA, which led us to speculate that increased TSP-1 expression may be the key factor in seizure generation *via* TGF- $\beta$ 1 pathway activation. We obtained similar results with SIS3, a potent and selective

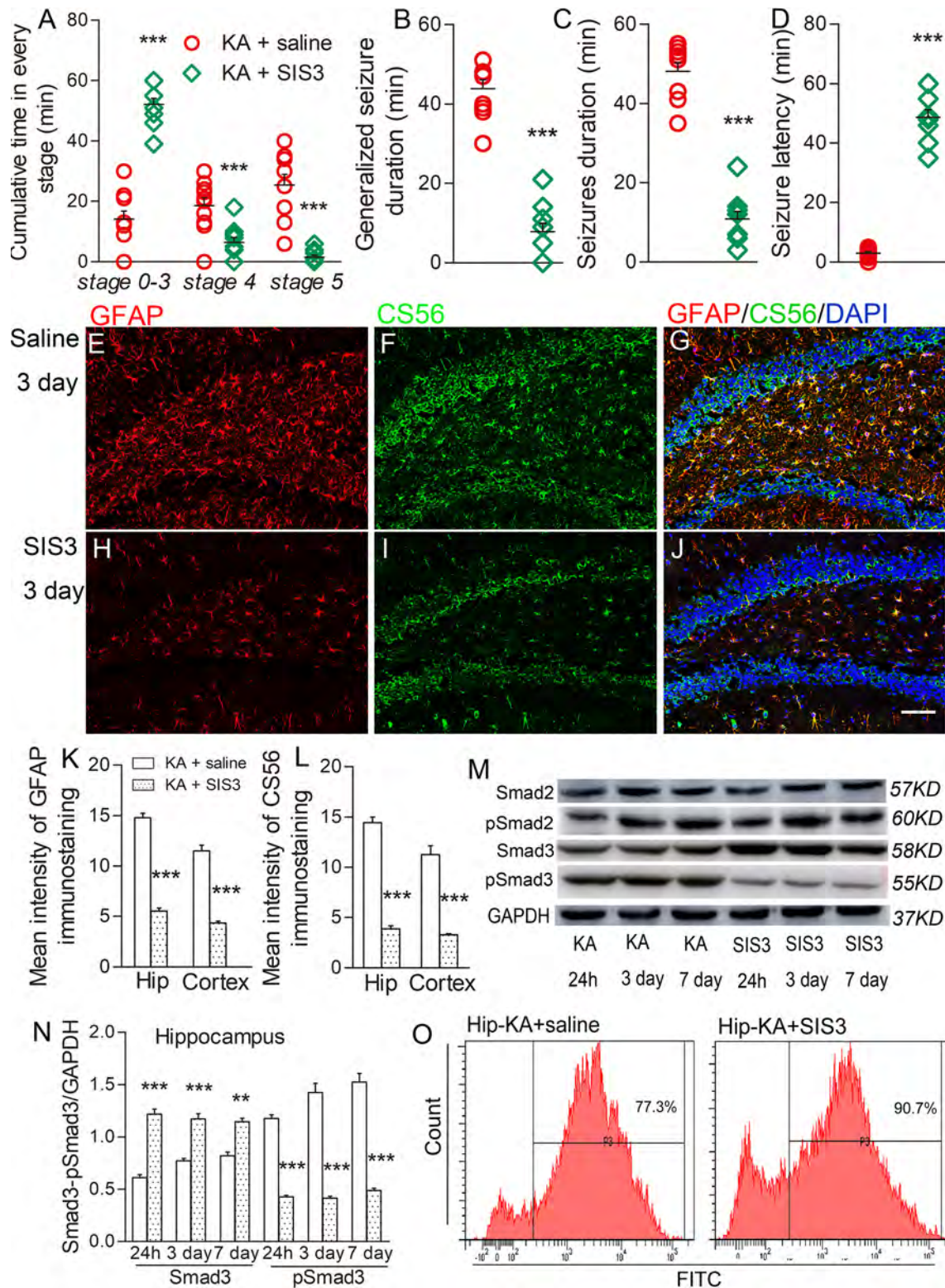


**Fig. 7** Effects of SIS3 in the KA-induced SE model. **A–D** SIS3 altered the cumulative times in each stage (**A**), shortened GSDs (**B**) and seizure durations (**C**), and increased the latencies (**D**,  $n = 10$ /group). **E–L** Representative images (**E–J**) and statistics (**K**, **L**) for the immunoreactivity for GFAP and CS56 in controls and after SIS3 treatment (scale bar, 100  $\mu$ m;  $n = 6$ /group). **M**, **N** Western blots

and statistics showing SIS3-induced changes in the levels of Smad2/3 and pSmad2/3. **O** Flow cytometry-based quantification of hippocampal Smad3 (3 days,  $n = 6$ /group). The data are shown as the mean  $\pm$  SEM. **\*\*** $P < 0.01$ , **\*\*\*** $P < 0.001$  vs. controls. Hip, hippocampus.

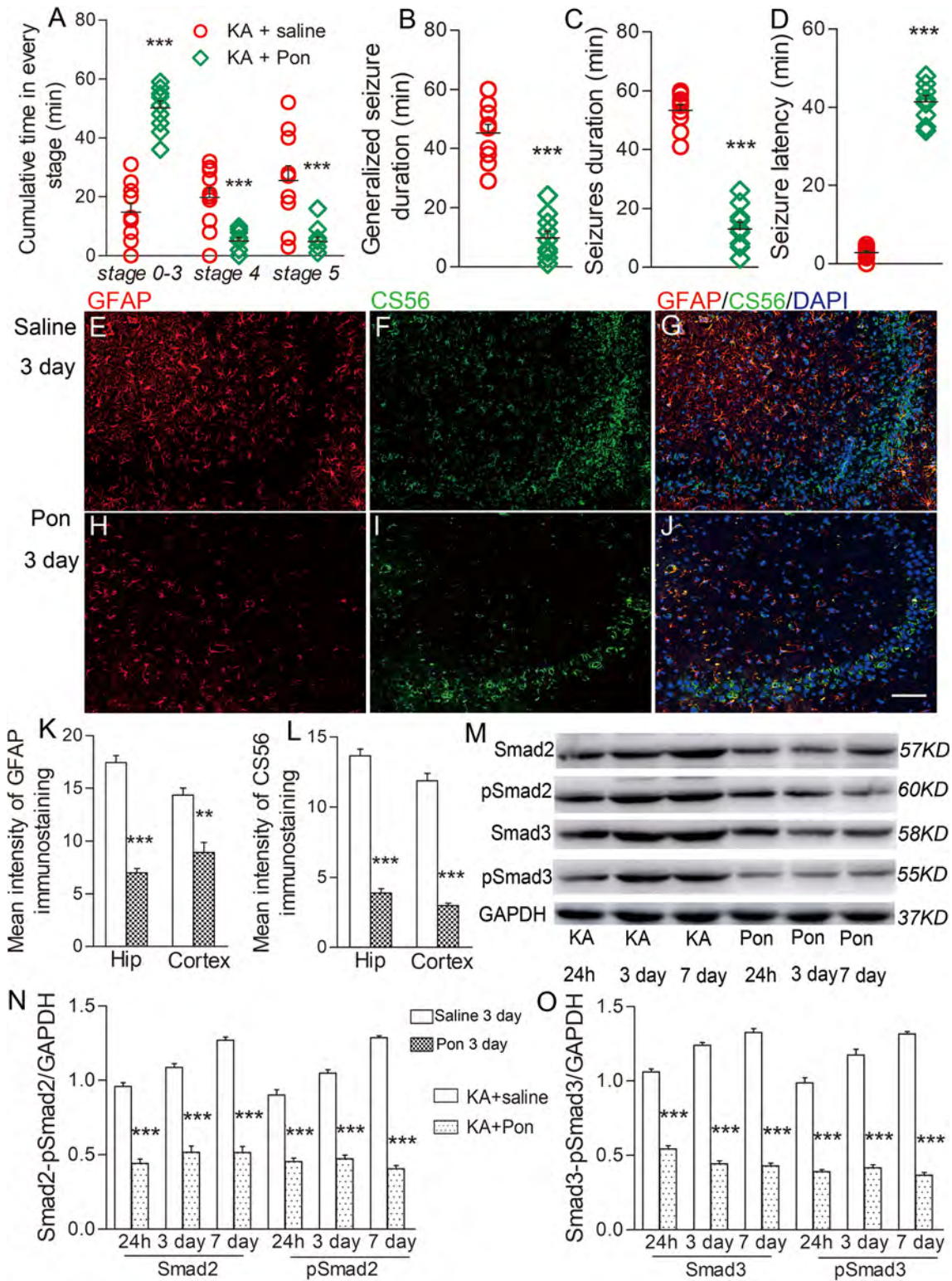


**Fig. 8** Effects of ponatinib in the KA-induced SE model. **A–D** Ponatinib altered the cumulative times in each stage (**A**), shortened GSDs (**B**) and seizure durations (**C**), and increased the latencies (**D**) ( $n = 10/\text{group}$ ). **E–L** Representative images (**E–J**) and statistics (**K, L**) of immunoreactivity for GFAP and CS56 in the hippocampus

of controls and after KA and ponatinib treatment (scale bar, 100  $\mu\text{m}$ ;  $n = 6/\text{group}$ ). **M–O** Western blots (**M**) and statistics (**N, O**) showing ponatinib-induced changes in the levels of Smad2/3 and pSmad2/3. The data are shown as the mean  $\pm$  SEM.  $**P < 0.01$ ,  $***P < 0.001$  vs. controls. Hip, hippocampus; Pon, ponatinib.

inhibitor of TGF- $\beta$ 1-regulated Smad3 phosphorylation [51]. This indicates that increased Smad3 phosphorylation, induced by TSP-1 and TGF- $\beta$ 1, may be the key factor underlying KA-induced astrogliosis and seizures.

Ponatinib is a multi-target tyrosine kinase inhibitor suitable for treating cases of chronic myelogenous leukemia that are otherwise resistant to complex amino-acid kinase inhibitors [50]. Ponatinib modulates the TGF- $\beta$ 1/pSmad2/3 pathway [48], which contributes to seizures. In our study, ponatinib also alleviated KA-induced seizures and astrogliosis. These results point to the inhibitory effect of ponatinib, further supporting the contribution of pSmad2/3 to astrogliosis and seizures.

As reported in previous studies, we found increased hippocampal and cortical immunoreactivity for GFAP and CS56 in KA-treated rats. Hippocampal dysregulation is crucial for epileptic seizures induced by several kindling stimuli [51, 52]. Similar to the hippocampus, the cortex has been shown to be an important region for the propagation of epileptic discharges, and most interictal-like discharges originating in the cortex show secondary propagation [53–56]. Our results confirm the increased immunoreactivity of GFAP and CS56 in KA-treated rats. Moreover, this increase was attenuated by siRNA or pharmacological intervention to inhibit the TSP-1/TGF- $\beta$ 1/pSmad2/3 pathway. These results support the possible contribution of the TSP-1-regulated pathway directly or indirectly to KA-induced astrogliosis. Moreover, since astrogliosis contributes to both acute seizures and chronic epilepsy [6, 7], we speculate that the TSP-1/TGF- $\beta$ 1/pSmad2/3 pathway may also contribute to spontaneous recurrent seizures, in addition to KA-induced SE.

In conclusion, astrocytes increase TSP-1 levels in response to KA-induced SE, subsequently activating the TGF- $\beta$ 1/Smad2/3 pathway, perhaps in astrocytes or other cell types, thereby increasing astrogliosis. Interfering with either TSP-1 or TGF- $\beta$ 1 signaling reduces seizure severity and astrogliosis, indicating that inhibiting the TSP-1/TGF- $\beta$ 1/Smad2/3 pathway is a potential therapeutic target for seizure management.

**Acknowledgements** This work was supported by the National Natural Science Foundation of China (81573412), the Key Research and Development Plan (2018GSF121004), and the Natural Science Foundation of Shandong Province, China (ZR2014JL055).

**Conflict of interest** The authors declare that they have no conflict of interest.

## References

- Johannessen SI, Gran L, Sillanpaa M, Johnson T. Intractable Epilepsy. Petersfield, UK: Wrightson Biomedical Publishing 1995: 1–12.
- Leppik IE. Intractable epilepsy in adults. *Epilepsy Res* 1992, 5: 7–11.
- Wilcox KS, Gee JM, Gibbons MB, Tvrdik P, White JA. Altered structure and function of astrocytes following status epilepticus. *Epilepsy Behav* 2015, 49: 17–19.
- Coulter DA, Steinhilber C. Role of astrocytes in epilepsy. *Cold Spring Harb Perspect Med* 2015, 5: a022434.
- Devinsky O, Vezzani A, Najjar S, De Lanerolle NC, Rogawski MA. Glia and epilepsy: excitability and inflammation. *Trends Neurosci* 2013, 36: 174–184.
- Guo D, Zou J. Rapamycin attenuates acute seizure-induced astrocyte injury in mice *in vivo*. *Sci Rep* 2017, 7: 2867.
- Robel S. Astroglial scarring and seizures: a cell biological perspective on epilepsy. *Neuroscientist* 2016, 23: 152–168.
- Okada-Tsuchioka M, Segawa M, Kajitani N, Hisaoka-Nakashima K, Shibasaki C, Morinobu S, *et al.* Electroconvulsive seizure induces thrombospondin-1 in the adult rat hippocampus. *Prog Neuropsychopharmacol Biol Psychiatry* 2014, 48: 236–244.
- Shi Y, Massagué J. Mechanisms of TGF-beta signaling from cell membrane to the nucleus. *Cell* 2003, 113: 685–700.
- Cacheaux LP, Ivens S, David Y, Lakhter AJ, Bar-Klein G, Shapira M, *et al.* Transcriptome profiling reveals TGF-beta signaling involvement in epileptogenesis. *J Neurosci* 2009, 29: 8927–8935.
- Bar-Klein G, Cacheaux LP, Kamintsky L, Prager O, Weissberg I, Schoknecht K, *et al.* Losartan prevents acquired epilepsy via TGF- $\beta$  signaling suppression. *Ann Neurol* 2014, 75: 864–875.
- Weissberg I, Wood L, Kamintsky L, Vazquez O, Milikovsky DZ, Alexander A, *et al.* Albumin induces excitatory synaptogenesis through astrocytic TGF- $\beta$ /ALK5 signaling in a model of acquired epilepsy following blood–brain barrier dysfunction. *Neurobiol Dis* 2015, 78: 115–125.
- Yu CY, Gui W, He HY, Wang XS, Zuo J, Huang L, *et al.* Neuronal and astroglial TGF $\beta$ -Smad3 signaling pathways differentially regulate dendrite growth and synaptogenesis. *Neuro-molecular Med* 2014, 16: 457–472.
- Krishna SM, Golledge J. The role of thrombospondin-1 in cardiovascular health and pathology. *Int J Cardiol* 2013, 168: 692–706.
- Hou M, Bao X, Luo F, Chen X, Liu L, Wu M. HMGA2 modulates the TGF $\beta$ /Smad, TGF $\beta$ /ERK and Notch signaling pathways in human lens epithelial-mesenchymal transition. *Curr Mol Med* 2018, 18: 71–82.
- Moustakas A, Souchelnyskiy S, Heldin CH. Smad regulation in TGF-beta signal transduction. *J Cell Sci* 2001, 114: 4359–4369.
- Cui L, Wang Y, Yu R, Li B, Xie S, Gao Y, *et al.* Jia-Shen decoction-mediated serum inhibits angiotensin-II induced cardiac fibroblast proliferation via the TGF- $\beta$ 1/Smad signaling pathway. *Mol Med Rep* 2016, 14: 1610–1616.
- Sun H, Ma L, Zhang Y, Pan X, Wang C, Zhang J, *et al.* A purinergic P2 receptor family-mediated increase in thrombospondin-1 bolsters synaptic density and epileptic seizure activity in the amygdala-kindling rat model. *Front Cell Neurosci* 2018, 12: 302.
- Racine RJ. Modification of seizure activity by electrical stimulation. II. Motor seizure. *Electroencephalogr Clin Neurophysiol* 1972, 32: 281–294.
- Jinnin M, Ihn H, Tamaki K. Characterization of SIS3, a novel specific inhibitor of Smad3, and its effect on transforming growth factor-beta1-induced extracellular matrix expression. *Mol Pharmacol* 2006, 69: 597–607.
- Miyazawa K, Shinozaki K, Hara T, Furuya T, Miyazono K. Two major Smad pathways in TGF-beta superfamily signalling. *Genes Cells* 2002, 7: 1191–1204.
- Wang D, Zhang X, Wang M, Zhou D, Pan H, Shu Q, *et al.* Early activation of astrocytes does not affect amyloid plaque load in an

- animal model of Alzheimer's disease. *Neurosci Bull* 2018, 34: 912–920.
23. Chen G, Luo X, Qadri MY, Berta T, Ji RR. Sex-dependent glial signaling in pathological pain: distinct roles of spinal microglia and astrocytes. *Neurosci Bull* 2018, 34: 98–108.
  24. Okuda H. A review of functional heterogeneity among astrocytes and the CS56-specific antibody-mediated detection of a subpopulation of astrocytes in adult brains. *Anat Sci Int* 2018, 93: 161–168.
  25. Christopherson KS, Ullian EM, Stokes CC, Mullen CE, Hell JW, Agah A, *et al.* Thrombospondins are astrocyte-secreted proteins that promote CNS synaptogenesis. *Cell* 2005, 120: 421–433.
  26. Xu J, Xiao N, Xia J. Thrombospondin 1 accelerates synaptogenesis in hippocampal neurons through neuropilin 1. *Nat Neurosci* 2010, 13: 22–24.
  27. Iruela-Arispe ML, Liska DJ, Sage EH, Bornstein P. Differential expression of thrombospondin 1, 2, and 3 during murine development. *Dev Dyn* 1993, 197: 40–56.
  28. Yu K, Ge J, Summers JB, Li F, Liu X, Ma P, *et al.* TSP-1 secreted by bone marrow stromal cells contributes to retinal ganglion cell neurite outgrowth and survival. *PLoS One* 2008, 3: e2470.
  29. Cahoy JD, Emery B, Kaushal A, Foo LC, Zamanian JL, Christopherson KS, *et al.* A transcriptome database for astrocytes, neurons, and oligodendrocytes: a new resource for understanding brain development and function. *J Neurosci* 2008, 28: 264–278.
  30. Eroglu C, Allen NJ, Susman MW, O'Rourke NA, Park CY, Ozkan E, *et al.* Gabapentin receptor alpha2delta-1 is a neuronal thrombospondin receptor responsible for excitatory CNS synaptogenesis. *Cell* 2009, 139: 380–392.
  31. Santolini I, Celli R, Cannella M, Imbriglio T, Guiducci M, Parisi P, *et al.* Alterations in the  $\alpha 2 \delta$  ligand, thrombospondin-1, in a rat model of spontaneous absence epilepsy and in patients with idiopathic/genetic generalized epilepsies. *Epilepsia* 2017, 58: 1993–2001.
  32. Mendus D, Rankin-Gee EK, Mustapha M, Porter BE. Increased sensitivity to kindling in mice lacking TSP1. *Neuroscience* 2015, 305: 302–308.
  33. Egbenya DL, Hussain S, Lai YC, Xia J, Anderson AE, Davanger S. Changes in synaptic AMPA receptor concentration and composition in chronic temporal lobe epilepsy. *Mol Cell Neurosci* 2018, 92: 93–103.
  34. Lorgen JØ, Egbenya DL, Hammer J, Davanger S. PICK1 facilitates lasting reduction in GluA2 concentration in the hippocampus during chronic epilepsy. *Epilepsy Res* 2017, 137: 25–32.
  35. Pfeifer FW, Barres BA. Synaptic efficacy enhanced by glial cells *in vitro*. *Science* 1997, 277: 1684–1687.
  36. Lafyatis R. Transforming growth factor  $\beta$ -at the centre of systemic sclerosis. *Nat Rev Rheumatol* 2014, 10: 706–719.
  37. Cheng C, Lau SK, Doering LC. Astrocyte-secreted thrombospondin-1 modulates synapse and spine defects in the fragile X mouse model. *Mol Brain* 2016, 9: 74.
  38. Hayashi H, Sakai T. Biological significance of local TGF-beta activation in liver diseases. *Front Physiol* 2012, 3: 12.
  39. Sweetwyne MT, Murphy-Ullrich JE. Thrombospondin 1 in tissue repair and fibrosis: TGF-beta-dependent and independent mechanisms. *Matrix Biol* 2012, 31: 178–186.
  40. Tran MD, Furones-Alonso O, Sanchez-Molano J, Bramlett HM. Trauma-induced expression of astrocyte thrombospondin-1 is regulated by P2 receptors coupled to protein kinase cascades. *Neuroreport* 2012, 23: 721–726.
  41. Kawarada Y, Inoue Y, Kawasaki F, Fukuura K, Sato K, Tanaka T, *et al.* TGF-beta induces p53/Smads complex formation in the PAI-1 promoter to activate transcription. *Sci Rep* 2016, 6: 35483.
  42. Chin GS, Liu W, Peled Z, Lee TY, Steinbrech DS, Hsu M, *et al.* Differential expression of transforming growth factor-beta receptors I and II and activation of Smad 3 in keloid fibroblasts. *Plast Reconstr Surg* 2001, 108: 423–429.
  43. Zhang R, Wu Y, Xie F, Zhong Y, Wang Y, Xu M, *et al.* RGMA mediates reactive astrogliosis and glial scar formation through TGFbeta1/Smad2/3 signaling after stroke. *Cell Death Differ* 2018, 25: 1503–1516.
  44. Ivens S, Kaufer D, Flores LP, Bechmann I, Zumsteg D, Tomkins O, *et al.* TGF-beta receptor-mediated albumin uptake into astrocytes is involved in neocortical epileptogenesis. *Brain* 2007, 130: 535–547.
  45. Yu Y, Li J, Zhou H, Xiong Y, Wen Y, Li H. Functional importance of the TGF- $\beta$ 1/Smad3 signaling pathway in oxygen-glucose-deprived (OGD) microglia and rats with cerebral ischemia. *Int J Biol Macromol* 2018, 116: 537–544.
  46. Tichauer JE, Flores B, Soler E, Eugenin-von Bernhardt L, Ramírez G, von Bernhardt R. Age-dependent changes on TGF $\beta$ 1 Smad3 pathway modify the pattern of microglial cell activation. *Brain Behav Immun* 2014, 37: 187–196.
  47. Yu W, Du Y, Zou Y, Wang X, Stephani U, Lü Y. Smad anchor for receptor activation contributes to seizures in temporal lobe epilepsy. *Synapse* 2017, 71: 3.
  48. Christensen KV, Leffers H, Watson WP, Sánchez C, Kallunki P, Egebjerg J. Levetiracetam attenuates hippocampal expression of synaptic plasticity-related immediate early and late response genes in amygdala-kindled rats. *BMC Neurosci* 2010, 11: 9.
  49. Chen Y, Shimotake A, Matsumoto R, Kunieda T, Kikuchi T, Miyamoto S, *et al.* The 'when' and 'where' of semantic coding in the anterior temporal lobe: Temporal representational similarity analysis of electrocorticogram data. *Cortex* 2016, 79: 1–13.
  50. Qu Y, Zhang L, Kang Z, Jiang W, Lv C. Ponatinib ameliorates pulmonary fibrosis by suppressing TGF-beta1/Smad3 pathway. *Pulm Pharmacol Ther* 2015, 34: 1–7.
  51. Hsu D. The dentate gyrus as a filter or gate: a look back and a look ahead. *Prog Brain Res* 2007, 163: 601–613.
  52. Heinemann U, Beck H, Dreier JP, Ficker E, Stabel J, Zhang CL. The dentate gyrus as a regulated gate for the propagation of epileptiform activity. *Epilepsy Res* 1992, 7: 273–280.
  53. Petit LF, Jalabert M, Buhler E, Malvache A, Peret A, Chauvin Y, *et al.* Normotopic cortex is the major contributor to epilepsy in experimental double cortex. *Ann Neurol* 2014, 76: 428–442.
  54. Bernasconi A, Martinez V, Rosa-Neto P, D'Agostino D, Bernasconi N, Berkovic S, *et al.* Surgical resection for intractable epilepsy in "double cortex" syndrome yields inadequate results. *Epilepsia* 2001, 42: 1124–1129.
  55. Mai R, Tassi L, Cossu M, Francione S, Lo Russo G, Garbelli R, *et al.* A neuropathological, stereo-EEG, and MRI study of subcortical band heterotopia. *Neurology* 2003, 60: 1834–1838b.
  56. Parker CS, Clayden JD, Cardoso MJ, Rodionov R, Duncan JS, Scott C, *et al.* Structural and effective connectivity in focal epilepsy. *Neuroimage Clin* 2018, 17: 943–952.



# NLRP3 Deficiency Attenuates Secondary Degeneration of Visual Cortical Neurons Following Optic Nerve Injury

Zhou Zhang<sup>1</sup> · Wenyi Liu<sup>1</sup> · Yubin Huang<sup>2</sup> · Linlin Luo<sup>1</sup> · Xiaofeng Cai<sup>1</sup> · Yunjia Liu<sup>1</sup> · Liqianyu Ai<sup>1</sup> · Jun Yan<sup>3</sup> · Sen Lin<sup>1</sup> · Jian Ye<sup>1</sup>

Received: 7 April 2019 / Accepted: 26 July 2019 / Published online: 26 November 2019  
© Shanghai Institutes for Biological Sciences, CAS 2019

**Abstract** In the visual pathway, optic nerve (ON) injury may cause secondary degeneration of neurons in distal regions, such as the visual cortex. However, the role of the neuroinflammatory response in regulating secondary impairment in the visual cortex after ON injury remains unclear. The NOD-like receptor family pyrin domain containing 3 (NLRP3) is an important regulator of neuroinflammation. In this study, we established a mouse model of unilateral ON crush (ONC) and showed that the expression of NLRP3 was significantly increased in the primary visual cortex (V1) as a response to ONC and that the NLRP3 inflammasome was activated in the contralateral V1 1 days–14 days after ONC. Ablation of the NLRP3 gene significantly decreased the trans-neuronal degeneration within 14 days. Visual electrophysiological function was improved in NLRP3<sup>-/-</sup> mice. Taken together, these findings suggest that NLRP3 is a potential therapeutic

target for protecting visual cortical neurons against degeneration after ON injury.

**Keywords** NLRP3 · Visual cortex · Optic nerve injury · Visual cortical degeneration

## Introduction

In the visual system, in addition to the direct damage to the axons and somata in the primary site under pathological conditions such as ocular trauma and high intraocular pressure, neurons within the visual pathway also suffer from anterograde (retina to visual cortex) or retrograde (visual cortex to retina) injuries, which are characterized by distal neural degeneration, programmed cell death, and increased inflammatory cytokines, accompanied by the recruitment and activation of glial cells [1–4]. However, little is known about the initial factors and pathological mechanisms responsible for these secondary changes; relevant therapies to prevent dysfunction are still unavailable.

Inflammation performs the dual roles of damage and repair in the central nervous system (CNS) and has also been reported to be a key factor in secondary injury [5]. An important component of human innate immunity, cell pattern-recognition receptors, such as toll-like receptors [6] and NOD-like receptors [7], are activated by pathogen-associated molecular patterns (PAMPs) and damage-associated molecular patterns (DAMPs), fused into a multimeric complex by binding to the adaptor molecule apoptosis-associated speck-like protein containing a caspase-1 recruitment domain (ASC) and procaspase-1, named the inflammasome. The inflammasome is capable of converting immature pro-interleukin (IL)-1 $\beta$  and pro-IL-

**Electronic supplementary material** The online version of this article (<https://doi.org/10.1007/s12264-019-00445-x>) contains supplementary material, which is available to authorized users.

✉ Sen Lin  
sam.lin@tmmu.edu.cn

✉ Jian Ye  
yejian1979@163.com

<sup>1</sup> Department of Ophthalmology, Research Institute of Surgery and Daping Hospital, Army Medical Center of the People's Liberation Army (PLA), Army Medical University, Chongqing 400042, China

<sup>2</sup> Shenzhen Institutes of Advanced Technology, Chinese Academy of Sciences, Shenzhen 518000, China

<sup>3</sup> Department 1, Research Institute of Surgery and Daping Hospital, Army Medical Center of the PLA, Army Medical University, Chongqing 400042, China

18 to mature forms by procaspase-1 self-cleavage, thereby triggering the innate inflammatory response [8–10]. In addition, activated caspase-1 promotes the maturation of gasdermin D (GSDMD), which ultimately mediates the pro-inflammatory form of programmed cell death termed pyroptosis [11]. In the inflammasome family, the nucleotide-binding domain leucine-rich repeat (LRR)–pyrin domain containing 3 or NOD-like receptor family pyrin domain containing 3 (NLRP3) inflammasome has been well characterized, for the abnormal activation of the NLRP3 inflammasome has been shown to be implicated in many CNS disorders [12, 13], diabetes mellitus [14, 15], and autoimmune diseases [16, 17]. Accumulating evidence has shown that inflammasomes participate in the onset and progression of secondary brain injury [18–20] and glaucoma [21]. Furthermore, activation of the NLRP3 inflammasome in microglia has been implicated in retinal ganglion cell loss after optic nerve (ON) injury [22].

Studies on secondary lesions have shown that the breach of the blood-brain barrier following ON injury is associated with the recruitment of peripheral mononuclear macrophages and neutrophils [3] and the inflammatory response upon NLRP3 activation of glia [22, 23]. Furthermore, the expression of NLRP3 in neurons has been documented [24–27]. Concerning its possible involvement in secondary/distal damage in the CNS, it is imperative to establish whether the NLRP3 inflammasome is activated trans-synaptically after ON injury and whether its effect on visual cortical neurons is responsible for secondary neuronal degeneration. To address this issue, we established a mouse model of unilateral ON crush (ONC). Activation of the NLRP3 inflammasome in the primary visual cortex (V1) was found to be associated with the progression of neuronal injury. The inflammatory cytokines in V1 of the NLRP3<sup>-/-</sup> brain were decreased within 14 days, the number of apoptotic and degenerative neurons was decreased, and the indexes of visual electrophysiology were also improved in NLRP3-knockout mice.

## Materials and Methods

### Animals

Adult C57BL/6J male mice (WT) 8–10 weeks old and weighing 20 g–24 g were purchased from the Animal Center of The Army Medical University (AMU). Age- and weight-matched NLRP3<sup>-/-</sup> mice (JAX Cat. No. 021302) were purchased from The Jackson Laboratory (Bar Harbor, ME). The NLRP3<sup>-/-</sup> mice were confirmed by polymerase chain reaction (PCR) (Figs. S1 and S2). The primer sequences used were as follows: 5'-TGCCTGCTCTTTA CTGAAGG-3' (mutant forward); 5'-TCAGTTTCCTTGG

CTACCAGA-3' (WT forward); 5'-TTCCATTACAGT-CACTCCAGATGT-3' (common reverse). The animals were housed in a 12/12 h light/dark schedule in a specific pathogen-free facility, with free access to irradiated food and sterile water.

### Experimental Design

The sample size per experiment was determined based on previous publications with similar methodologies. All experiments were performed 3 times. All the data were included in analysis.

### Surgical Procedure for Optic Nerve Crush

The control group consisted of mice that received no operation (naïve) and mice that received sham surgery on the left eye (sham). In the experimental group, the left eye was subjected to ONC. Briefly, animals were anesthetized by intraperitoneal injection of 1% pentobarbital. Using aseptic technique, a minimal incision was performed in the temporal area of the conjunctiva of the left eye, and the extraocular muscles were gently separated to expose the ON, which was crushed with fine, self-closing forceps 1.5 mm behind the eyeball for 10 s without damaging the blood vessels [28, 29]. In the sham operation, the ON was exposed by using the same protocol but without crushing. The eyes were treated with antibiotic ointment after surgery. The mice were then kept on a warming pad until fully awake. There were no postoperative infections. All animal procedures were conducted in accordance with the Guidelines on the Use of Animals from the NIH and the Institutional Animal Care and Use Committee of AMU and were approved by the Animal Ethics Committee of AMU.

### RNA Isolation and Quantitative Real Time Polymerase Chain Reaction (qRT-PCR)

Animals were euthanized and V1 was dissected out according to the mouse brain atlas (The Mouse Brain in Stereotaxic Coordinates, Academic Press, New York, 2001). Total RNA of the contralateral and ipsilateral V1 was extracted with an RNeasy RNA isolation kit (Qiagen, Hilden, Germany), and reverse transcribed with a Prime Script<sup>TM</sup> RT reagent Kit (Takara, Dalian, China) according to the manufacturer's instructions. qRT-PCR was performed on a CFX96 real-time instrument/C1000 Thermal Cycler (Bio-Rad, Hercules, CA) using the SYBR method (Quanta BioSciences, Gaithersburg, MA).

The primer sequences used for qRT-PCR were as follows:

NLRP3: F-AAAGGAAGTGGACTGCGAGA, R-TTCA AACGACTCCCTGGAAC;

NLRP1: F-TTAGATGAGCATGCCATTGC, R-ACTC CTGAAGACACAAGTGG;

NLRC4[NLR family CARD (caspase recruitment domain)-containing 4]: F-GGAAAGTGCAAGGCTCT-GAC, R-TGTCTGCTTCCTGATTGTGC;

NLRP6: F-CTGTTCTGAGCTACTGCGTGAG, R-AG GCTCTTCTTCTTCTTCTCCTG;

AIM2(Absent in Melanoma 2): F-AGCCTGAACA-GAAACAGATGG, R-CTTCTTGGGTCTCAAACGTGA.

### Western Blot

Freshly-dissected V1 tissue was combined with RIPA (89900, Thermo Fisher Scientific, Waltham, MA) and protease inhibitor cocktail (78438, Thermo Fisher Scientific, Waltham, MA) to obtain the lysate. After centrifugation at  $12,000 \times g$  at  $4^{\circ}\text{C}$  for 15 min, the supernatant was collected and the protein concentration was measured with an Enhanced BCA Protein Assay Kit (P0009, Beyotime, Shanghai, China). Equal amounts of lysate (50 mg) were separated on SDS polyacrylamide gel and transferred to polyvinylidene difluoride membranes (IPVH00010, Millipore, Burlington, MA) with continuous current (250 mA) for 0.5 h–2 h. The membranes were washed in Tris-buffered saline (TBS, pH 7.4) containing 0.1% Tween-20 (TBS-T) and blocked in 5% non-fat milk in TBS-T for 2 h at room temperature (RT). Then, the membranes were incubated with primary antibodies recognizing mouse NLRP3 (AG-20B-0014-C100, 1:500, AdipoGen Life Science, Liestal, Switzerland), ASC (Santa Cruz, Dallas, TX), caspase-1 (AB 1871, 1:1000, Chemicon, Temecula, CA), IL-1 $\beta$  (AF-401-NA, 1:1000, R&D Systems, Minneapolis, MN), AIM2 (ab93015, 1:500, Abcam, Cambridge, MA), and  $\beta$ -actin (AP0731, 1:5000, Bioworld, Bloomington, MN) overnight at  $4^{\circ}\text{C}$ . After three washes with TBS-T for 10 min each, the membranes were incubated with horseradish peroxidase-conjugated secondary antibodies (1:2000, R&D Systems, Minneapolis, MN) for 2 h at RT. The signals were detected with a chemiluminescence reagent (ECL, GE Healthcare, Shanghai, China), and images were acquired by a chemiluminescent detection system (Thermo Fisher Scientific, Waltham, MA). Densitometric quantification of the specific band intensities was normalized to  $\beta$ -actin in the same blot.

### Immunostaining

Mouse brains were fixed in freshly prepared 4% paraformaldehyde at  $4^{\circ}\text{C}$  for 24 h and then embedded in OCT compound (Sakura Finetek, San Diego, CA). Cryosections (20  $\mu\text{m}$ ) were permeabilized with PBS containing 0.2% Triton X-100 at RT for 30 min. Sections were

blocked with the appropriate sera and then incubated overnight at  $4^{\circ}\text{C}$  with primary antibodies for NLRP3 (1:400, AdipoGen Life Science, Liestal, Switzerland) and NeuN (#24307, 1:200, Cell Signaling Technology, Danvers, MA). After three washes, the sections were incubated with the appropriate fluorescent secondary antibodies (Alexa Fluor 488 and 594, 1:400, Life Technologies, Carlsbad, CA) for 1 h at RT. The slides were then stained with DAPI and mounted. Images were captured using an SP-8 confocal microscope (Leica, Wetzlar, Germany).

### TUNEL

Apoptotic neurons in contralateral V1 sections were stained using an *In Situ* Cell Death Detection Kit according to the manufacturer's protocol (TMR red, 12156792910, Roche, Mannheim, Germany). Briefly, the cryosections were washed with PBS, permeabilized in citrate-Triton buffer (0.1%), and then incubated with TUNEL working solution for 1 h at  $37^{\circ}\text{C}$  in a humid cassette avoiding light. The samples were then processed for NeuN double-labeling (see above) after a PBS wash. The images were captured with the SP-8 confocal microscope. TUNEL+ NeuN+ cells were randomly counted *via* FIJI software (<https://imagej.nih.gov/ij/>), and the numbers of positive cells from the same optical fields (low-power) in each animal were averaged.

### Fluoro-Jade C (FJC) Staining

Staining was carried out according to the manufacturer's protocol, with modifications. Briefly, slides were first immersed in a solution of 1% sodium hydroxide in 80% ethanol for 5 min, followed by 70% ethanol and a distilled water rinse for 2 min. Then, the slides were incubated in 0.06% potassium permanganate for 9 min. Following a 2-min water rinse, a 0.0001% solution of Fluor-Jade® C (AG325-30MG, Chemicon, Temecula, CA) dissolved in a 0.1% acetic acid vehicle was added to the slides and left for 15 min. The slides were then rinsed through three changes of distilled water (1 min per change), dried on a slide warmer at  $50^{\circ}\text{C}$  for 5 min, cleared in xylene for 1 min, and then coverslipped with DPX (Sigma). The stained slides were photographed with the SP-8 confocal microscope. The number of FJC-positive cells from the same optical fields (low-power) of each animal was averaged.

### Flash Visual Evoked Potentials (F-VEPs)

To evaluate the visual electrophysiological function of mice with ONC or sham surgery, F-VEPs were measured on days 7 and 14 after ONC. Electrodes located at the primary visual cortexes were the active (positive)

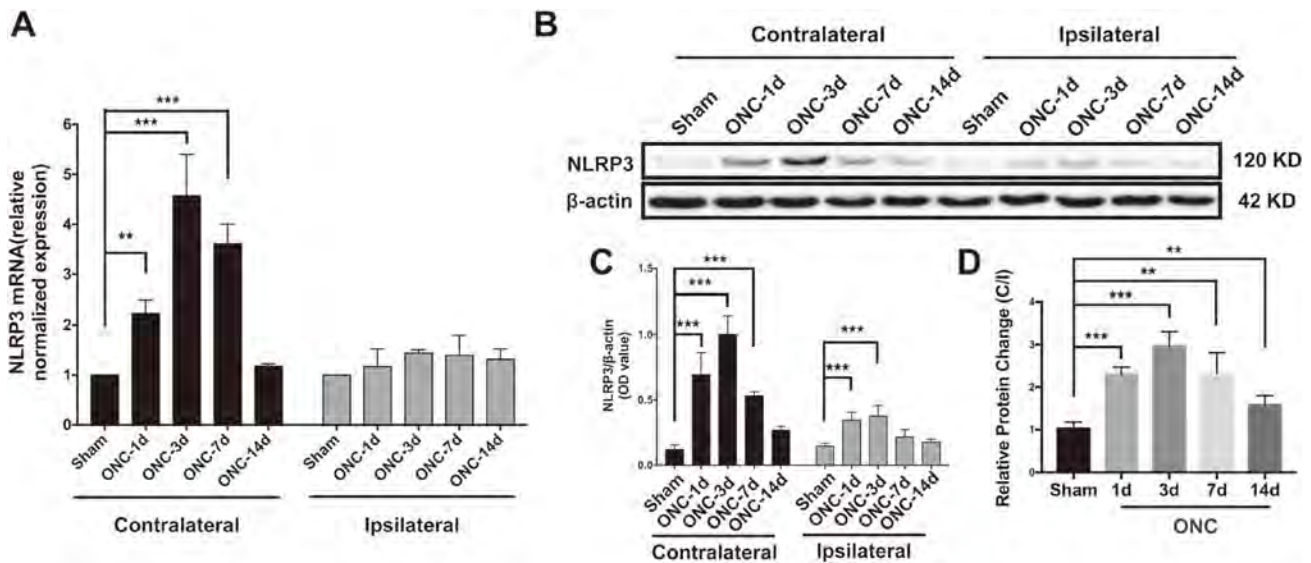


**Fig. 1** NLRP3 expression is significantly upregulated in primary visual cortex after optic nerve crush (ONC). **A, B** The mRNA and protein levels of NLRP3 in contralateral and ipsilateral V1 as determined by qRT-PCR and Western blot, respectively.

**C** Quantification of NLRP3 protein levels in V1. **D** Relative protein change is presented as the ratio of contralateral to ipsilateral protein levels (C/I ratio). \*\* $P < 0.01$ , \*\*\* $P < 0.001$  versus sham group,  $n = 4$ .

electrodes, and an electrode placed at the frontal cortex was the reference (negative) electrode. The ground electrode was inserted into the tail. While an eye was being tested, the contralateral eye was covered by a lightproof patch; the apparatus reduced interference from electrical noise (60 Hz) and the heartbeat. In each F-VEP experiment, 50 successive flash stimuli of 10  $\mu$ s duration and 1 Hz frequency were delivered (intensity 120 mJ–200 mJ). In each animal, the amplitudes of three main waveforms from stimulus onset were recorded, and the P2 amplitude with respect to baseline was analyzed.

### Statistical Analysis

Data are presented as the mean  $\pm$  SEM. The unpaired Student's *t*-test was applied to assess the differences between two groups. One-way analysis of variance (ANOVA) followed by the Tukey test was used for multiple comparisons. A *P*-value  $< 0.05$  was considered statistically significant. All results were analyzed using GraphPad Prism software (GraphPad Software, Inc., La Jolla, CA).

## Results

### NLRP3 Expression is Elevated in Contralateral Primary Visual Cortex After Optic Nerve Crush

In previous studies, increased expression of NLRP3 has been reported in the local cerebral cortex after traumatic

brain injury and cerebral ischemia [30, 31]. However, no study has described its expression pattern in V1 after anterior visual pathway injury. First, using qRT-PCR, we demonstrated elevated NLRP3 levels in the contralateral V1 after ONC. The RNA expression of NLRP3 was upregulated on day 1 and was further increased to its highest level on day 3. Then, the relative mRNA level decreased to the levels in the naïve (Fig. S3A) and sham groups on day 14 (Fig. 1A). However, no significant changes in the mRNA levels of NLRP3 in the ipsilateral V1 were found throughout the 14 days after ONC. Consistent with the qRT-PCR results, increased protein levels of NLRP3 in the contralateral V1 in response to ONC were shown by Western blotting (Fig. 1B). The densitometric ratio of NLRP3 to  $\beta$ -actin in ONC mice was nearly 22-fold higher than that of the naïve (Fig. S3 B, C) and sham groups on day 1 and progressively increased until day 3; subsequently, the ratio gradually decreased. On the ipsilateral side, however, the protein level of NLRP3 in the ONC mice was significantly higher on days 1 and 3 than in their sham-treated littermates, and then gradually declined to levels similar to those of the sham controls (Fig. 1B, C).

The ratio of NLRP3 protein levels in the contralateral V1 to those in the ipsilateral V1 (C/I) was significantly higher 1 day after ONC than in the sham group and further increased on day 3. Then, a substantial decrease in the ratio occurred on day 7 but was still significantly higher than that in the sham mice (Fig. 1D). Taken together, these results suggest that the pronounced activation of NLRP3 in the contralateral V1 acts as a response to ONC.

### NLRP3 is Upregulated in Contralateral V1 Neurons Following Optic Nerve Crush

In rodent species, > 95% of the axons of retinal ganglion cells decussate at the chiasma and project to the contralateral recipient nuclei [32]. qRT-PCR and Western blot demonstrated that the increased expression of NLRP3 induced by ONC was prominent in contralateral V1. To determine whether the upregulated NLRP3 was located within the neurons of V1, we performed double immunolabeling using NLRP3 and neuronal nuclei (NeuN) antibodies. NLRP3 expression was hardly detectable in neurons in both the naïve (data not shown) and sham groups, while a significant increase in NLRP3-positive staining was observed in the neurons 1 day after ONC (Fig. 2A). A schematic overview of the regions of interest used for quantification in contralateral V1 is shown in Fig. 2B. The number of NeuN+NLRP3+ double stained cells was significantly higher and was approximately 13.4-fold greater than that of the sham group on day 3. A

notable decrease in double-positive cells occurred 7 days after ONC (Fig. 2A, C).

We next calculated the ratios of NeuN+NLRP3+ *versus* total NeuN+ neurons in the contralateral V1 of the ONC and sham-treated mice. The ratio was significantly higher on day 1 in the ONC than in the sham groups and reached a peak on day 3, when the maximum number of NeuN+NLRP3+ double-positive cells occurred. The ratio was significantly lower on day 7 due to the decreased number of double-positive neurons (Fig. 2D), and remained significantly higher than the sham group on day 14 (Fig. 2D). These results demonstrate that NLRP3 in the contralateral V1 neurons is upregulated in response to ONC within 14 days.

### NLRP3 Inflammasome Components ASC, Caspase-1 (p20), and GSDMD are Activated After ONC

Since NLRP3 was upregulated mainly in the contralateral V1, we next asked whether the increased NLRP3 mediated

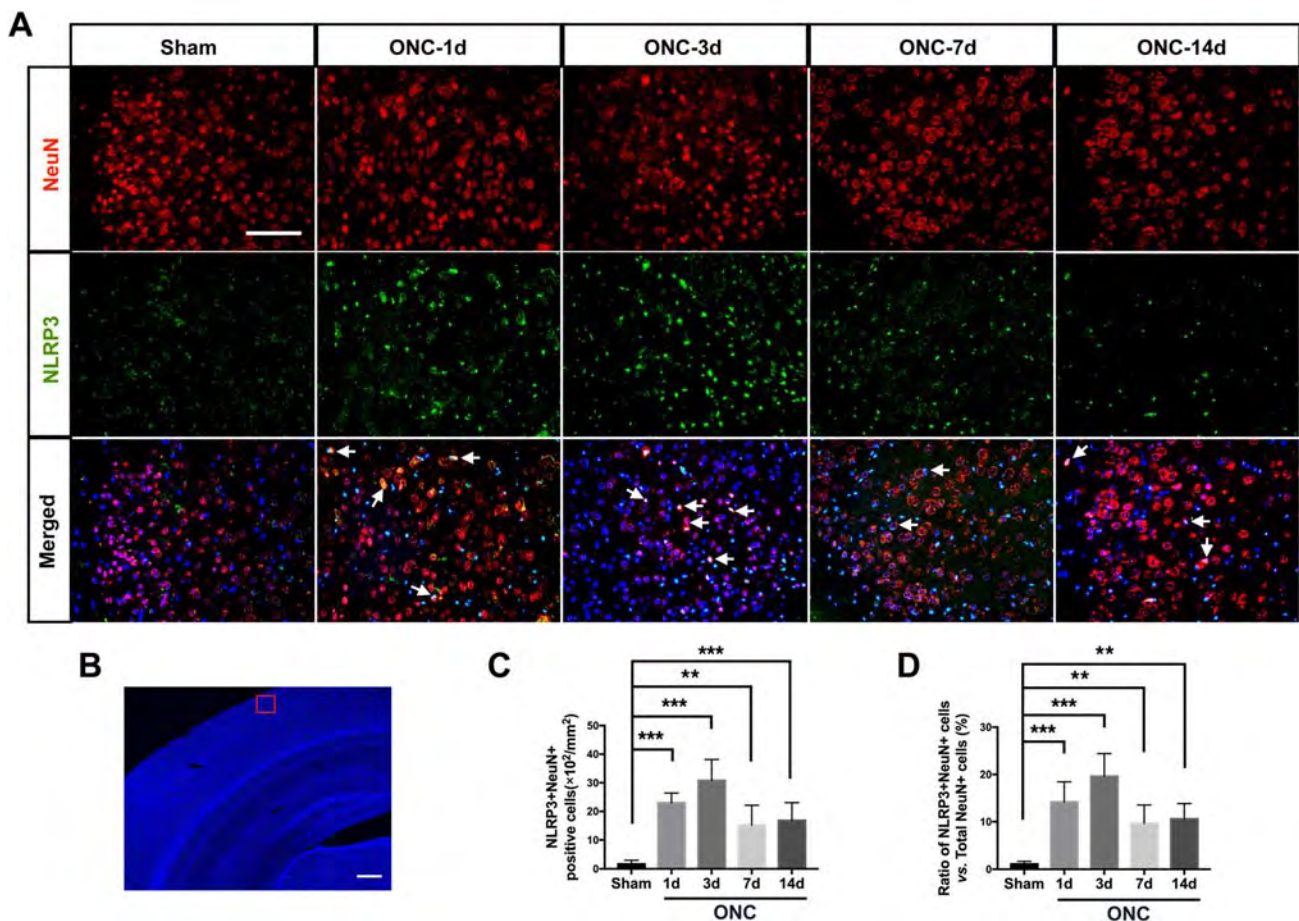


**Fig. 2** NLRP3 is activated in neurons of contralateral V1 1 day after ONC. **A** Double immunostaining for NeuN (red) and NLRP3 (green) in contralateral V1. Nuclear counterstaining by DAPI in merged images is pseudocolored in dark blue. Arrows indicate NeuN+NLRP3+ cells. Scale bar, 100  $\mu\text{m}$ . **B** Region of interest for

quantification in contralateral V1. Scale bar, 500  $\mu\text{m}$ . **C** Quantification of NeuN+NLRP3+ cells. **D** Ratio of NeuN+NLRP3+ to total NeuN+ neurons. Data are presented as the mean  $\pm$  SEM.  $**P < 0.01$ ,  $***P < 0.001$  vs sham group,  $n = 6$ .

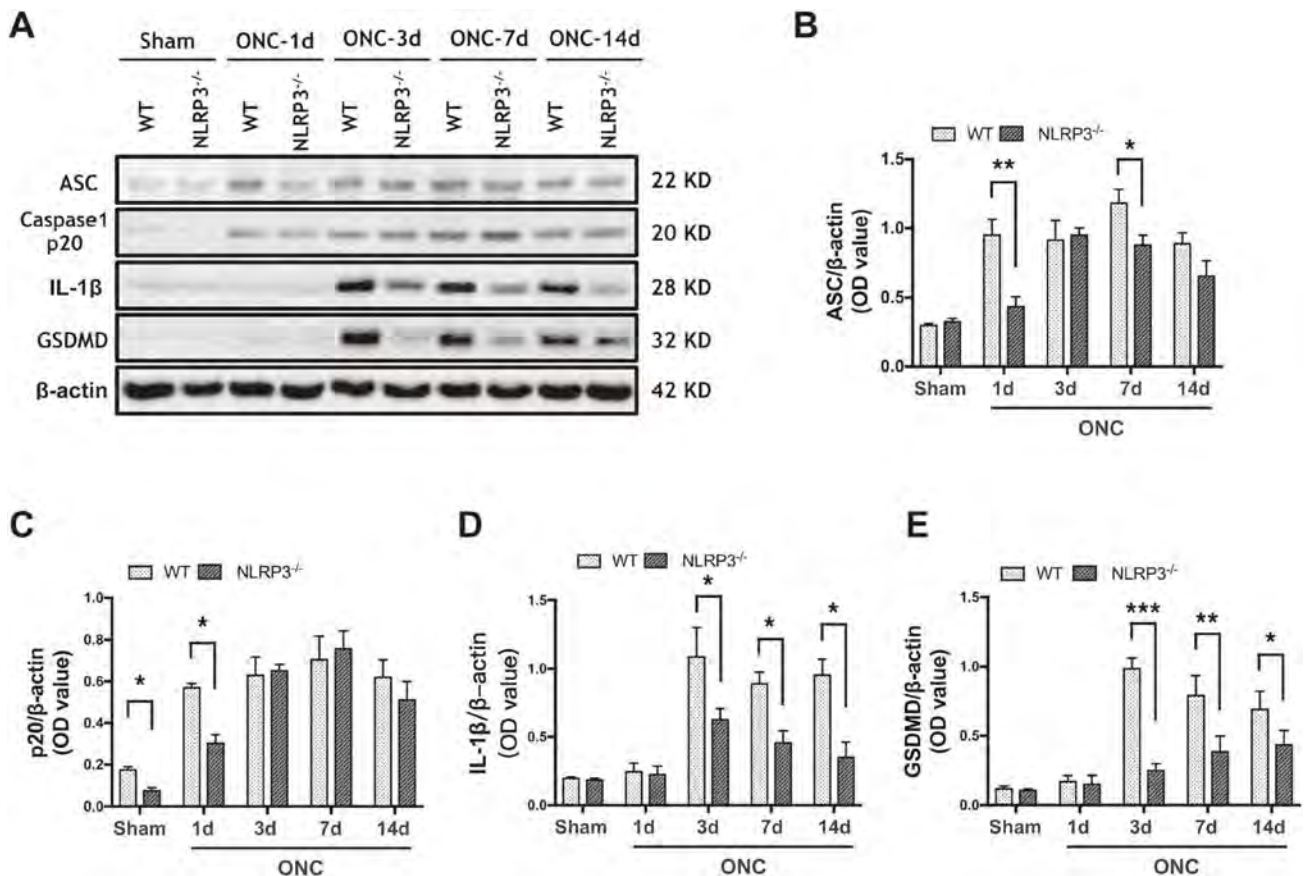


**Fig. 3** The expression levels of ASC, caspase-1 (p20), IL-1 $\beta$ , and cleaved GSDMD in the contralateral V1 of wild type (WT) mice and NLRP3<sup>-/-</sup> mice change following ONC. **A** Western blots showing the protein levels in contralateral V1.  $\beta$ -actin served as loading control.

**B–E** Quantification of the changes in protein levels of ASC, caspase-1 (p20), IL-1 $\beta$ , and cleaved GSDMD. Data are presented as the mean  $\pm$  SEM. \* $P < 0.05$ , \*\* $P < 0.01$ , \*\*\* $P < 0.001$ ,  $n = 4$ .

the formation of inflammasomes in the same region. We examined the inflammasome components ASC and caspase-1 and downstream cytokines. In WT mice, the protein level of ASC was significantly upregulated in the contralateral V1 on day 1 and continued to increase in the period between 3 and 14 days, indicating the active assembly of NLRP3 inflammasomes in response to ONC (Fig. 3A, B). The increase of cleaved caspase-1 (p20) was evident 1 day after ONC, had progressively increased by days 3 and 7 (Fig. 3A, C), and was maintained up to day 14. No significant difference in the protein level of IL-1 $\beta$  in ONC mice and sham controls was found on day 1, then it significantly increased on day 3 and persisted on days 7 and 14 after ONC (Fig. 3A, D). However, in NLRP3<sup>-/-</sup> mice with ONC, the protein level of ASC was significantly lower than that in the WT group on days 1 and 7. No difference was found on day 3 due to the significantly increased protein level of ASC in the V1 of NLRP3<sup>-/-</sup> brains (Fig. 3A, B). The protein level of p20 in V1 of NLRP3<sup>-/-</sup> brains was significantly lower than that of WT 1 day after ONC; however, there was no significant difference

between the two genotypes over the rest of the experimental period (Fig. 3A, C). Although no significant difference occurred 1 day after ONC, the protein level of IL-1 $\beta$  in NLRP3<sup>-/-</sup> V1 was significantly lower than in WT littermates on days 3, 7, and 14 (Fig. 3A, D). We also found changes in the protein level of GSDMD, the dominant factor mediating pyroptosis, which is processed by cleaved caspase-1. In the V1 of WT brains, the expression of GSDMD was significantly upregulated on days 3, 7, and 14. As expected, the protein levels of GSDMD in V1 of NLRP3<sup>-/-</sup> brains were significantly lower than those of the WT group at each time point. Of note, a significant increase occurred in NLRP3<sup>-/-</sup> V1 14 days after ONC (Fig. 3A, E). These results suggest that the ONC-induced NLRP3 inflammasome activation partially contributes to the increases of caspase-1, IL-1 $\beta$ , and GSDMD in the contralateral V1. In addition, GSDMD-mediated pyroptosis may occur in the contralateral V1 after ONC.

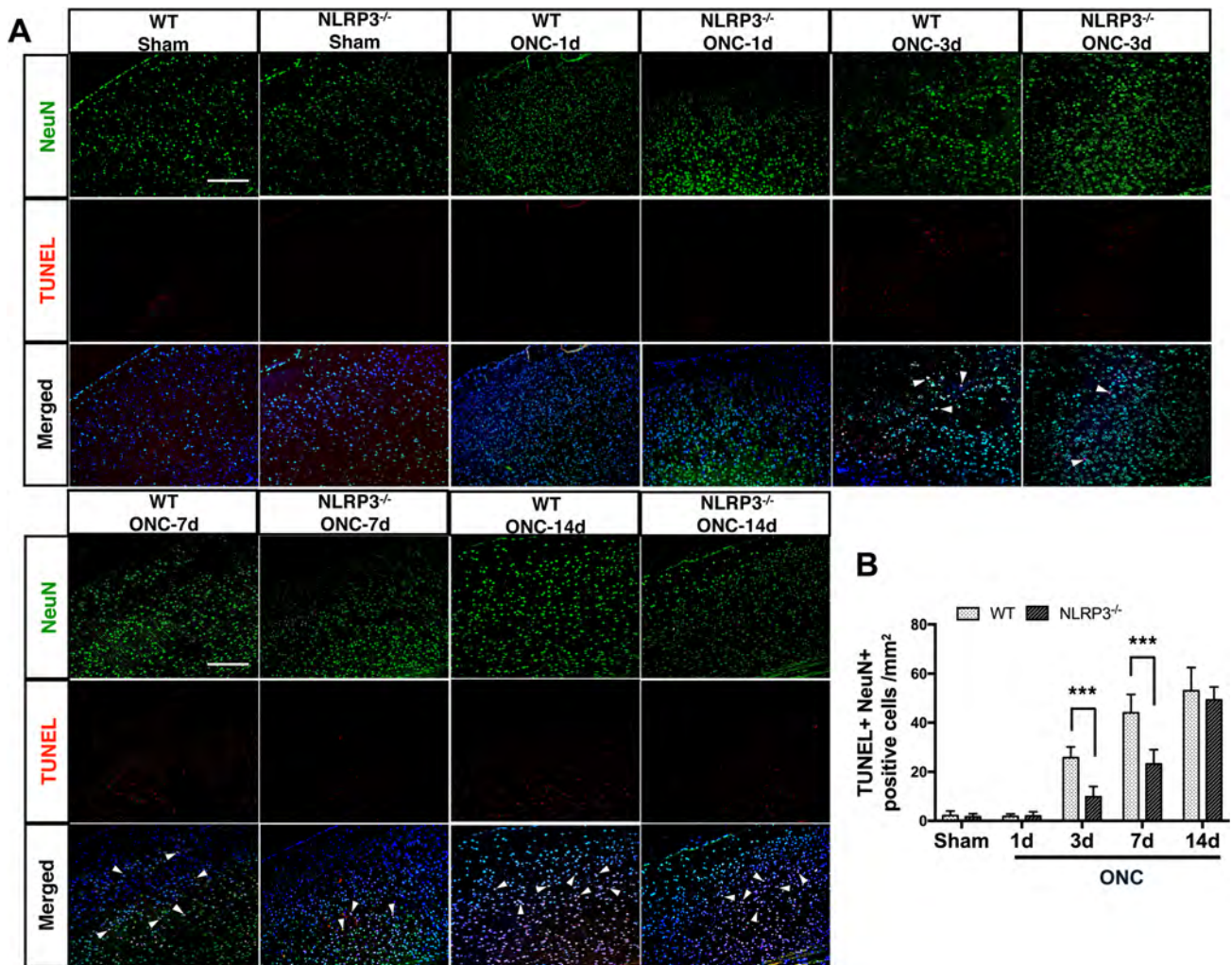


**Fig. 4** Apoptotic neurons in the contralateral V1 of WT and NLRP3<sup>-/-</sup> brains after ONC. **A** Double staining for TUNEL (red) and NeuN (green) in the contralateral V1. Nuclear counterstaining by DAPI in merged images is pseudocolored in dark blue. Arrowheads

indicate NeuN+TUNEL+ cells. Scale bars, 200  $\mu$ m. **B** Quantification of TUNEL+NeuN+ cells. Data are presented as the mean  $\pm$  SEM. \*\*\* $P < 0.001$ ,  $n = 6$ .

#### Ablation of NLRP3 Alleviates Apoptosis of Neurons in V1 Following ONC

Programmed cell death is known to play a major role in the spread of neurodegeneration [33]. As neuronal apoptosis in V1 has been reported after ON axotomy [3], we next determined the effect of NLRP3 deletion on neuronal apoptosis using TUNEL staining. The numbers of TUNEL+NeuN+ double-positive cells showed little difference in the contralateral V1 of both WT and NLRP3<sup>-/-</sup> brains 1 day after ONC compared to sham controls. In WT V1, the number of double-positive cells was significantly higher on day 3 than in NLRP3<sup>-/-</sup> mice and sham controls, and was further increased in the 7- to 14- day period. However, the differences in the number of double-positive cells between WT and NLRP3<sup>-/-</sup> were not significant on day 14 due to the substantial increase of TUNEL+NeuN+

cells in NLRP3<sup>-/-</sup> V1 (Fig. 4A, B). In other words, the results suggest that knocking out the NLRP3 gene delays ONC-induced neuronal apoptosis within 7 days.

#### Ablation of NLRP3 Delays Neuronal Degeneration in Contralateral V1 after ONC

Given that the ONC-induced trans-neuronal injury resulted not only in apoptosis but also in degeneration, to further determine the protective effect of NLRP3 depletion on the secondary degeneration in V1, we used FJC, an anionic fluorochrome, to selectively identify degenerating neurons [34]. The numbers of FJC-positive cells in the contralateral V1 of both WT and NLRP3<sup>-/-</sup> brains were not significantly higher than that in sham controls on day 1 (Fig. 5A). The number of FJC-positive cells in WT mice was significantly higher on day 3 than in sham-treated

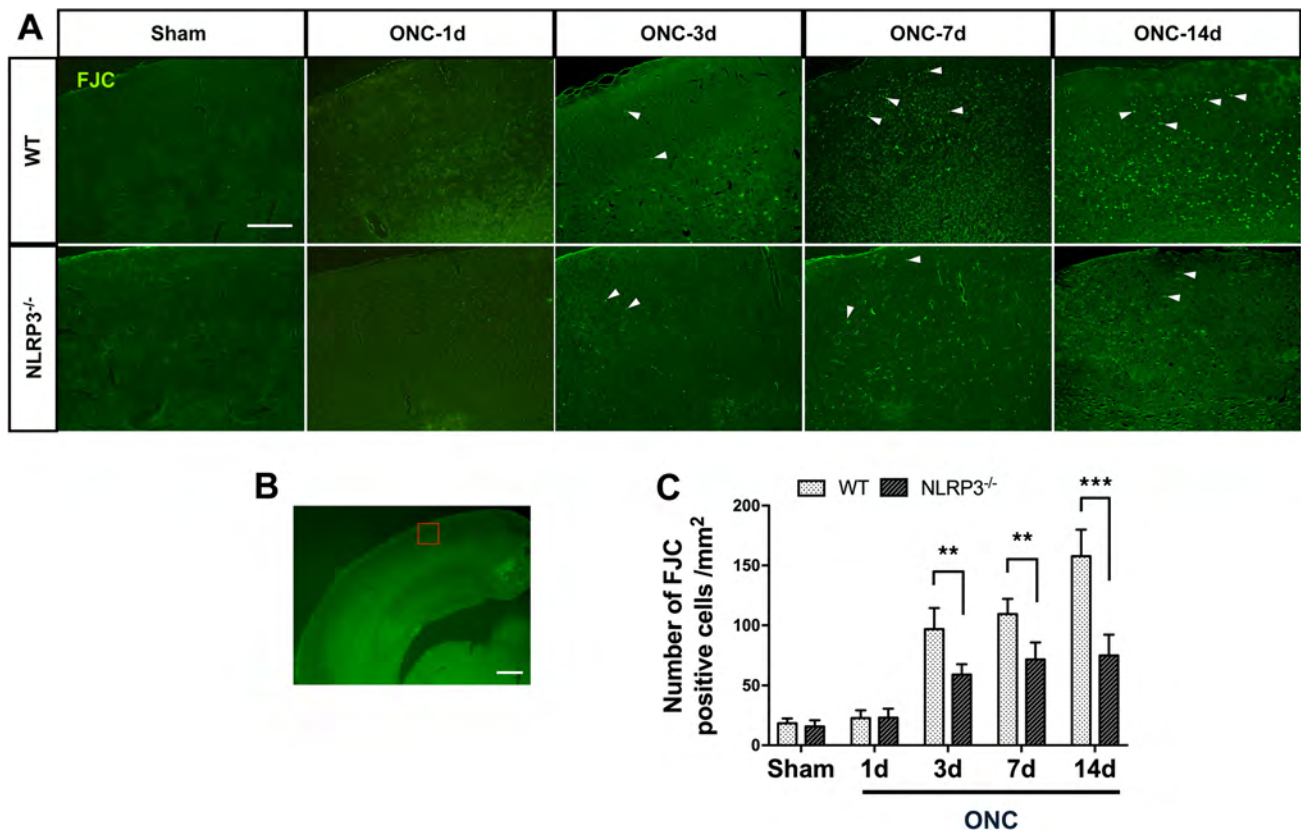


**Fig. 5** FJC staining of contralateral V1 in WT and NLRP3<sup>-/-</sup> mice after ONC. **A** Confocal images showing the differences in FJC staining between WT and NLRP3<sup>-/-</sup> mice. Scale bar, 200  $\mu$ m.

littermates and continued to increase through 7 and 14 days. As expected, the numbers of FJC-positive cells were significantly lower in V1 of NLRP3<sup>-/-</sup> brains than in WT littermates for the remainder of the observation period (Fig. 5A, C). A schematic overview of the regions of interest used for quantification in contralateral V1 is shown in Fig. 5B. The results suggest that a portion of neurons in the contralateral V1 undergo degeneration due to ONC, and ablation of NLRP3 delays the degeneration for at least 14 days.

#### Visual Function is Improved in NLRP3-Knockout Mice Following ONC

The results of TUNEL and FJC staining demonstrated that knocking out the NLRP3 gene plays a protective role in the apoptosis and degeneration of V1 neurons after crush injury. Next, we asked whether visual cortical function was also improved by ablation of NLRP3. F-VEPs were recorded to determine the differences in the visual electrophysiological function between WT and NLRP3<sup>-/-</sup> mice after ONC. The VEP P2 amplitudes were significantly lower in both WT and NLRP3<sup>-/-</sup> mice after ONC than in

**B** Region of interest used for quantification. Scale bar, 500  $\mu$ m. **C** Quantification of FJC-positive cells. Data are presented as the mean  $\pm$  SEM. \*\* $P$  < 0.01, \*\*\* $P$  < 0.001,  $n$  = 6.

sham controls. Notably, the VEP P2 waveform and amplitude from the contralateral hemisphere were significantly improved in the NLRP3<sup>-/-</sup> mice compared to the WT mice on 7 and 14 days (Fig. 6A, B), while the differences were barely detectable in the ipsilateral hemisphere in these mice (Fig. 6C), indicating that the visual cortical activity in contralateral hemisphere suffered more severely from ONC due to the decussation of axonal projection, and the mitigation effect of NLRP3 gene knockout within 14 days after ONC.

#### AIM2 Expression is Altered in Contralateral V1 in a Time-Dependent Manner Following ONC

Considering that the NLRP3 gene was globally knocked out in the animals used in this study, and the expression of ASC, caspase-1 (p20), and IL-1 $\beta$  was not substantially suppressed in V1 of the NLRP3<sup>-/-</sup> brain after ONC (Fig. 3C, D), we speculated that there is a compensatory effect of other inflammasomes that might be responsible for cytokine maturation. Therefore, we next determined whether other inflammasome analogues were activated in the contralateral V1 after crush injury, especially in the

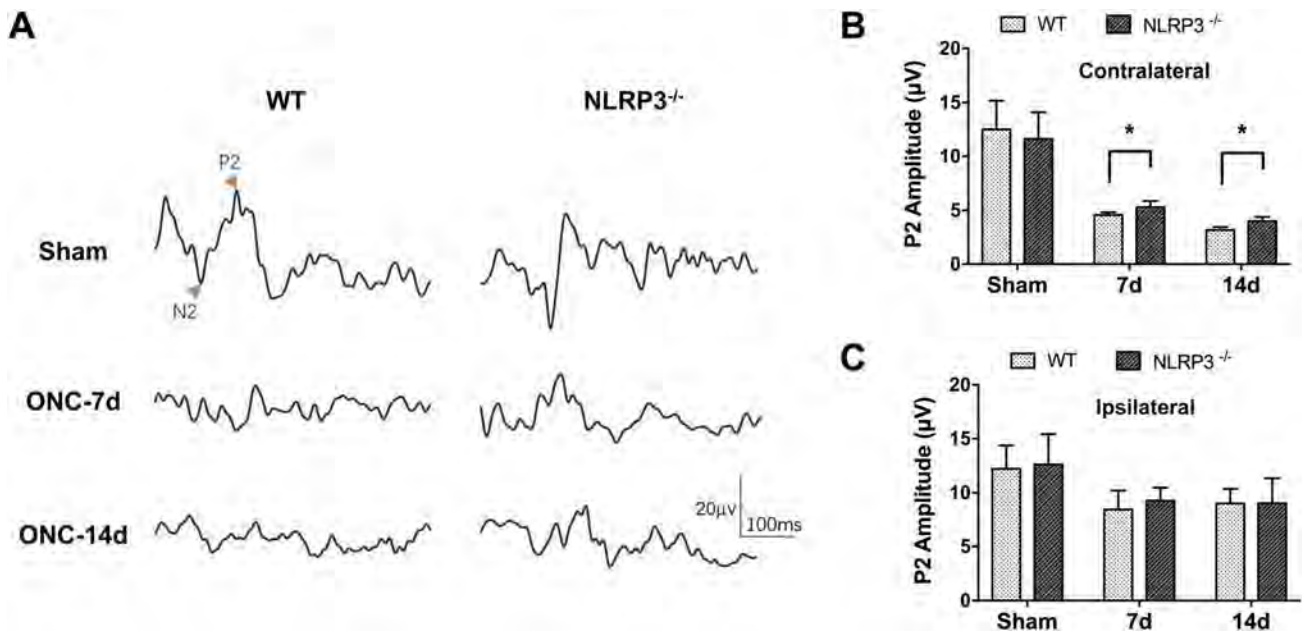


**Fig. 6** Ablation of NLRP3 mitigates the ONC-induced decrease in the VEP P2 amplitude. **A** Representative waveforms in the contralateral hemisphere (with respect to ONC) of WT and NLRP3<sup>-/-</sup> mice. **B**,

**C** Quantification of the VEP P2 amplitude in the contralateral (**B**) and ipsilateral hemispheres (**C**). Data are presented as the mean  $\pm$  SEM. \* $P < 0.05$ ,  $n = 6$  for sham groups and  $n = 8$  for ONC groups.

absence of NLRP3. The mRNA levels of AIM2, NLRP1, NLRP6, and NLRC4 were assessed by qRT-PCR. The results showed that the mRNA expression of AIM2 in the V1 of NLRP3<sup>-/-</sup> brains was significantly upregulated by  $\sim 5.9$ -fold ( $16.14 \pm 3.19$  vs  $2.79 \pm 0.13$ ) compared with WT littermates on day 7, and the difference remained significant through day 14. The mRNA level of NLRP1 was also significantly increased in NLRP3<sup>-/-</sup> V1 on days 7 and 14, as was that of NLRC4 on day 7, all compared to WT littermates. However, the changes in NLRP6 expression were hardly detectable over the observational period in both WT and NLRP3<sup>-/-</sup> mice (Fig. 7A).

Since the mRNA level of AIM2 increased dramatically in V1 of the NLRP3<sup>-/-</sup> brain after ONC, we speculated that AIM2 was a candidate for further study. We next determined whether the protein level of AIM2 was also prominent in the V1 of the NLRP3<sup>-/-</sup> brain. Western blots revealed that the protein level of AIM2 was significantly upregulated 3 days after crush injury in both WT and NLRP3<sup>-/-</sup> mice, while the level was significantly higher in the V1 of NLRP3<sup>-/-</sup> brains than in WT littermates on day 14 (Fig. 7B, C). These findings suggest that AIM2 is activated in V1 after ONC and that its significant upregulation in NLRP3<sup>-/-</sup> V1 may account for the compensatory effect on inflammatory cytokine maturation.

## Discussion

The spread of neuronal degeneration, such as delayed secondary damage, occurs in distal brain regions that are anatomically connected to the proximal site of the initial infarction by axonal projections [35]. In the field of neuro-ophthalmology, prior to vision loss at the end stage, dysfunctionality of the distal regions in the visual pathway has been reported in the early or progressive stage of glaucoma and ocular trauma [36–38]. For instance, ocular hypertension undermines synaptic connections and induces progressive thinning of the visual cortex [39, 40]. So more comprehensive neurological examinations and visual functional analyses of the visual cortex have been recommended [41–44], and treatment should not be limited to rescue of the optic nerve and the alleviation of ocular hypertension but should also include protection of the distal related brain regions in the early stage. Therefore, it is urgent to seek effective therapies to meet this clinical need.

In the current study, ONC triggered upregulation of NLRP3 in contralateral V1, together with activated NLRP3 inflammasome components, indicating the immediate response of this canonic inflammasome in visual cortex spatially separated from the site of the initial lesion. Meanwhile, co-localization of NLRP3 and NeuN suggests that NLRP3 can be activated in visual cortical neurons upon ONC. Depletion of NLRP3 attenuated the apoptosis and degeneration of V1 neurons susceptible to ONC within

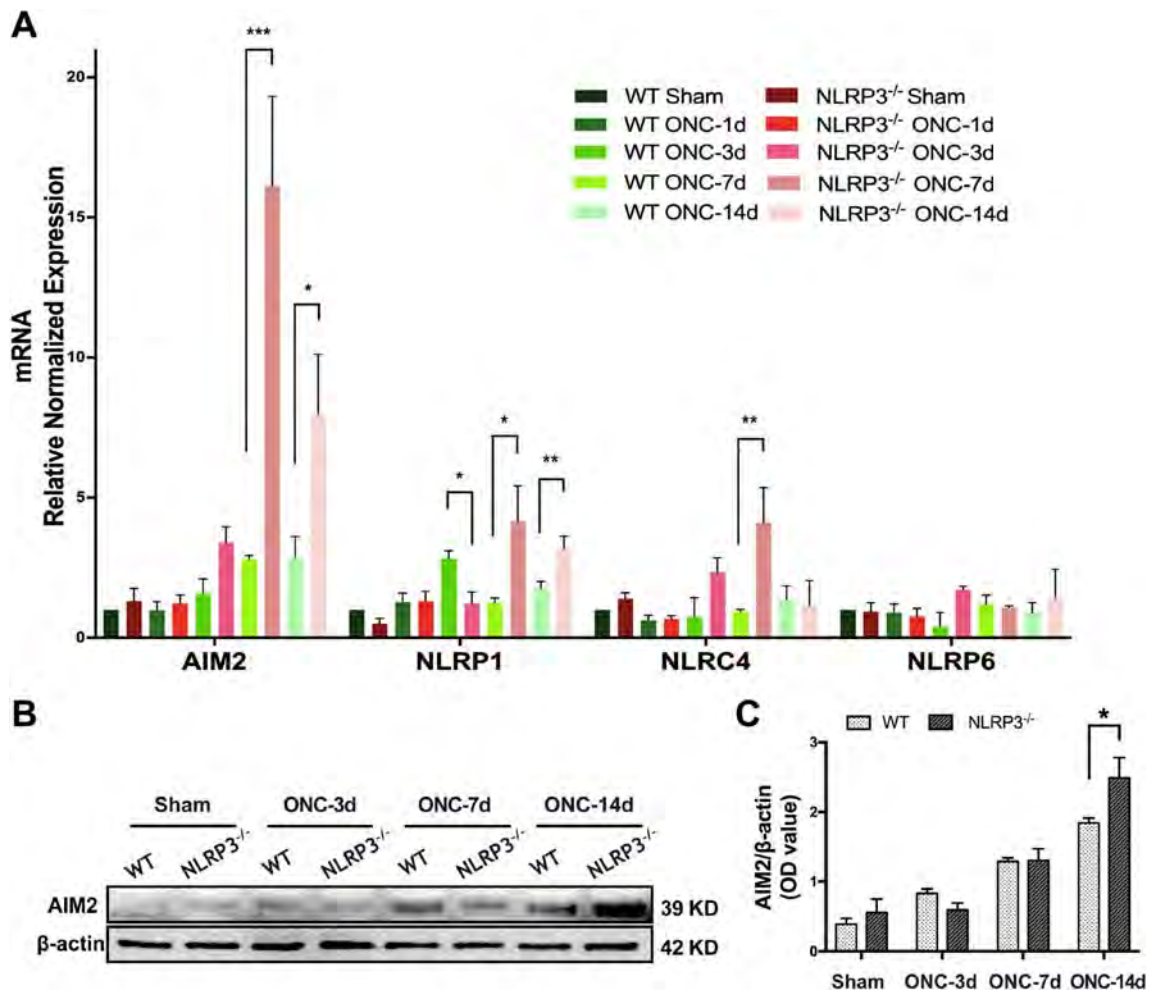


**Fig. 7** The expression levels of AIM2, NLRP1, NLRC4, and NLRP6 are altered in contralateral V1 after ONC. **A** qRT-PCR results of the mRNA levels of AIM2, NLRP1, NLRC4, and NLRP6 in the contralateral V1 of WT and NLRP3<sup>-/-</sup> mice. **B** Western blots showing

the expression of AIM2 in the contralateral V1 of WT and NLRP3<sup>-/-</sup> mice. **C** Quantification of the protein levels of AIM2. Data are presented as the mean ± SEM. \**P* < 0.05, *n* = 5.

7 days. The index of visual electrophysiology was also improved in NLRP3 gene-knockout mice. To our knowledge, this is the first evidence of NLRP3 activation in the visual cortex and its implications in anterograde neurodegeneration.

The receptor molecules that sense exogenous threats or endogenous stress, such as pathogen-associated molecular patterns and DAMPs, recruit scaffold partners (ASCs) and lead to the assembly of inflammasomes. The inflammasome family has > 20 members [45, 46], among which the NLRP3 inflammasome is the best characterized because of its activation by diverse stimuli and its extensive participation in a variety of immunoresponsive processes, especially sterile inflammation [47]. Involvement of the NLRP3 inflammasome in the secondary insults of traumatic brain injury [48], intracerebral hemorrhage [49], and cerebral ischemia [50] has been well documented, suggesting that NLRP3 can be activated trans-neuronally due

to its high sensitivity. On the other hand, cortical neurons are ‘blinded’ by the interruption of input after ON injury. Taken together, we speculated that the direct and immediate response possibly occurs in the visual cortical neurons.

Along with NLRP3 activation, neurons in the primary visual cortex were compromised in our findings. There is a possibility that some form of ‘damage initiators’ are delivered trans-synaptically *via* the visual pathway. Whether NLRP3 itself is a form of ‘transmitter’ or is activated by other stimuli, such as high-mobility group box 1 (HMGB1) [51], reactive oxygen species (ROS) [52], and DAMPs [53], remains unclear. In addition, the current study did not exclude the activation of NLRP3 in microglia and astrocytes, which may also contribute to anterograde degeneration. Future work is needed on the NLRP3 triggering mechanism and the combined effect of NLRP3 activation in neurons and glia in this type of trans-neuronal

injury. Moreover, in primate species, ~ 40% of retinal ganglion cell axons decussate to the contralateral side at the chiasma and terminate in layers I, IV, and VI of the lateral geniculate nucleus before projecting to the visual cortex [32]. This poses a more complicated scenario in terms of anterograde degeneration that we cannot thoroughly investigate in rodent models.

Interestingly, the activated NLRP3 inflammasome was not fully responsible for the maturation of caspase-1 (p20) and IL-1 $\beta$  after ONC because paradoxically increased expression of ASC and p20 occurred in NLRP3<sup>-/-</sup> mice at specific time points. Therefore, we hypothesize that a compensatory mechanism of other inflammatory mediators exists. Like NLRP3, AIM2, NLRP1, NLRP6, and NLRC4 are also mediators of the inflammatory response through inflammasome formation. Previous studies have elucidated their effects in CNS disorders, especially in CNS injury [54–57]. Strikingly, AIM2, a member of the hemopoietic IFN-inducible nuclear 200 family [58], which is activated by viral, bacterial, and host ectopic dsDNA, was significantly upregulated in the contralateral V1 of the NLRP3<sup>-/-</sup> brain after ONC. Our studies are now focusing on the interaction and synergistic effect of NLRP3 and AIM2 in secondary neuronal degeneration.

In conclusion, our findings demonstrate that the activation of NLRP3 is responsible for the anterograde degeneration of visual cortical neurons after ONC. Inhibition of NLRP3, especially in the early stage, might be a potential method of neuroprotection.

**Acknowledgements** We would like to thank Prof. Yuan-Guo Zhou from the Army Medical Center of the People's Liberation Army and Prof. Feng Mei from the Army Medical University (AMU) for project consultation and data evaluation, and thank Prof. Bo Peng from Shenzhen Institutes of Advanced Technology, Chinese Academy of Sciences, for technical support. This work was supported by the National Natural Science Foundation of China (81570840 and 81200926), the Academician-Led Science and Technological Innovation of Chongqing (cstc2017jcyj-yszxX0006), and the Research Foundation of the Department of Ophthalmology in Daping Hospital, AMU (9-2543).

**Conflict of interest** The authors claim that there are no conflicts of interest.

## References

- Shou TD. Visual functional changes during acute elevation of intraocular pressure. *Neurosci Bull* 2006, 22: 235–238.
- You Y, Gupta VK, Graham SL, Klistorner A. Anterograde degeneration along the visual pathway after optic nerve injury. *PLoS One* 2012, 7: e52061.
- Smith NM, Giacci MK, Gough A, Bailey C, McGonigle T, Black AMB, *et al.* Inflammation and blood-brain barrier breach remote from the primary injury following neurotrauma. *J Neuroinflamm* 2018, 15: 201.
- Dengler-Criss CM, Smith MA, Inman DM, Wilson GN, Young JW, Criss SD. Anterograde transport blockade precedes deficits in retrograde transport in the visual projection of the DBA/2J mouse model of glaucoma. *Front Neurosci* 2014, 8: 290.
- David S, Kroner A. Repertoire of microglial and macrophage responses after spinal cord injury. *Nat Rev Neurosci* 2011, 12: 388–399.
- Bourgeois C, Kuchler K. Fungal pathogens—a sweet and sour treat for toll-like receptors. *Front Cell Infect Microbiol* 2012, 2: 142.
- Martinon F, Burns K, Tschopp J. The inflammasome: a molecular platform triggering activation of inflammatory caspases and processing of proIL-beta. *Mol Cell* 2002, 10: 417–426.
- Latz E, Xiao TS, Stutz A. Activation and regulation of the inflammasomes. *Nat Rev Immunol* 2013, 13: 397–411.
- Vladimer GI, Marty-Roix R, Ghosh S, Weng D, Lien E. Inflammasomes and host defenses against bacterial infections. *Curr Opin Microbiol* 2013, 16: 23–31.
- Abulafia DP, de Rivero Vaccari JP, Lozano JD, Lotocki G, Keane RW, Dietrich WD. Inhibition of the inflammasome complex reduces the inflammatory response after thromboembolic stroke in mice. *J Cereb Blood Flow Metab* 2009, 29: 534–544.
- Shi J, Zhao Y, Wang K, Shi X, Wang Y, Huang H, *et al.* Cleavage of GSDMD by inflammatory caspases determines pyroptotic cell death. *Nature* 2015, 526: 660–665.
- Halle A, Hornung V, Petzold GC, Stewart CR, Monks BG, Reinheckel T, *et al.* The NALP3 inflammasome is involved in the innate immune response to amyloid-beta. *Nat Immunol* 2008, 9: 857–865.
- Liu SB, Mi WL, Wang YQ. Research progress on the NLRP3 inflammasome and its role in the central nervous system. *Neurosci Bull* 2013, 29: 779–787.
- Carlos D, Costa FR, Pereira CA, Rocha FA, Yaochite JN, Oliveira GG, *et al.* Mitochondrial DNA activates the NLRP3 inflammasome and predisposes to type 1 diabetes in murine model. *Front Immunol* 2017, 8: 164.
- Lee J, Wan J, Lee L, Peng C, Xie H, Lee C. Study of the NLRP3 inflammasome component genes and downstream cytokines in patients with type 2 diabetes mellitus with carotid atherosclerosis. *Lipids Health Dis* 2017, 16: 217.
- Lu A, Li H, Niu J, Wu S, Xue G, Yao X, *et al.* Hyperactivation of the NLRP3 inflammasome in myeloid cells leads to severe organ damage in experimental lupus. *J Immunol* 2017, 198: 1119–1129.
- Inoue M, Chen PH, Siecinski S, Li QJ, Liu C, Steinman L, *et al.* An interferon-beta-resistant and NLRP3 inflammasome-independent subtype of EAE with neuronal damage. *Nat Neurosci* 2016, 19: 1599–1609.
- Ma MW, Wang J, Dhandapani KM, Brann DW. NADPH oxidase 2 regulates NLRP3 inflammasome activation in the brain after traumatic brain injury. *Oxid Med Cell Longev* 2017, 2017: 6057609.
- Lee SW, de Rivero Vaccari JP, Truettner JS, Dietrich WD, Keane RW. The role of microglial inflammasome activation in pyroptotic cell death following penetrating traumatic brain injury. *J Neuroinflamm* 2019, 16: 27.
- de Rivero Vaccari JP, Lotocki G, Marcillo AE, Dietrich WD, Keane RW. A molecular platform in neurons regulates inflammation after spinal cord injury. *J Neurosci* 2008, 28: 3404–3414.
- Albalawi F, Lu W, Beckel JM, Lim JC, McCaughey SA, Mitchell CH. The P2X7 receptor primes IL-1beta and the NLRP3 inflammasome in astrocytes exposed to mechanical strain. *Front Cell Neurosci* 2017, 11: 227.
- Puyang Z, Feng L, Chen H, Liang P, Troy JB, Liu X. Retinal ganglion cell loss is delayed following optic nerve crush in NLRP3 knockout mice. *Sci Rep* 2016, 6: 20998.

23. Xu Z, Fouda AY, Lemtalsi T, Shosha E, Rojas M, Liu F, *et al.* Retinal neuroprotection from optic nerve trauma by deletion of arginase 2. *Front Neurosci* 2018, 12: 970.
24. Zou J, Crews FT. Inflammasome-IL-1beta signaling mediates ethanol inhibition of hippocampal neurogenesis. *Front Neurosci* 2012, 6: 77.
25. Chen P, He L, Pang X, Wang X, Yang T, Wu H. NLRP3 is expressed in the spiral ganglion neurons and associated with both syndromic and nonsyndromic sensorineural deafness. *Neural Plast* 2016, 2016: 3018132.
26. Fann DY, Lim YA, Cheng YL, Lok KZ, Chunduri P, Baik SH, *et al.* Evidence that NF-kappaB and MAPK signaling promotes NLRP inflammasome activation in neurons following ischemic stroke. *Mol Neurobiol* 2018, 55: 1082–1096.
27. von Herrmann KM, Salas LA, Martinez EM, Young AL, Howard JM, Feldman MS, *et al.* NLRP3 expression in mesencephalic neurons and characterization of a rare NLRP3 polymorphism associated with decreased risk of Parkinson's disease. *NPJ Parkinsons Dis* 2018, 4: 24.
28. Lin S, Liang Y, Zhang J, Bian C, Zhou H, Guo Q, *et al.* Microglial TIR-domain-containing adapter-inducing interferon-beta (TRIF) deficiency promotes retinal ganglion cell survival and axon regeneration via nuclear factor-kappaB. *J Neuroinflamm* 2012, 9: 39.
29. Zhou JX, Liu YJ, Chen X, Zhang X, Xu J, Yang K, *et al.* Low-intensity pulsed ultrasound protects retinal ganglion cell from optic nerve injury induced apoptosis via Yes associated protein. *Front Cell Neurosci* 2018, 12: 160.
30. Ismael S, Nasoohi S, Ishrat T. MCC950, the selective inhibitor of nucleotide oligomerization domain-like receptor protein-3 inflammasome, protects mice against traumatic brain injury. *J Neurotrauma* 2018, 35: 1294–1303.
31. Ye X, Shen T, Hu J, Zhang L, Zhang Y, Bao L, *et al.* Purinergic 2X7 receptor/NLRP3 pathway triggers neuronal apoptosis after ischemic stroke in the mouse. *Exp Neurol* 2017, 292: 46–55.
32. Leamey CA PD, Dreher B. Comparative survey of the mammalian visual system with reference to the mouse. In: Chalupa, Williams RW (Eds). *Eye, Retina, and Visual System of the Mouse*. MIT Press, 2008: 35–60.
33. Cusack CL, Swaheri V, Hampton Henley W, Michael Ramsey J, Deshmukh M. Distinct pathways mediate axon degeneration during apoptosis and axon-specific pruning. *Nat Commun* 2013, 4: 1876.
34. Schmued L. Fluoro-Jade C results in ultra high resolution and contrast labeling of degenerating neurons. *Brain Res* 2005, 1035: 24–31.
35. Block F, Dihne M, Loos M. Inflammation in areas of remote changes following focal brain lesion. *Prog Neurobiol* 2005, 75: 342–365.
36. Lawlor M, Danesh-Meyer H, Levin LA, Davagnanam I, De Vita E, Plant GT. Glaucoma and the brain: Trans-synaptic degeneration, structural change, and implications for neuroprotection. *Surv Ophthalmol* 2018, 63: 296–306.
37. Lam DY, Kaufman PL, Gabelt BT, To EC, Matsubara JA. Neurochemical correlates of cortical plasticity after unilateral elevated intraocular pressure in a primate model of glaucoma. *Invest Ophthalmol Vis Sci* 2003, 44: 2573–2581.
38. Vasalauskaite A, Morgan JE, Sengpiel F. Plasticity in adult mouse visual cortex following optic nerve injury. *Cereb Cortex* 2019, 29: 1767–1777.
39. Dekeyster E, Aerts J, Valiente-Soriano FJ, De Groef L, Vreysen S, Salinas-Navarro M, *et al.* Ocular hypertension results in retinotopic alterations in the visual cortex of adult mice. *Curr Eye Res.* 2015, 40: 1269–1283.
40. Yu L, Xie L, Dai C, Xie B, Liang M, Zhao L, *et al.* Progressive thinning of visual cortex in primary open-angle glaucoma of varying severity. *PLoS One* 2015, 10: e0121960.
41. Lindsey JD, Scadeng M, Dubowitz DJ, Crowston JG, Weinreb RN. Magnetic resonance imaging of the visual system in vivo: transsynaptic illumination of V1 and V2 visual cortex. *Neuroimage* 2007, 34: 1619–1626.
42. Chan KC, So KF, Wu EX. Proton magnetic resonance spectroscopy revealed choline reduction in the visual cortex in an experimental model of chronic glaucoma. *Exp Eye Res* 2009, 88: 65–70.
43. Li X, Li X. The antidepressant effect of light therapy from retinal projections. *Neurosci Bull* 2018, 34: 359–368.
44. Duan J, Fu H, Zhang J. Activation of parvalbumin-positive neurons in both retina and primary visual cortex improves the feature-selectivity of primary visual cortex neurons. *Neurosci Bull* 2017, 33: 255–263.
45. de Zoete MR, Palm NW, Zhu S, Flavell RA. Inflammasomes. *Cold Spring Harb Perspect Biol* 2014, 6: a016287.
46. Janowski AM, Sutterwala FS. Atypical inflammasomes. *Methods Mol Biol* 2016, 1417: 45–62.
47. Freeman L, Guo H, David CN, Brickey WJ, Jha S, Ting JP. NLR members NLRC4 and NLRP3 mediate sterile inflammasome activation in microglia and astrocytes. *J Exp Med* 2017, 214: 1351–1370.
48. Irrera N, Pizzino G, Calo M, Pallio G, Mannino F, Fama F, *et al.* Lack of the Nlrp3 inflammasome improves mice recovery following traumatic brain injury. *Front Pharmacol* 2017, 8: 459.
49. Ma Q, Chen S, Hu Q, Feng H, Zhang JH, Tang J. NLRP3 inflammasome contributes to inflammation after intracerebral hemorrhage. *Ann Neurol* 2014, 75: 209–219.
50. Tong Y, Ding ZH, Zhan FX, Cai L, Yin X, Ling JL, *et al.* The NLRP3 inflammasome and stroke. *Int J Clin Exp Med* 2015, 8: 4787–4794.
51. Frank MG, Weber MD, Fonken LK, Hershman SA, Watkins LR, Maier SF. The redox state of the alarmin HMGB1 is a pivotal factor in neuroinflammatory and microglial priming: A role for the NLRP3 inflammasome. *Brain Behav Immun* 2016, 55: 215–224.
52. Minutoli L, Puzzolo D, Rinaldi M, Irrera N, Marini H, Arcoraci V, *et al.* ROS-mediated NLRP3 inflammasome activation in brain, heart, kidney, and testis ischemia/reperfusion injury. *Oxid Med Cell Longev* 2016, 2016: 2183026.
53. Rubartelli A. DAMP-mediated activation of NLRP3-inflammasome in brain sterile inflammation: the fine line between healing and neurodegeneration. *Front Immunol* 2014, 5: 99.
54. Kaushal V, Dye R, Pakavathkumar P, Foveau B, Flores J, Hyman B, *et al.* Neuronal NLRP1 inflammasome activation of Caspase-1 coordinately regulates inflammatory interleukin-1-beta production and axonal degeneration-associated Caspase-6 activation. *Cell Death Differ* 2015, 22: 1676–1686.
55. Wang PF, Li ZG, Zhang Y, Ju XH, Liu XW, Zhou AM, *et al.* NLRP6 inflammasome ameliorates brain injury after intracerebral hemorrhage. *Front Cell Neurosci* 2017, 11: 206.
56. Adamczak SE, de Rivero Vaccari JP, Dale G, Brand FJ, 3rd, Nonner D, Bullock MR, *et al.* Pyroptotic neuronal cell death mediated by the AIM2 inflammasome. *J Cereb Blood Flow Metab* 2014, 34: 621–629.
57. Denes A, Coutts G, Lenart N, Cruickshank SM, Pelegrin P, Skinner J, *et al.* AIM2 and NLRC4 inflammasomes contribute with ASC to acute brain injury independently of NLRP3. *Proc Natl Acad Sci U S A* 2015, 112: 4050–4055.
58. Fernandes-Alnemri T, Yu JW, Datta P, Wu J, Alnemri ES. AIM2 activates the inflammasome and cell death in response to cytoplasmic DNA. *Nature* 2009, 458: 509–513.



# Propofol Attenuates $\alpha$ -Synuclein Aggregation and Neuronal Damage in a Mouse Model of Ischemic Stroke

Yuzhu Wang<sup>1,2</sup> · Dan Tian<sup>2</sup> · Changwei Wei<sup>1</sup> · Victoria Cui<sup>3</sup> · Huan Wang<sup>2</sup> · Yanbing Zhu<sup>2</sup> · Anshi Wu<sup>1</sup> · Yun Yue<sup>1</sup>

Received: 26 February 2019 / Accepted: 3 June 2019 / Published online: 13 September 2019  
© Shanghai Institutes for Biological Sciences, CAS 2019

**Abstract**  $\alpha$ -Synuclein is a soluble monomer abundant in the central nervous system. Aggregates of  $\alpha$ -synuclein, consisting of higher-level oligomers and insoluble fibrils, have been observed in many chronic neurological diseases and are implicated in neurotoxicity and neurodegeneration.  $\alpha$ -Synuclein has recently been shown to aggregate following acute ischemic stroke, exacerbating neuronal damage. Propofol is an intravenous anesthetic that is commonly used during intravascular embolectomy following acute ischemic stroke. While propofol has demonstrated neuroprotective properties following brain injury, the mechanism of protection in the setting of ischemic stroke is unclear. In this study, propofol administration significantly reduced the neurotoxic aggregation of  $\alpha$ -synuclein, decreased the infarct area, and attenuated the neurological deficits after ischemic stroke in a mouse model. We then demonstrated that the propofol-induced reduction of  $\alpha$ -synuclein aggregation was associated with increased mammalian target of

rapamycin/ribosomal protein S6 kinase beta-1 signaling pathway activity and reduction of the excessive autophagy occurring after acute ischemic stroke.

**Keywords** Propofol ·  $\alpha$ -Synuclein · Autophagy · Stroke · Neuroprotection

## Introduction

$\alpha$ -Synuclein is a 14-kDa protein encoded by the *Snc*a gene, which is highly conserved among vertebrates. Making up as much as 1% of all proteins in the cytosol of neurons,  $\alpha$ -synuclein is found mainly in the presynaptic terminals [1–3].  $\alpha$ -Synuclein can transit between several different conformations, including soluble monomers (14 kDa), oligomers and higher-level oligomers (26–180 kDa), and insoluble fibrils (> 180 kDa) [4, 5]. *In vivo*,  $\alpha$ -synuclein likely exists in monomeric form and as a helically-folded tetramer which may confer resistance to pathologic aggregation [6].

The association between chronic diseases of the central nervous system, including Parkinson's disease and Alzheimer's disease, and the presence of  $\alpha$ -synuclein aggregates is well known [5, 9]. However, the role of  $\alpha$ -synuclein in acute injury of the brain has been little studied.  $\alpha$ -Synuclein aggregates, consisting of higher-level oligomers and insoluble fibrils, are thought to have neurotoxic properties and are implicated in severe neuronal loss and the eventual development of neurological deficits [7, 8].  $\alpha$ -Synuclein interacts specifically with proteins involved in the regulation of oxidative phosphorylation and mitochondrial function, and its oligomers increase the level of oxidative stress in neurons [10, 11]. The overexpression of *Snc*a and increased production of  $\alpha$ -synuclein have been

Yuzhu Wang and Dan Tian have contributed equally to this work.

**Electronic supplementary material** The online version of this article (<https://doi.org/10.1007/s12264-019-00426-0>) contains supplementary material, which is available to authorized users.

✉ Anshi Wu  
wuanshi88@163.com

✉ Yun Yue  
yueyun@hotmail.com

<sup>1</sup> Department of Anesthesiology, Beijing Chaoyang Hospital, Capital Medical University, Beijing 100020, China

<sup>2</sup> Experimental and Translational Research Center, Beijing Friendship Hospital, Capital Medical University, Beijing 100050, China

<sup>3</sup> Washington University School of Medicine, St. Louis, MI, USA

shown to exacerbate autophagy following ischemic stroke [12, 13]. While both oxidative phosphorylation and autophagy are vital physiological processes, they prove detrimental at high levels following acute ischemic brain injury [14, 15].

Propofol (2,6-disopropylphenol) is the most commonly used intravenous general anesthetic in emergency procedures. Studies have suggested that propofol administration reduces the infarct size and improves the outcome of acute ischemic stroke [16, 17]. However, the neuroprotective mechanism of propofol in this setting remains obscure. In this study, we hypothesized that propofol decreases  $\alpha$ -synuclein aggregation and decreases ischemic stroke-induced excessive autophagy *via* the mammalian target of rapamycin (mTOR)/ribosomal protein S6 kinase beta-1 (S6K1) signaling pathway. We tested this hypothesis in a mouse model of acute ischemic stroke and evaluated  $\alpha$ -synuclein aggregation, infarct area, neurological deficits, gene expression profiles, and autophagy following treatment with propofol.

## Materials and Methods

### Animals and Treatment

All experimental procedures were approved by the Institutional Animal Care and Use Committee of Capital Medical University (AEEI-2018-120). Specific pathogen-free C57BL/6 J mice (25 g–30 g) were raised with free access to water and standard food. Ischemic stroke in the right focal somatosensory cortex was created using a previously published protocol [18–20].

In brief, the procedure was performed under 1.5% isoflurane (#R510-22, RWD Life Science, San Diego, CA) for maintenance of anesthesia. The selected branch of the right middle cerebral artery was permanently ligated with 10-0 suture (#w2790, Ethicon, Somerville, NJ), with temporary clamping of the bilateral common carotid arteries for 7 min. Mice were given propofol (16 mg/kg, #260929, Fresenius Kabi, Bad Homburg, Germany) by intraperitoneal injection (IP) or the same volume of 0.9% normal saline (1.6 mL/kg, IP) at the time of reperfusion. They received additional maintenance IP propofol (10–12 mg/kg every half-hour) or the same volume of 0.9% normal saline for two hours, in consideration of the rapid induction of anesthesia for emergency surgery for acute ischemic stroke. Only skin dissection was performed in the sham procedure group. The sham group was also given 0.9% normal saline IP during and after the procedure. The skin incision was closed using Vetbond tissue adhesive (#1469SB, 3 M Company, MN). Mice were returned to their cages after recovery from anesthesia.

Body temperature was monitored and maintained with a heating pad during anesthesia and surgery. All procedures were conducted between 09:30 and 11:30.

### Western Blot Analysis

Infarcted cortex was harvested 24 h after stroke. Thermo M-PER mammal Protein Extract Reagent (#78501, Waltham, MA) with complete protease inhibitor cocktail tablets (#11697498001, Roche, Basel, Switzerland) and PhosSTOP™ phosphatase inhibitor cocktail tablets (#04906845001, Roche) were used for sample homogenization. The homogenate was then separated using SDS-PAGE and transferred onto nitrocellulose membranes (0.2  $\mu$ m). The blots were blocked in Tris-buffered saline containing 0.5% Tween-20 (#P9416, Sigma, St. Louis, MO) and Difco skim milk (10% *m/v*, #232100, BD, San Jose, Canada) for 1 h after transfer. The blocked membrane was incubated with primary antibody overnight at 4°C, followed by secondary antibody for 1 h at room temperature. HRP immunoblots were developed using Immobilon Western Chemiluminescent HRP Substrate (#WBKLS0500, Millipore, MA, USA). Blots were exposed to Molecular Imager (ChemiDo XRS +, Bio-Rad, Hercules, CA) and analyzed with ImageJ software (Version 1.52).

The antibodies used for western blot were anti-LC3B (1:2000 dilution, #L7543, Sigma), anti- $\alpha$ -synuclein (1:1500 dilution, #2642, Cell Signaling Technology, Beverly, MA), anti-S6K1 phospho T389 (1:500 dilution, #ab2571, Abcam, Cambridge, UK), anti-S6K1 (1:10000 dilution, #ab32529, Abcam), anti- $\beta$ -actin (1:5000 dilution, #A5316, Sigma), goat anti-rabbit IgG (1:150000 dilution, #A0545, Sigma), and goat anti-mouse IgG (1:150000 dilution, #A9044, Sigma). A pre-stained protein ladder (#26616, Thermo Scientific, Waltham, MA) was used as the molecular weight marker.

### Immunofluorescence

Frozen brain tissue was cut into 10  $\mu$ m-thick coronal sections on a cryostat vibratome (Leica CM 1860, Wetzlar, Germany) 24 h after stroke. The sections were fixed in 4% paraformaldehyde for 20 min and permeabilized with 0.3% Triton-X 100 (Sigma) for 15 min. The sections were then blocked with 10% fetal bovine serum for 60 min at room temperature and incubated with primary antibody (anti-LC3B, 1:500 dilution, #L7543, Sigma; Anti-NeuN, 1:1000 dilution, #ab104224, Abcam) and secondary antibody (#A-21206 and #A10036, Invitrogen, Carlsbad, CA) overnight at 4 °C. DAPI Fluoromount-G (#36308ES11, Yeasen, Shanghai, China) was used as the mounting medium. Imaging was performed using the Olympus microscope

system and analyzed *via* the ImageJ (Version 1.52) automatic puncta analysis procedure.

### Transcriptome Sequencing

RNA from the infarcted cortex was sequenced at 24 h after ischemic stroke. The RNA Library Prep Kit for Illumina (#E7530L, NEB, MA, USA) and index codes were used to attribute sequences in each sample. RNA Library concentrations were measured using the RNA Assay Kit in Qubit 3.0 (#Q10211, Thermo Scientific, Waltham, MA) for preliminary quantification. The Bio analyzer 2100 System (Agilent Technologies, CA) was used to assess the insert size. Qualified inserts were further quantified using the Step One Plus Real-Time PCR System (#4376600, Thermo Scientific). The index-coded sample library was clustered using the cBot cluster generation system (HiSeq PE Cluster Kit v4-Cbot-HS, Illumina, CA) and sequenced on the Illumina platform.

### 2,3,5-Triphenyl Tetrazolium Chloride (TTC)

#### Staining

Mice were sacrificed 72 h after stroke. The brain was cut coronally into 1-mm slices. After staining with 2% TTC (#T8877, Sigma) for 15 min at 37°C in darkness, the slices were fixed in 4% paraformaldehyde at 4°C for 12 h. The whole area and infarct area of each section were measured with ImageJ (Version 1.52). The results are expressed as the ratio of infarct volume to whole brain volume  $\times 100\%$ .

#### Behavioral Testing

Experimenters were blinded to study group during all behavioral tests. In the sticky-label test, a square ( $2 \times 2 \text{ mm}^2$ ) of medical adhesive tape (3 M Company) was placed on the mouse forepaw. The mice were then allowed to move freely. The latency and time to remove the tape were recorded. The latency was defined as the time between tape placement and the animal's first attempt to remove it; *i.e.* shaking its paw or biting the tape. The right and left forepaws were tested separately in an alternating manner, with an interval of at least 10 min. Testing with the right forepaw was considered to be the ipsilateral sticky-label test, and testing with the left forepaw the contralateral sticky-label test, relative to the induced lesion. Mice were trained 3 times a day on each forepaw for 3 days prior to stroke. The same procedure was performed 24 h after stroke.

The whisker tests were performed as previously described to assess fine neurological deficits [21]. In mice, sensation in the whiskers projects to the contralateral barrel cortex of S1 (Fig. 1E), which is specifically covered in the

stroke model used in this study [22]. In the whisker-evoked forelimb placing test, a mouse was gently held by the torso and the whiskers on one side were brushed against the corner of a platform to elicit ipsilateral forelimb placement on the platform. For the whisker-evoked cross-midline forelimb placing test, a mouse was held by the torso and rotated 45° onto its side. Then, the whiskers on the lower side were brushed perpendicularly against the edge of the corner platform to elicit contralateral (upper side) forelimb placement on the platform. The eyes were covered to avoid visual input during the tests. In both tests, if the mouse could place the forelimb on the platform after brushing the whisker, it was recorded as a success. If the mouse remained motionless or moved and failed to place its forelimb on the platform, it was recorded as a failure. Trials in which the animal struggled were not counted. Testing with brushing of the right whiskers was considered ipsilateral, and testing with the left whiskers contralateral, relative to the induced lesion (Fig. 1F). Mice underwent 10 training trials a day on the whiskers on both sides in the whisker-evoked forelimb placing and cross-midline tests for 3 days prior to stroke. The same procedures were used during testing at 24 h after stroke.

#### Bioinformatics and Statistical Analysis

R (Version 5.2.0, New Zealand) was used for bioinformatics and statistical analysis. Following transcriptome sequencing, differentially-expressed genes (DEGs) between the propofol and stroke groups were identified using DEseq2 (<https://github.com/mikelove/DESeq2>). Term enrichment analysis with Bonferroni correction was performed using the Kyoto Encyclopedia of Genes and Genomes (KEGG), the KEGG Orthology-Based Annotation System, and the Gene Ontology (GO) Consortium databases. STRING (Version 10.5, Cambridgeshire, UK) was used for protein-protein interaction (PPI) network analysis. The Database for Annotation, Visualization, and Integrated Discovery (DAVID Bioinformatics Resources, Version 6.8) was used for statistical analysis. Benjamini-Hochberg correction-adjusted *P* values were used in all bioinformatics analyses. Two-tailed *t*-tests were used to compare TTC-staining data in the stroke and propofol groups. Bonferroni-adjusted one-way ANOVA was used to analyze western blot, immunofluorescence and behavioral tests. The expression levels of p-S6 K were adjusted by the corresponding total S6 K protein levels, and other protein levels were adjusted by the corresponding  $\beta$ -actin. The expression levels in the stroke and propofol groups were normalized to the sham group. Data are presented as the average with standard deviation.

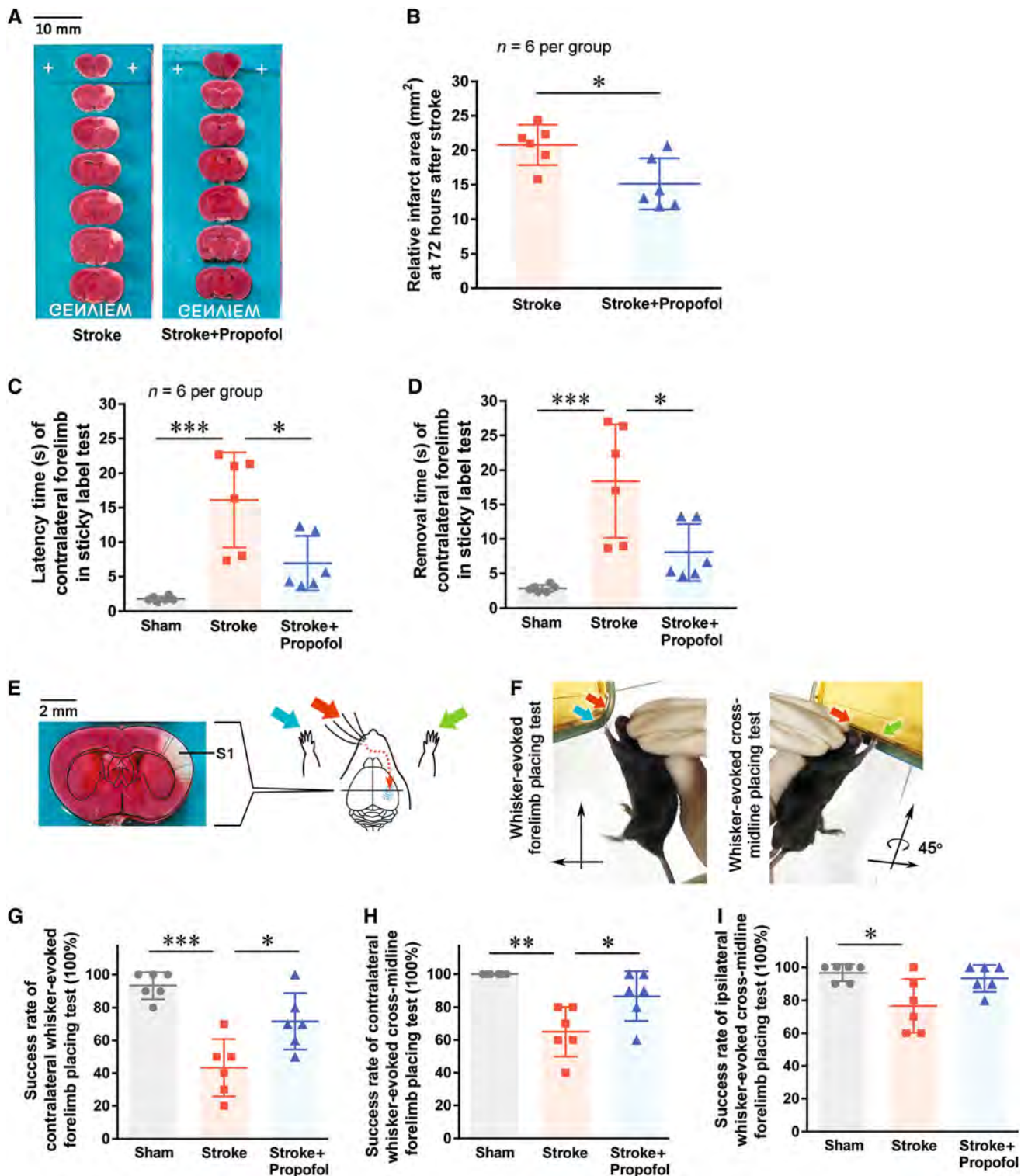


**Fig. 1** Propofol reduces the neurological deficit after ischemic stroke. **A** Typical TTC staining results. The viable area of each slice is stained red, while the infarcted area is white. **B** Relative infarct area measured 72 h after stroke. **C** and **D** Latency and removal time in the sticky-label test 24 h after stroke. **E** Schematic of the stroke region

and whisker tests. **F** Images of the whisker-evoked placing tests. **G** Contralateral whisker-evoked forelimb placing test. **H** Contralateral cross-midline placing test. **I** Ipsilateral cross-midline test.  $*P < 0.05$ ,  $**P < 0.01$ ,  $***P < 0.001$ .

## Results

### Propofol Reduces the Infarct Size After Ischemic Stroke

TTC staining showed a relative reduction of 27.10% of the infarct area in the propofol group compared to the stroke group ( $P = 0.016$ ) (Fig. 1A, B).

### Propofol Improves the Neurological Outcome After Ischemic Stroke

In the contralateral sticky-label test, both the latency and removal time were significantly longer after ischemic stroke than in the sham group ( $P < 0.0001$ ) (Fig. 1C, D). These delays were significantly reduced with propofol administration. Mice receiving propofol after ischemic stroke did not have significant differences in performance on the contralateral sticky-label test compared to the sham group ( $P = 0.329$ ). There were no differences between groups for the ipsilateral sticky-label test. These results suggested that propofol treatment alleviates the stroke-induced neurological deficit.

In the contralateral whisker-evoked forelimb placing test and cross-midline test, the mice receiving propofol after stroke achieved higher success rates than the stroke group ( $P = 0.015$  and  $P = 0.025$ ) (Fig. 1G, H). There was no significant difference in success rate between groups for the ipsilateral whisker-evoked forelimb placing test. In the ipsilateral whisker-evoked cross-midline forelimb placing test, mice in the propofol group achieved a higher success rate than those in the stroke group (Fig. 1I,  $P = 0.019$  sham *vs* stroke;  $P = 1.00$  sham *vs* propofol;  $P = 0.056$  stroke *vs* propofol). The mice receiving propofol after ischemic stroke did not have significant differences in success rate compared to the sham group in any of the whisker tests.

### Propofol Attenuates the Ischemia-Induced $\alpha$ -Synuclein Aggregation Early After Ischemic Stroke

Fibrils of  $\alpha$ -synuclein, which have high molecular weight of 180 kDa, were minimally expressed in the sham group, while significant aggregation of  $\alpha$ -synuclein into fibrils was observed following ischemic stroke (Fig. 2A). In mice receiving propofol, stroke-induced  $\alpha$ -synuclein aggregation into fibrils was remarkably reduced at 24 h compared to the stroke group ( $P < 0.001$ ) (Fig. 2A, B). The relative protein levels of  $\alpha$ -synuclein oligomers, with molecular weights of 26–180 kDa, also decreased after ischemic stroke ( $P < 0.01$ ) (Fig. 2A, C). Propofol administration had minimal effect on the total  $\alpha$ -synuclein ( $P = 0.587$ ) (Fig. 2E). The levels of monomeric  $\alpha$ -synuclein and total

$\alpha$ -synuclein did not change significantly after ischemic stroke or propofol administration (Fig. 2A, D and E). These results suggest that the treatment with propofol specifically attenuates the levels of  $\alpha$ -synuclein fibrils after ischemic stroke.

### Propofol Alters the Gene Expression Profile in Infarcted Cortex After Ischemic Stroke

To investigate the mechanism by which propofol alleviates  $\alpha$ -synuclein and improves the prognosis of stroke, we sequenced RNA from the infarcted cortex 24 h after ischemic stroke. From a total of 20,606 expressed genes identified, 141 DEGs were down-regulated and 28 DEGs were up-regulated in the propofol group compared to the stroke group ( $P < 0.05$ , absolute value of logarithmic fold change  $> 1.00$ ) (Fig. 3A).

For the down-regulated DEGs in the propofol group, term-enrichment analysis identified 4 terms from the KEGG and 3 terms from the GO database after Bonferroni correction (Fig. 3B). Gene set C0 denotes 9 down-regulated DEGs which notably represent the overlap between the 4 identified KEGG terms Parkinson disease, Huntington disease, Alzheimer disease, and oxidative phosphorylation (Fig. 3C). Gene set C0 also had prominent overlap with down-regulated DEGs enriched in the GO term mitochondrial inner membrane (Fig. 3C, D). Figure 3D is a heatmap of relative expression levels of down-regulated DEGs in the propofol group which were enriched in KEGG terms and the GO term protein heterodimerization activity. No down-regulated DEGs were significantly enriched in the biological process type of GO terms after Bonferroni correction. No up-regulated DEGs were significantly enriched in any GO or KEGG pathway after Bonferroni correction.

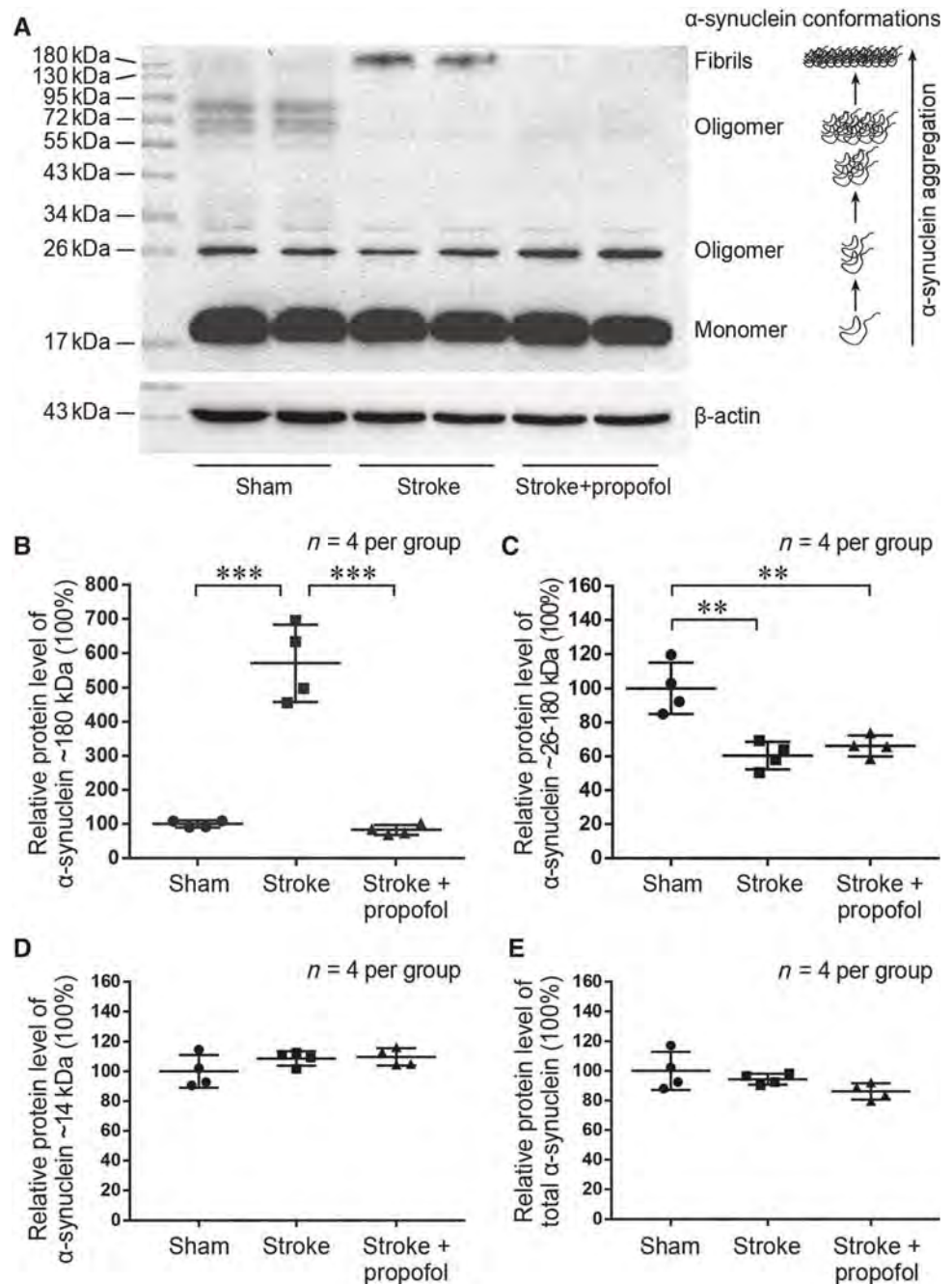
There was no significant difference in the gene expression levels of  $\alpha$ -synuclein in the propofol and stroke groups on RNA sequencing. This result corresponded with the unchanged protein expression level of total  $\alpha$ -synuclein in immunoblot analysis (Fig. 2E), suggesting that propofol regulates  $\alpha$ -synuclein after transcription.

### Propofol is Involved in the Crosstalk Between $\alpha$ -Synuclein, Proteins Encoded by Enriched Down-Regulated DEGs, and Proteins Involved in Autophagy

To investigate the relationship between transcriptional changes in DEGs and  $\alpha$ -synuclein protein aggregation, PPI network analysis was performed using STRING. Proteins encoded by the down-regulated DEGs enriched in the KEGG term oxidative phosphorylation and the GO term

**Fig. 2** Propofol reduces stroke-induced  $\alpha$ -synuclein aggregation at 24 h post-stroke.

**A** Western blots of  $\alpha$ -synuclein in the sham, stroke, and stroke + propofol groups. **B–D** Relative protein expression levels of  $\alpha$ -synuclein at 180, 26–180, and 14 kDa molecular weights. **E** Relative protein expression levels of total  $\alpha$ -synuclein. \*\* $P < 0.01$ , \*\*\* $P < 0.001$ .



protein heterodimerization activity were correlated with  $\alpha$ -synuclein and genes of mTOR-modulated autophagy (Fig. 3E). These PPI results suggest that propofol treatment is involved in interactions between  $\alpha$ -synuclein and autophagy-associated proteins after ischemic stroke. Since both *Snca* and autophagy-related genes from the PPI network analysis were not significantly changed in our RNA sequencing analysis (Fig. 3E, all  $P$  values  $> 0.05$ ), it is possible that propofol plays roles in the regulation of autophagy and  $\alpha$ -synuclein aggregation after transcription.

### Propofol Attenuates the Increased Autophagy After Ischemic Stroke

To test the hypothesis that propofol decreases the post-stroke  $\alpha$ -synuclein aggregation *via* the regulation of autophagy, we focused on typical proteins in the autophagy pathways. The gene *Map1lc3a*, which was identified as a node in the PPI analysis (Fig. 3E), encodes both microtubule-associated protein light chain 3 I (LC3 I) and II (LC3 II) [23], which are involved in autophagy. Western blot analysis showed that the LC3 II:I ratio increased early

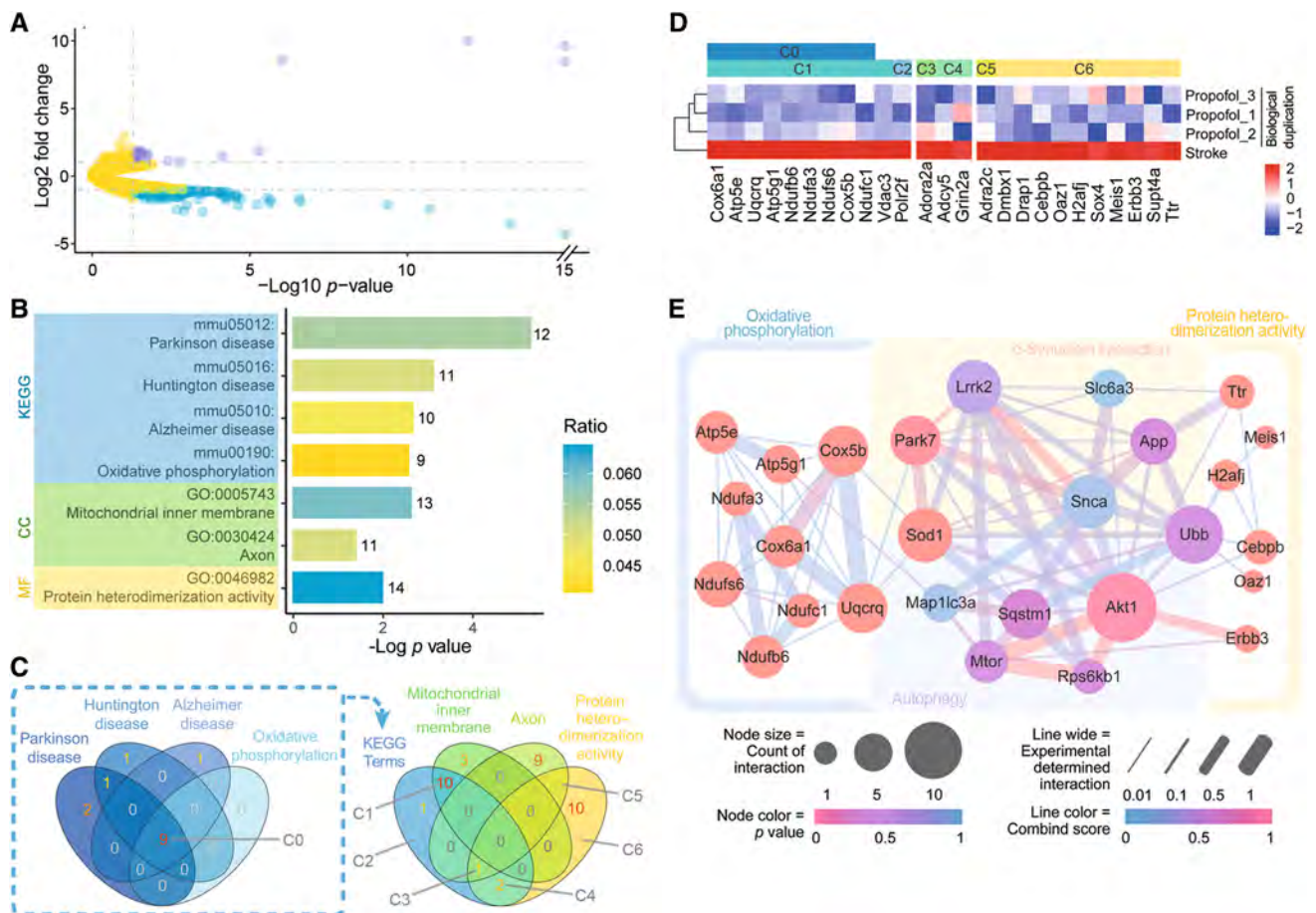


**Fig. 3** Differentially-expressed genes (DEGs) in the stroke and propofol groups identified using RNA-sequencing. **A** Volcano plot showing upregulated (violet) and downregulated (blue) DEGs in the infarcted areas of mice treated with propofol (yellow, genes without significant changes in expression). **B** KEGG and GO term-enrichment analysis of downregulated DEGs. **C** Venn plot of terms identified in enrichment analysis. **D** Heatmaps of down-regulated DEGs enriched in KEGG terms and protein heterodimerization activity. **E** Protein-

protein interaction network analysis of proteins encoded by DEGs enriched in terms of oxidative phosphorylation and protein heterodimerization activity, proteins related with  $\alpha$ -synuclein, and proteins that regulate the mTOR-autophagy pathway. KEGG, Kyoto Encyclopedia of Genes and Genomes; GO, Gene Ontology; CC, Cellular Component; MF, Molecular Function. All *P* values based on RNA sequencing analysis.

after stroke, with a prominent increase at 24 h, followed by a decrease at 72 h (Fig. 4A). Corrected *P*-values between groups are shown in Table S1. The increase in LC3 II:I ratio was rescued after propofol administration when compared to the stroke group (*P* < 0.001) (Fig. 4B).

As the *Sqstm1* gene was identified as a node in the PPI analysis (Fig. 3E), we measured the degradation of sequestosome 1 (ubiquitin-binding protein p62) encoded by this gene, to further investigate if autophagic flux was affected by propofol [24]. Immunoblot analysis showed that the p62 levels were reduced after ischemic stroke and preserved in the propofol group (*P* = 0.002) (Fig. 4C).

Immunofluorescence was further used to detect the autophagy of LC3 [24]. In the propofol group, the total area of punctate LC3 was higher than that in the sham group but to a lesser extent than that in the stroke group (*P* < 0.001) (Fig. 4E). In both stroke and propofol groups, LC3 puncta

displayed a qualitative overlap with NeuN, a neuronal nuclear antigen used as a biomarker for neurons.

These results suggested that autophagy is increased 24 hours after stroke and this stroke-induced autophagy is attenuated by propofol.

### Propofol Increases the Activity of the mTOR/S6K1 Signaling Pathway to Inhibit Autophagy

To study the regulatory mechanism of propofol in stroke-induced autophagy, we focused on its upstream mediator, ribosomal protein S6K1. Encoded by *Rps6kb1*, S6K1 is one of the main downstream targets of mTOR and its involvement was predicted in the PPI network analysis. We measured the activation of the mTOR/S6K1 signaling pathway *via* the phosphorylation of S6K1 by mTOR [25]. The ratio of phosphorylated S6K1 to S6K1 decreased

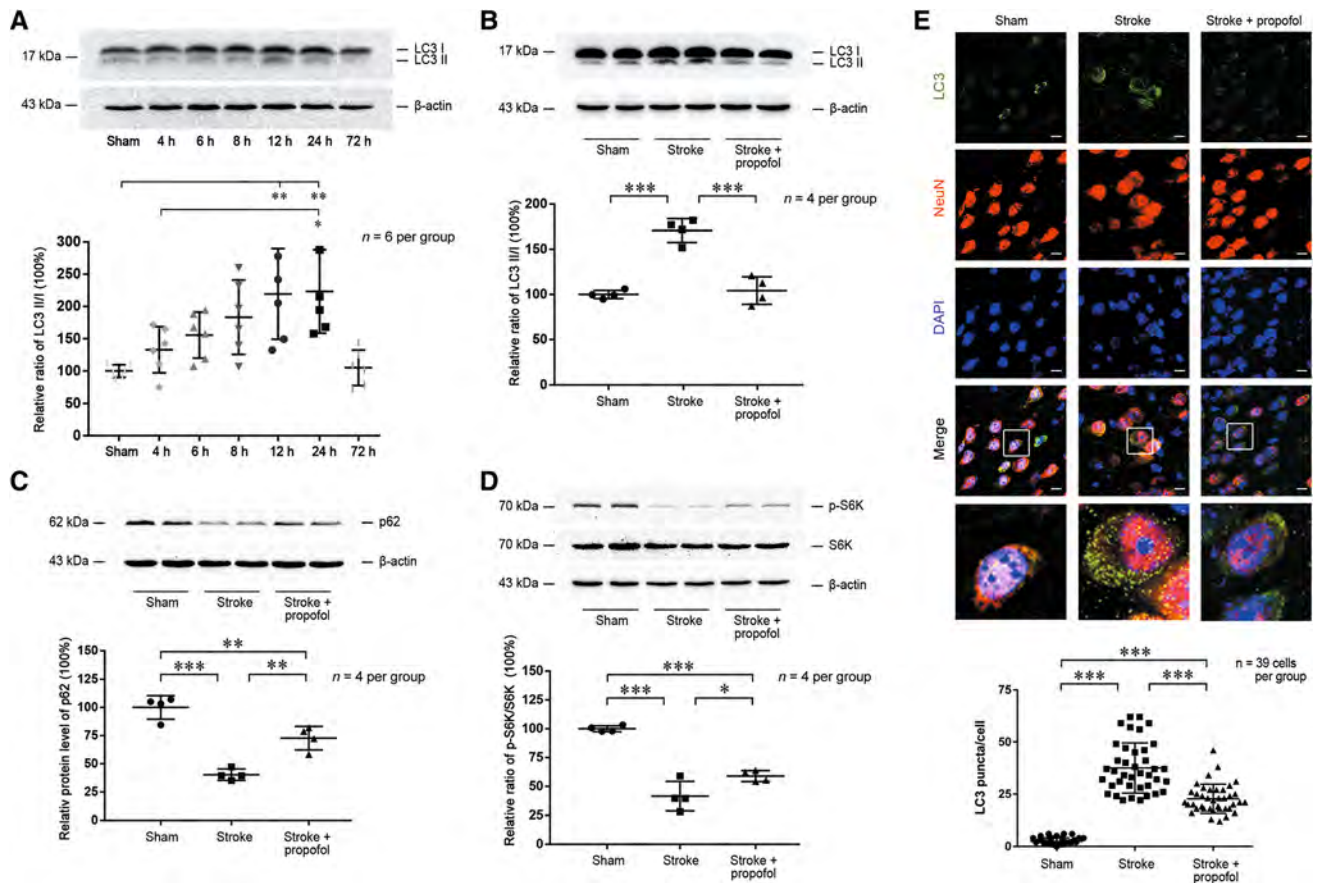


**Fig. 4** Propofol increases the mTOR/S6K1 pathway activity to alleviate stroke-induced abnormal autophagy. **A** Western blots of LC3 in the stroke group from 4 h to 72 h post-stroke. **B–D** Western blots (upper panels) and statistics (lower panels) of differential protein expression levels of LC3, p62, and pS6K/S6K among sham, stroke, and propofol groups 24 h post-stroke. **E** Upper panels,

photomicrographs of immunofluorescence of LC3 puncta merged with NeuN and DAPI in the sham, stroke, and propofol groups 24 h post-stroke. Scale bars, 10  $\mu$ m. Lower panel, statistics for LC3 puncta merged with NeuN in randomly-selected sections from each group ( $n = 39$  random cells/group from four mice/group;  $*P < 0.05$ ,  $**P < 0.01$ ,  $***P < 0.001$ ).

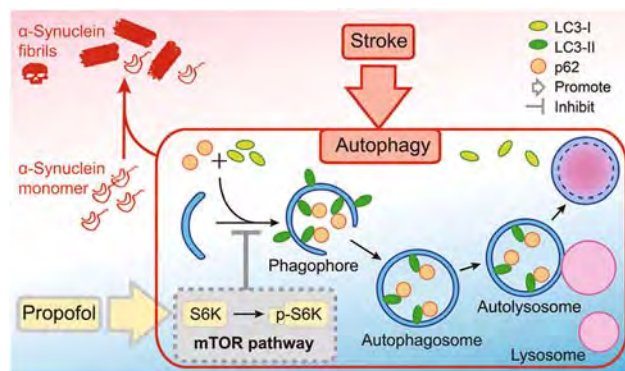


**Fig. 5** Proposed mechanism for the neuroprotective action of propofol in ischemic stroke. Propofol decreases  $\alpha$ -synuclein aggregation to reduce the increased level of autophagy after stroke *via* activation of the mTOR/S6K1 signaling pathway.

significantly after ischemic stroke, indicating decreased mTOR/S6K1 pathway activity. This effect was partially reversed by propofol ( $P < 0.05$ ) (Fig. 4D). Based on these

results, we suggest that propofol decreases autophagy after ischemic stroke *via* increased activation of the mTOR/S6K1 signaling pathway (Fig. 5).

### Discussion

In this study, we demonstrated that treatment with propofol inhibits  $\alpha$ -synuclein aggregation and reduces the neurological deficits following acute ischemic stroke. Previous studies have shown that abnormal aggregation of  $\alpha$ -synuclein has serious neurotoxic effects in the long-term chronic progression of neurodegeneration [5]. We argue and emphasize that, even in the short time-frame of acute ischemic stroke, the neurotoxic effects of  $\alpha$ -synuclein aggregation cannot be underestimated and may be prevented.

After ischemic stroke,  $\alpha$ -synuclein in neurons aggregates into higher-level oligomers and insoluble fibrils,

which are difficult to degrade once formed [36]. These aggregates induce mitochondrial damage and disrupt oxidative phosphorylation [32], leading to greater oxidative stress [11]. Oxidative stress in turn leads to additional accumulation of additional  $\alpha$ -synuclein aggregates [33]. Furthermore, both  $\alpha$ -synuclein and oxidative stress augment autophagy, including negative regulation of the mTOR/S6K1 pathway by  $\alpha$ -synuclein overexpression [26, 27, 34, 35]. We suggest that propofol can break this vicious cycle by preventing the initial aggregation of  $\alpha$ -synuclein and reducing the initial peak of autophagy in the early stage of ischemic stroke.

In our mouse model, ischemic stroke resulted in measurable sensory and motor neurological deficits at 24 h. Our results concur with previous studies showing significant aggregation of  $\alpha$ -synuclein into insoluble fibrils and higher-level oligomers following stroke. With propofol treatment after stroke, the levels of  $\alpha$ -synuclein fibrils were significantly reduced. Total infarct size on post-stroke pathology and neurological deficits were similarly attenuated with propofol administration. Furthermore, transcriptome sequencing identified down-regulated DEGs associated with the major neurodegenerative diseases Parkinson disease, Huntington disease, and Alzheimer disease, and oxidative phosphorylation on term-enrichment analysis. The finding that total  $\alpha$ -synuclein levels on immunoblot analysis and RNA sequencing were both unchanged after propofol treatment supports the hypothesis that propofol regulates  $\alpha$ -synuclein aggregation after transcription.

We further investigated the neuroprotective mechanism of propofol in the setting of acute ischemic stroke, focusing on the increased level of autophagy after stroke as previously reported. PPI network analysis showed that the proteins encoded by DEGs that were down-regulated after propofol treatment were related to both  $\alpha$ -synuclein and proteins of mTOR-modulated autophagy. Markers of autophagy and autophagic flux were reduced by propofol treatment, and this was accompanied by an increase in mTOR/S6K1 pathway activity.

This study has several limitations. First, although we showed that propofol decreases both  $\alpha$ -synuclein aggregation and stroke-induced autophagy, and identified interactions between  $\alpha$ -synuclein and the mTOR/S6K1 signaling pathway using sequencing analysis, further experiments are needed to verify the relationship between  $\alpha$ -synuclein and the mTOR/S6K1 signaling pathway in our stroke model. Besides, additional investigation is needed on the relationship between  $\alpha$ -synuclein aggregation and neurological damage after acute ischemic stroke, since  $\alpha$ -synuclein interacts with numerous proteins involved in the regulation of mitochondrial function, oxidative stress, autophagy,

vesicular trafficking, signal transduction, and synaptic transmission [11, 27].

Besides, in addition to reducing  $\alpha$ -synuclein aggregation, propofol may improve stroke outcomes through other mechanisms. Recent studies have shown that propofol has an important capacity of trapping liposome-bound proteins at the presynaptic terminal [28]. Moreover,  $\alpha$ -synuclein is not only primarily expressed at the presynaptic terminal, but also promotes liposome-bound protein complex assembly [3].  $\alpha$ -Synuclein also binds to membrane lipids to induce membrane curvature, a key process in the initialization of autophagy [3, 29–31]. Nevertheless, in addition to the mTOR/S6K1 signaling pathway, other pathways involved in autophagic flux might be affected by  $\alpha$ -synuclein [27]. Further investigations are needed for these possibilities.

Previous studies have reported increased  $\alpha$ -synuclein fibrils and oligomers after stroke [12], while we found increased  $\alpha$ -synuclein fibrils and decreased  $\alpha$ -synuclein oligomers after ischemic stroke. This phenomenon might be attributed to the rapid pathological changes caused by acute ischemic stroke, which resulted in the aggregation of  $\alpha$ -synuclein oligomers into fibrils at the time point we examined (24 h after ischemic stroke), and might be due to the different ischemic model used in our study. Nevertheless,  $\alpha$ -synuclein fibrils are already known to be detrimental [7, 8]. However, it is yet in dispute whether  $\alpha$ -synuclein oligomers (26–180 kDa) are neurotoxic, which might differ between soluble and insoluble oligomers, and between oligomers and higher-level oligomers of  $\alpha$ -synuclein [7, 8]. These issues need further studies.

In conclusion, propofol treatment after ischemic stroke decreases  $\alpha$ -synuclein aggregation and reduces stroke-induced autophagy associated with activation of the mTOR/S6K1 pathway. By exerting this neuroprotective effect, propofol treatment may improve the prognosis following acute ischemic stroke.

**Acknowledgements** We thank Mengyao Qu and Yushang Zao for surgical assistance with the mouse stroke model. This work was supported by the National Natural Science Foundation of China (81771139) and the Beijing Natural Science Foundation (7194270).

**Conflict of interest** All authors claim that there are no conflicts of interest.

## References

1. Iwai A, Masliah E, Yoshimoto M, Ge N, Flanagan L, de Silva HA, *et al.* The precursor protein of non-A beta component of Alzheimer's disease amyloid is a presynaptic protein of the central nervous system. *Neuron* 1995, 14: 467–475.

2. Chandra S, Chen X, Rizo J, Jahn R, Südhof TC. A broken alpha-helix in folded alpha-synuclein. *J Biol Chem* 2003, 278: 15313–15318.
3. Burré J, Sharma M, Tsetsenis T, Buchman V, Etherton MR, Südhof TC. Alpha-synuclein promotes SNARE-complex assembly *in vivo* and *in vitro*. *Science* 2010, 329: 1663–1667.
4. Diógenes MJ, Dias RB, Rombo DM, Vicente Miranda H, Maiolino F, Guerreiro P, *et al.* Extracellular alpha-synuclein oligomers modulate synaptic transmission and impair LTP via NMDA-receptor activation. *J Neurosci* 2012, 34: 11750–11762.
5. Wong YC, Krainc D.  $\alpha$ -Synuclein toxicity in neurodegeneration: mechanism and therapeutic strategies. *Nat Med* 2017, 23: 1–13.
6. Bartels T, Choi JG, Selkoe DJ.  $\alpha$ -Synuclein occurs physiologically as a helically folded tetramer that resists aggregation. *Nature* 2011, 477: 107–110.
7. Pieri L, Madiona K, Bousset L, Melki R.  $\alpha$ -Synuclein and Huntingtin exon 1 assemblies are toxic to the cells. *Biophys J* 2012, 102: 2894–2905.
8. Winner B, Jappelli R, Maji SK, Desplats PA, Boyer L, Aigner S, *et al.* *In vivo* demonstration that  $\alpha$ -synuclein oligomers are toxic. *Proc Natl Acad Sci U S A* 2011, 108: 4194–4199.
9. Sharon R, Bar-Joseph I, Frosch MP, Walsh DM, Hamilton JA, Selkoe DJ. The formation of highly soluble oligomers of alpha-synuclein is regulated by fatty acids and enhanced in Parkinson's disease. *Neuron* 2003, 37: 583–595.
10. Bonini NM, Giasson BI. Snaring the function of alpha-synuclein. *Cell* 2005, 123: 359–361.
11. Cremades N, Cohen SI, Deas E, Abramov AY, Chen AY, Orte A, *et al.* Direct observation of the interconversion of normal and toxic forms of alpha-synuclein. *Cell* 2012, 149: 1048–1059.
12. Unal-Cevik I, Gursoy-Ozdemir Y, Yemisci M, Lule S, Gurer G, Can A, *et al.* Alpha-synuclein aggregation induced by brief ischemia negatively impacts neuronal survival *in vivo*: a study in [A30P]alpha-synuclein transgenic mouse. *J Cereb Blood Flow Metab* 2011, 31: 913–23.
13. Kim T, Mehta SL, Kaimal B, Lyons K, Dempsey RJ, Vemuganti R. Poststroke induction of  $\alpha$ -synuclein mediates ischemic brain damage. *J Neurosci* 2016, 36: 7055–7065.
14. Ham PB, Raju R. Mitochondrial function in hypoxic ischemic injury and influence of aging. *Prog Neurobiol* 2017, 157: 92–116.
15. Wang P, Shao BZ, Deng Z, Chen S, Yue Z, Miao CY. Autophagy in ischemic stroke. *Prog Neurobiol* 2018, 163–164: 98–117.
16. Gelb AW, Bayona NA, Wilson JX, Cechetto DF. Propofol anesthesia compared to awake reduces infarct size in rats. *Anesthesiology* 2002, 96: 1183–1190.
17. Zhang J, Xia Y, Xu Z, Deng X. Propofol suppressed hypoxia/reoxygenation-induced apoptosis in HBVSMC by regulation of the expression of Bcl-2, Bax, Caspase3, Kir6.1, and p-JNK. *Oxid Med Cell Longev* 2016, 2016: 1–11.
18. Song M, Yu SP, Mohamad O, Cao W, Wei ZZ, Gu X, *et al.* Optogenetic stimulation of glutamatergic neuronal activity in the striatum enhances neurogenesis in the subventricular zone of normal and stroke mice. *Neurobiol Dis* 2017, 98: 9–24.
19. Wei ZZ, Zhang JY, Taylor TM, Gu X, Zhao Y, Wei L. Neuroprotective and regenerative roles of intranasal Wnt-3a administration after focal ischemic stroke in mice. *J Cereb Blood Flow Metab* 2017, 38: 404–421.
20. Xiong B, Li A, Lou Y, Chen S, Long B, Peng J, *et al.* Precise cerebral vascular atlas in stereotaxic coordinates of whole mouse brain. *Front Neuroanat* 2017, 11: 128.
21. Woodlee MT, Asseo-García AM, Zhao X, Liu SJ, Jones TA, Schallert T. Testing forelimb placing across the midline reveals distinct, lesion-dependent patterns of recovery in rats. *Exp Neurol* 2005, 191: 310–317.
22. Feldmeyer D, Brecht M, Helmchen F, Petersen CC, Poulet JF, Staiger JF, *et al.* Barrel cortex function. *Prog Neurobiol* 2013, 103: 3–27.
23. Klionsky DJ, Abdelmohsen K, Abe A, Abedin MJ, Abeliovich H, Acevedo Arozena A, *et al.* Guidelines for the use and interpretation of assays for monitoring autophagy (3rd edition). *Autophagy* 2016, 12: 1–222.
24. Mizushima N, Yoshimori T. How to interpret LC3 immunoblotting. *Autophagy* 2007, 3: 542–545.
25. Magalhaes J, Gegg ME, Migdalska-Richards A, Doherty MK, Whitfield PD, Schapira AH. Autophagic lysosome reformation dysfunction in glucocerebrosidase deficient cells: relevance to Parkinson disease. *Hum Mol Genet* 2016, 25: 3432–3445.
26. Gao S, Duan C, Gao G, Wang X, Yang H. Alpha-synuclein overexpression negatively regulates insulin receptor substrate 1 by activating mTORC1/S6K1 signaling. *Int J Biochem Cell Biol* 2015, 64: 25–33.
27. Button RW, Roberts SL, Willis TL, Hanemann CO, Luo S. Accumulation of autophagosomes confers cytotoxicity. *J Biol Chem* 2017, 292: 13599–13614.
28. Bademosi AT, Steeves J, Karunanithi S, Zalucki OH, Gormal RS, Liu S, *et al.* Trapping of Syntaxin1a in presynaptic nanoclusters by a clinically relevant general anesthetic. *Cell Rep* 2018, 22: 427–440.
29. Bendor JT, Logan TP, Edwards RH. The function of alpha-synuclein. *Neuron* 2013, 79: 1044–1066.
30. Menzies FM, Fleming A, Caricasole A, Bento CF, Andrews SP, Ashkenazi A, *et al.* Propagation of pathological  $\alpha$ -synuclein in marmoset brain. *Acta Neuropathol Commun* 2017, 5: 5–12.
31. Menzies FM, Fleming A, Caricasole A, Bento CF, Andrews SP, Ashkenazi A, *et al.* Autophagy and neurodegeneration: pathogenic mechanisms and therapeutic opportunities. *Neuron* 2017, 93: 1015–1034.
32. Grassi D, Howard S, Zhou M, Diaz-Perez N, Urban NT, Guerrero-Given D, *et al.* Identification of a highly neurotoxic alpha-synuclein species inducing mitochondrial damage and mitophagy in Parkinson's disease. *Proc Natl Acad Sci U S A* 2018, 115: E2634–E2643.
33. Binolfi A, Limatola A, Verzini S, Kosten J, Theillet F, Rose HM, *et al.* Intracellular repair of oxidation-damaged  $\alpha$ -synuclein fails to target C-terminal modification sites. *Nature Commun* 2016, 7: 10251.
34. Liu J, Wang X, Lu Y, Duan C, Gao G, Lu L, *et al.* Pink1 interacts with  $\alpha$ -synuclein and abrogates  $\alpha$ -synuclein-induced neurotoxicity by activating autophagy. *Cell Death Dis* 2017, 8: e3056.
35. Zhao QD, Viswanadhapalli S, Williams P, Shi Q, Tan C, Yi X, *et al.* NADPH oxidase 4 induces cardiac fibrosis and hypertrophy through activating Akt/mTOR and NF $\kappa$ B signaling pathways. *Circulation* 2015, 131: 643–655.
36. Fink AL. The aggregation and fibrillation of  $\alpha$ -synuclein. *Acc Chem Res* 2006, 39: 628–634.



# The Risk and Prevention of Novel Coronavirus Pneumonia Infections Among Inpatients in Psychiatric Hospitals

Yuncheng Zhu<sup>1</sup> · Liangliang Chen<sup>2</sup> · Haifeng Ji<sup>2</sup> · Maomao Xi<sup>3</sup> · Yiru Fang<sup>1,5,6</sup> · Yi Li<sup>4</sup>

Received: 14 February 2020 / Accepted: 16 February 2020 / Published online: 25 February 2020  
© Shanghai Institutes for Biological Sciences, CAS 2020

## Dear Editor,

Since the middle of December 2019, human-to-human transmission of novel coronavirus pneumonia (NCP, also called COVID-19) has occurred among close contacts [1]. After the outbreak on January 21, 2020, it was swiftly included among the Class B infectious diseases stipulated in the Law of the People's Republic of China on the Prevention and Control of Infectious Diseases, and measures for prevention and control of Class A infectious diseases were adopted. At 21:27 on February 12, 2020, the China News Network updated information to include epidemic data from the National Health Commission and official channels in Hong Kong, Macao, and Taiwan

---

Yuncheng Zhu, Liangliang Chen, and Haifeng Ji have contributed equally to this work.

---

✉ Yiru Fang  
yirufang@aliyun.com

✉ Yi Li  
psylee@163.com

- <sup>1</sup> Shanghai Mental Health Center, Shanghai Jiao Tong University School of Medicine, Shanghai 200030, China
- <sup>2</sup> Shanghai Changning Mental Health Center (Affiliated to East China Normal University), Shanghai 200335, China
- <sup>3</sup> Institute of Burns, Tongren Hospital of Wuhan University (Wuhan Third Hospital), Wuhan 430000, China
- <sup>4</sup> Affiliated Wuhan Mental Health Center, Tongji Medical College of Huazhong University of Science and Technology, Wuhan 430012, China
- <sup>5</sup> CAS Center for Excellence in Brain Science and Intelligence Technology, Shanghai 200031, China
- <sup>6</sup> Shanghai Key Laboratory of Psychotic Disorders, Shanghai 201108, China

regions: the highest death rate was in Wuhan City (Table 1). Overload of inpatients at hospitals may play a negative role in the overall therapeutic effect and contribute to the death rate.

At the same time, with the related law promulgated, Wuhan Mental Health Center (WMHC) announced the closed management of inpatients (visit prohibited), and this was followed by other psychiatric hospitals nationwide. Unfortunately, on February 8, China News Weekly exclusively reported that nosocomial infection had occurred in WMHC. Up to February 8, ~ 50 patients and 30 medical staff in WMHC were diagnosed with NCP, so WMHC became the first psychiatric hospital in China with clustered nosocomial infections. The official spokesman of WMHC revealed to the media that delay of information on infections increased the chance of infection in the early stage, such as unawareness of the infection and the mode of transmission, as well as the possibility of an asymptomatic incubation period, similar to the situation of other general hospitals in Wuhan.

## Related Risk Factors

Three elements are responsible for the infection of hospitalized psychotic patients: source of infection (patients with NCP), transmission route (human-to-human droplet transmission), and susceptibility (patients without insight). A similar outbreak occurred in 2003 that has parallels with the emergence of NCP: the severe acute respiratory syndrome (SARS), which killed 349 of 5327 probable cases (6.6%) reported in mainland China [2]. Compared to the mean incubation period of 6.4 days of SARS [3], the 5.2 days of the 2019 new Coronavirus (SARS-CoV-2) means it is more infectious [1]. Although

**Table 1** Outbreak status of novel coronavirus pneumonia from the National Health Commission (21:27 on Feb 12, 2020)

	Diagnosed	Cured	Dead
Global	45204	5084	1117 (2.471%)
Asia	45124	5075	1117 (2.475%)
China	44763	5034	1116 (2.493%)
Hubei	33366	2668	1068 (3.200%)
Wuhan	19558	1379	820 (4.192%)

the death rate from NCP (2.5%) is lower than that of SARS, unfortunately, the number of deaths doubles that of SARS although the outbreak started less than two months ago. Thus, the Chinese government has realized the severity of the NCP outbreak.

Staff working in psychiatric hospitals were not notified of factors that may increase the risk and outbreak, but these may include the following:

1. The wards are often closed and crowded;
2. As is common in psychiatric hospitals, the wards of WMHC were not designed to the standards for isolation against infectious respiratory disease, nor are they equipped with negative pressure devices;
3. Now is the season of high incidence of respiratory diseases, which led to the initial underestimating of NCP as a common disease;
4. The source of infection cannot be found in a timely manner because the patients are neither sensitive to nor concerned about the news after long-term social isolation;
5. It is difficult for psychiatric patients to accept and cooperate with self-isolation measures for cutting off the NCP infection route in time;
6. Medical staff in the psychiatric specialty lack knowledge in coping with infectious diseases;
7. A practical clinical path has not yet been promulgated for preventing infectious diseases in such isolated groups;
8. Patients with psychoses have slowed perception of changes to the external environment, and lack a sense of self-protection;
9. More emphasis is placed on the “stability” of the patient’s condition and not causing trouble, resulting in insufficient subjectivity of medical staff in psychiatric hospitals.

Clearly, even supported by the nearby Pulmonary Medicine Department, emergency facilities are far from sufficient. We know that the healthcare workload for NCP is extremely great, particularly under the condition of human-to-human transmission.

## Lessons to Learn

Not only in China, any mistake in prevention and control can critically strike local health systems worldwide. It has been noted in the Diagnosis and Treatment of Pneumonia Caused by New Coronavirus Infection (Trial Version 5) that the incubation period is generally 3–7 days, and the longest is 24 days [4]. Fourteen days of observation have been announced by the authorities.

We need to consider the absence of objective measures, subjective deficiencies, and points that need to be changed. In case of aggravation or recurrence in a psychotic patient, the physician should take precautions before receiving a patient for hospitalization. Psychiatrists ought to aware that psychiatric patients are a susceptible group, so they should be carefully treated and fully prepared for admission and hospitalization. Clearly, it is more difficult for these patients to go through the proper procedures than healthy persons. Especially for pre-hospital assessment and virus isolation, every necessary step must be followed and cannot be simplified at the current unusual time.

During the hospital stay, the closure measures should be strictly enforced, because some family members have still been able to deliver materials to the hospital even when visits are prohibited. The first case of NCP diagnosed in WMHC was a patient with Alzheimer’s disease. This patient might have been infected by outside goods brought by a family member. This phenomenon still occurs in the closed psychotic hospitals in China, with the most common reason being the tradition of reunion at Chinese New Year. Besides, experts have noted that if infected, the elderly and those with underlying diseases are more likely to develop severe pulmonary disease. Long-term hospitalized patients with mental disorders with comorbidity such as hypertension, diabetes, and other chronic diseases are more vulnerable than the general population [5]. Before the occurrence of this public health issue, such risks had not been fully discussed.

Meanwhile, with the rapid development of information technology, far beyond that of the SARS period, such psychological influences spread more widely *via* the mainstream media and “We Media”. The long-term psychological implications of infectious diseases should not be ignored. These are likely to cause a secondary disaster due to stress and psychological distress even after the NCP is over [6]. These severe psychological stress factors could facilitate the onset of existing mental illness, for example, causing a serious delusion generalized by the epidemic situation. As a result, psychiatric hospitals will be burdened with extra pressure.

The key conclusions from this section are: observation, threshold, isolation, and prevention.

## Possible Coping Strategies

Once the novel coronavirus is imported into a public place, its speed of transmission is beyond control. To reduce the risk of infection at an early stage, all possible methods should be undertaken, such as to restrict hospitalization, expedite discharge, prohibit visits, provide physical supplies, and provide psychological assistance.

A 14-day clinical observation period is indispensable before formal hospitalization procedures. It has been suggested that an observation room outside the routine ward should be set up for isolation and observation, so as to ensure the safety of patients with mental disorders during isolation. In particular, patients who cannot control their behavior should be more carefully assessed and stricter protective constraints than usual should be implemented. The intensive use of ward beds will increase the inconvenience of emergency deployment, the potential rate of cross infections, and the error rates due to fatigue of medical staff under high pressure. Therefore, remitted patients should be transferred to an outpatient clinic as soon as possible. Home quarantine has proved to be an effective way in these days [7], especially in less-affected provinces in China.

The usual psychiatric ward is densely staffed and lacks sufficient space for activities and ventilation, which is conducive to the transmission of the novel coronavirus. Once exogenous infection occurs, transmission can be rapid and extremely hard to control. Therefore, the complete isolation of mental health centers has been recommended during the NCP epidemic. Specific measures to be considered are as follows:

1. Fourteen days under observation in hospital is the key to reducing hospital infection;
2. A pre-admission observation ward needs to be arranged immediately;
3. A detailed understanding of the patient's recent travel history in Hubei province, as well as the close contact history with suspected or confirmed patients;
4. Based on the risk level of a latent infectious patient, the physician should make a firm decision on whether the patient should be transferred to the designated hospital for treatment set by the local government;
5. Medical, nursing, logistics support, and canteen staff should limit their approaches to the hospital and have their temperature taken before entering and leaving the ward;
6. Temporarily prohibit on-site visits, and replace them with video chat. In principle, only food and clothing from government-approved institutions are acceptable;
7. More psychological services should be provided by community workers and family doctors to help the hospital to communicate about the restriction of visitors, so as to obtain consent on the necessity of these temporary arrangements;
8. Ensure that family members know that the patients receive sufficient daily necessities from the hospital, so as to eliminate the worries and doubts of family members;
9. The skills of medical staff in the psychiatric specialty needs to be improved in identifying and treating physical diseases.

Panic is inevitable among patients and medical staff and timely mental health care for dealing with the novel coronavirus outbreak is urgently needed [8]. At present, it has been reported that many local hospital workers in Wuhan, especially nurses, have been confronting occupational exhaustion. Inevitably, the overloaded working conditions lead to mental health problems such as serious psychosomatic disorders and a decline in decision making and execution [9]. Psychological services and crisis interventions are needed at an early stage to reduce anxiety, depression, and post-traumatic stress disorder (PTSD) in almost all groups during such a stressful period. However, we should note that the premise of providing such services is to follow the advice in this paper, to isolate infected patients and cut off the transmission route to protect vulnerable people. Once a psychological consultation room is set up in a general hospital, the manager should pay attention to the redesign of the layout, formulate strict measures to prevent infection, and increase the protective equipment at work to ensure that consultations are conducted in a safe environment. Online psychotherapy is recommended. Where there is no sufficient preventative facility for the epidemic, psychiatrists and counselors are currently suggested to do more work over the phone, and *via* internet applications such as WeChat.

The guiding principles divide the population affected by NCP into 6 categories and 4 levels and require the first-level population to be the focus of psychological crisis intervention. Then the intervention shall be gradually expanded to the second, third, and fourth levels, and finally, involve all populations. Common psychological and behavioral issues that have emerged from the outbreak, as well as psychological crisis interventions and principles have been explained in detail [10]. In order to alleviate the current acute stress responses of individuals and patients and reduce the incidence of psychological distress or PTSD, we should take appropriate measures for the support of public mental health. Probable practices are as follows:

1. Disseminating knowledge on mental health to the public;
2. Setting up psychological counseling hotlines nationwide;

3. Launching individualized psychological support by psychiatrists and psychologists;
4. Encouraging public and private physicians to provide psychological assistance;
5. Encouraging voluntary support by infected survivors;
6. Developing mental health insurance for special periods.

Last but not least, we should identify high-risk individuals in a timely manner, and avoid the occurrence of extreme events such as suicide, impulsive behavior, and group psychological crisis [10]. We know that, to prevent and control nosocomial infections, it is essential to take measures to monitor patients outside the hospital. Probable practices for psychotic patients are:

1. Lengthening the duration of prescriptions for stable outpatients;
2. Ensuring remote monitoring for unstable outpatients;
3. Early warning of the risk for patients needing hospitalization and rapid precaution planning.

### Further Perspectives

Generally, a psychiatric hospital is required to provide mental health services to millions of local residents while hospital administrators have many difficulties in cutting off exogenous infections completely without higher administrative direction. The management system for psychiatric hospitals in China is still incomplete for responding well to public emergencies. We expect that the Government of China will promulgate targeted and operable laws and regulations as soon as possible to ensure the organization and personnel deployment for medical staff after this epidemic. A precise policy is essential for orderly treatment in psychiatric hospitals nationwide.

**Acknowledgements** We thank all the members of the Shanghai Medical Team dispatched to Wuhan and Liqiong Huang for

proofreading the manuscript. This work was supported by the National Key Research and Development Program of China (2016YFC1307100), the National Natural Science Foundation of China (81771465 and 81930033), and the Research Project of Changning District Health Committee of Shanghai Municipality, China (20194Y013).

### References

1. Li Q, Guan X, Wu P, Wang X, Zhou L, Tong Y, *et al.* Early transmission dynamics in Wuhan, China, of novel coronavirus-infected pneumonia. *N Engl J Med* 2020. <https://doi.org/10.1056/NEJMoa.2001316>.
2. Cui Y, Zhang ZF, Froines J, Zhao J, Wang H, Yu SZ, *et al.* Air pollution and case fatality of SARS in the People's Republic of China: an ecologic study. *Environ Health* 2003, 2: 2–15.
3. Chan-Yeung M, Xu RH. SARS: epidemiology. *Respirology* 2003, 8: 1440–1843.
4. Chang, Lin M, Wei L, Xie L, Zhu G, Dela Cruz CS, *et al.* Epidemiologic and clinical characteristics of novel coronavirus infections involving 13 patients outside Wuhan, China. *JAMA* 2020. <https://doi.org/10.1001/jama.2020.1623>
5. Lobo-Escolar A, Saz P, Marcos G, Quintanilla MA, Campayo A, Lobo A. Somatic and psychiatric comorbidity in the general elderly population: results from the ZARADEMP project. *J Psychosom Res* 2008, 65: 347–355.
6. Lee AM, Wong JG, McAlonan GM, Cheung V, Cheung C, Sham PC, *et al.* Stress and psychological distress among SARS survivors 1 year after the outbreak. *Can J Psychiatry* 2007, 52: 233–240.
7. Enserink M. SARS. Researcher told to stay home after China trip. *Science* 2003, 300: 1216.
8. Xiang YT, Yang Y, Li W, Zhang L, Zhang Q, Cheung T, *et al.* Timely mental health care for the 2019 novel coronavirus outbreak is urgently needed. *Lancet Psychiatry* 2020, 4: 30046–30048.
9. Kang L, Li Y, Hu S, Chen M, Yang C, Yang BX, *et al.* The mental health of medical workers in Wuhan, China dealing with the 2019 novel coronavirus. *Lancet Psychiatry* 2020. pii: S2215-0366(20)30047-X. [https://doi.org/10.1016/s2215-0366\(20\)30047-X](https://doi.org/10.1016/s2215-0366(20)30047-X).
10. Ma N, Ma H, Li LJ. Reading and analysis of the guiding principles of emergent psychological crisis intervention in the novel coronavirus pneumonia. *Chin J Psychiatry* 2020, 53: E001–E001.



# Microglia Research in the 100th Year Since Its Discovery

Anthony D. Umpierre<sup>1</sup> · Long-Jun Wu<sup>1,2,3</sup>

Received: 18 December 2019 / Accepted: 9 January 2020 / Published online: 26 February 2020  
© Shanghai Institutes for Biological Sciences, CAS 2020

In 1919, Pio del Rio-Hortega first described a class of cells residing in the brain with a tiny soma and branched architecture distinguishable from astrocytes and neurons. These cells, called microglia or mesoglia, have come to be appreciated as resident immune cells in the central nervous system (CNS). In the year 2019, we review the three most recent advances in microglia research in this 100th year since their discovery (Fig. 1). We first discuss their transcriptional diversity, which allows us to appreciate the heterogeneity of microglia across species, development, diseases, and brain regions. We also highlight recent stem cell-based approaches that allow us to study human microglia. We further review new signaling mechanisms that expand our understanding of how microglia sense synaptic changes and alter neural circuits. Ultimately, 100 years of microglial research demonstrates their incredible adaptation and plasticity, playing roles in neural development, brain homeostasis, and neurological disorders far beyond their anticipated immunological function.

## Transcriptomic Analyses Reveal the Heterogeneity of Microglia

2019 marks a year with major advances in understanding microglial heterogeneity (Fig. 1A). Single-cell RNA sequencing (SC-RNAseq) beautifully characterizes the transcriptional diversity and conservation of microglia across millions of years of evolution [1]. Within a species, SC-RNAseq has helped to define clusters of transcriptionally distinct microglia. In mice, microglia have unique transcriptional profiles across development (particularly between the embryonic and postnatal periods) and across brain regions [2]. In addition, highly distinct microglial clusters have emerged in disease contexts, specific to either neurodegeneration or demyelination [2]. Similarly, human microglia also demonstrate clusters of transcriptional diversity between non-pathological gray and white matter, and between the healthy and tumoral portions of resected tissue [3]. These findings suggest that microglia can be stratified based on multiple axes of transcriptional diversity (Fig. 1A). Microglial heterogeneity can also serve as a critical lens through which to investigate brain diseases. Towards this end, studies of *Hoxb8*, one of the first markers found to differentiate microglial subtypes, demonstrate the interesting role of this subpopulation in complex behavior. The loss of *Hoxb8* in microglia particularly exacerbates pathological behaviors and anxiety in females through an as-yet unknown mechanism involving circulating sex hormones [4].

The challenge for the coming decade will be the selective functional investigation of transcriptionally unique sub-populations of microglia to evaluate their role in the intact brain. To do so, we look forward to new tools that enable researchers to distinctively label microglial populations based on transcriptomics profiles, in the

✉ Long-Jun Wu  
wu.longjun@mayo.edu

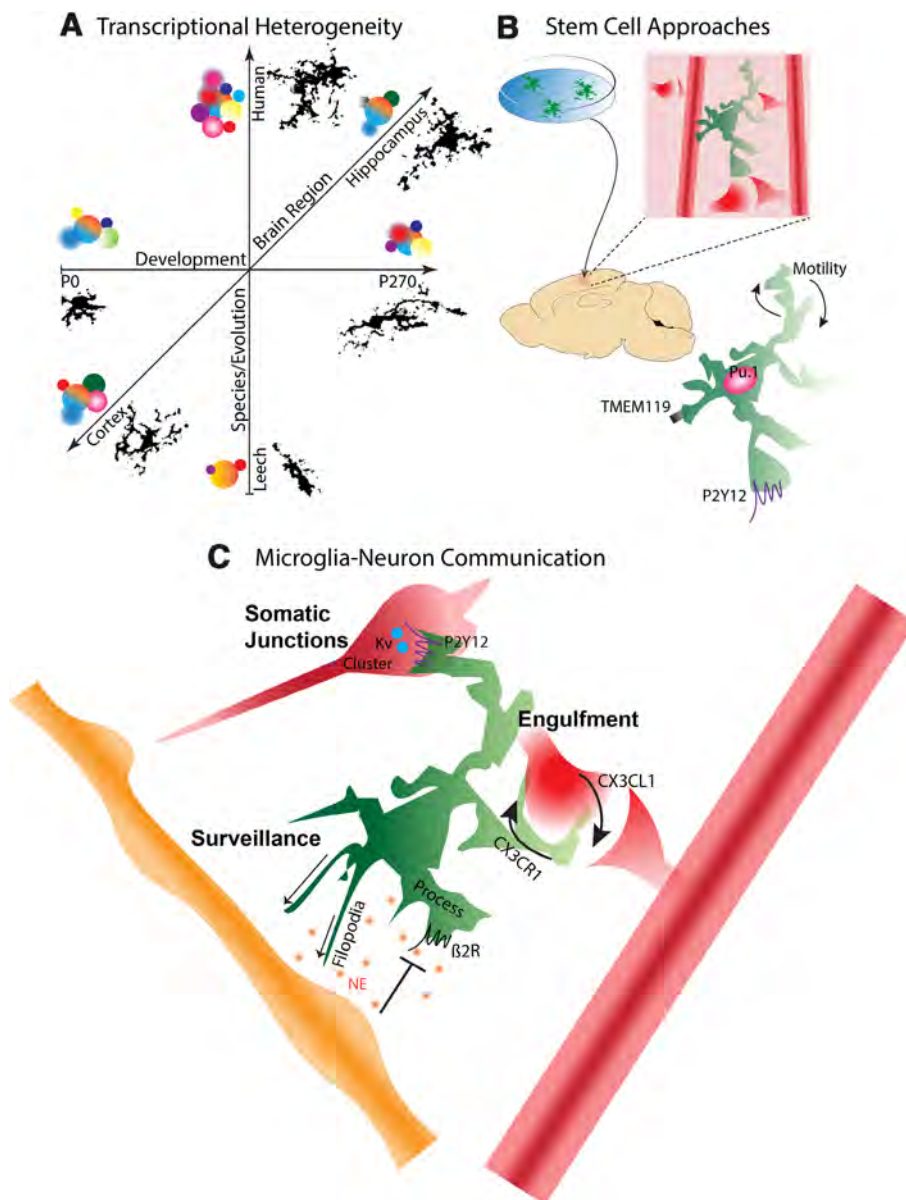
<sup>1</sup> Department of Neurology, Mayo Clinic, Rochester, MN 55905, USA

<sup>2</sup> Department of Neuroscience, Mayo Clinic, Jacksonville, FL 32224, USA

<sup>3</sup> Department of Immunology, Mayo Clinic, Rochester, MN 55905, USA

**Fig. 1** Key microglial research advances in the year 2019.

**A** Single-cell RNAseq studies show that microglial transcriptional diversity spans species, development, and brain regions in addition to noted differences in pathology. **B** Human stem cells can be induced to differentiate into microglia and implanted into the mouse brain. In this context, human microglia display canonical motility characteristics and have lineage (e.g. Pu.1, a transcription factor) and signature gene expression (e.g. the P2Y12 receptor and transmembrane protein TMEM119). **C** Novel signaling mediates microglia-neuron communication. Neuronal somatic ATP release is sensed by microglial P2Y12 receptors, forming somatic junctions between neuronal somata and microglial processes at sites with clustered potassium channels (Kv). Neuronal fractalkine (CX3CL1) signaling to the microglial receptor CX3CR1 is the basis for activity-dependent engulfment in the barrel cortex. Tonic norepinephrine (NE) from adrenergic neurons arrests microglial process surveillance through  $\beta$ 2 receptors in awake mice while also promoting nanoscale surveillance by smaller filopodia structures.



absence of a singular defining gene. Such an advance seems particularly necessary to understand the sub-populations of human microglia, which have the greatest transcriptional diversity [1].

### Stem Cell Approaches to Study Human Microglia

2019 has also seen an explosion in stem cell-based approaches to study human microglia (Fig. 1B). Technical advances in the past few decades have culminated in our ability to derive microglia from blood monocytes [5], embryonic cell lines [6], hematopoietic stem cells [7], or human induced pluripotent stem cells [8]. These microglia-

like human cells can be successfully engrafted into the developing mouse brain [6–8].

Microglia-like cells implanted into the mouse are replete with microglial signature genes [6–8], maintain markers of the myeloid lineage [7, 8], and adopt a ramified morphology [6–8] (Fig. 1B). These studies also demonstrate that human microglia display canonical motility characteristics and injury responses [7, 8]. At the same time, however, these human-derived microglia can take on a substantially different transcriptional profile in response to Alzheimer's disease (AD) pathology from neighboring mouse microglia [6, 7]. Interestingly, microglia from patients with schizophrenia even maintain their enhanced phagocytic capacity *in vitro* relative to microglia-like cells from healthy controls [5]. Because stem cells retain the genetic

profile of their source, stem cell techniques now enable researchers to study species-specific and patient-specific microglial responses to a uniform pathological context. Given the key role that microglia-driven inflammation plays in the amyloid-beta and tau pathology of AD [9], placing human microglia in a uniform AD model system could yield key insights into gene–environment interactions. Of interest, future studies would also be able to isolate and study human microglia from genetically high-risk and low-risk populations.

Apart from generating microglia from human stem cells, progress has also been made in generating neurons from adult microglia. Finding ways to reprogram microglia, with their relatively strong capacity to regenerate, could be an early step in combating neuronal loss. Towards this end, progress has been made in reprogramming adult microglia, even *in vivo*, using the transcription factor NeuroD1 [10]. Reprogrammed cells take on a neuronal transcriptional and epigenetic profile, but future work is needed to determine whether these cells properly integrate into circuitry.

### Novel Signaling Regulates Bidirectional Microglial-Neuron Communication

Key studies in 2019 have expanded our knowledge of which microglial receptors mediate critical functions such as synaptic engulfment and microenvironmental surveillance (Fig. 1C). For example, fractalkine ligand (CX3CL1) signaling to the microglial fractalkine receptor (CX3CR1) has recently been shown to be a key regulator of synapse elimination in the barrel cortex [11]. As suggested by RNAseq and validated by genetic and pharmacological approaches, neuronal cleavage of the soluble CX3CL1 by the metalloprotease ADAM10 signals to CX3CR1 to begin an active engulfment process.

In addition, new studies have also expanded our understanding of microglial  $\beta_2$  receptors in network interactions (Fig. 1C). Two studies have recently revealed that the  $\beta_2$  adrenergic receptor plays an important role in regulating microglial process surveillance in awake mice [12, 13]. These studies showed that tonic norepinephrine (NE) levels in the awake mouse attenuate the extent to which microglial processes survey their surroundings. In tandem, NE promotes tiny filopodia at the ends of these arrested microglial processes to search the local milieu, promoting a “nanoscale” level of surveillance dependent on cAMP [14]. At the systems level, approaches that dampen local or global NE levels (such as anesthesia) permit microglial process outgrowth and increase microglia-neuron contact time [12, 13]. An early implication of this interaction is that prolonged NE- $\beta_2$  signaling can negatively impact certain forms of visual plasticity [13]. In

contrast to prolonged NE- $\beta_2$  signaling, a key future question is whether a reduction in NE- $\beta_2$  signaling during sleep creates a more permissive environment for microglia to alter the synaptic landscape, contributing to plasticity.

By 2019, the role of microglia in plasticity has been well established through immunological signaling mechanisms during development [15] and pathology (e.g. hypoxia) [16]. However, the role of microglia in learning and plasticity is not merely restricted to development and immunological signaling. Recent work also demonstrates that microglia can influence motor learning or the maintenance of long-term potentiation through their release of brain-derived neurotrophic factor [17, 18].

Finally, one of the last discoveries of 2019 expands our understanding of the well-known P2Y<sub>12</sub> receptor. Previously, P2Y<sub>12</sub> has been recognized for its role in mediating microglial process interactions with neuronal synapses [19]. In addition, neuronal somata have recently been described for their inclusion of unique microdomains, which recruit microglial processes. These mitochondria-rich sites generate activity-dependent release of ATP, which recruits microglial processes through the P2Y<sub>12</sub> receptor [20]. Given the role of microglial P2Y<sub>12</sub> signaling in neuroprotection during stroke and acute seizures [19, 20], it is possible that somatic as well as synaptic microglial contacts are both critical for how microglia exert P2Y<sub>12</sub>-dependent effects. Future studies are necessary to understand exactly how microglial P2Y<sub>12</sub> signaling dampens neuronal activity and increases neuroprotection through each interaction site. Altogether, research in 2019 has greatly expanded our knowledge of the microglial signaling repertoire and its impact on the neuronal landscape. The mechanisms identified highlight both immunological and neuronal signaling axes that inform and influence neuroimmune function.

### Conclusion

The 100th anniversary of microglial research has made great strides in understanding microglial transcriptional diversity and their circuit functions. While microglia are often referred to as innate immune cells of the CNS, one of the most unanticipated discoveries of the past 100 years is the ability for microglia to sense and influence neuronal networks as part of normal development. These discoveries suggest that microglia are an integral part of neuronal circuitry. Moving forward, transcriptomics will continue to provide the road map for understanding microglial response profiles in the healthy and diseased brains. A necessary next step is to begin to use this wealth of knowledge to identify rationale candidates (receptors and signals) for detailed functional studies. Ultimately,

combining the strengths of transcriptional and functional approaches is necessary to identify key mechanisms mediating normal and pathological interactions. As we come to better understand their circuit function, we anticipate the promising development of microglia-specific therapeutics for treating neurological disorders in the decades to come.

**Acknowledgements** This insight was supported by a National Institutes of Health (NIH) F32 grant (NS114040) and the Mayo Foundation and NIH R01 grants (NS088627 and NS112144).

## References

- Geirsdottir L, David E, Keren-Shaul H, Weiner A, Bohlen SC, Neuber J, *et al.* Cross-species single-cell analysis reveals divergence of the primate microglia program. *Cell* 2019, 179: 1609–1622.
- Masuda T, Sankowski R, Staszewski O, Böttcher C, Amann L, Sagar, *et al.* Spatial and temporal heterogeneity of mouse and human microglia at single-cell resolution. *Nature* 2019, 566: 388–392.
- Sankowski R, Böttcher C, Masuda T, Geirsdottir L, Sagar, Sindram E, *et al.* Mapping microglia states in the human brain through the integration of high-dimensional techniques. *Nat Neurosci* 2019, 22: 2098–2110.
- Tränkner D, Boulet A, Peden E, Focht R, Van Deren D, Capocchi M. A microglia sublineage protects from sex-linked anxiety symptoms and obsessive compulsion. *Cell Rep* 2019, 29: 791–799.
- Sellgren CM, Gracias J, Watmuff B, Biag JD, Thanos JM, Whittredge PB, *et al.* Increased synapse elimination by microglia in schizophrenia patient-derived models of synaptic pruning. *Nat Neurosci* 2019, 22: 374–385.
- Mancuso R, Van Den Daele J, Fattorelli N, Wolfs L, Balusu S, Burton O, *et al.* Stem-cell-derived human microglia transplanted in mouse brain to study human disease. *Nat Neurosci* 2019, 22: 2111–2116.
- Hasselmann J, Coburn MA, England W, Figueroa Velez DX, Kiani Shabestari S, Tu CH, *et al.* Development of a chimeric model to study and manipulate human microglia *in vivo*. *Neuron* 2019, 103: 1016–1033.
- Svoboda DS, Barrasa MI, Shu J, Rietjens R, Zhang S, Mitalipova M, *et al.* Human iPSC-derived microglia assume a primary microglia-like state after transplantation into the neonatal mouse brain. *Proc Natl Acad Sci U S A* 2019, 116: 25293–25303.
- Ising C, Venegas C, Zhang S, Scheiblich H, Schmidt SV, Viera-Saecker A, *et al.* NLRP3 inflammasome activation drives tau pathology. *Nature* 2019, 575: 669–673.
- Matsuda T, Irie T, Katsurabayashi S, Hayashi Y, Nagai T, Hamazaki N, *et al.* Pioneer factor neuroD1 rearranges transcriptional and epigenetic profiles to execute microglia-neuron conversion. *Neuron* 2019, 101: 472–485.
- Gunner G, Cheadle L, Johnson KM, Ayata P, Badimon A, Mondo E, *et al.* Sensory lesioning induces microglial synapse elimination via ADAM10 and fractalkine signaling. *Nat Neurosci* 2019, 22: 1075–1088.
- Liu YU, Ying Y, Li Y, Eyo UB, Chen T, Zheng J, *et al.* Neuronal network activity controls microglial process surveillance in awake mice via norepinephrine signaling. *Nat Neurosci* 2019, 22: 1771–1781.
- Stowell RD, Sipe GO, Dawes RP, Batchelor HN, Lordy KA, Whitelaw BS, *et al.* Noradrenergic signaling in the wakeful state inhibits microglial surveillance and synaptic plasticity in the mouse visual cortex. *Nat Neurosci* 2019, 22: 1782–1792.
- Bernier LP, Bohlen CJ, York EM, Choi HB, Kamyabi A, Dissing-Olesen L, *et al.* Nanoscale surveillance of the brain by microglia via cAMP-regulated filopodia. *Cell Rep* 2019, 27: 2895–2908.
- Schafer DP, Lehrman EK, Kautzman AG, Koyama R, Mardinly AR, Yamasaki R, *et al.* Microglia sculpt postnatal neural circuits in an activity and complement-dependent manner. *Neuron* 2012, 74: 691–705.
- Zhang J, Malik A, Choi HB, Ko RW, Dissing-Olesen L, MacVicar BA. Microglial CR3 activation triggers long-term synaptic depression in the hippocampus via NADPH oxidase. *Neuron* 2014, 82: 195–207.
- Parkhurst CN, Yang G, Ninan I, Savas JN, Yates JR 3<sup>rd</sup>, Lafaille JJ, *et al.* Microglia promote learning-dependent synapse formation through brain-derived neurotrophic factor. *Cell* 2013, 155: 1596–1609.
- Zhou LJ, Peng J, Xu YN, Zeng WJ, Zhang J, Wei X, *et al.* Microglia are indispensable for synaptic plasticity in the spinal dorsal horn and chronic pain. *Cell Rep* 2019, 27: 3844–3859.
- Eyo UB, Peng J, Swiatkowski P, Mukherjee A, Bispo A, Wu LJ. Neuronal hyperactivity recruits microglial processes via neuronal NMDA receptors and microglial P2Y12 receptors after status epilepticus. *J Neurosci* 2014, 34: 10528–10540.
- Cserép C, Pósfai B, Lénárt N, Fekete R, László ZI, Lele Z, *et al.* Microglia monitor and protect neuronal function via specialized somatic purinergic junctions. *Science* 2020, 367: 528–537.



# Expert Consensus on the Care and Management of Patients with Cognitive Impairment in China

Academy of Cognitive Disorders of China (ACDC) · Yuliang Han<sup>1</sup> · Jianjun Jia<sup>2</sup> · Xia Li<sup>3</sup> · Yang Lv<sup>4</sup> · Xuan Sun<sup>5</sup> · Shanshan Wang<sup>5</sup> · Yongjun Wang<sup>6</sup> · Zhiwen Wang<sup>7</sup> · Jintao Zhang<sup>8</sup> · Jiong Zhou<sup>9</sup> · Yuying Zhou<sup>10</sup>

Received: 22 February 2019 / Accepted: 25 July 2019 / Published online: 2 December 2019  
© Shanghai Institutes for Biological Sciences, CAS 2019

**Abstract** The cognitive disease consensus was prepared by panels of health and public representatives based on actual clinical practice in Geriatric Departments in Chinese hospitals and a systematic literature review. This consensus reflects the medical knowledge accumulated by those experts and provides information about professional medical care and advice. A multidisciplinary panel of specialists (neurologists,

psychiatrists, and nursing specialists) reports an expert consensus on the medical knowledge accumulated from those experts and provides information about professional medical care and advice. The recommendations focus on the care and management of older adults with mild cognitive impairment, the objectives and methods of maintaining cognition and training, the assessments and measures of daily care for patients at different stages of dementia, the assessments and coping strategies for the behavioral and psychological symptoms of dementia, principles and suggestions for an appropriate living environment, arrangements for recreational activities, the care and management of patients with end-stage dementia, and suggestions for addressing stress in caregivers.

Authors are listed in alphabetical order by family name.

**Electronic supplementary material** The online version of this article (<https://doi.org/10.1007/s12264-019-00444-y>) contains supplementary material, which is available to authorized users.

✉ Jianjun Jia  
jjjianjun301@126.com

- <sup>1</sup> The 305 Hospital of People's Liberation Army, Beijing 100017, China
- <sup>2</sup> The Second Medical Center, People's Liberation Army (PLA) General Hospital, Beijing 100853, China
- <sup>3</sup> Shanghai Mental Health Center, Shanghai JiaoTong University School of Medicine, Shanghai 200030, China
- <sup>4</sup> The First Affiliated Hospital of Chongqing Medical University, Chongqing 630014, China
- <sup>5</sup> The Second Medical Center, PLA General Hospital, Beijing 100853, China
- <sup>6</sup> Shenzhen Institute of Mental Health, Shenzhen Kangning Hospital, Shenzhen 518020, China
- <sup>7</sup> Peking University School of Nursing, Beijing 100191, China
- <sup>8</sup> The 960th Hospital of People's Liberation Army, Taian 271000, China
- <sup>9</sup> The Second Affiliated Hospital, Zhejiang University School of Medicine, Hangzhou 310009, China
- <sup>10</sup> HuanHu Hospital of Nankai University, Tianjin 300350, China

**Keywords** Consensus · Healthcare · Management · Cognitive disorders

Cognition is the process by which the brain receives and processes external information to actively understand the world. Cognitive functions involve multiple areas, such as memory, attention, language, execution, reasoning, calculation, and orientation. Cognitive impairment refers to a dysfunction in one or more of these areas and affects the social function and quality of life of patients to different extents. Severe cognitive impairment may even lead to death. Cognitive impairment may be caused by multiple factors, including neurodegenerative diseases, cardiovascular and cerebrovascular diseases, nutritional and metabolic disorders, infections, trauma, tumors, and drug abuse. Cognitive impairment is divided into two stages based on severity: mild cognitive impairment (MCI) and dementia. MCI is a transitional state when the cognitive function lies between normal function and dementia. The incidence of

MCI among the elderly population aged  $\geq 65$  years is 10%–20%, and >50% of patients with MCI progress to dementia within 5 years [1–4]. The percentage of individuals with MCI who develop dementia is 10 times greater than healthy elderly individuals [5]. Therefore, MCI interventions are critical to delay the occurrence and development of dementia.

Dementia is defined as a group of diseases characterized by cognitive impairment and accompanied by psychological and behavioral symptoms, leading to reduced daily living abilities. Based on the etiology, dementia is categorized into several types, including Alzheimer's disease (AD), vascular dementia, frontotemporal dementia, dementia with Lewy bodies, among which AD is the most common, accounting for 30%–50% of all dementia cases [6]. In 2018, approximately 50 million people worldwide were living with dementia. Approximately 152 million people are estimated to be diagnosed with dementia by 2050 [7]. In China, 14% of the population aged 60 years or older had dementia in 2015, and this value will reach  $\sim 33\%$  by 2050. The number of individuals with dementia in China ranked first in the world in 2015, imposing heavy burdens on families and society [8]. Therefore, dementia care has become an integral part of treatment. The majority of dementia caregivers include direct caregivers for individuals with dementia and their partners, such as spouses, children, home-service personnel, physicians, nurses, care providers for the elderly, community service personnel, and social workers. Appropriate care and management can delay disease progression in patients with dementia and improve their quality of life, leading to an extended life span and alleviating the stress on caregivers. Developed countries have established relatively complete dementia care models. The promotion of a dementia care and management model that is suitable for China is an important problem that demands a prompt solution.

Dementia care and management models are of two main types: home care and residential care. Home care includes day care centers, part-time nanny care services, full-time nanny care services, and on-site health care services. Residential care includes senior citizen homes, dementia care institutions, assisted living facilities for the elderly, nursing homes, and dementia units. In China, the majority of patients with dementia use the home care model, and caregivers are mainly family members and close relatives [9]. However, because of changes in the family structure and an incomplete dementia care system, the establishment of a consensus cognitive impairment care and management plan that is suitable for the national conditions in China is urgently needed.

We have systematically reviewed the literature in related fields published in the last 10 years, combined with the most recent research progress, and formulated the

expert consensus described below after a collective discussion among the members of the expert group (see supplementary material). This consensus is based on the current status of dementia care in China and takes advantage of care and management experiences from other countries to offer guidance and suggestions for dementia caregivers in China, including the following: (1) MCI care and management; (2) cognitive maintenance and training; (3) daily care; (4) care and management of psychological behaviors; (5) living environment setting; (6) arrangements for recreational activities; (7) care and management of patients with end-stage dementia; and (8) suggestions for addressing stress in caregivers.

## MCI Care and Management

### Informing a Patient of an MCI Diagnosis

MCI is a common problem among the elderly population. The outcomes of MCI are stabilization, reversal to normal functions, or progression to dementia, so some patients with MCI have a poor prognosis. Informing a patient about an MCI diagnosis often involves legal and ethical issues. The key to communication is reasonable informed consent. Certain techniques and procedures are required when determining whether to directly inform and how to inform the patient and family members about the diagnosis. Studies conducted in various countries suggest that the majority of patients would like to know the diagnosis of MCI, and common reasons include “can plan for the future”, “have the right to know” and “can select treatment options”, while the reasons for not wanting to know include “will feel sad and depressed” and “knowing the truth does not help” [10]. According to recent research conducted in China, most patients would like to be informed about the true status of their diagnosis and would like family members to know, but they would like to be notified in neutral terms, such as “cognitive impairment”, “memory loss”, “brain degeneration” and “Alzheimer's disease” [11]. In general, both options have pros and cons. Currently, after confirmation of an MCI diagnosis, the recommended practice is that physicians should first sufficiently communicate with the patient's family members and then, depending on the circumstances, directly communicate with the patient. The content of the communication includes assessments of treatable risk factors, the risk ratio of conversion from MCI to dementia, whether a biomarker examination is needed to determine the possibility of a progression towards dementia, and possible interventions. The content of the communication should be beneficial for follow-up and management and minimize potential harm to the patient.

## Care and Management of Patients with MCI

Both clinical physicians and patients hope to begin interventions early during the MCI stage to delay or prevent the development and progression of dementia. Therefore, a comprehensive and detailed memory profile should be established at a patient's first visit and archived as the baseline condition; the reversible risk factors that cause further cognitive impairment are also assessed in detail [12]. Moreover, a cognitive assessment should be performed every six months. During the assessment, the patient should be accompanied by a family member, friend, or close associate. Importantly, the assessment results are only used as a diagnostic reference, and not as a diagnostic conclusion. After the assessment, the patient should be informed of the importance of early diagnosis and interventions, and they should be notified that an approved drug for the treatment of MCI is currently unavailable. Notably, joint interventions, including the comprehensive management of risk factors, cognitive training, exercise therapy and family care, social interactions, and treatment of depression, are beneficial for preventing or delaying dementia. The follow-up management should be voluntary on the part of the patient, and from the perspective of protecting the patient's interests, the patient's choice of included family members should be completely respected. During follow-up, methods to achieve the continuous management of the patient must be discussed, with the aim of establishing effective, rigorous, practical, and smooth communication and to provide the patient with integral and continuous medical services. Using the current diagnostic criteria, some misdiagnosis of MCI occurs [13], and the MCI misdiagnosis rate can be reduced through regular follow-up visits. Regular health education sessions are recommended, including methods to identify cognitive impairment at an early stage, methods to perform visits and follow-ups, methods to correct unhealthy living habits and control risk factors, and methods to improve self-care [14]. A survey of five cities in China indicated that the majority of the population has a poor awareness of AD [15] and a high demand exists for skilled care [16], which can be learned from the health education of Chinese communities in other countries [17]. The management of a population with chronic diseases should be strengthened, and medical personnel in the community should be regularly trained. Health care workers in community health service institutions should receive systematic training, including the early identification and timely referral of individuals with a high risk of cognitive impairment. Patients and caregivers should also receive regular health education. Therefore, the care and management of patients with MCI should be based on the establishment of memory profiles, regular follow-up visits, and health education.

## Maintenance of the Personal Rights of Patients with MCI

For patients with a confirmed diagnosis of MCI, physicians should inform the patients and their family members of the uncertainty of the diagnosis and prognosis. Physicians should suggest that the patients and their family members discuss long-term plans together, such as the establishment of living wills, safe driving, financial and property planning, decisions regarding medical and research participation, and entrusting specific individuals to represent their legal interests (financial and medical affairs) [12, 18], which are beneficial for the maintenance of the personal rights of patients with MCI. In addition, many countries have regulations on the regular review or cancellation of motor vehicle driver licenses of elderly individuals or patients with dementia. In China, the *Regulations of the Motor Vehicle Driver License Application and Use* also stipulates that individuals with dementia are not allowed to drive motor vehicles. However, these regulations do not provide a detailed explanation of MCI. Relevant information should be provided to patients with MCI and relatives.

## Cognitive Maintenance and Training

### The Objective of Cognitive Maintenance and Training

A patient's cognitive dysfunction and the severity of the condition should be assessed. Individualized cognitive training should be provided based on the assessment results, possible etiology, and the patient's circumstances to help maintain the current cognitive status and restore or partially restore impaired cognitive function as much as possible, thereby delaying the clinical progression of the disease and improving the patient's quality of life.

### Methods for Cognitive Maintenance and Training

#### Management of Relevant Factors, such as the Etiology and Causes

The patient's diet, exercise level, mentality, social support and past medical history, and current status should be comprehensively understood, and the relevant etiology and causes should be confirmed together with specialists. Based on the assessment results, the caregivers should implement a nutritional and drug treatment plan in daily life, observe the effects and adverse reactions of all drugs, and provide regular feedback.

## Cognitive Function Training

Training should combine individualized and standardized aspects, including a combination of individual and group training, traditional and modern medicine, family and societal elements, specialized treatment, and daily life activities, and should include assessments. Five to six 1-hour cognitive training sessions are recommended weekly, with an individualized duration and intensity that is focused on the patient's needs.

1. Assessment of cognitive functions: Detailed training plans should be created and executed according to the range and severity of cognitive impairment, the patient's condition, and the available medical and social resources near the family and in the surrounding area. Novel and complex cognitive stimulations are believed to be more effective [19].
2. Common training methods:
  - (1) Memory training: This type of training helps maintain a patient's long-term memory by allowing them to look at old photographs and recall past events and by encouraging the patient to tell their personal stories. This type of training improves the patient's logical reasoning by guiding them to classify and recall pictures, phrases, or objects. Short-term memory can be improved by having the patient recall numbers and dates, repeat phone numbers, and recall the names of previously presented objects, such as pens, glasses, and keys. The patient's delayed memory ability can be trained by showing him/her several items encountered in their daily activities, such as pens, glasses, and keys, and asking the patient to recall the names of the previously presented objects 5 min later or by guiding the patient to recall a piece of information, repeating the information and repeating the process with extended durations. In addition, other specific therapeutic techniques, such as vanishing cues, errorless learning, and internal *versus* external memory strategies, would be useful, but they are limited to the transfer of memory training to daily functions.
  - (2) Orientation training: We recommend that orientation training is incorporated into daily life. This can yield two results with half the effort by choosing memories for training and strengthening times, locations, and figures to which the patient is emotionally attached and shows interest.
  - (3) Verbal communication skill training: Methods for communication and interaction that are acceptable to the patient are recommended to help maintain their verbal communication skills. During this process, the patient should be encouraged and praised. The ability to express oneself can be trained by prompting the patient to name and describe picture cards, starting with easy tasks and progressing to more difficult tasks. Writing skills can be strengthened through transcription, dictation, writing based on pictures, and keeping a diary. The corresponding brain functions can also be activated by reading and singing.
  - (4) Visual space

and executive ability training: The patient should undergo targeted training on the items related to daily living activities, such as getting dressed, going to the restroom, bathing, identifying coins, making and receiving phone calls, and turning the TV on and off. More complicated items can also be included, such as using the washer and withdrawing money from the bank. If the patient makes mistakes during training, they should be taught in an encouraging way and should not be blamed or forced to make choices or recall things.

- (5) Calculation training: The difficulty of the training should be incrementally increased according to disease status. Simple arithmetic calculations are more beneficial. If a patient is unable to complete all the above training sessions, they are still beneficial for producing a comprehensive cognitive improvement by training a single cognitive area [20]. Better effects can be achieved using computer-assisted cognitive training [21, 22].

## Daily Care

Individualized daily care that is centered on the patient and takes the maximum advantage of the patient's remaining functions is recommended. A patient's independence can be promoted and maintained by allowing autonomous behaviors. Patients should also be encouraged to participate in meaningful and interesting activities, eat a healthy and balanced diet, and engage in regular exercise.

## Assessments

The daily living activities that can be assessed through communication with the patient/caregiver and physical examinations include vision, hearing, oral hygiene, physical ability, nutrition, function, and family environment. The assessment of daily living activities includes two aspects: basic activities of daily living, such as eating, getting dressed and taking a shower, and instrumental activities of daily living, such as managing money, shopping, driving and taking medications. Common scales for activity assessments include the Alzheimer's Disease Assessment Scale–Activities of Daily Living, the Instrumental Activities of Daily Living (IADL) scale and the Disability Assessment for Dementia scale [23]. The Mini Nutritional Assessment Short-Form is recommended as a regular assessment of the patient's nutritional status. If the patient is at an advanced stage of cognitive impairment and has an active eating disorder or behavioral symptoms, their nutritional status can be assessed using the Aversive Feeding Behaviors Inventory scale, the Edinburgh Feeding Evaluation in Dementia questionnaire, and the Eating

Behavior Scale to improve eating and nutrition issues [12, 24]. Physical ability is typically assessed by measuring grip strength, pace, and the Short Physical Performance Battery scale.

## Suggestions for Stratified Care

### Mild Dementia

The daily living activities of patients at this stage of the disease are partially impaired, and require assistance to improve and maintain their instrumental activities of daily living, such as managing money, taking public transportation, performing housework, and using appliances. Caregivers should not provide excessive care but instead urge patients to take care of themselves. Patients should have regular lives; pay attention to their diets, nutrition, and cleaning; exercise appropriately; and participate in social activities they enjoy to ensure that they are able to maintain independent living activities at a high level for as long as possible.

### Moderate Dementia

At this stage, cognitive functions gradually decline and the patient's daily living ability decreases. Caregivers must assist patients with many types of obstacles encountered in daily life. Patients should perform simple and regular self-care tasks with the help of caregivers. Caregivers should cultivate patients' confidence and security.

### Severe Dementia

At this stage, patients generally have lost their ability to take care of themselves. Caregivers should particularly focus on oral hygiene, nutritional status, and excretion to avoid complications such as aspiration pneumonia, pressure sores, and deep vein thrombosis.

## Daily Care Measures

### Basic Daily Living Activities

**(1) Eating:** For patients with any stage of cognitive impairment, caregivers should provide a pleasant dining environment, reasonable meals, and colorful, aromatic and tasty dishes according to the patient's preference. An attempt to improve cognitive functions with nutritional supplements is not recommended for patients without a nutrient deficiency [18, 24]. Patients should be encouraged to take food orally and avoid diet restrictions. If oral food

intake is <50% of the expected amount for >10 days due to disease progression or irritation, the patient should undergo tube feeding to provide enteral nutritional supplements through an indwelling nasogastric tube or gastrostomy. If contraindications exist or the patient is intolerant of tube feeding, parenteral nutrition can be administered for a short period of time [18]. Patients with dysphagia or who are fed nasally should receive focused care to prevent aspiration and choking risks. However, invasive treatments aiming to "keep the patient alive at all costs" do not extend the lifespan or improve the quality of life [25]. **(2) Dressing:** The choice of clothing should be simplified, and patients should be encouraged to dress and undress themselves. Assistance should be provided to patients who experience difficulty getting dressed. Patients should be informed, and their privacy should be protected during this process [26]. **(3) Cleaning and grooming:** Patients should be encouraged and guided to complete cleaning and grooming processes, such as hair combing, tooth brushing, shaving, and nail clipping. Patients who are unable to complete oral care procedures should be assisted in maintaining oral hygiene. Patients' teeth and dentures should be examined regularly. **(4) Outdoor activities and exercise:** Exercise should be based on long-term regular aerobic exercise and resistance training. The form of exercise can be determined individually according to the past preferences of the patient [27]. Walking, jogging, aerobics, dancing, tai chi, and progressive resistance exercises are all appropriate. During exercise, patients should perform the exercises they are capable of completing and move carefully to prevent injuries. When patients with end-stage dementia have difficulties in completing exercises, caregivers should help the patients move their muscles and joints to prevent complications such as joint deformation and muscle atrophy. **(5) Bathing and skin cleansing:** Caregivers should create a comfortable bathing environment and respect patients' habits. Patients should take baths regularly. The bathing process should be simplified, and scentless, low or neutral pH, and fat-containing soaps should be used. The skin should be moisturized with body lotion to prevent itching caused by dryness. Caregivers should also pay attention to skin damage. For patients who refuse to take baths, caregivers should look for reasons, such as fear of water, fear of being undressed, or the lack of privacy, and address these fears in an appropriate manner. **(6) Using the bathroom and incontinence:** Patients with mild or moderate cognitive impairment should be encouraged to use the bathroom independently. Assistance should be provided to patients with difficulties, such as ensuring that the patient knows where the bathroom is located and renovating the bathroom if needed [28]. In cases of incontinence, caregivers should consider potential causes and seek treatment. Patients with unknown causes of

incontinence should use the bathroom regularly and change their lifestyle to accommodate this condition. Diapers or a waterproof mattress should be used when necessary. Bedding should be changed and cleaned regularly.

### Instrumental Living Activities

**(1) Shopping:** Patients should be encouraged to shop with a shopping list. Caregivers should help patients find shopping locations, and patients should choose the right products themselves. Caregivers can help the patients with payment [29]. **(2) Driving and taking public transportation:** When patients have basically normal cognitive functions, they should be accompanied by caregivers when driving. If a patient has a score  $>1$  on the clinical dementia rating scale, they should stop driving [30–32]. When patients travel by public transportation, caregivers should accompany them and help them find stations and routes. **(3) Cooking:** Caregivers should know a patient's cooking habits and guide them in preparing cooking materials. The patient can then complete the cooking steps according to the recipe. When necessary, caregivers should remind the patient about appropriate techniques and help ensure a safe cooking process. **(4) Housekeeping:** Caregivers should encourage and assist patients to participate in as many housework activities as possible, such as washing dishes and clothes, making the bed, and sweeping. **(5) Telephone use:** Caregivers should know the patient's past ability to use a phone, remind them to search for phone numbers, and encourage and guide them to make independent phone calls. **(6) Medication management:** Caregivers should supervise patients in taking medications, observe adverse reactions, and prevent excessive use or misuse of medications. If patients refuse to take their medications, caregivers should identify the causes and seek professional help when necessary. **(7) Financial management:** Caregivers should know their patient's financial management capability and remind or assist them in paying bills, such as water, power, gas, and phone bills. Caregivers should assist legal guardians in helping patients with financial issues.

### Care and Management of Psychological Behaviors

Behavioral and psychological symptoms of dementia (BPSD) are defined as abnormalities or disruptions of perceptions, mood, and thoughts during the development and progression of cognitive impairment, including hallucinations, illusions, delusions, anxiety, depression, indifference, irritability, impulsive behaviors, and behavioral disinhibition [33]. BPSD is very stressful for patients but also imposes a substantial burden on caregivers.

### BPSD Care Principles

1. Combine professional care and family care.
2. Understand the patient's characteristics, including personality, hobbies, remaining abilities, and previous experiences, and identify patient-centered care approaches.
3. Regularly assess the effects of care and continuously improve them. Care for the behavioral and psychological symptoms should cover the entire disease course.
4. Non-pharmacological care interventions are preferred for BPSD care, and drug treatments should also be combined with non-medication interventions. The intervention methods should be administered incrementally and assessed prior to and after the intervention to ensure that the care methods are continuously improved.
5. Protect the safety of patients and keep them away from dangerous items.

### BPSD Identification and Assessment

A prerequisite for alleviating BPSD is their correct identification and assessment. The predisposing factors, manifestations, duration, frequency, and intensity of the symptoms and their effects on the patient and caregiver should be recorded in detail. Assessment has been performed using instruments such as the Narcissistic Personality Inventory Questionnaire and the Global Deterioration Scale [34, 35].

### BPSD Interventions

- (1) Delusion: Delusion is often a source of a patient's insecurity. Delusions of being robbed or persecuted are common symptoms. Caregivers should provide support to the patient through their speech and behavior, such as giving the patient the "banking deposit book" or "stolen money". Delusions can also be addressed through non-pharmacological methods, such as music, art, and cognitive therapies [36].
- (2) Hallucination: Careful observation and recording can help caregivers discover the triggers of hallucinations. Gentle treatment of the patient, providing distractions and reducing hostility and distrust are all helpful in alleviating symptoms. Glasses and hearing aids should be used for patients with visual and hearing impairments. Dangerous items such as knives, scissors, and ropes should be stored in safe places. Patients should be kept away from gas, and the doors and windows should be closed to prevent accidents.
- (3) Agitation/aggression: The causes and precipitating factors for agitation/aggression should first be determined. Methods such as persuasion, explanation, or distraction can help calm the patient. Safety measures should be implemented without restricting a patient's movements. The agitation symptoms and aggressive behavior can be alleviated by providing ample

opportunities to participate in games, music therapy [37], touch therapy [38], aromatherapy [39], and daylight exposure therapy [40]. (4) Depression/dysthymia: The patient should remain in a safe and quiet environment. Exposure to a sufficient amount of natural sunshine and music and verbal communication can effectively prevent and alleviate depression [41, 42]. Suicide and self-injury should be prevented in patients with severe depression. Patients should be treated by specialists in a timely manner. (5) Anxiety: For patients with mild to moderate symptoms, group reminiscence therapy, touch therapy, and play therapy can provide opportunities to increase social interactions, enhance their pleasure, and enrich their daily life, which subsequently helps to alleviate anxiety [43]. (6) Elation/euphoria: This symptom is manifested by excessive happiness, satisfaction, increased talking, and patient's facial expressions of a naïve and uncoordinated impression. The caregiver should respect the patient and should not force them to stop but instead listen patiently, gently comfort and persuade them to ensure that their elation/euphoria does not affect the safety of the patient or surrounding people. The caregiver can adjust the environment as needed, shift the patient's attention, and avoid irritating language and behavior. The caregiver can also increase the patient's activity and arrange for them to listen to music, watch TV, play chess, read newspapers, or engage in other activities according to their hobbies and interests to maintain a good state. (7) Apathy/indifference: Apathy and indifference are common symptoms experienced by patients with dementia. Caregivers must improve the patient's care in daily life [44], including the diet, daily life, personal hygiene and assistance with performing moderate physical exercise. (8) Disinhibition: For patients who are impulsive, speak rudely, swear, or are sexually hyper-excited, caregivers should prevent violent impulsive behavior without arguing, correcting, or engaging face-to-face conflict. The caregivers can distract a patient's attention and let them perform active exercises to minimize the symptoms. Patients should be treated in a timely manner if they have severe disinhibited behavior [45]. (9) Irritability/emotional instability: The cause, triggers and characteristics of this behavior must be identified, and stimuli that easily trigger emotional fluctuations should be avoided. A patient's fluctuating emotions can also be alleviated or calmed through non-drug treatments, such as soothing music therapy, physical activities, or sunbathing. (10) Abnormal activities: Patients with repetitive language or other abnormal behaviors can be comforted, neglected, or distracted. For patients with a tendency to leave safe areas, the incidence of becoming lost can be reduced by setting up an appropriate environment or arranging numerous daytime activities [46]. (11) Sleeping/night behavior: Patients with this type of symptom should avoid becoming

too hungry or too full before going to sleep, and their daytime activities and physical exercise levels should be increased. Night-time sounds and light stimulation should be reduced and potentially accompanied by individualized music therapy [47]. Patients with daytime rhythm disorders and "sunset syndromes" can receive phototherapy [48, 49]. (12) Appetite and eating disorders: For patients with a reduced appetite, causes should be actively sought and treated in a timely manner. In addition, timely interventions should be provided for patients with eating disorders. Caregivers should help feed patients with end-stage dementia. (13) Medications that improve the cognitive function of patients with moderate to severe BPSD are the basic treatment for dementia. Currently, commonly used medications include cholinesterase inhibitors and N-methyl-D-aspartate receptor antagonists, among which memantine is highly effective in alleviating hallucinations, agitation, aggressiveness, and severe stereotypic behaviors [50]. Non-drug therapy is the primary option for BPSD. If non-drug interventions are ineffective, a combination of drug treatments and non-drug interventions is recommended [41, 42]. Antipsychotics, antidepressants, and benzodiazepines may be used for a short period, when necessary.

## Living Environment Setting

### Principles in Establishing the Living Environment

Along with decreasing cognitive function, patients often exhibit a decreased ability to orient and adapt to the environment. Patients are more prone to falls and becoming lost, and an unfamiliar environment and inappropriate environmental stimulation can increase a patient's insecurity, which may induce agitation [51]. Therefore, friendly living environments should be established for patients with cognitive impairment according to the following principles: (1) ensure the safety of the environment to prevent accidental injuries and getting lost or falling, (2) maintain the stability and familiarity of the environment and avoid sudden changes, (3) design time and orientation clues to facilitate time and location orientation, and (4) provide proper sensory stimuli.

### Suggestions for Establishing the Living Environment Setting

#### Ensure Environmental Safety

(1) Prevent falls: Furniture should be as simple as possible, and clutter and sharp corners should be minimized. Non-

slip materials should be used for the floor, and the floor should be quickly dried in the event of a spill. Stairs should not be located in the active area, and small carpets should be avoided to prevent tripping [52]. Handrails should be installed next to the toilet and bath, and automatic night-lights should be installed in the bedroom, hallway, and bathroom [53]. (2) Prevent getting lost: Locks that the patient is unable to open easily should be installed. Curtains and pictures can be used to hide exits. Modern electronics such as door and window sensing devices, remote alarm systems, and electronic positioning devices should be used [54, 55]. Caregivers should inform neighbors and relevant personnel in the community about the condition of the patient so they can receive timely assistance. Care institutions can use circular or ring-shaped architectural designs. (3) Manage hazardous items: Toxic, harmful, sharp, or fragile items, such as medications, knives, scissors, glass containers, detergents, expired food, chopsticks, and toothbrushes, should be locked up. Gas and power safety and alarm devices should be installed. We recommend that the gas valve is shut off [56] and that seasonings are stored properly in the kitchen to prevent the patient from mistakenly eating them. The power sources of small appliances such as ovens, microwaves, and electric kettles should be turned off, and the temperature of the water heater should be decreased. Mirrors should be removed for patients with end-stage dementia.

#### **Ensure that the Environment is Stable and Familiar**

(1) Patients with cognitive impairment should live in an environment with which they are as familiar as possible and avoid sudden changes in the residence (such as moving, intermittently staying at children's homes, or moving to care institutions), layout, and items in the living space [51]. (2) If the patient must change their residence, items with which they are familiar or like, such as small pieces of furniture, photos, pictures, and souvenirs, should be placed in the living area to help them identify their new environment [52]. (3) Institutions that treat patients with cognitive impairment should create small units and home-like environments, such as letting the patients have their own rooms and providing a living room, small kitchen, and dining room resembling a home. Some of the patient's own furniture, photos, and items should be included in their room, and frequent room changes should be avoided [51, 57].

#### **Design Orientation Clues**

(1) Time and direction clues: Large clocks and calendars should be placed in prominent locations in the active areas, including the bedroom, living room, and dining room.

Pictures showing the current season and upcoming holidays should be designed to help patients identify time [58]. (2) Directional guidance signs: Photos or pictures that the patient is able to recognize should be attached to the door to help them identify their own room. Simply designed direction signs, such as words or patterns, to guide patients in locating the bathroom, kitchen, or dining room, should be used. Daily supplies should be placed in stable and prominent locations, and the outsides of cabinets and drawers should be labelled [59].

#### **Provide Proper Sensory Stimulation**

(1) Light stimulation: The active areas should maintain bright and uniform natural or artificial light and avoid glare or dim light. The mirror should be placed in a location that will not easily produce reflections. Strong sunlight should be blocked with curtains [52, 60]. (2) Color stimulation: The walls, curtains and sheets should have warm and bright colors. Brightly colored photos, pictures, decorations, flowers, and plants should be hung or placed in the living space. (3) Sound stimulation: Noises and excessive quiet should be avoided. Appropriate sound stimulation should be maintained based on the patient's preference, such as playing songs, music, plays, and comic dialogues the patient likes [61]. For patients who are bedridden and unable to leave their room/residence, the use of recording or projection technology to allow the patient to listen to sounds from nature, such as birds or ocean sounds, is recommended [62]. (4) Tactile stimulation: Items evoking different tactile sensations, such as sponges and sand, should be placed in the living area [52]. Simulation dolls or pets that the elderly patient likes should be provided [63, 64]. (5) Olfactory stimulation: The windows should be opened regularly for ventilation, to remove odors from the room and maintain a supply of fresh air. (6) If possible, care facilities should establish a multi-sensory stimulation room that uses light, music, aroma, and various objects to provide multiple sensory stimuli for patients with cognitive impairment [65].

#### **Maintain Privacy and Sociality**

(1) Privacy: A private environment can provide physical and psychological safety for the patient. The patient should be provided with their own space according to past living habits [66]. Curtains are recommended for care facilities or 2-person or multi-person rooms. (2) Sociality: Spaces should be set up for group activities such as activity rooms, living rooms, dining rooms, and reading rooms [67].

## Arrangements for Recreational Activities

### Principles of Recreational Activity Arrangements

Active participation in recreational activities can provide patients with cognitive impairment opportunities for self-expression and social interaction, which is beneficial for maintaining personal abilities and provides pleasant experiences. The arrangement of recreational activities should follow the principles described below. (1) Activities should have a proper level of difficulty that matches the patient's existing physical function and cognitive ability. Activities that are too difficult are frustrating and activities that are too easy may be boring. (2) The activities should combine a patient's interests and preferences and make them happy. Caregivers should note the patient's reactions during and after the activity, as well as the completion status, to draw conclusions and help the patient find appropriate activities in which to participate. (3) The difficulty and participation mode of the activities should be flexibly adjusted. Turning the activities into tasks and forcing the patients to participate should be avoided. Patients should be encouraged and guided during the activities. (4) The duration of each activity should not be too long, and the patients should not be too "busy" [68].

### Suggestions for Recreational Activity Arrangements

**(1) Physical exercise:** Physical exercise helps strengthen the physique and maintain social functions. Caregivers should guide patients with cognitive impairment in performing regular activities [69] such as walking, strolling around a park, hiking, performing tai chi, and other health exercises. Caregivers can also lead the patients in limb and finger activities, such as swinging the upper limbs and performing finger exercises [52, 70]. **(2) Family activities:** Family members are the most important social support system for patients with cognitive impairment. Activities performed with family members are the most familiar and safest experiences for patients [71]. Therefore, caregivers should create opportunities for patients and family members to dine, chat, take walks, go shopping, and perform simple household tasks, such as picking and washing vegetables, cooking, dishwashing, cleaning the desk, stuffing and addressing envelopes, and gardening. For patients who are housed in care institutions, caregivers should create more opportunities for family members to visit [72]. The establishment of a simulated supermarket that allows patients to buy their preferred daily necessities with tokens is recommended. **(3) Reminiscence activities:** If patients with cognitive impairment still have some memory function, activities that stimulate their memories

of past events or experiences, such as looking through and talking about old photos, listening to old songs, watching old movies, talking about past events, and revisiting old places, are recommended [42, 73]. **(4) Sensory and cognitive stimulation:** Suitable sensory and cognitively stimulating activities based on the patient's preferences and existing abilities are recommended, such as singing, listening to music, following the beat of music, touching flowers, smelling the scents of flowers or perfume [74], receiving a massage or emotional touch [75], and interacting with pets [42]. Patients can perform some manual activities, such as origami, paper-cutting, flower-arranging, weaving, beading, jigsaw puzzles, interacting with building blocks, playing pick-up sticks, writing, drawing, and coloring. Caregivers can also perform some activities together with the patients such as simple calculations, labelling and classifying items, and playing chess and cards; however, patients should not be forced to perform difficult calculations [71, 76].

## Care and Management of Patients with End-Stage Dementia

End-stage dementia is defined as the state at which the dementia has progressed to the most severe stage. Memory and other cognitive functions are severely impaired. Patients have no autonomous needs, have lost the ability to complete daily living activities, and have urinary and fecal incontinence. Common complications include dysphagia, fever, and lung infections [26]. At this stage, the clinical dementia rating scale score is 3 and patients have a score of 7 on the Global Deterioration Scale. Patients with end-stage dementia require complete care from others. Palliative and soothing care is typically provided to these patients.

### Deciding on Care and Medical Treatment Plans

Soothing therapy and hospice care are usually administered to patients with end-stage dementia. Both physicians and guardians must coordinate to determine care and medical treatment plans. The decision can be made through an open family interview. The physician informs the patient's guardian of the prognosis, options, and medical principles to be followed and answers any of the guardian's questions. The guardian can decide on a care and medical treatment plan that is suitable for the patient based on the patient's will and family customs.

If soothing therapy and hospice care are determined to be the appropriate management, these treatments can be

provided at home or in a retirement home, nursing home, hospice site, or other institution.

### Suggestions for End-Stage Care

Under current Chinese law, if the guardian decides to actively extend the patient's life, the patient should be sent to a medical institution that is able to provide nasal feeding, gastrostomy, or parenteral nutrition as needed [77]. In the presence of an infection or organ failure, necessary treatments and rescue measures should be administered to extend the patient's life in an appropriate manner.

The adoption of soothing therapy and hospice care does not mean that the patient is allowed to die, but instead, this care is provided under the principles of reducing pain and maintaining patient dignity [78]. If the guardian decides on this option, the patient typically receives care through one of the following methods:

- (1) Eating difficulty: The patient should be fed small amounts of food multiple times per day.
- (2) Respiratory tract infection: The physician's advice should be followed. Caregivers should let the patient inhale oxygen, turn him/her over, pat his/her back, aspirate sputum, and administer the appropriate medication.
- (3) Urinary tract infection: The urethra, vulva, and perineum must be cleaned regularly. The patient should be replenished with a sufficient amount of water. The patient's bladder is flushed when necessary.
- (4) Pressure sores: The patient's position must be shifted regularly and the patient should be assisted with some mild activities on the bed. The patient's clothes are changed regularly and the skin is kept clean and dry to prevent pressure sores. If conditions allow, the patient can use an air bed.
- (5) Pain: Analgesic medication should be provided according to the doctor's advice.
- (6) Oral care: The patient's mouth should be kept clean and moist.
- (7) Other: It should be determined whether the patient is comfortable and peaceful. The patient's dignity should be maintained. The patient should be continuously assessed and the care measures updated when needed. Touch, music, and other means should be used to pacify the patient.

### Suggestions for Addressing Stress in Caregivers

#### Definition and Classification of the Stress Experienced by Caregivers of Patients with Cognitive Impairment

Caregiver stress, also known as caregiver burden, refers to various adverse effects on the emotions, economics, health, and mentality of caregivers while caring for patients [79]. The main burdens on caregivers of patients with dementia include psychological (including social psychology), physical, and economic burdens, among which the psychological burden is the most important. Caregiver stress affects the caregiver's physical and mental health. Fifty-nine percent of home-based caregivers of patients with dementia have very high levels of psychological stress and 40% have depression; only 5%–17% of caregivers of patients with other disorders experience depression [80]. The ratio of caregivers with depression increases as dementia progresses [81]. For many caregivers, the care provided often affects their own health. Caregivers are more susceptible to other diseases or complications when caring for patients with dementia [82]. For example, caregivers have a higher risk of hypertension and cardiovascular diseases [83, 84].

#### The Manifestation of Stress in Caregivers of Patients with Cognitive Impairment

Although financial burdens are included in the stress experienced by the caregivers of patients with cognitive impairment, the most prominent manifestations are physical and psychological stress. Detailed manifestations include an attitude of denial, anxiety, irritability, frustration, emotional instability, insomnia, social difficulties, distraction, exhaustion, and fatigue. For example, caregivers may deny the dementia diagnosis of their family member. They are anxious about the future. They are angry with the patient, themselves and others. Their beliefs are shaken after a series of setbacks. They often wake in the middle of the night or have nightmares. They are lonely but are not willing to interact with friends. They have difficulty in focusing their attention and cannot complete complicated tasks. These stresses gradually cause mental and physical damage, leading to weight loss or gain, and caregivers often suffer from chronic diseases.

#### Factors Affecting the Stress Experienced by Caregivers of Patients with Cognitive Impairment

Factors affecting the stress experienced by caregivers of patients with dementia are complicated and related to the characteristics of the caregiver, the disease status of the

patient, and the care environment (family status). These factors mainly include the closeness of the relationship between caregiver and patient, the gender of the caregiver, how they cope with stress, ethnic, and cultural differences, the patient's dementia symptoms and BPSD, and encouragement and support from other family members.

## Addressing Caregiver Stress

### Stress Assessment

According to the Basic Activities of Daily Living questionnaire and the IADL questionnaire, the time spent each day providing care for a patient with dementia is an important metric when studying the indirect financial burden of dementia [85]. The Zarit Burden Interview (ZBI) scale is used to assess the stress of caregivers [69]. The short form or filtered version of this scale has also been used to assess caregiver stress. In addition, caregiver stress has been assessed using the Cardio Stress Index, the Screen for Caregiver Burden, the Simplified ZBI scale, the Positive Aspects of Caregiving scale and the Coping with Stress Scale.

### Methods of Addressing Caregiver Stress

The burden of the caregivers of patients with dementia can be alleviated by providing effective and targeted interventions and follow-up, which then conserve comprehensive health resources (by delaying the time for which patients visit a professional care institution) to achieve the eventual goal of alleviating the financial burden and pressure of dementia on society. The main methods for alleviating caregiver stress are described below. (I) Adjusting psychological and social stress: (1) Caregivers' mental stress, and physical and psychological status should be assessed regularly by specialists. Medical personnel can become involved in caring for the patient with dementia and provide professional guidance, proactive health education and psychosocial support to alleviate the care burden [86, 87]. (2) Caregivers should adjust their attitude and understanding and learn to effectively cope with stress. Caregivers should block out some time for themselves and perform activities that make them happy and fulfilled. (3) Trust should be established between the caregiver, patient, friends, and family members. The caregivers should not blame themselves when the patient experiences a difficulty, and they should understand that difficulties arise with disease progression. The caregivers should also establish a communication mechanism to ensure that they can seek help in a timely manner when they are unable to cope with the psychological pressure. (4) A professional team of

nurses, physiotherapists, and doctors should provide online counselling services and support for the caregivers, while caregivers can communicate with each other on a website. (5) A complete social support system should be established to reduce the burden on caregivers. Through social gatherings or regular family meetings, caregivers can share and discuss the difficulties they face and their experiences. They can also seek help from social support agencies to allow them some time to relax and take a break. (6) A psychological education plan should be developed, and cognitive behavioral therapy should be used to encourage caregivers to learn psychological relaxation techniques, which are beneficial to both the patients and caregivers [88, 89]. (II) Addressing physical stress: (1) The caregivers should be encouraged to pay attention to and maintain their own health. (2) Physicians should anticipate potential problems during patient care and interview the caregivers during patient visits to assess the caregiver's health status and potential problems. Physicians can then provide appropriate medical suggestions based on the caregiver's health status. (3) Attendance at some pleasant leisure recreational activities is beneficial for the caregiver's physical and mental health. Caregivers should also choose nutritious and preferred food. (4) Caregiver knowledge of dementia should be improved, and they should be provided care plans and coping techniques, such as training in proper patient transportation methods. (5) The use of new technologies can improve patient function and reduce dependence on caregivers. For example, the use of equipment to assist caregivers with moving patients who are unable to move can reduce the physical burden on caregivers. (6) Regular day and holiday care should be arranged. Caregivers require vacations, rest, and recreation time to ensure that they are physically and mentally rested. (III) Addressing financial burdens: (1) The financial burden and relevant factors related to the care of patients with dementia should be assessed to provide a reference for the development of proper medical care plans, new health care policies, social resource support plans, and medical insurance plans [90, 91]. (2) According to previous studies, anti-dementia medication can reduce medical costs, which then reduces the caregiver's financial burden [92]. (3) Improving the care abilities and financial status of caregivers might also alleviate their financial burden.

In the process of caring for patients with dementia, medical staff should establish a communication mechanism with caregivers and family members to jointly evaluate and address various problems. Non-drug interventions should be implemented as the main measure, and the principle of individualization should be emphasized. In addition, while focusing on patients, medical professionals should also monitor the pressure and response of caregivers.

## References

- Behrman S, Valkanova V, Allan CL. Diagnosing and managing mild cognitive impairment. *Practitioner* 2017, 261: 17–20.
- Langa KM, Levine DA. The diagnosis and management of mild cognitive impairment: a clinical review. *JAMA* 2014, 312: 2551–2561.
- Sanford AM. Mild cognitive impairment. *Clin Geriatr Med* 2017, 33: 325–337.
- Petersen RC. Mild cognitive impairment. *Continuum (Minneapolis)* 2016, 22: 404–418.
- Manly JJ, Tang MX, Schupf N, Stern Y, Vonsattel JP, Mayeux R. Frequency and course of mild cognitive impairment in a multiethnic community. *Ann Neurol* 2008, 63: 494–506.
- Alzheimer's Association. 2018 Alzheimer's disease facts and figures. *Alzheimers Dement* 2018, 14: 367–429.
- Alzheimer's Disease International (ADI). World Alzheimer Report, 2018.
- Wang LN. Pay close attention to dementia patients health caregivers' issue. *Chin J Intern Med* 2006, 45: 266.
- Yang Z, Zhang DM, Chen R, Hu Z. A survey on care and caregiver of people with dementia in five provinces in China. *Anhui Med J* 2013, 34: 847–850.
- van den Dungen P, van Kuijk L, van Marwijk H, van der Wouden J, Moll van Charante E, van der Horst H, *et al.* Preferences regarding disclosure of a diagnosis of dementia: a systematic review. *Int Psychogeriatr* 2014, 26: 1603–1618.
- Zou Y, Song N, Hu YB, Gao Y, Zhang YQ, Zhao QH, *et al.* Caregivers' attitude toward disclosure of Alzheimer's disease diagnosis in Urban China. *Int Psychogeriatr* 2017, 29: 1849–1855.
- Petersen RC, Lopez O, Armstrong MJ, Getchius TSD, Ganguli M, Gloss D, *et al.* Practice guideline update summary: Mild cognitive impairment: Report of the Guideline Development, Dissemination, and Implementation Subcommittee of the American Academy of Neurology. *Neurology* 2018, 90: 126–135.
- Edmonds EC, Delano-Wood L, Jak AJ, Galasko DR, Salmon DP, Bondi MW, *et al.* "Missed" mild cognitive impairment: high false-negative error rate based on conventional diagnostic criteria. *J Alzheimers Dis* 2016, 52: 685–691.
- Whitlatch CJ, Orsulic-Jeras S. Meeting the informational, educational, and psychosocial support needs of persons living with dementia and their family caregivers. *Gerontologist* 2018, 58: S58–S73.
- Zeng F, Xie WT, Wang YJ, Luo HB, Shi XQ, Zou HQ, *et al.* General public perceptions and attitudes toward Alzheimer's disease from five cities in China. *J Alzheimers Dis* 2015, 43: 511–518.
- Xu L, Hsiao HY, Denq W, Chi I. Training needs for dementia care in China from the perspectives of mental health providers: who, what, and how. *Int Psychogeriatr* 2018, 30: 929–940.
- Woo BKP. An evaluation of YouTube in disseminating dementia knowledge to older Chinese in Britain. *Int Psychogeriatr* 2018, 30: 1575.
- Burla C, Rego G, Nunes R. Alzheimer, dementia and the living will: a proposal. *Med Health Care Philos* 2014, 17: 389–395.
- Gates NJ, Sachdev P. Is cognitive training an effective treatment for preclinical and early Alzheimer's disease? *J Alzheimers Dis* 2014, 42 Suppl 4: S551–559.
- Corbett A, Owen A, Hampshire A, Grahn J, Stenton R, Dajani S, *et al.* The effect of an online cognitive training package in healthy older adults: an online randomized controlled trial. *J Am Med Dir Assoc* 2015, 16: 990–997.
- Liang JH, Xu Y, Lin L, Jia RX, Zhang HB, Hang L. Comparison of multiple interventions for older adults with Alzheimer disease or mild cognitive impairment: A PRISMA-compliant network meta-analysis. *Medicine (Baltimore)* 2018, 97: e10744.
- Hill NT, Mowszowski L, Naismith SL, Chadwick VL, Valenzuela M, Lampit A. Computerized cognitive training in older adults with mild cognitive impairment or dementia: a systematic review and meta-analysis. *Am J Psychiatry* 2017, 174: 329–340.
- Kojima G. Quick and simple FRAIL scale predicts incident activities of daily living (ADL) and instrumental ADL (IADL) disabilities: A systematic review and meta-analysis. *J Am Med Dir Assoc* 2018, 19: 1063–1068.
- Volkert D, Chourdakis M, Faxen-Irving G, Fruhwald T, Landi F, Suominen MH, *et al.* ESPEN guidelines on nutrition in dementia. *Clin Nutr* 2015, 34: 1052–1073.
- Finucane T. Thinking about life-sustaining treatment late in the life of a demented person. *Georgia Law Rev* 2001, 35: 691–705.
- Bartley MM, Suarez L, Shafi RMA, Baruth JM, Benarroch AJM, Lapid MI. Dementia care at end of life: current approaches. *Curr Psychiatry Rep* 2018, 20: 50.
- Goncalves AC, Cruz J, Marques A, Demain S, Samuel D. Evaluating physical activity in dementia: a systematic review of outcomes to inform the development of a core outcome set. *Age Ageing* 2018, 47: 34–41.
- Illiffe S, Wilcock J, Drennan V, Goodman C, Griffin M, Knapp M, *et al.* Changing practice in dementia care in the community: developing and testing evidence-based interventions, from timely diagnosis to end of life (EVIDEM). Southampton (UK): NIHR Journals Library, 2015.
- Bidzan L, Bidzan M, Pachalska M. The effects of intellectual, physical, and social activity on further prognosis in mild cognitive impairment. *Med Sci Monit* 2016, 22: 2551–2560.
- Sinnott C, Foley T, Forsyth J, McLoughlin K, Horgan L, Bradley CP. Consultations on driving in people with cognitive impairment in primary care: A scoping review of the evidence. *PLoS One* 2018, 13: e0205580.
- Frank CC, Lee L, Molnar F. Driving assessment for people with dementia. *Can Fam Physician* 2018, 64: 744.
- Hamdy RC, Kinser A, Kendall-Wilson T, Depelteau A, Whalen K, Culp J. Driving and patients with dementia. *Gerontol Geriatr Med* 2018, 4: 2333721418777085.
- Kales HC, Gitlin LN, Lyketsos CG. Assessment and management of behavioral and psychological symptoms of dementia. *BMJ* 2015, 350: h369.
- Jecmenica-Lukic M, Pekmezovic T, Petrovic IN, Tomic A, Svetel M, Kostic VS. Use of the Neuropsychiatric inventory to characterize the course of neuropsychiatric symptoms in progressive supranuclear palsy. *J Neuropsychiatry Clin Neurosci* 2018, 30: 38–44.
- Lin X, Haralambous B, Pachana NA, Bryant C, LoGiudice D, Goh A, *et al.* Screening for depression and anxiety among older Chinese immigrants living in Western countries: The use of the Geriatric Depression Scale (GDS) and the Geriatric Anxiety Inventory (GAI). *Asia Pac Psychiatry* 2016, 8: 32–43.
- Wang G, Albayrak A, van der Cammen TJM. A systematic review of non-pharmacological interventions for BPSD in nursing home residents with dementia: from a perspective of ergonomics. *Int Psychogeriatr* 2018: 1–13.
- Elliott M, Gardner P. The role of music in the lives of older adults with dementia ageing in place: A scoping review. *Dementia (London)* 2018, 17: 199–213.
- Woods DL, Dimond M. The effect of therapeutic touch on agitated behavior and cortisol in persons with Alzheimer's disease. *Biol Res Nurs* 2002, 4: 104–114.
- Yang MH, Lin LC, Wu SC, Chiu JH, Wang PN, Lin JG. Comparison of the efficacy of aroma-acupressure and aromatherapy for the treatment of dementia-associated agitation. *BMC Complement Altern Med* 2015, 15: 93.

40. Konis K, Mack WJ, Schneider EL. Pilot study to examine the effects of indoor daylight exposure on depression and other neuropsychiatric symptoms in people living with dementia in long-term care communities. *Clin Interv Aging* 2018, 13: 1071–1077.
41. Abraha I RJ, Trotta FM, Dell'Aquila G, Cruz-Jentoft A, Petrovic M, Gudmundsson A, *et al.* Systematic review of systematic reviews of non-pharmacological interventions to treat behavioural disturbances in older patients with dementia. The SENATOR-OnTop series. *BMJ Open* 2017, 16: e012759.
42. Scales K, Zimmerman S, Miller SJ. Evidence-based nonpharmacological practices to address behavioral and psychological symptoms of dementia. *Gerontologist* 2018, 58: S88–S102.
43. Blake M. Group reminiscence therapy for adults with dementia: a review. *Br J Community Nurs* 2013, 18: 228–233.
44. Theleritis C, Siarkos K, Politis AA, Katirtzoglou E, Politis A. A systematic review of non-pharmacological treatments for apathy in dementia. *Int J Geriatr Psychiatry* 2018, 33: e177–e192.
45. Garriga M, Pacchiarotti I, Kasper S, Zeller SL, Allen MH, Vazquez G, *et al.* Assessment and management of agitation in psychiatry: Expert consensus. *World J Biol Psychiatry* 2016, 17: 86–128.
46. Sarkamo T, Laitinen S, Numminen A, Kurki M, Johnson JK, Rantanen P. Pattern of emotional benefits induced by regular singing and music listening in dementia. *J Am Geriatr Soc* 2016, 64: 439–440.
47. Guarnieri B, Musicco M, Caffarra P, Adorni F, Appollonio I, Arnaldi D, *et al.* Recommendations of the Sleep Study Group of the Italian Dementia Research Association (SINDem) on clinical assessment and management of sleep disorders in individuals with mild cognitive impairment and dementia: a clinical review. *Neurol Sci* 2014, 35: 1329–1348.
48. Dowling GA, Graf CL, Hubbard EM, Luxenberg JS. Light treatment for neuropsychiatric behaviors in Alzheimer's disease. *West J Nurs Res* 2007, 29: 961–975.
49. Burns A, Allen H, Tomenson B, Duignan D, Byrne J. Bright light therapy for agitation in dementia: a randomized controlled trial. *Int Psychogeriatr* 2009, 21: 711–721.
50. Suzuki H, Inoue Y, Nishiyama A, Mikami K, Gen K. Clinical efficacy and changes in the dosages of concomitantly used psychotropic drugs in memantine therapy in Alzheimer's disease with behavioral and psychological symptoms on dementia. *Ther Adv Psychopharmacol* 2013, 3: 123–128.
51. Soril LJ, Leggett LE, Lorenzetti DL, Silvius J, Robertson D, Mansell L, *et al.* Effective use of the built environment to manage behavioural and psychological symptoms of dementia: a systematic review. *PLoS One* 2014, 9: e115425.
52. Guideline Adaptation Committee. *Clinical Practice Guidelines and Principles of Care for People with Dementia*. Sydney: Guideline Adaptation Committee, 2016.
53. Konno R, Stern C, Gibb H. The best evidence for assisted bathing of older people with dementia: a comprehensive systematic review. *JBIC Database of Systematic Reviews and Implementation Reports* 2013, 11: 123–212.
54. Topfer LA. GPS locator devices for people with dementia. *CADTH Issues in Emerging Health Technologies*. Ottawa (ON): Canadian Agency for Drugs and Technologies in Health, 2016: 147.
55. White EB, Montgomery P. Electronic tracking for people with dementia: an exploratory study of the ethical issues experienced by carers in making decisions about usage. *Dementia (London)* 2014, 13: 216–232.
56. Guidelines and Protocols Advisory Committee. *Cognitive Impairment: Recognition, Diagnosis and Management in Primary Care* 2014.
57. Kok JS, van Heuvelen MJ, Berg IJ, Scherder EJ. Small scale homelike special care units and traditional special care units: effects on cognition in dementia; a longitudinal controlled intervention study. *BMC Geriatr* 2016, 16: 47.
58. The National Institute for Health and Care Excellence (NICE). *Dementia: assessment, management and support for people living with dementia and their carers (NG97)* 2018.
59. Andrews J. A guide to creating a dementia-friendly ward. *Nurs Times* 2013, 109: 20–21.
60. Chiu HL, Chan PT, Chu H, Hsiao SS, Liu D, Lin CH, *et al.* Effectiveness of light therapy in cognitively impaired persons: a metaanalysis of randomized controlled trials. *J Am Geriatr Soc* 2017, 65: 2227–2234.
61. van der Steen JT, Smaling HJ, van der Wouden JC, Bruinsma MS, Scholten RJ, Vink AC. Music-based therapeutic interventions for people with dementia. *Cochrane Database Syst Rev* 2018, 7: CD003477.
62. Lin LW, Weng SC, Wu HS, Tsai LJ, Lin YL, Yeh SH. The effects of white noise on agitated behaviors, mental status, and activities of daily living in older adults with dementia. *J Nurs Res* 2018, 26: 2–9.
63. Ng QX, Ho CY, Koh SS, Tan WC, Chan HW. Doll therapy for dementia sufferers: A systematic review. *Complement Ther Clin Pract* 2017, 26: 42–46.
64. Travers C, Brooks D, Hines S, O'Reilly M, McMaster M, He W, *et al.* Effectiveness of meaningful occupation interventions for people living with dementia in residential aged care: a systematic review. *JBIC Database System Rev Implement Rep* 2016, 14: 163–225.
65. Lorusso LN, Bosch SJ. Impact of multisensory environments on behavior for people with dementia: a systematic literature review. *Gerontologist* 2018, 58: e168–e179.
66. International Psychogeriatric Association. *IPA Complete Guides to Behavioral and Psychological Symptoms of Dementia (BPSD)* 2015.
67. Garcia LJ, Hebert M, Kozak J, Senecal I, Slaughter SE, Aminzadeh F, *et al.* Perceptions of family and staff on the role of the environment in long-term care homes for people with dementia. *Int Psychogeriatr* 2012, 24: 753–765.
68. Lyketos CG, Colenda CC, Beck C, Blank K, Doraiswamy MP, Kalunian DA, *et al.* Position statement of the American Association for Geriatric Psychiatry regarding principles of care for patients with dementia resulting from Alzheimer disease. *Am J Geriatr Psychiatry* 2006, 14: 561–572.
69. Fleiner T, Leucht S, Forstl H, Zijlstra W, Haussermann P. Effects of short-term exercise interventions on behavioral and psychological symptoms in patients with dementia: a systematic review. *J Alzheimers Dis* 2017, 55: 1583–1594.
70. Barreto Pde S, Demougeot L, Pillard F, Lapeyre-Mestre M, Rolland Y. Exercise training for managing behavioral and psychological symptoms in people with dementia: A systematic review and meta-analysis. *Ageing Res Rev* 2015, 24: 274–285.
71. Roland KP, Chappell NL. Meaningful activity for persons with dementia: family caregiver perspectives. *Am J Alzheimers Dis Other Demen* 2015, 30: 559–568.
72. Castro-Monteiro E, Alhayek-Ai M, Diaz-Redondo A, Ayala A, Rodriguez-Blazquez C, Rojo-Perez F, *et al.* Quality of life of institutionalized older adults by dementia severity. *Int Psychogeriatr* 2016, 28: 83–92.
73. Duru Asiret G, Kapucu S. The effect of reminiscence therapy on cognition, depression, and activities of daily living for patients With Alzheimer disease. *J Geriatr Psychiatry Neurol* 2016, 29: 31–37.
74. Olley R, Morales A. Systematic review of evidence underpinning non-pharmacological therapies in dementia. *Aust Health Rev* 2018, 42: 361–369.

75. Wu J, Wang Y, Wang Z. The effectiveness of massage and touch on behavioural and psychological symptoms of dementia: A quantitative systematic review and meta-analysis. *J Adv Nurs* 2017, 73: 2283–2295.
76. Searson R, Hendry AM, Ramachandran R, Burns A, Purandare N. Activities enjoyed by patients with dementia together with their spouses and psychological morbidity in carers. *Aging Ment Health* 2008, 12: 276–282.
77. Raposo VL. Lost in ‘Culturation’: medical informed consent in China (from a Western perspective). *Med Health Care Philos* 2019, 22: 17–30.
78. Stewart JT, Schultz SK. Palliative care for dementia. *Psychiatr Clin North Am* 2018, 41: 141–151.
79. Zarit SH, Todd PA, Zarit JM. Subjective burden of husbands and wives as caregivers: a longitudinal study. *Gerontologist* 1986, 26: 260–266.
80. Mausbach BT, Chattillion EA, Roepke SK, Patterson TL, Grant I. A comparison of psychosocial outcomes in elderly Alzheimer caregivers and noncaregivers. *Am J Geriatr Psychiatry* 2013, 21: 5–13.
81. Seeher K, Low LF, Reppermund S, Brodaty H. Predictors and outcomes for caregivers of people with mild cognitive impairment: a systematic literature review. *Alzheimers Dement* 2013, 9: 346–355.
82. Fonareva I, Oken BS. Physiological and functional consequences of caregiving for relatives with dementia. *Int Psychogeriatr* 2014, 26: 725–747.
83. Shaw WS, Patterson TL, Ziegler MG, Dimsdale JE, Semple SJ, Grant I. Accelerated risk of hypertensive blood pressure recordings among Alzheimer caregivers. *J Psychosom Res* 1999, 46: 215–227.
84. Vitaliano PP, Scanlan JM, Zhang J, Savage MV, Hirsch IB, Siegler IC. A path model of chronic stress, the metabolic syndrome, and coronary heart disease. *Psychosom Med* 2002, 64: 418–435.
85. Wang G, Cheng Q, Zhang S, Bai L, Zeng J, Cui PJ, *et al.* Economic impact of dementia in developing countries: an evaluation of Alzheimer-type dementia in Shanghai, China. *J Alzheimers Dis* 2008, 15: 109–115.
86. Tang SH, Chio OI, Chang LH, Mao HF, Chen LH, Yip PK, *et al.* Caregiver active participation in psychoeducational intervention improved caregiving skills and competency. *Geriatr Gerontol Int* 2018, 18: 750–757.
87. Wang Z, Ma C, Han H, He R, Zhou L, Liang R, *et al.* Caregiver burden in Alzheimer’s disease: Moderation effects of social support and mediation effects of positive aspects of caregiving. *Int J Geriatr Psychiatry* 2018. <https://doi.org/10.1002/gps.4910>.
88. Forstmeier S, Maercker A, Savaskan E, Roth T. Cognitive behavioural treatment for mild Alzheimer’s patients and their caregivers (CBTAC): study protocol for a randomized controlled trial. *Trials* 2015, 16: 526.
89. Sepe-Monti M, Vanacore N, Bartorelli L, Tognetti A, Giubilei F, Caregiver Study Group Savvy. The Savvy Caregiver Program: a probe multicenter randomized controlled pilot trial in caregivers of patients affected by Alzheimer’s disease. *J Alzheimers Dis* 2016, 54: 1235–1246.
90. Pozet A, Lejeune C, Bonnet M, Dabakuyo S, Dion M, Fagnoni P, *et al.* Evaluation of efficacy and efficiency of a pragmatic intervention by a social worker to support informal caregivers of elderly patients (The ICE Study): study protocol for a randomized controlled trial. *Trials* 2016, 17: 531.
91. Nguyen TA, Nguyen H, Pham T, Nguyen TH, Hinton L. A cluster randomized controlled trial to test the feasibility and preliminary effectiveness of a family dementia caregiver intervention in Vietnam: The REACH VN study protocol. *Medicine (Baltimore)* 2018, 97: e12553.
92. Black CM, Lipton RB, Thiel E, Brouillette M, Khandker R. Relationship between treatment initiation and healthcare costs in Alzheimer’s disease. *J Alzheimers Dis* 2019, 68: 1575–1585.



REVIEW

# A Review of Functional Near-Infrared Spectroscopy Studies of Motor and Cognitive Function in Preterm Infants

Quan Wang<sup>1,3,4</sup> · Guang-Pu Zhu<sup>1,2,3</sup> · Li Yi<sup>5</sup> · Xin-Xin Cui<sup>1,3</sup> · Hui Wang<sup>1,2,3</sup> · Ru-Yi Wei<sup>1</sup> · Bing-Liang Hu<sup>3</sup>

Received: 29 April 2019 / Accepted: 23 July 2019 / Published online: 12 November 2019  
© Shanghai Institutes for Biological Sciences, CAS 2019

**Abstract** Preterm infants are vulnerable to brain injuries, and have a greater chance of experiencing neurodevelopmental disorders throughout development. Early screening for motor and cognitive functions is critical to assessing the developmental trajectory in preterm infants, especially those who may have motor or cognitive deficits. The brain imaging technology functional near-infrared spectroscopy (fNIRS) is a portable and low-cost method of assessing cerebral hemodynamics, making it suitable for large-scale use even in remote and underdeveloped areas. In this article, we review peer-reviewed, scientific fNIRS studies of motor performance, speech perception, and facial recognition in preterm infants. fNIRS provides a link between hemodynamic activity and the development of brain functions in preterm infants. Research using fNIRS

has shown different patterns of hemoglobin change during some behavioral tasks in early infancy. fNIRS helps to promote our understanding of the developmental mechanisms of brain function in preterm infants when performing motor or cognitive tasks in a less-restricted environment.

**Keywords** Functional near infrared spectroscopy · Preterm infant · Motor performance · Speech perception · Facial recognition · Cerebral hemodynamics

## Introduction

In 2015, a survey of children under five showed that 2.7 million died during the neonatal period [1]. Preterm birth is the leading cause of child mortality in almost all high- and middle-income countries [2]. The complications of preterm birth are the largest direct cause of neonatal mortality, accounting for 35% of the world's 3.10 million deaths each year, and at least 50% of all neonatal deaths [3]. Although advances in perinatal medical care have contributed to an increase in the survival rate of newborns, disorders of higher brain functions among surviving infants are still a crucial issue in perinatal medicine [4–7]. The gestational age (GA) of preterm neonates is generally <37 complete weeks [8]. Incomplete development of some organs may cause preterm infants to be unable to adapt to the outside world and prone to hypoxia and infection [9]. These may increase the risk of cerebral palsy, learning disabilities, and visual impairment in preterm infants, affecting long-term physical health and cognitive function [10]. The effects of preterm birth may last a lifetime, placing a heavy burden on the families, society, and medical institutions [11].

Brain imaging techniques can provide valuable information about brain development, and opportunities to link

Quan Wang and Guang-Pu Zhu have contributed equally to this work.

✉ Quan Wang  
wangquan@opt.ac.cn

✉ Bing-Liang Hu  
hbl@opt.ac.cn

- <sup>1</sup> Key Laboratory of Spectral Imaging Technology, Xi'an Institute of Optics and Precision Mechanics of the Chinese Academy of Sciences, Xi'an 710119, China
- <sup>2</sup> University of Chinese Academy of Sciences, Beijing 100049, China
- <sup>3</sup> Key Laboratory of Biomedical Spectroscopy of Xi'an, Xi'an Institute of Optics and Precision Mechanics of the Chinese Academy of Sciences, Xi'an 710119, China
- <sup>4</sup> Child Study Center, Yale School of Medicine, Yale University, New Haven, CT 06520, USA
- <sup>5</sup> School of Psychological and Cognitive Sciences and Beijing Key Laboratory of Behavior and Mental Health, Peking University, Beijing 100871, China

brain development to human behavior [12]. The traditional brain imaging techniques are mainly magnetic resonance imaging (MRI), electroencephalography (EEG), and computerized tomography (CT). However, CT scans generate radiation, and frequent scanning may affect brain development, so they are not recommended for preterm infants. MRI scans are not suitable for motor or cognitive function studies in preterm infants either. First, MRI has little tolerance for head movements [13]. Since it is almost impossible for a preterm infant to keep still for any length of time, the MRI scan must be done while the infant is asleep. The alternative is to sedate or anesthetize the infant before performing the scan, which may make parents reluctant to allow an MRI scan on their child. Second, a cognitive task is the most effective method for studying cognitive development, but sleeping infants cannot accomplish such tasks. Third, studying the brain function of preterm infants while they are performing natural behaviors requires long-term bedside monitoring with an instrument that is portable and possesses high ecological validity. These goals are difficult to achieve using MRI. Finally, the cost of MRI equipment is relatively high, and the availability of MRI units in low-income countries remains poor. A survey has shown that, in West Africa, 84 MRI units serve a population of 372,551,411 [14]. The lack of brain imaging equipment has led to higher mortality in preterm infants in low-income countries. A report from the World Health Organization showed that the mortality rate of preterm infants in low-income countries is ~9 times higher than that in high-income countries [15]. Although EEG is less restricted and more readily accepted by parents than MRI or CT, it is not suitable for developmental studies in preterm infants due to poor spatial localization. Accurate localization of the active areas in the brain is vital in studies of motor and cognitive function.

Functional near-infrared spectroscopy (fNIRS) is a brain imaging technology that is much more suitable for preterm infants than MRI, CT, or EEG. fNIRS devices are usually attached to the participant's scalp, where optodes (optical sensor devices) emit near-infrared light. The light penetrates the soft tissues and bone and is absorbed by oxy- and deoxy-hemoglobin. Light detectors absorb the scattered light emitted by the optode and quantify the concentration of hemoglobin. fNIRS captures changes in cerebral oxygen saturation by measuring the intensity of scattered light in the active areas of the brain. Compared with traditional functional brain imaging technologies, fNIRS is less susceptible to noise and requires less restriction of head or body activity than MRI and CT [16]. Also, it has more accurate spatial localization of the active cerebral areas than EEG. In addition, fNIRS is relatively low-cost and so can be promoted on a large scale. Some fNIRS studies in resource-poor and remote areas have confirmed its

suitability during infancy and its potential for field-based neuroimaging research on cognitive function [17, 18]. If fNIRS is widely used, more families with preterm infants will have access to brain imaging, even in remote and underdeveloped areas. Studies have shown that early intervention is helpful for neurodevelopmental outcomes in preterm infants, especially those who may have motor or cognitive deficits [19–21]. The common use of fNIRS also helps the early identification and diagnosis of these deficits, so that the affected infants can benefit from early intervention.

Infancy is the most vigorous stage of growth and development in a person's life. Motor, hearing, and visual skills are all developing at this stage. In the late 1970s to mid-1980s, fNIRS was first used to study infants [22–24] and it is now widely used in research and clinical environments to monitor cerebral oxygen saturation in preterm infants with various conditions, such as apnea [25], intraventricular hemorrhage [26], and medication effects [27]. Many studies have confirmed the feasibility of using fNIRS to assess cerebral autoregulation [28, 29], and researchers have found that developmentally linked or acquired dysfunction of cerebral autoregulation is closely associated with the occurrence of brain injury. In recent years, some research has used fNIRS to compare cerebral oxygenation in preterm and term infants and assess the brain functions in preterm infants to explore their developmental trajectories.

There are already some reviews of fNIRS applications in exploring the brain function of preterm or term infants. Lloyd-Fox *et al.* [30] reviewed the achievements in neurodevelopment and the advantages of fNIRS in infant research. They focused on advances in techniques and the progress of methods in research design and the analysis of hemodynamic responses. Quaresima *et al.* [31] reviewed studies of cortical activation in the classical language region in newborns, children, and adults using fNIRS instruments of varying complexity. Wolf *et al.* [32] overviewed the instrumentation available, compared the advantages and limitations based on the underlying principles, and reviewed the application of fNIRS to measure oxygen saturation in the brain, liver, gastrointestinal tract, and peripheral tissue. However, there is no systematic review of fNIRS studies for the assessment of motor and cognitive function in preterm infants while performing tasks. In this review, we focused on studies assessing the brain function of preterm infants using fNIRS and were particularly interested in three functions: motor performance, speech perception, and facial recognition. We specifically concentrated on differences in cerebral hemodynamic responses between preterm and term infants when exposed to the same stimuli.

## fNIRS Studies in Preterm Infants

We conducted a literature search first using PubMed. Subsequently, Google Scholar was used to supplement relevant articles. The keywords used in the searches were “near infrared spectroscopy”, “NIRS”, “preterm”, “pre-mature”, “neonate”, “infant”, “speech”, “language”, “motor”, “movement”, and “face”. Next, the “Related Articles” function was used to broaden the search. The reference sections of all relevant studies were examined to identify additional papers. This literature search concluded in May 2019. Studies were limited to articles in English.

Included studies involved the use of fNIRS to assess brain function in preterm human neonates. Articles on animal experiments did not fulfill the inclusion criteria. Trials in both awake and sleep states were considered. Studies that examined the effect of drugs or breastfeeding on neonatal cerebral hemodynamics were excluded. In addition, research assessing cerebral oxygenation during hypoxic ischemic attacks or surgery in preterm infants was not considered. The search strategy is summarized in Fig. 1. Preterm infants were included as subjects in each study. Their GA was <37 weeks, and chronological ages were no more than one year. The brain function in preterm infants was assessed at hospitals in all studies.

According to the papers meeting the inclusion criteria, studies were classified into three areas: motor performance, speech perception, and facial recognition (Table 1). Our main concern was the cerebral hemodynamic responses in preterm infants exposed to visual, auditory, or motor stimuli. Also, we compared the cerebral hemodynamic responses between preterm and term infants, and explored the effect of preterm birth on different brain functions in infants.

## Motor Performance

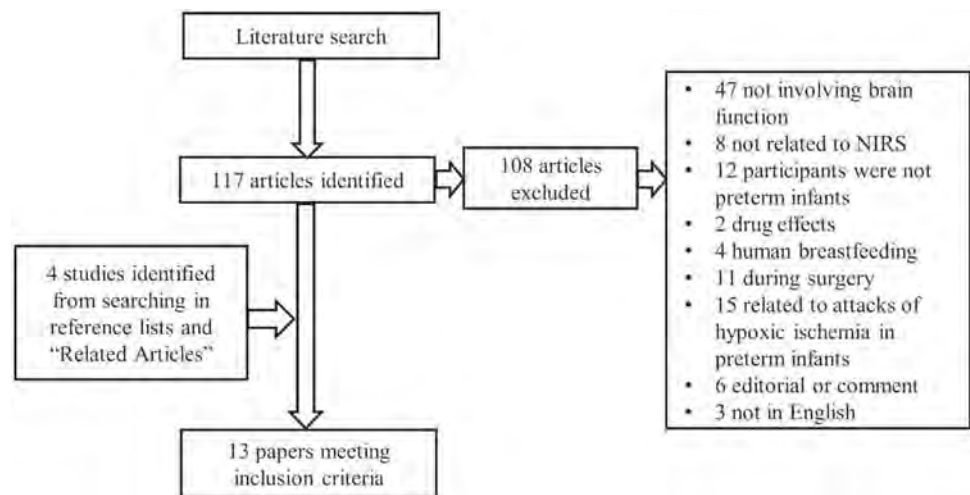
The fetus develops rapidly between 20 and 37 weeks GA, and many sensorimotor networks are established during the second half of pregnancy. Therefore, motor development is one of the most affected areas in preterm birth and may cause many restrictions in later life. An fNIRS study indicated that motor impairment might be associated with cerebral hypoxia during the transition immediately after birth in preterm infants [33]. A recent meta-analysis of 11 studies assessed the prevalence of motor impairments in school-aged children born prematurely after the 1990s, and reported it as ranging from 19.0% to 40.5% [34].

Neonatal motor performance is closely associated with the development of the sensorimotor cortex. fNIRS is practical for studying the role of cortical sensorimotor

function in motor behavior. Isobe *et al.* [35] performed passive knee movements on healthy term infants and preterm infants (GA: 24–35 weeks; median, 29.6 weeks) on days 3–57 during sedated sleep. They found that oxyhemoglobin (HbO) and total hemoglobin (tHb) increased in the primary sensorimotor area of all neonates, and the local deoxyhemoglobin (HHb) decreased in 6 of 7 neonates in response to contralateral knee movement. However, during ipsilateral knee movement, HbO and tHb showed slighter changes. To study this further, Kusaka *et al.* [36] added the stimulation of passive elbow and knee movement in term infants and preterm infants (GA: 24–41 weeks; median, 29.6 weeks) on days 3–99. The fNIRS results showed a significant difference in the area and degree of response between contralateral and ipsilateral movements. They found that contralateral knee and elbow movement caused a marked increase in HbO in a larger area of the sensorimotor cortex, while ipsilateral knee and elbow movement caused smaller changes in HbO in a smaller area.

Apart from the passive motor behavior in a sleeping state, researchers have demonstrated that fNIRS can be used to identify the activation of sensorimotor areas in awake infants. Kashou *et al.* [37] compared the durations of HbO changes in the left and right hemispheres of preterm neonates (mean postmenstrual age (PMA): 41.6–47.0 weeks) between palmar, plantar, and oromotor stimuli, and found that the oromotor stimuli resulted in a 50% greater response than the palmar or plantar stimuli. de Oliveira *et al.* [38] compared motor performance between term and preterm infants (GA <34 weeks) at 6 months chronological age using fNIRS and the Bayley Scales of Infant Development, Third Edition (Bayley-III). Motor performance was similar in full-term and preterm infants, but the hemodynamic responses were different. During sensorimotor stimulation, the cerebral activation response in full-term infants was contralateral, whereas the response in preterm infants was predominantly bilateral. The preterm group also exhibited a longer latency for the hemodynamic response than the full-term group. In 2019, de Oliveira *et al.* [39] conducted a longitudinal study with preterm and full-term infants at 6 and 12 months of age. In response to sensorimotor stimulation, preterm infants showed wider bilateral activation at 6 months, and an exclusively contralateral and more local activation response at 12 months. However, the 12-month-old preterm group continued to show a larger activation area than the full-term group of the same age. This may indicate that the brains of preterm infants are less specialized. Allievi *et al.* [40] saw a maturational trend toward faster, higher amplitude, and more spatially dispersed functional responses in the brains of preterm neonates (PMA: 32–45 weeks). They also found that, in preterm infants at

**Fig. 1** Literature search strategy. The systematic search strategy highlights the number of articles acquired in the original search, the justification for rejection of certain articles, and the total number of articles included for systematic review, data extraction, and analysis.



a PMA equivalent to full-term infants, there was a decrease in both response amplitude and interhemispheric functional connectivity, and an increase in spatial specificity, culminating in the establishment of a sensorimotor functional response similar to that seen in adults.

The above studies show that in both the awake and sedated sleep states, the sensorimotor functions in preterm infants can be imaged and evaluated with fNIRS. Moreover, fNIRS can detect real-time activation responses in cortex, and this can be complimentary to movement assessment scales such as Bayley-III. Therefore, fNIRS has the potential to supplement the developmental assessment of behavioral responses.

## Speech Perception

Many studies have shown that preterm infants have speech perception abilities. Mahmoudzadeh *et al.* [41] recorded cortical responses in the temporal and frontal areas using fNIRS in preterm infants at ~30 weeks PMA. The results showed that these infants could discriminate two syllables (*/ba/versus/ga/*) and the gender of a human voice (male *vs* female). When preterm infants were exposed to auditory stimuli in the form of utterances made by their mothers and female nurses, the active response in the right frontal area was different. In addition, they could discriminate between their mothers' utterances and those of female nurses [42].

Language disorder is a major concern among preterm infants. fNIRS studies are important for understanding the physiological mechanisms underlying brain functions in preterm infants. A study conducted by Naoi *et al.* [43] examined cerebral activation and functional connectivity in response to infant-directed speech and adult-directed speech in term and preterm infants (mean PMA: 275.4 days) using a 94-channel NIRS instrument. Cerebral

activation in response to speech stimuli in preterm infants was higher in the right temporal region and inter-hemisphere connectivity was higher than in full-term controls. This was especially evident in regions known to be involved in speech processing, such as the temporal and temporo-parietal regions, suggesting that preterm infants follow different developmental trajectories due to differences in intrauterine and extrauterine development.

Studying the cerebral hemodynamics of speech perception in preterm infants is valuable for early diagnosis and intervention for speech development deficits. fNIRS research on adults and infants has indicated that speech stimulation typically causes an increase in HbO and a slight simultaneous decrease in HHb [44]. However, Arimitsu *et al.* [45] found that preterm infants (GA: 26–36 weeks) do not always have the same patterns of hemoglobin change as full-term infants in response to phonemic or prosodic contrasts. They further found that the proportion of preterm infants with atypical hemodynamic patterns decreased, and finally became the same as that of term infants when they reached a corrected age of 38 weeks. These results reflected that the cerebral cortices of preterm infants may not initially be fully functional and the higher brain functions of preterm infants develop gradually before the projected due date. Arimitsu *et al.* [46] tested 80 infants (GA: 26–41 weeks) from 33 to 41 weeks PMA, and found that as PMA increased, hemodynamic regulation and the functional system for phonemic and prosodic processing developed and became consistent with term infants by the projected due date. The maturity of the hemodynamic response may reflect the development of language functions in preterm infants. Results also suggested that hearing infant-directed speech is helpful for the development of speech function in preterm infants, and that early intervention has a positive effect on speech perception disorders [46].

**Table 1** Summary of fNIRS studies on motor and cognitive functions in preterm infants.

Study	fNIRS System	Method	Key finding
<i>Motor performance</i>			
Isobe <i>et al.</i> [34]	NIR topography, Hitachi	Flexed and extended the right or left leg at the knee joint	HbO and tHb increase during contralateral knee movement
Kusaka <i>et al.</i> [35]	24 multichannel NIRS, Hitachi	Flexed and extended the knee or elbow joint	Significant difference in the area and degree of response between contralateral and ipsilateral movement
Kashou <i>et al.</i> [36]	NIRScout imaging system, NIRx	Palmar, plantar, and oromotor stimulation	Oromotor stimulus resulted in a 50% greater response than palmar or plantar stimuli
Pansy <i>et al.</i> [32]	INVOS Cerebral/somatic oximeter monitor	crSO <sub>2</sub> ; assessed short-term neurological outcome by GMA	Motor impairment possibly associated with cerebral hypoxia
de Oliveira <i>et al.</i> [37]	NIRScout Tandem 1616, NIRx	Micro-direct-current motor held against right hand	Activation response bilateral and latency longer in preterms
de Oliveira <i>et al.</i> [38]	NIRScout Tandem 1616, NIRx	Micro-motor grasped in hand	12-month old preterm infants showed a contralateral response but the activation area was larger than 12-month-old term infants
<i>Speech perception</i>			
Saito <i>et al.</i> [41]	NIRO200, Hamamatsu Photonics	Auditory stimuli (mother's voice, nurse's voice, or white noise)	Preterm infants reacted differently to different voice stimuli
Mahmoudzadeh <i>et al.</i> [40]	Imagent, ISS	Four syllables/ba/and/ga/produced by French male and female speakers; standard, deviant voice, and deviant phoneme trials	Preterm infants discriminated two syllables (/ba/vs/ga/) and human voice (male vs female).
Naoi <i>et al.</i> [42]	ETG-7000, Hitachi	Speech and non-speech auditory stimuli	Preterm infants: decreased activity in response to speech stimuli in the right temporal region, and increased interhemispheric connectivity
Arimitsu <i>et al.</i> [44]	Not mentioned	Phonemic contrast (/itta/vs/itte/), and prosodic contrast (/itta/and/itta?/)	Hemoglobin change pattern became the same as that of term infants at 38 weeks CGA
Arimitsu <i>et al.</i> [45]	ETG 4000, Hitachi	Phonemic contrast (/itta/vs/itte/), and prosodic contrast (/itta/and/itta?/)	Alterations in hemodynamic regulation and the functional system for phonemic and prosodic processing in preterm infants catch up by their projected due dates
<i>Facial recognition</i>			
Carlsson <i>et al.</i> [57]	NIRO 300, Hamamatsu Photonics	Pictures of the mothers and unknown women	Alteration or delay of the maturation of the occipitotemporal pathway may cause difficulties in face recognition in preterms
Frie <i>et al.</i> [59]	NIRO 300 or NIRO 200, Hamamatsu Photonics	Gray background, mother's face, an unknown face	Different cortical face recognition processes than term-born infants

Abbreviations: HbO, oxyhemoglobin; tHb, total hemoglobin; crSO<sub>2</sub>, cerebral regional oxygen saturation; GMA, general movement assessment; CGA, corrected gestational age.

## Facial Recognition

The ability to distinguish and recognize faces is necessary for social interaction. At birth, infants are able to distinguish between facial and non-facial patterns and prefer face-like patterns [47]. This ability is likely associated with cortical circuits [48–50]. The infant is exposed to faces and the cortical circuits begin to develop at 2 months [51]. Between 6 and 8 months, an infant can identify a face [52, 53]. fMRI studies suggest that the right temporal lobe,

prefrontal cortex, and fusiform gyrus are the most important areas for facial recognition processes [54, 55]. Injury of these areas may be associated with impaired facial recognition in preterm infants. Such an impairment could affect social interactions, and may lead to depression or anxiety.

fNIRS provides a way to measure cerebral activity during face processing by monitoring changes in HbO, HHb, and tHb concentrations [56, 57]. It also offers a method of exploring the neurodevelopmental mechanism

of facial recognition. A study by Carlsson *et al.* [58] found that infants at 6–9 months exhibit a higher activation-related hemodynamic response in the right fronto-temporal cortex when exposed to an image of their mother's face than to an unknown face. The results suggested that the right fronto-temporal cortex is involved in facial recognition processes at this age. They further hypothesized that an alteration or delay in the maturation of the occipitotemporal pathway may cause facial recognition impairments [59]. Frie *et al.* [60] compared cortical hemodynamic responses to known and unknown facial stimuli between extremely preterm infants (corrected age: 6–10 months) and full-term infants. They found that preterm infants had a significantly smaller hemodynamic response in the right frontotemporal areas when looking at their mother's face compared to an unknown face, which was opposite to the response of term infants [60]. These results suggest that preterm infants have different cortical facial recognition processes than term infants, possibly due to disruption of the subcortical system associated with an innate ability to prioritize face-like patterns over non-face-like patterns.

## Summary and Perspectives

The studies reviewed above analyzed the relationships between hemodynamic activity and motor and cognitive development in preterm infants. We focused on three aspects of brain development (motor performance, speech perception, and facial recognition), and found that preterm infants have different, even opposite responses to the same stimuli when compared to term infants. These differences may have a few different causes. First, during the last 3 months of pregnancy, the fetal auditory system undergoes functional development [61, 62]. Preterm infants have a shorter GA, so the hemodynamic response to speech stimuli may be affected by their immature brains after birth. Second, differences in intra- and extra-uterine developmental environments may cause differences in hemodynamic patterns between preterm and term infants. Compared to a term infant, a preterm infant at an equivalent PMA has less intrauterine experience and more extrauterine experience. In addition, preterm infants are generally treated in neonatal intensive care units and receive more facial and sound stimuli than their term counterparts. In the first few weeks after birth, overstimulation in the neonatal intensive care unit may have long-term effects on brain size and function in preterm infants [63]. This experience could affect cerebral hemodynamic responses to speech or facial stimuli. Finally, these differences between pre- and full-term infants may be caused by immature neural networks and angiogenesis in preterm infants. After oxygen consumption accompanying

neuronal activity, the supply of oxygen is not efficiently delivered to the area of active neurons in the cerebral cortex [64], leading to abnormal changes of HbO and HHb in certain brain regions of preterm infants.

Different hemodynamic responses in preterm infants suggest that their brain functions may not develop at first. However, these functions gradually develop before the projected due date and eventually become the same as those of term infants at an equivalent PMA. In motor performance, the differences in lateralization of evoked sensorimotor cortex responses in term and preterm infants indicate that a considerable degree of functional lateralization develops during the first months of postnatal life. Similar phenomena have been found in the auditory cortex. As for phonemic and prosodic perception, the phoneme is generally processed in the left-temporal area, while prosody activates the right-temporal area in term infants and adults [65, 66]. After 39 weeks PMA, preterm infants begin to show functional laterality in the auditory cortex and gradually resemble term infants [46]. The research reviewed above also suggests that early intervention facilitates the development of cognitive functions. fNIRS is useful for early screening and intervention in the developmental problems of preterm infants.

The preterm infant is at elevated risk of cognitive deficits and developmental disorders. The fNIRS studies in preterm infants described in this article mainly focused on the first year after birth, which is the critical development period. Over the past 40 years [67], fNIRS has continuously developed and much progress has been made [68]. This is mainly due to its advantages. fNIRS will continue to develop as a methodology because its potential is still far from fully utilized.

Although fNIRS has apparent advantages, there are several challenges that limit its applications. fNIRS has poor spatial resolution and limited penetration depth [69, 70]. When assessing cerebral oxygenation saturation, the distance between the optode and the detector is at least 2 cm, which limits the spatial resolution [71]. In addition, the signal-to-noise ratio (SNR) in fNIRS is lower than in MRI. Many research groups have tried novel methods to overcome these shortcomings, such as combining fNIRS with other imaging methods. Chiarelli *et al.* [72] integrated fNIRS with EEG to monitor the neonatal brain, and showed that this provides additional information about the electrical and metabolic hemodynamic activities of the cerebral cortex, and has higher sensitivity and specificity. In preterm infants, combined techniques can provide new insights into brain function and help us better understand impairments.

In addition to poor spatial resolution, limited penetration depth, and a low SNR, there are other challenges when using fNIRS to study brain functions in preterm infants.

Although fNIRS does not have strict head-movement limitations like MRI, sliding of the probe or changes in the intensity of the near-infrared light can result in spurious signals (motion artifacts) at the corresponding detector [73]. Motion artifacts may affect study results by masking actual changes of HbO and HHb. These artifacts may also influence baseline data. Motion artifacts can be reduced with hardware and software optimization, as well as by calming the preterm infant during the experiment, thereby reducing unnecessary motion caused by anxiety. Another challenge is that the results of fNIRS studies of the same brain function in preterm infants may be different [74]. This may be because different experimental designs are used in different studies [75]. In addition, differences in chronological ages and developmental levels among different studies also influence the results. Future research needs to weigh the comfort of the subjects, spatial resolution of the hardware, and potential for motion artifacts. At the same time, larger sample sizes are needed to replicate experiments.

As an imaging technique, fNIRS establishes a correspondence between brain activity and brain areas by measuring HbO and HHb concentrations, and promotes our understanding of brain development in preterm infants. This will inevitably help us to identify critical periods for intervention in atypical development, thereby reducing the risk of motor and cognitive disorders and minimizing the impact of preterm birth on infants. However, the current fNIRS research in preterm infants still has many limitations. Apart from the three areas reviewed, the developmental mechanisms of other brain functions are still unclear. Further studies with fNIRS are needed to better understand the mechanisms of brain functions in preterm infants.

**Acknowledgements** This review was supported by the Key Laboratory of Biomedical Spectroscopy of Xi'an Municipality, China (Y839S11D0Z) and an Autonomous Deployment Project of Xi'an Institute of Optics and Precision Mechanics of the Chinese Academy of Sciences (Y855W31213). We thank Zhou-Feng Zhang and Tao Yu for providing critical suggestions on the paper. The suggestions of Rui-Na Dai are also acknowledged. And thanks for the help of Chi Gao and Xin-Ming Zhang.

**Conflict of interest** The authors claim that there are no conflicts of interest.

## References

- Liu L, Oza S, Hogan D, Chu Y, Perin J, Zhu J, *et al.* Global, regional, and national causes of under-5 mortality in 2000–15: an updated systematic analysis with implications for the sustainable development goals. *Lancet* 2016, 388: 3027–3035.
- Liu L, Johnson HL, Cousens S, Perin J, Scott S, Lawn JE, *et al.* Global, regional, and national causes of child mortality: an updated systematic analysis for 2010 with time trends since 2000. *Lancet* 2012, 379: 2151–2161.
- Lawn JE, Kerber K, Enweronu-Laryea C, Cousens S. 3.6 million neonatal deaths—what is progressing and what is not? *Semin Perinatol* 2010, 34: 371–386.
- Mwaniki MK, Atieno M, Lawn JE, Newton CR. Long-term neurodevelopmental outcomes after intrauterine and neonatal insults: a systematic review. *Lancet* 2012, 379: 445–452.
- Luu TM, Vohr BR, Schneider KC, Katz KH, Tucker R, Allan WC, *et al.* Trajectories of receptive language development from 3 to 12 years of age for very preterm children. *Pediatrics* 2009, 124: 333–341.
- Bhutta AT, Cleves MA, Casey PH, Cradock MM, Anand K. Cognitive and behavioral outcomes of school-aged children who were born preterm: a meta-analysis. *JAMA* 2002, 288: 728–737.
- Aarnoudse-Moens CSH, Weisglas-Kuperus N, van Goudoever JB, Oosterlaan J. Meta-analysis of neurobehavioral outcomes in very preterm and/or very low birth weight children. *Pediatrics* 2009, 124: 717–728.
- Steer P. The epidemiology of preterm labour. *BJOG* 2005, 112: 1–3.
- Logitharajah P, Rutherford MA, Cowan FM. Hypoxic-ischemic encephalopathy in preterm infants: antecedent factors, brain imaging, and outcome. *Pediatric Res* 2009, 66: 222.
- Rogers LK, Velten M. Maternal inflammation, growth retardation, and preterm birth: insights into adult cardiovascular disease. *Life Sci* 2011, 89: 417–421.
- Butler AS, Behrman RE. Preterm birth: causes, consequences, and prevention. Washington: National Academies Press, 2007.
- Fan L, Jiang T. Mapping underlying maturational changes in human brain. *Neurosci Bull* 2017, 33: 478–480.
- Sumitani S, Tanaka T, Tayoshi SY, Ota K, Kameoka N, Ueno SI, *et al.* Activation of the prefrontal cortex during the wisconsin card sorting test as measured by multichannel near-infrared spectroscopy. *Neuropsychobiology* 2006, 53: 70–76.
- Ogbole GI, Adeyomoye AO, Badu-Pepurah A, Mensah Y, Nzeh DA. Survey of magnetic resonance imaging availability in West Africa. *Pan Afr Med J* 2018, 30: 240.
- March of Dimes, PMNCH, Save the children, WHO. Born Too Soon: The Global Action Report on Preterm Birth. CP Howson, MV Kinney, JE Lawn (Eds). World Health Organization, Geneva, 2012.
- Wilcox T, Biondi M. fNIRS in the developmental sciences. *Wiley Interdiscip Rev Cognit Sci* 2015, 6: 263–283.
- Lloyd-Fox S, Papademetriou M, Darboe MK, Everdell NL, Wegmuller R, Prentice AM, *et al.* Functional near infrared spectroscopy (fNIRS) to assess cognitive function in infants in rural Africa. *Sci Rep* 2014, 4: 4740.
- Lloyd-Fox S, Moore S, Darboe M, Prentice A, Papademetriou M, Blasi A, *et al.* fNIRS in Africa & Asia: an objective measure of cognitive development for global health settings. *FASEB J* 2016, 30: 1149.1118–1149.
- Gross RT. Enhancing the outcomes of low-birth-weight premature infants: a multisite randomized trial. *JAMA* 1990, 263: 3035–3042.
- Nurcombe B, Howell DC, Rauh VA, Teti DM, Ruoff P, Brennan J. An intervention program for mothers of low-birthweight infants: preliminary results. *J Am Acad Child Adolesc Psychiatry* 1984, 23: 319–325.
- Van Hus J, Jeukens-Visser M, Koldewijn K, Holman R, Kok J, Nollet F, *et al.* Early intervention leads to long-term developmental improvements in very preterm infants, especially infants with bronchopulmonary dysplasia. *Acta Paediatr* 2016, 105: 773–781.

22. Brazy JE, Lewis DV, Mitnick MH, vander Vliet FFJ. Noninvasive monitoring of cerebral oxygenation in preterm infants: preliminary observations. *Pediatrics* 1985, 75: 217–225.
23. Wyatt J, Delpy D, Cope M, Wray S, Reynolds E. Quantification of cerebral oxygenation and haemodynamics in sick newborn infants by near infrared spectrophotometry. *Lancet* 1986, 328: 1063–1066.
24. Benaron DA, Benitz WE, Ariagno RL, Stevenson DK. Noninvasive methods for estimating in vivo oxygenation. *Clin Pediatr* 1992, 31: 258–273.
25. Yamamoto A, Yokoyama N, Yonetani M, Uetani Y, Nakamura H, Nakao H. Evaluation of change of cerebral circulation by SpO<sub>2</sub> in preterm infants with apneic episodes using near infrared spectroscopy. *Pediatr Int* 2003, 45: 661–664.
26. Zhang Y, Chan GS, Tracy MB, Lee QY, Hinder M, Savkin AV, *et al.* Cerebral near-infrared spectroscopy analysis in preterm infants with intraventricular hemorrhage. *Conf Proc IEEE Eng Med Biol Soc* 2011: 1937–1940.
27. Dani C, Bertini G, Reali MF, Tronchin M, Wiechmann L, Martelli E, *et al.* Brain hemodynamic changes in preterm infants after maintenance dose caffeine and aminophylline treatment. *Neonatology* 2000, 78: 27–32.
28. Hummel E, Kooi E, Verhagen E, Bos A. 592 cerebral autoregulation during 24 hours in preterm infants measured by near-infrared spectroscopy. *Pediatr Res* 2010, 68: 303–308.
29. Alderliesten T, Lemmers PM, Smarius JJ, van de Vosse RE, Baerts W, van Bel F. Cerebral oxygenation, extraction, and autoregulation in very preterm infants who develop peri-intraventricular hemorrhage. *J Pediatrics* 2013, 162: 698–704.
30. Lloyd-Fox S, Blasi A, Elwell C. Illuminating the developing brain: the past, present and future of functional near infrared spectroscopy. *Neurosci Biobehav Rev* 2010, 34: 269–284.
31. Quaresima V, Bisconti S, Ferrari M. A brief review on the use of functional near-infrared spectroscopy (fNIRS) for language imaging studies in human newborns and adults. *Brain Lang* 2012, 121: 79–89.
32. Wolf M, Naulaers G, van Bel F, Kleiser S, Greisen G. A review of near infrared spectroscopy for term and preterm newborns. *J Near Infrared Spectrosc* 2012, 20: 43–55.
33. Pansy J, Baik N, Schwabegger B, Scheuchenegger A, Pichler-Stachl E, Avian A, *et al.* Cerebral hypoxia during immediate transition after birth and short term neurological outcome. *Early Hum Dev* 2017, 110: 13–15.
34. Williams J, Lee KJ, Anderson PJ. Prevalence of motor-skill impairment in preterm children who do not develop cerebral palsy: a systematic review. *Dev Med Child Neurol* 2010, 52: 232–237.
35. Isobe K, Kusaka T, Nagano K, Okubo K, Yasuda S, Kondo M, *et al.* Functional imaging of the brain in sedated newborn infants using near infrared topography during passive knee movement. *Neurosci Lett* 2001, 299: 221–224.
36. Kusaka T, Isobe K, Miki T, Ueno M, Koyano K, Nakamura S, *et al.* Functional lateralization of sensorimotor cortex in infants measured using multichannel near-infrared spectroscopy. *Pediatric Res* 2011, 69: 430–435.
37. Kashou NH, Dar IA, Hasenstab KA, Nahhas RW, Jadcherla SR. Somatic stimulation causes frontoparietal cortical changes in neonates: a functional near-infrared spectroscopy study. *Neurophotonics* 2016, 4: 011004.
38. de Oliveira SR, de Paula Machado ACC, de Paula JJ, de Moraes PHP, Nahin MJS, de Castro Magalhães L, *et al.* Association between hemodynamic activity and motor performance in six-month-old full-term and preterm infants: a functional near-infrared spectroscopy study. *Neurophotonics* 2017, 5: 011016.
39. de Oliveira SR, Machado ACC, de Paula JJ, Novi SL, Mesquita RC, de Miranda DM, *et al.* Changes of functional response in sensorimotor cortex of preterm and full-term infants during the first year: An fNIRS study. *Early Hum Dev* 2019, 133: 23–28.
40. Allievi AG, Arichi T, Tusor N, Kimpton J, Arulkumaran S, Counsell SJ, *et al.* Maturation of sensori-motor functional responses in the preterm brain. *Cereb Cortex* 2015, 26: 402–413.
41. Mahmoudzadeh M, Dehaene-Lambertz G, Fournier M, Kongolo G, Goudjil S, Dubois J, *et al.* Syllabic discrimination in premature human infants prior to complete formation of cortical layers. *Proc Natl Acad Sci U S A* 2013, 110: 4846–4851.
42. Saito Y, Fukuhara R, Aoyama S, Toshima T. Frontal brain activation in premature infants' response to auditory stimuli in neonatal intensive care unit. *Early Hum Dev* 2009, 85: 471–474.
43. Naoi N, Fuchino Y, Shibata M, Niwa F, Kawai M, Konishi Y, *et al.* Decreased right temporal activation and increased inter-hemispheric connectivity in response to speech in preterm infants at term-equivalent age. *Front Psychol* 2013, 4: 94. <https://doi.org/10.3389/fpsyg.2013.00094>.
44. Vermeij A, Van Beek AH, Rikkert MGO, Claassen JA, Kessels RP. Effects of aging on cerebral oxygenation during working-memory performance: a functional near-infrared spectroscopy study. *PLoS One* 2012, 7: e46210.
45. Arimitsu T, Minagawa Y, Takahashi T, Ikeda K. Assessment of developing speech perception in preterm infants using near-infrared spectroscopy. *NeoReviews* 2015, 16: e481–e489.
46. Arimitsu T, Minagawa Y, Yagihashi T, Uchida MO, Matsuzaki A, Ikeda K, *et al.* The cerebral hemodynamic response to phonetic changes of speech in preterm and term infants: The impact of postmenstrual age. *NeuroImage* 2018, 19: 599–606.
47. Johnson MH, Dziurawiec S, Ellis H, Morton J. Newborns' preferential tracking of face-like stimuli and its subsequent decline. *Cognition* 1991, 40: 1–19.
48. Johnson MH. Subcortical face processing. *Nat Rev Neurosci* 2005, 6: 766.
49. Haan MD, Pascalis O, Johnson MH. Specialization of neural mechanisms underlying face recognition in human infants. *J Cognit Neurosci* 2002, 14: 199–209.
50. Turati C, Bulf H, Simion F. Newborns' face recognition over changes in viewpoint. *Cognition* 2008, 106: 1300–1321.
51. Morton J, Johnson MH. CONSPEC and CONLERN: a two-process theory of infant face recognition. *Psychol Rev* 1991, 98: 164–181.
52. Gauthier I, Nelson CA. The development of face expertise. *Curr Opin Neurobiol* 2001, 11: 219–224.
53. Courage ML, Reynolds GD, Richards JE. Infants' attention to patterned stimuli: developmental change from 3 to 12 months of age. *Child Dev* 2006, 77: 680–695.
54. Haxby JV, Hoffman EA, Gobbini MI. The distributed human neural system for face perception. *Trends Cognit Sci* 2000, 4: 223–233.
55. Kanwisher N, McDermott J, Chun MM. The fusiform face area: a module in human extrastriate cortex specialized for face perception. *J Neurosci* 1997, 17: 4302–4311.
56. Otsuka Y, Nakato E, Kanazawa S, Yamaguchi MK, Watanabe S, Kakigi R. Neural activation to upright and inverted faces in infants measured by near infrared spectroscopy. *Neuroimage* 2007, 34: 399–406.
57. Nakato E, Otsuka Y, Kanazawa S, Yamaguchi MK, Watanabe S, Kakigi R. When do infants differentiate profile face from frontal face? A near-infrared spectroscopic study. *Hum Brain Mapp* 2009, 30: 462–472.
58. Carlsson J, Lagercrantz H, Olson L, Printz G, Bartocci M. Activation of the right fronto-temporal cortex during maternal facial recognition in young infants. *Acta Paediatr* 2008, 97: 1221–1225.
59. Dutton GN, Jacobson LK. Cerebral visual impairment in children. *Semin Neonatol* 2001, 6: 477–485.

60. Frie J, Padilla N, Áden U, Lagercrantz H, Bartocci M. Extremely preterm-born infants demonstrate different facial recognition processes at 6–10 months of corrected age. *J Pediatr* 2016, 172: 96–102. e101.
61. Birnholz JC, Benacerraf BR. The development of human fetal hearing. *Science* 1983, 222: 516–518.
62. Hall JW. Development of the ear and hearing. *J Perinatol* 2000, 20: S12–S20.
63. Le Grand R, Mondloch CJ, Maurer D, Brent HP. Neuroperception: Early visual experience and face processing. *Nature* 2001, 410: 890.
64. Raichle ME, MacLeod AM, Snyder AZ, Powers WJ, Gusnard DA, Shulman GL. A default mode of brain function. *Proc Natl Acad Sci U S A* 2001, 98: 676–682.
65. Minagawa-Kawai Y, Cristià A, Dupoux E. Cerebral lateralization and early speech acquisition: A developmental scenario. *Dev Cognit Neurosci* 2011, 1: 217–232.
66. Sato Y, Mori K, Furuya I, Hayashi R, Minagawa-Kawai Y, Koizumi T. Developmental changes in cerebral lateralization during speech processing measured by near infrared spectroscopy. *Jpn J Logoped Phoniater* 2003, 44: 165–171.
67. Jobsis FF. Noninvasive, infrared monitoring of cerebral and myocardial oxygen sufficiency and circulatory parameters. *Science* 1977, 198: 1264–1267.
68. Scholkman F, Kleiser S, Metz AJ, Zimmermann R, Pavia JM, Wolf U, *et al.* A review on continuous wave functional near-infrared spectroscopy and imaging instrumentation and methodology. *Neuroimage* 2014, 85: 6–27.
69. Horaguchi T, Ogata Y, Watanabe N, Yamamoto M. Behavioral and near-infrared spectroscopy study of the effects of distance and choice in a number comparison task. *Neurosci Res* 2008, 61: 294–301.
70. Irani F, Platek SM, Bunce S, Ruocco AC, Chute D. Functional near infrared spectroscopy (fNIRS): an emerging neuroimaging technology with important applications for the study of brain disorders. *Clin Neuropsychol* 2007, 21: 9–37.
71. Ernst LH, Schneider S, Ehlis AC, Fallgatter AJ. Functional near infrared spectroscopy in psychiatry: a critical review. *J Near Infrared Spectrosc* 2012, 20: 93–105.
72. Chiarelli AM, Zappasodi F, Di Pompeo F, Merla A. Simultaneous functional near-infrared spectroscopy and electroencephalography for monitoring of human brain activity and oxygenation: a review. *Neurophotonics* 2017, 4: 041411.
73. Aslin RN, Mehler J. Near-infrared spectroscopy for functional studies of brain activity in human infants: promise, prospects, and challenges. *J Biomed Opt* 2005, 10: 011009.
74. Jenny C, Biallas M, Trajkovic I, Fauchere JC, Bucher HU, Wolf M. Reproducibility of cerebral tissue oxygen saturation measurements by near-infrared spectroscopy in newborn infants. *J Biomed Opt* 2011, 16: 097004.
75. Pichler G, Wolf M, Roll C, Weindling M, Greisen G, Wardle S, *et al.* Recommendations to increase the validity and comparability of peripheral measurements by near infrared spectroscopy in neonates. *Neonatology* 2008, 94: 320–322.



# NEUROSCIENCE BULLETIN

Impact Factor

# 4.246

Q2

2018 Journal Citation Report  
(Clarivate Analytics, 2019)



**NEUROSCIENCE BULLETIN 神经科学通报 (Monthly)**

Vol. 36 No. 3 March 15, 2020

**Sponsored by:** Shanghai Institutes for Biological Sciences, Chinese Academy of Sciences  
Chinese Neuroscience Society  
Second Military Medical University

**Editors-in-Chief:** Shumin Duan, Ru-Rong Ji

**Edited by:** Editorial Board of *Neuroscience Bulletin*

319 Yueyang Road, Building 31 B, Room 405, Shanghai 200031, China

Phone: +86-21-54922863; Fax: +86-21-54922833

E-mail: [nsb@sibs.ac.cn](mailto:nsb@sibs.ac.cn); <http://www.neurosci.cn>

**Editors:** Bin Wei, Xu Jiang, Zhi-Rui Liu

**Published by:** Shanghai Institutes for Biological Sciences, Chinese Academy of Sciences (320 Yueyang Road, Shanghai)

**Printed by:** Shanghai Shengtong Times Printing Co., Ltd (A6, No. 2888, Caolang Highway, Jinshan District, Shanghai)

**Overseas Distributed by:** Springer Nature

**Home Distributed by:** Local Post Offices

ISSN 1673-7067

CN 31-1975/R

Post Office Code Number: 4-608

Permit of Ad. Number: 3100420130051

Price: ¥ 100.00

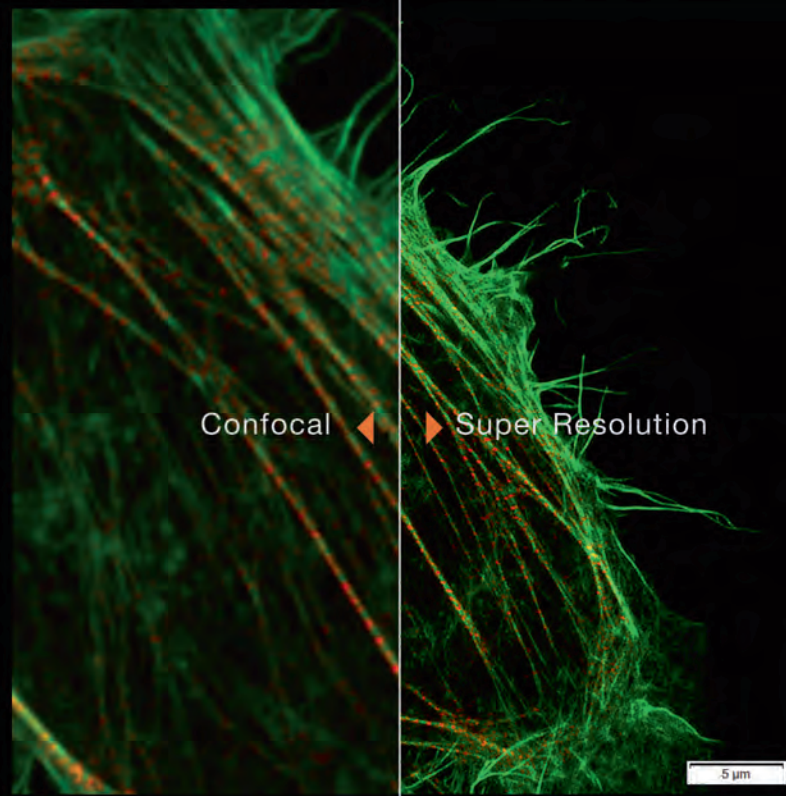
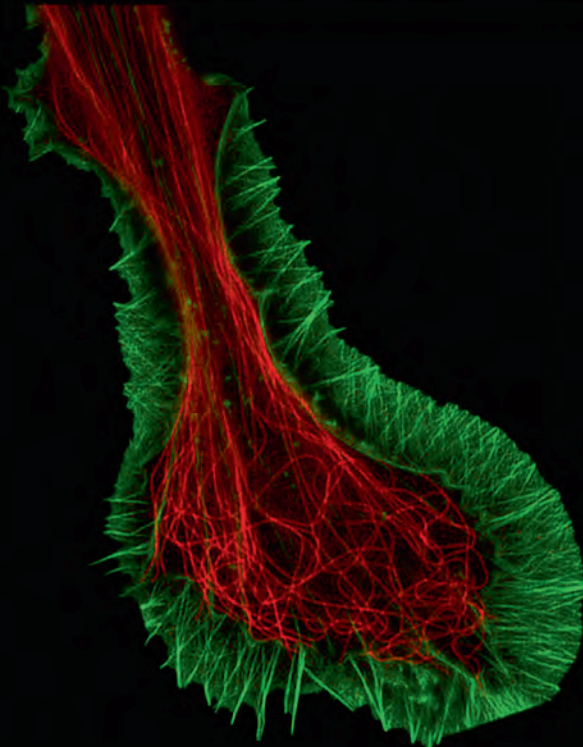
ISSN 1673-7067



9 771673 706209

兼顾分辨率和速度的

转盘共聚焦活细胞超分辨系统 **SpinSR10**



- 分辨率高达110nm的实时超分辨率成像
- 专有反卷积算法进一步提升图像质量
- 宽视野成像，速度高达 200fps
- 特色硅油物镜可以实现活细胞深层成像
- 宽场、共聚焦、超分辨率模式自由切换
- 功能强大的智能cellSens软件平台



奥林巴斯（北京）销售服务有限公司

北京朝阳区酒仙桥路10号恒通商务园B12C座2F (北京) 010-59756006  
 上海市徐汇区淮海中路1010号嘉华中心11楼 (上海) 021-51582084  
 广州市环市东路403号广州电子大厦16楼 (广州) 020-61227171

陕西省西安市新城区尚德路85号太平洋保险大厦8F

湖北省武汉市江岸区中山大道1628号武汉天地企业中心5号7楼701单元  
 四川省成都市人民南路四段三号来福士广场T1-11楼  
 辽宁省沈阳市沈河区友好街10号新地中心1号楼3501室

(西安) 029-87206108

(武汉) 027-82718838

(成都) 028-86703700

(沈阳) 024-23342084